LOAN DOCUMENT

PHOTOGRAPH THIS SHEET

DTIC ACCESSION NUMBER

LEVEL

INVENTORY

0

Proceedings of the Workshop on the Microcalorimetry. . .

DOCUMENT IDENTIFICATION

19 May 99

DISTRIBUTION STATEMENT A
Approved for Public Release
Distribution Unlimited

DISTRIBUTION STATEMENT

NTIS GRA&I
DTIC TRAC
UNANNOUNCED
JUSTIFICATION

BY

DISTRIBUTION/

AVAILABILITY CODES

DISTRIBUTION	AVAILABILITY AND/OR SPECIAL	
A-1		

DISTRIBUTION STAMP

DATE ACCESSIONED

DATE RETURNED

19991213 057

DATE RECEIVED IN DTIC

REGISTERED OR CERTIFIED NUMBER

PHOTOGRAPH THIS SHEET AND RETURN TO DTIC-FDAC

HANDLE WITH CARE

DTIC FORM 70A JUN 94

DOCUMENT PROCESSING SHEET

PREVIOUS EDITION MAY BE USED UNTIL STOCK IS EXHAUSTED.

LOAN DOCUMENT

DTIC QUALITY INSPECTED 4

University of
HUDDERSFIELD

PROCEEDINGS OF THE WORKSHOP ON THE MICROCALORIMETRY OF ENERGETIC MATERIALS

17-19TH May 1999

LEEDS, UNITED KINGDOM

REPORT DOCUMENTATION PAGE

Form Approved
OMB No. 0704-0188

1. AGENCY USE ONLY *(Leave blank)*	2. REPORT DATE	3. REPORT TYPE AND DATES COVERED
	MAY 1999	Final 17-19 May 1999

4. TITLE AND SUBTITLE
Proceedings of the Workshop on the Microcalorimetry of Energetic Materials

5. FUNDING NUMBERS

6. AUTHOR(S)
Trevor Griffiths, Workshop Chairman

7. PERFORMING ORGANIZATION NAME(S) AND ADDRESS(ES)
University of Huddersfield
Leeds, United Kingdom

8. PERFORMING ORGANIZATION REPORT NUMBER

9. SPONSORING/MONITORING AGENCY NAME(S) AND ADDRESS(ES)
DERA
Fort Halstead, UK

10. SPONSORING/MONITORING AGENCY REPORT NUMBER

11. SUPPLEMENTARY NOTES

12a. DISTRIBUTION/AVAILABILITY STATEMENT
Approved for public release, distribution is unlimited.

12b. DISTRIBUTION CODE

13. ABSTRACT *(Maximum 200 words)*
Eighteen papers were presented at the workshop about uses of microcalorimetry as a tool to study servicelife of gun propellants, ageing, stability, heat generation, thermal decomposition of energetic plastisizers, modelling, absorbant surfaces, absolute alibration, corrosion rate, DSC studies, compatibility of energetic materials, sample preparations and measuring conditions.

14. SUBJECT TERMS
Pyrotechnics, microcalorimetry, energetic materials, Workshop proceedings

15. NUMBER OF PAGES

16. PRICE CODE

17. SECURITY CLASSIFICATION OF REPORT	18. SECURITY CLASSIFICATION OF THIS PAGE	19. SECURITY CLASSIFICATION OF ABSTRACT	20. LIMITATION OF ABSTRACT
Unclassified	Unclassified	Unclassified	SAR

GENERAL INSTRUCTIONS FOR COMPLETING SF 298

The Report Documentation Page (RDP) is used in announcing and cataloging reports. It is important that this information be consistent with the rest of the report, particularly the cover and title page. Instructions for filling in each block of the form follow. It is important to ***stay within the lines*** to meet ***optical scanning requirements***.

Block 1. Agency Use Only *(Leave blank)*.

Block 2. Report Date. Full publication date including day, month, and year, if available (e.g. 1 Jan 88). Must cite at least the year.

Block 3. Type of Report and Dates Covered. State whether report is interim, final, etc. If applicable, enter inclusive report dates (e.g. 10 Jun 87 - 30 Jun 88).

Block 4. Title and Subtitle. A title is taken from the part of the report that provides the most meaningful and complete information. When a report is prepared in more than one volume, repeat the primary title, add volume number, and include subtitle for the specific volume. On classified documents enter the title classification in parentheses.

Block 5. Funding Numbers. To include contract and grant numbers; may include program element number(s), project number(s), task number(s), and work unit number(s). Use the following labels:

C	- Contract	**PR**	- Project
G	- Grant	**TA**	- Task
PE	- Program Element	**WU**	- Work Unit Accession No.

Block 6. Author(s). Name(s) of person(s) responsible for writing the report, performing the research, or credited with the content of the report. If editor or compiler, this should follow the name(s).

Block 7. Performing Organization Name(s) and Address(es). Self-explanatory.

Block 8. Performing Organization Report Number. Enter the unique alphanumeric report number(s) assigned by the organization performing the report.

Block 9. Sponsoring/Monitoring Agency Name(s) and Address(es). Self-explanatory.

Block 10. Sponsoring/Monitoring Agency Report Number. *(If known)*

Block 11. Supplementary Notes. Enter information not included elsewhere such as: Prepared in cooperation with...; Trans. of...; To be published in.... When a report is revised, include a statement whether the new report supersedes or supplements the older report.

Block 12a. Distribution/Availability Statement. Denotes public availability or limitations. Cite any availability to the public. Enter additional limitations or special markings in all capitals (e.g. NOFORN, REL, ITAR).

- **DOD** - See DoDD 5230.24, "Distribution Statements on Technical Documents."
- **DOE** - See authorities.
- **NASA** - See Handbook NHB 2200.2.
- **NTIS** - Leave blank.

Block 12b. Distribution Code.

- **DOD** - Leave blank.
- **DOE** - Enter DOE distribution categories from the Standard Distribution for Unclassified Scientific and Technical Reports.
- **NASA** - Leave blank.
- **NTIS** - Leave blank.

Block 13. Abstract. Include a brief *(Maximum 200 words)* factual summary of the most significant information contained in the report.

Block 14. Subject Terms. Keywords or phrases identifying major subjects in the report.

Block 15. Number of Pages. Enter the total number of pages.

Block 16. Price Code. Enter appropriate price code *(NTIS only)*.

Blocks 17. - 19. Security Classifications. Self-explanatory. Enter U.S. Security Classification in accordance with U.S. Security Regulations (i.e., UNCLASSIFIED). If form contains classified information, stamp classification on the top and bottom of the page.

Block 20. Limitation of Abstract. This block must be completed to assign a limitation to the abstract. Enter either UL (unlimited) or SAR (same as report). An entry in this block is necessary if the abstract is to be limited. If blank, the abstract is assumed to be unlimited.

TABLE OF CONTENTS

PREFACE

This document is a compilation of the papers presented at the Workshop on Microcalorimetry of Energetic Materials which was held in Leeds UK between 17 - 19th May 1999. The workshop was organised by the Centre for Thermal Studies, Huddersfield University and DERA, Explosive and Pyrotechnic Assessment (WS3C). The workshop was attended by 45 delegates representing 12 countries and 18 papers were presented. Attendees represented government, industry, academia and instrument manufacturers who had on display some of their instrumentation.

No workshop can be successful without the backing and support from various organisations and individuals therefore I would like to acknowledge the following: firstly DERA for their support and Dr P Barnes (CESO(N)) for contributing towards the cost of publishing these Proceedings.

I personally would like to thank those who helped me to organise the Workshop and gave unstinting support. Among these are the Centre of Thermal Studies, Huddersfield University, in particular Professor Ted Charsley and his staff, Ms Sarah Goodall and Mr Jim Rooney. Since they were in the vicinity of the Workshop they had the job of finding a suitable venue and of arranging the social programme. The success of this 2nd Workshop is due to their hard work in ensuring everything ran smoothly and attending to the needs of the delegates. Again I would like to thank the Chevin Lodge Hotel for the lecture facilities, comfortable accommodation and good food. Also to the staff of Bedern Hall for helping to make the conference dinner a pleasant occasion.

Other individuals I would like to thank are Mr Tony Cardell for his assistance and helpful discussions on organising the Workshop and putting together the Workshop Programme. Thanks to Mr Jim Queay who has collated the papers ready for publishing. I would also like to express my gratitude to Dr Bernie Douda and Dr Bill Hubble for their support and for promoting the Workshop in the USA. I wish to recognise the work of Mrs Janet Smith who typed all the sections which were not papers.

On behalf of myself and everyone associated with organising the Workshop, thanks to Dr Peter Laye who did a magnificent job in leading, in what turned out to be a difficult final discussion and highlighting the conclusions of the delegates.

Finally I would like to thank all the session chairmen, all the authors who submitted papers, which resulted in an interesting technical programme, and especially all the delegates for making the effort to attend for without you there would have been no Workshop.

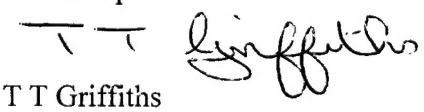

T T Griffiths
(Workshop Chairman)

ABSTRACT

The use of Heat Flow Calorimetry (HFC) Data to Enhance / Optimize the Service Life Evaluation of Gun Propellant

James A. Wilson
NSWC Crane Division
300 Highway 361
Crane IN 47522

The Service Life assessment of Naval Gun propellant has changed little in the last 40 years. The primary thrust of the Navy evaluation program has been to determine when the propellant will become chemically unstable. This has been accomplished by visually monitoring the release of nitrogen oxides (most often a red color fume). This process is extremely limited in its ability to predict of the impending end of service life.

The current process used by Crane has three elements: 1) conducting kinetic testing , 2) perform accelerated aging , and 3) performing functional testing. This process is very effective, but, would require many, many years to evaluate all of the numerous ammunition lots. This paper will outline a study conducted by NSWC Crane, which may revolutionize the manner in which the service life evaluation of gun ammunition is conducted. The basic thrust of the study was to compare the HFC (microcalorimetry) traces of a specific ammunition lot to the functional performance of that same lot. The goal of this effort is to establish if HFC traces could be used as a screening function so that ammunition lots with questionable performance attributes could be identified and evaluated early in the Service Life program.

This paper will present the results of this study, outline the potential benefits to both the logistics manager and the war fighter, and present a basic plan to speed up the validation process.

THE USE OF HEAT FLOW CALORIMETRY (HFC) TO OPTIMIZE THE SERVICE LIFE EVALUATION OF GUN PROPELLANT

BACKGROUND

Gun propellant contains nitrate esters (nitrocellulose, nitroglycerin, or both). Nitrate esters are by their very nature, unstable. During the course of storage, gun propellant slowly and spontaneously releases nitrogen oxides (a red color fume). Stabilizer is added to the propellant at the time of manufacturing to serve as a "trap" for the oxides. Without the stabilizer, or when the stabilizer content is low, the liberated nitrogen oxides can catalyze the decomposition of the original nitrate esters. This reaction is exothermic and may eventually lead to autocatalysis (self-ignition) of the gun propellant. Propellants are subjected to test throughout their lifetime to assure that they remain in a stable condition safe for storage and handling. Due to the expense of this process and the assumption that chemical stability will be bad before performance will suffer, no effort is made to assess performance.

In review of the US Army and Navy gun propellant evaluation history for the last 75 years, it seems there has been a tremendous amount of frustration. The studies of fuming process of many types of propellants indicated that the test is simply a pass or fail test with no quantifiable content. Review of the cause of one incident that occurred in 1976 at ARDEC, revealed that the red fume produced in the test could fade in a few days. At some time after the red fume fading, many of the samples would self-ignite. Therefore the time-to-fume test is clearly not an accurate and safe predictive test method. Today the degradation process is more completely understood by routinely using High Pressure Liquid Chromatography (HPLC) analysis to quantify the effective stabilizer contents remained in the propellant. The HPLC data is useful for assessment of the current stability condition, however, it does not predict the future safe storage life of the propellant and cannot be correlated to performance. The NATO test method has improved the capability of future shelf life prediction by combining the HPLC analysis of the stabilizer levels before and after accelerated aging test (65.5°C for 60 or 120 days). The NATO test method is based on a kinetic model established by the observed rate of stabilizer depletion. However, the complexity of the solid state kinetics may make it very difficult to derive a rate law truly representing the propellant degradation process.

Since 1988, NSWC Crane Division has been involved in developing a method that can determine the safe storage life of the gun propellant as well as assuring long range performance. This new method used both the HPLC and HFC to establish long term chemical stability as well as defining a very accurate accelerated aging program for the ammunition under test. By aging a portion of the subject ammunition to predetermined ages, the functional testing of the rounds will reveal any long range performance trends. This new program is called the **Predictive Surveillance (PS) Program** due to its ability to make long range stability and performance predictions.

Predictive Surveillance

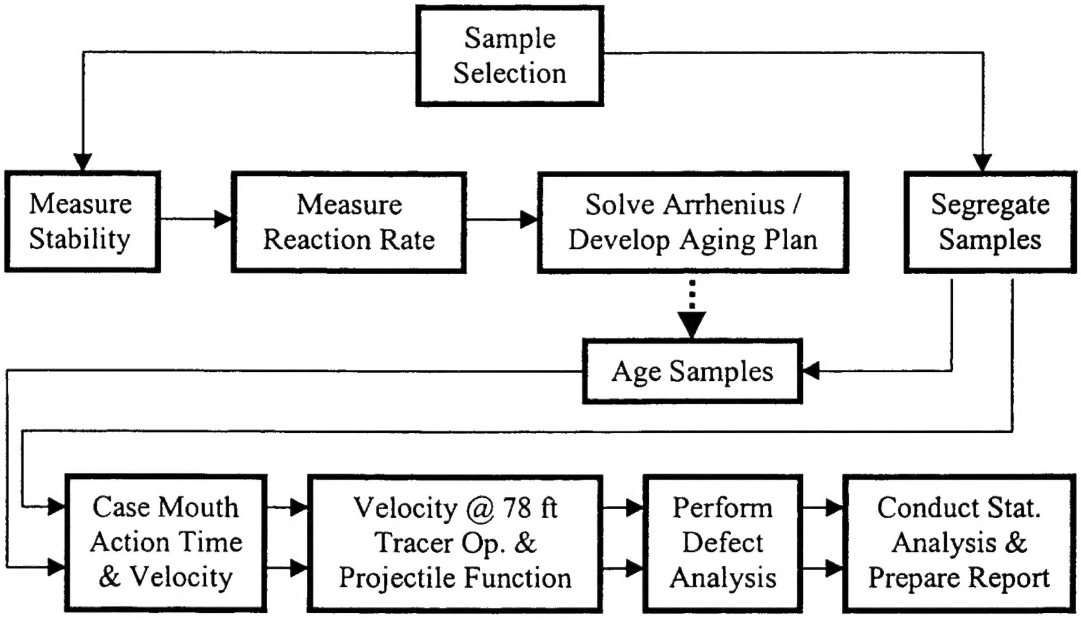

Evaluation Sample Strategy

Since all service life classifications of small caliber ammunition is made by ammunition lot number, and since historical data reveals that gun propellant is very heterogeneous, it is imperative that each ammunition lot be evaluated. When any evaluation activity first looks at the inventory of a modern small caliber ammunition series, the overwhelming size of the stockpile can be formidable. It is not uncommon to have more than two hundred ammunition lots for one series of ammunition. If indeed each lot had to be individually tested, the task would be extremely expensive and would most probably never accomplished. Since the propellant is the primary concern of the service life program, there is another method of evaluating the stockpile. By concentrating on propellant lots, the number of unique substrata can be reduced by approximately ten fold. This is due to the fact that each ammo lot is built with only one propellant lot and each propellant lot will be found in 9 to 14 or more ammo lots. By changing the sampling strategy from ammo lots to propellant lots the scope of the evaluation process becomes much more obtainable.

Test Sample Selection

A total of 10 separate ammunition lots were selected, obtained and tested. All of the ammunition lots were loaded with different propellant lots. A total of 35 rounds were randomly selected from each box of ammunition. Five round were disassembled and the propellant was removed. After the propellant was thoroughly mixed to a homogeneous state, the HFC and HPLC samples were taken. Of the remaining 30 rounds, 10 were to be aged 20 years, 10 were to be aged 10 years and 10 were left un-aged. All of the rounds

selected for functional testing were given an alphanumeric test sequence number. Individual lots were designated with a letter, (A-K), and each round had an additional number (1-30).

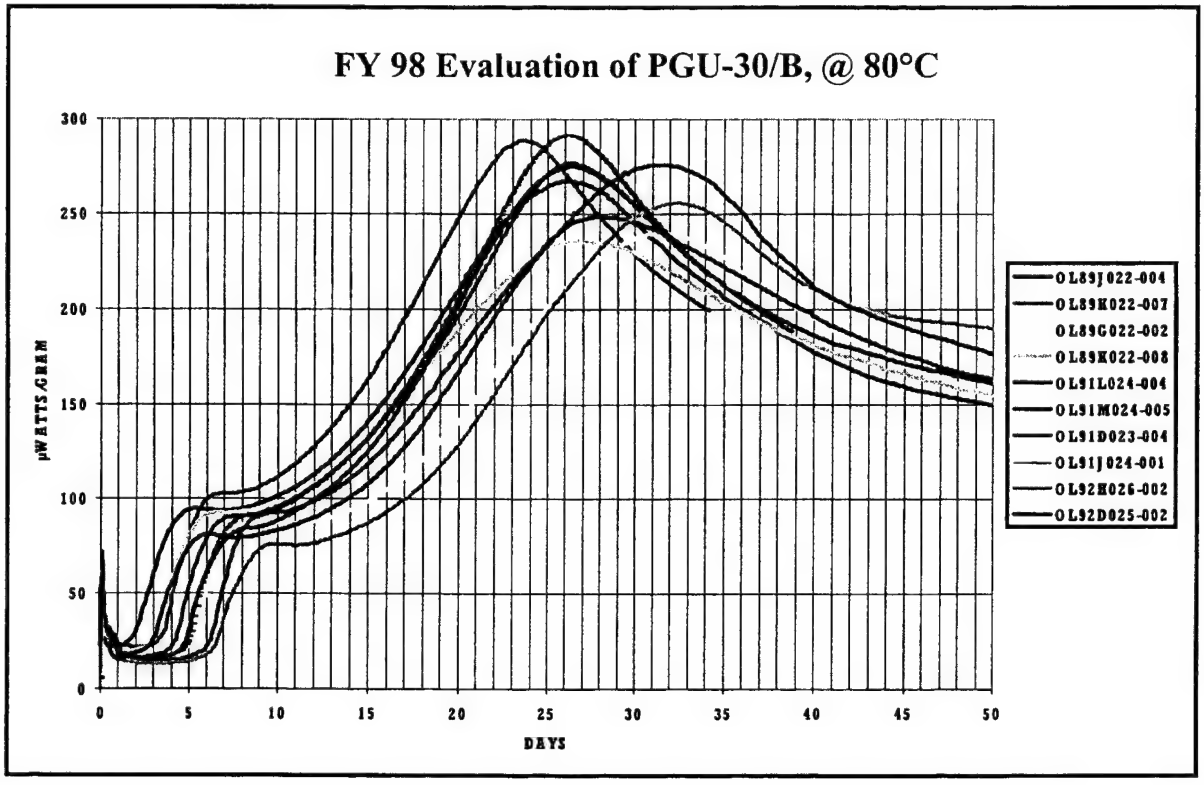

Heat Flow Calorimeter Analysis

The objective of the heat flow calorimetric analysis is to determine slow aging degradation, long-term chemical stability/compatibility, aging trend (i.e. accelerating factor), and shelf life of the gun propellants. The method is based on the measurement of the production (or consumption) of heat that accompanies chemical and physical transition from almost any energetic composition. The amount of heat produced is directly or indirectly proportional to the rate of degradation of the energetic composition. The net heat flow, in microwatts (μW), can be used to derive an accelerated aging plan through standard kinetics and thermodynamics equations (i.e. Arrhenius Equation). The extremely high sensitivity of the detector (0.2 μW) makes it possible to carry out measurements at temperatures closer to the real operational and storage conditions. Three Thermometric model TAM-2707 HFCs were used during this analysis.

HPLC (High Pressure Liquid Chromatography) Analysis

The objective of HPLC is to support the HFC in determining degradation trend of stabilizers in the propellant. The purity (percent) and rate of depletion (shelf life controlling) of the effective stabilizer can be determined. The HPLC analysis applies the principle of column chromatography combined with the state-of-art detecting system to separate and identify the propellant degradation products. The Water's model 150C ALC/GPC system is equipped with a photodiode array variable wavelength detector.

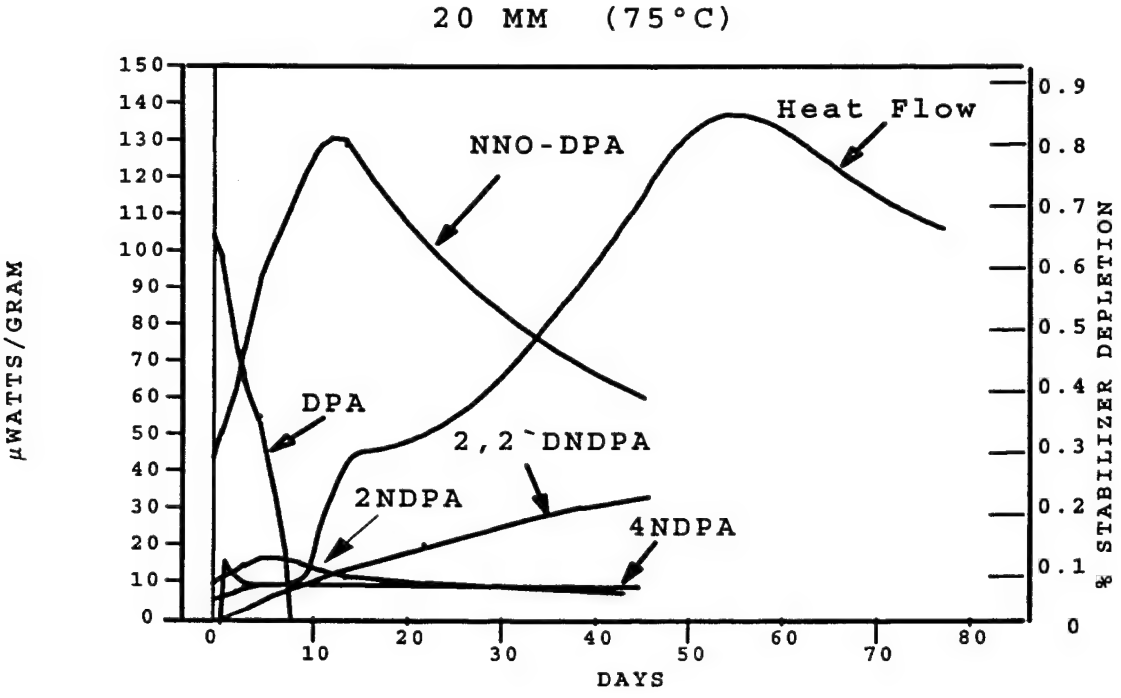

HPLC and HFC data charted together

Stabilizer and HFC

When the changes in the HPLC data are plotted on the same time frame as the HFC data, a number of concerns related to the HFC trace are answered. It is very apparent that the initial low rate of heat production is a direct result of the presence of DPA stabilizer. Once this stabilizer is depleted, the heat rate immediately rises. Although less positive, the second transition point on the HFC trace appears to be related to the level of the NNO-DPA daughter stabilizer. The same relative results have been noted in all cases where this data was collected.

Accelerated Aging

Based on the results of the kinetics (HFC) testing of this propellant, an acceleration plan was derived. Under this plan, the samples to be aged were exposed to a temperature of 62°C (144°F) for a predetermined period of time. The units to be aged to an artificial 10 years remained in the temperature chambers for 14 days and the 20 years samples for twice that period. A standard T & H chamber was used for the actual aging.

Function Firing Test

The aged and unaged cartridges were tested for chamber pressure, action time, projectile velocity at 78 feet, and tracer performance. All of the cartridges were conditioned to 70° ± 2° Fahrenheit (°F) prior to firing. The chamber pressure was measured with a PCB piezoelectric ballistic pressure transducer model 118A, and a PCB ballistic charge amplifier model 462B52 serial number 280. Transducer system calibration was conducted with a Pressure Products Industries static pressure calibration standard serial number AOH-17479. Signals from the ballistic transducer are feed into both an Oehler Model 82 ballistic computer and a Nicolet Pro 40 digital oscilloscope. The projectile velocity was measured using two photoelectric velocity screens placed at the standard position for 20mm ballistic testing. Tracer performance was determined visually by the use of a video recording system.

Functional Test Results

All cartridges fired on the initial valid attempt and there were no indications, from the performance variables, which would indicate abnormal projectile performance. Overall, 21 units had case mouth pressure readings higher than is acceptable for optimum performance of the gun. Only 12 of these out-of-specification tests could be considered major defects. All 12 major defects came from two lots, OL-92D025-002 and OL-92H026-002. In addition, all 12 came from rounds that had been artificially aged. A total of 40 units exhibited projectile velocity readings that failed to meet the minimum specification. The majority of these failures occurred on units aged to 10 and 20 years. Approximately half these failures occurred in one lot, OL-89G022-002. All (10 of 10) of the rounds from this lot aged to 10 years failed to meet minimum specification. With the exception of the three lots mentioned above, the performance of all the other lots was satisfactory.

Performance to HFC Correlation

Based on our HPLC stabilizer work, it was probable that there are indications from the HFC traces that could be indicative of actual propellant performance. In an effort to establish if any such correlation did exist, we looked at the HFC traces of the three lots which exhibited performance problems. By comparing the traces of satisfactory performers with those of the non-performers, it was apparent that there was at least one attribute that all three non-performing lot exhibited that the good lots did not, the peak heat rate was experienced after

30 days. All of the lots which exhibited satisfactory performance reached their peak heat flow rate prior to 30 days. When data from previous evaluations was also analyzed, the same phenomenon was also noted. Obviously the results form a sample size of only 20 lots is not very conclusive, however, the consistency of the results is very promising.

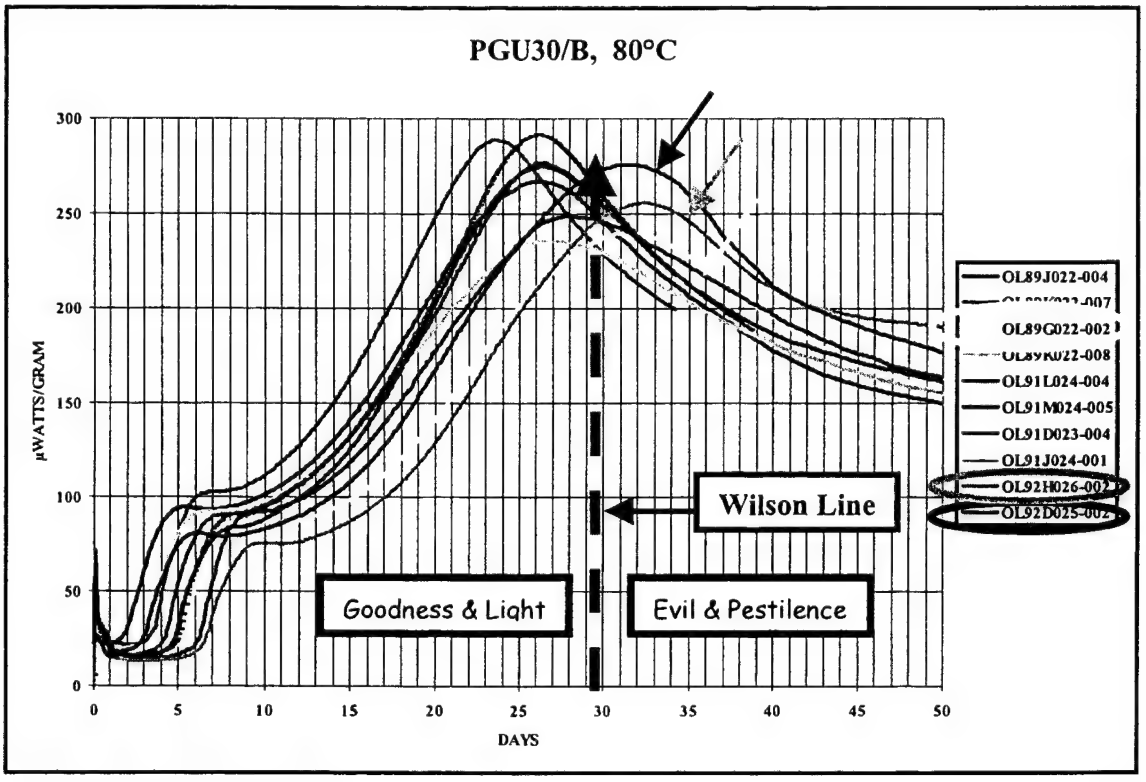

The validity of the "Wilson Line" would be established or invalidated eventually through normal surveillance testing, however, this could take many years to accomplish. The main concern with continuing our established pattern is the possibility that truly unserviceable or even unsafe strata might go undetected for many years. This represents an unacceptable treat to our war fighters and can not be tolerated. If the "Wilson Line" is assumed to be valid, a much more aggressive approach to the stockpile service life program can be assumed. By dramatically increasing the number of propellant lots that are kinetically tested each year while at the same time reducing the number that are functionally tested to only those lots with heat flow peaks occurring beyond 30 days, the entire stockpile could be evaluated in a very brief time period. Also, this would be accomplished with no increase in the baseline cost of the program. The only down side to this approach is that the number of lots with firing data would be greatly diminished during this period. If in the future the "Wilson Line" is determined to be non-valid, the author may suffer some discomfort, however, the actual downside risks to the war fighter are relatively minor.

Challenges

The new PS program satisfies many of the existing Gun Ammunition service life concerns:

1. Defines how long the propellant will be chemically stable.
2. Establishes if the propellant will perform satisfactory for the next 20 years.
3. Identifies low performing sub-strata prior to it becoming unserviceable so that these stocks can be expended in training rather than having to demil them.

While all of the above is true, there still remains a large number of programmatic challenges to be faced by the Gun Ammunition service life community:

1. Is there a method of interpreting the HFC traces that will accurately and consistently predict how propellant will perform when fired in a gun?
2. Will 20mm rounds ever enter an autocatalytic reaction which would result in self-ignition while in normal storage conditions?
3. Can the validity of the PS program be established with any meaningful level of statistical confidence? And if so, how?

Conclusion

The feasibility of using HFC to conduct the initial screening operation for small caliber gun propellant appears to be highly promising. If the results of the next two years of evaluation data continue in the same direction, HFC analysis should become a standard tool for both acquisition and service life efforts.

The use of Predictive Surveillance will have a direct and positive effect on the quality of the in-service gun ammunition stockpile and also provide the item managers the tools needed to effectively manage their assets.

Influence of storage on ageing of gun propellants in munition articles or in glass bottles

*Wim de Klerk** *and Niels v.d. Meer*

TNO Prins Maurits Laboratory, Researchgroup Properties Energetic Materials,
P.O. Box 45, 2280 AA Rijswijk, THE NETHERLANDS

ABSTRACT

Since the beginning of the nineties ammunition articles of the Dutch Ministry of Defense (MoD) are stored in temperature and humidity controlled bunkers of the Dutch army. However, the propellants kept at TNO-PML for surveillance purposes are stored in semi-closed glass bottles in a bunker with no climate control.

To compare the influence of ageing of both storage environments, a microcalorimetric program with IST (Isothermal Storage Test, an in house developed technique at TNO) is carried out on the propellants of 13 selected munition articles. Among them are new and old articles as well as small and large caliber.

A safe diameter of the propellants is calculated, which is characteristic for the self-ignition hazard. Furthermore, the heat production also gives an indication of the decrease of the calorific value for a storage period of 10 years in a moderate climate.

The experimental results showed that corresponding propellants have comparable heat production in the IST. As a consequence, the maximum heat generation and the calculated safe diameter of a sample couple are in the same order of magnitude. It could be concluded that thermal stability of the samples is not significantly affected by the different storage conditions. Only when the munition article has no metal casing, some differences may occur.

Keywords: explosives, microcalorimetry, ammunition, hazard, self-ignition, safe diameter

Introduction

Since the beginning of the seventies TNO-Prins Maurits Laboratory (TNO-PML) investigates the thermal stability of gun-propellants by isothermal microcalorimetry. The investigations are performed with IST (Isothermal Storage Test) at a temperature of 85 °C (358 K).
The investigated samples are stored in a bunker in semi-closed glass bottles. The bunker has no temperature and humidity control facilities. During the year there is a temperature profile from about 0 °C (over wintertime) till around 30 °C (over summer time).

* corresponding author, email : klerk@pml.tno.nl

Depending on the available mass of gun propellant the bottles are completely or partially filled. As a consequence of this variation in filling there is also a difference in oxygen cap in the bottle, which might have influence on the degradation process of the NC-based gun propellant.
The real ammunition articles containing the propellants are stored in the MoD bunkers. Since the beginning of the nineties these bunkers are humidity and temperature controlled.
The work presented in this paper is to investigate if there exists differences between the thermal stability of propellants stored at TNO and the same propellants in the munition article. Therefore 13 gun propellants are selected and are investigated by microcalorimetry.

Samples

All the investigated samples are identified by a unique KB/PH-number, which is assigned to the propellant by TNO-PML. The production year of the propellants is presented in Table 2.

Table 1: Chemical composition of the investigated gun propellants.

KB/PH number-1	KB/PH number-2	NC [%]	NGl [%]	EC [%]	DPA [%]	Vaseline [%]	Dibutyl-phtalate	Moisture [%]
3128	7259	92.7		1.0	1.1			1.2
3388	7260	57.8	25.2	2.2		0.4	4.4	0.4
3391	7261	61.6	27.0	2.2		0.4	2.4	0.3
3687	7262	56.5	23.9	2.3		0.4	4.7	0.5
3977 *	7263							
4767	7264	92.7		0.9	0.9		0.5	1.0
5109	7265	88.7		1.7	1.4			1.0
6384 *	7268							
6451 *	7269							
6479 *	7270							
6514 *	7272							
6832	7273	93.7			1.0			1.2
7084	7274	78.1	12.7	5.9	0.9		0.1	0.5

* : Composition not described on the propellant description sheet

In Table 1, the identifier KB/PH number-1 belongs to the propellant as stored at TNO-PML and KB/PH number-2 belongs to the army stored propellant. According to the above-mentioned table it can be concluded, that a variety of compositions (like single base and double bases, stabilised by EC and DPA) were investigated.

The ammunition articles and the year of production are listed in Table 2.

Table 2 : Age and application of the investigated propellants.

KB/PH number-1	KB/PH number-2	Year of production	NSN-code[1]	Weapon[2]
3128	7259	1953	0561	CTG tracer .303 inch
3388	7260	1954	3681	CTG 105 mm HE for Howitzers
3391	7261	1954	3681	CTG 105 mm HE for Howitzers
3687	7262	1955	3691	CTG 105 mm HE for Howitzers
3977	7263	1956	4411	Charge propelling 155 mm for Howitzer
4767	7264	1961	0801	CTG caliber .50 linked ball
5109	7265	1963	1272	CTG 40 mm HE for guns L/70
6384	7268	1980	2777	CTG 81 mm HE for Mortar
6451	7269	1980	0661	CTG 9 mm ball
6479	7270	1981	0611	CTG blank .303 inch
6514	7272	1982	0312	CTG 7.62 mm NATO ball
6832	7273	1986	1101	CTG 25 mm APDS-T
7084	7274	1991	0131	CTG caliber .30 carbine ball

[1] - NSN = NATO Stock Number
[2] - CTG = Cartridge

Storage Conditions

The storage conditions at TNO-PML are not controlled. During the year, there is a variation in temperature from about 0 °C till about 30 °C, as graphically shown in Figure 1 for the years 1995-1998.

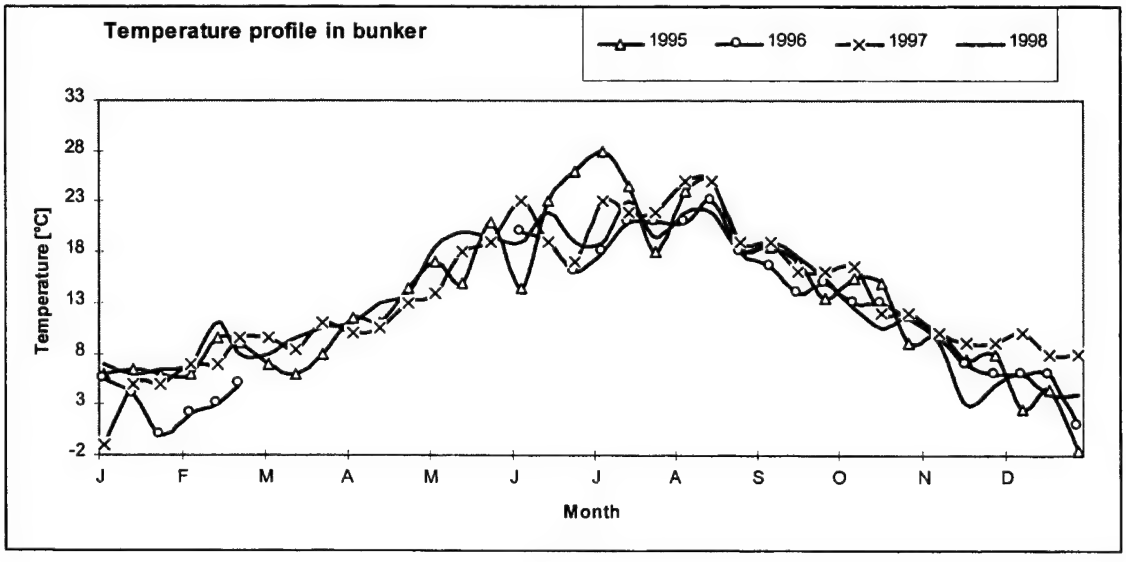

Figure 1 : Temperature profile in TNO-PML storage bunker.

Since the beginning of the nineties, the Dutch MoD has been storing most of their propellants under controlled conditions. These conditions mean, that the maximum relative humidity is limited to 50 % and the maximum temperature is 15 °C. Also the ammunitions are stored in metal cases, which are airtight.
Before the nineties storage of propellants was done in bunkers not fulfilling these conditions. At that time the conditions were the same as at TNO-PML. The great difference between TNO-PML and the MoD was, that at TNO all propellants were stored in semi-closed glass bottles. At MoD munition articles were packed in metal boxes, depending on the caliber.

Technique

The heat flow calorimeter or microcalorimeter is a sensitive heat generation measuring instrument. The technique has been used at TNO-PML since the late sixties [2]; the amount of gun propellant to be investigated is usually 5 gram. The Isothermal Storage Test (IST) (Fig. 2) consists of large heat sink (an aluminum block) which is kept at a constant temperature. In that block are two holes with a heat flow meter, e.g. a thermo-element, at the bottom of each hole.
The stainless steel sample vessel has a volume of 70 cm^3. After insertion of the sample vessel, temperature equilibration must be attained before the actual measurement can start, usually about 4 hours.

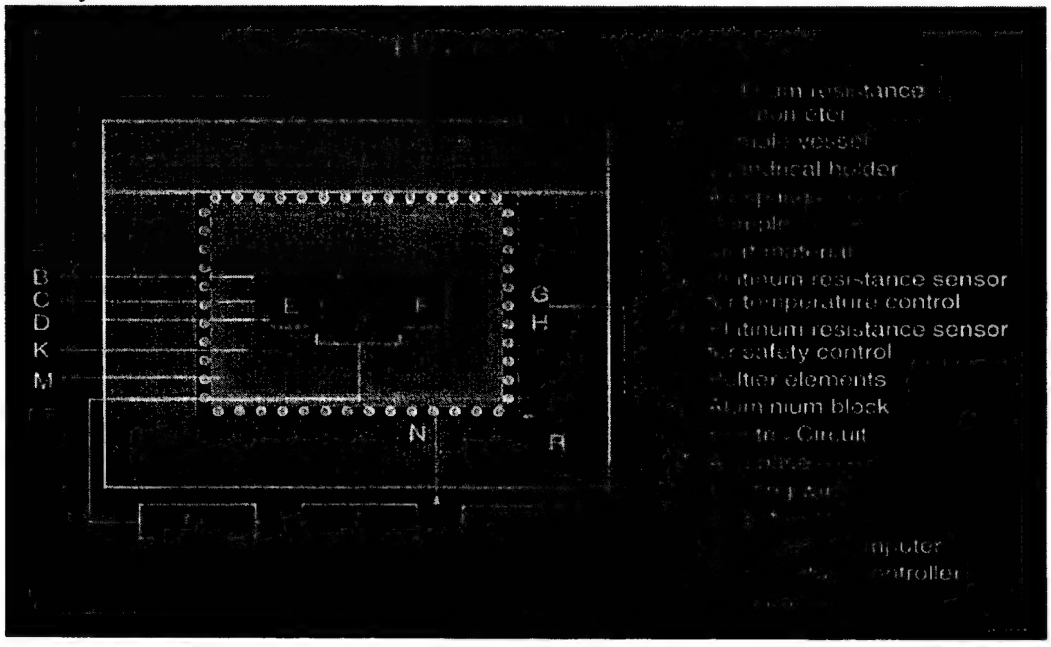

Figure 2 : Schematic design of the Isothermal Storage Test (IST)

Measurements can be performed in the temperature range 300 - 390 K, under confined or under atmospheric conditions [4]. Heat generations can be measured between the lower limit of 5 mW/kg and the upper limit of 5 W/kg with an accuracy of at least 30 % in the lower range to 5 % in the higher ranges.

For all the experiments in this project, a storage period of 168 hours at 85 °C was used, which is comparable with to natural ageing time of about 10 years at 30 °C.

Calculations

Safe diameter

The safe diameter is defined as the diameter of an infinite cylindrical container filled with propellant, for which self-ignition is excluded [1]. The safe diameter is calculated using the maximum value in the heat generation curve.

One of the NATO requirements is that propellants have to withstand temperatures up to 71 °C (344 K). This temperature has been observed in propellant cases subjected to direct sunlight. No account is taken of extreme conditions, which may occur under desert conditions [5].

According to Merzhanov [7] and Barendregt [6], the formula to calculate the safe diameter, D_{344}, is as follows;

$$D_{344} = \frac{2.7 * \lambda}{2} + \sqrt{\frac{(2.7 * \lambda)^2}{4} + \frac{4 * R T_a^2 * \delta_c * \lambda * \exp\left(\frac{E_a}{R}\left(\frac{1}{T_a} - \frac{1}{T_m}\right)\right)}{\rho_b * E_a * Q_{max}}} \qquad [m]$$

The following parameters are used [6]:

E_a	activation energy	100	[kJ/mol]
R	gasconstante	8.3144	[J/mol.K]
T_a	ambient temperature	344	[K]
T_m	measured temperature	358	[K]
δ_c	shape factor	2.00	[-] for a cylinder
λ	thermal conductivity		[W/m.K]
ρ_b	bulk density		[kg/m^3]
Q_{max}	maximum heat generation		[mW/kg]

Lambda (λ) and bulk density are determined for each KB/PH number.

Calorific value

The second quantity that can be derived from the IST-curve is the decrease in calorific value of the propellant, which is closely related to the ballistic stability of the propellant. In the literature [3] an empirical relation between the decrease in the muzzle velocity and the decrease in calorific value was reported.

An ageing period of 1.5 days at 85 °C in the IST corresponds to storage of 10 years at 20 °C (moderate climate). The decrease (delta Q) is calculated by integrating the Q vs. time curve from 4 till 36 hours.

Results / Discussion

In Table 3 a summary of the results from the IST experiments is presented. The Q_{max}-value is the maximum heat generation measured during an ageing period of 168 hours at 85 °C.

Table 3 : Results of IST experiments.

KB/PH nr.	Q_{max} [mW/kg]	D_{344} [m]	delta Q [%]		KB/PH nr.	Q_{max} [mW/kg]	D_{344} [m]	delta Q [%]
3128	65	0.61	0.16		7259	68	0.60	0.17
3388	65	0.74	0.17		7260	73	0.72	0.17
3391	70	0.64	0.17		7261	70	0.64	0.16
3687	85	0.59	0.22		7262	66	0.67	0.20
3977	71	0.56	0.16		7263	117	0.45	0.25
4767	78	0.51	0.21		7264	84	0.49	0.22
5109	79	0.49	0.14		7265	83	0.48	0.24
6384	64	0.65	0.15		7268	59	0.69	0.13
6451	116	0.45	0.25		7269	109	0.47	0.26
6479	125	0.43	0.31		7270	135	0.42	0.29
6514	141	0.39	0.43		7272	139	0.39	0.43
6832	56	0.56	0.10		7273	41	0.64	0.05
7084	139	0.39	0.38		7274	146	0.38	0.36

From this table a first global conclusion is that the differences in Q_{max} and delta Q are not significant between the propellant stored at TNO-PML and the propellant stored in munition articles at the MoD. In the following, some results are discussed in more detail.

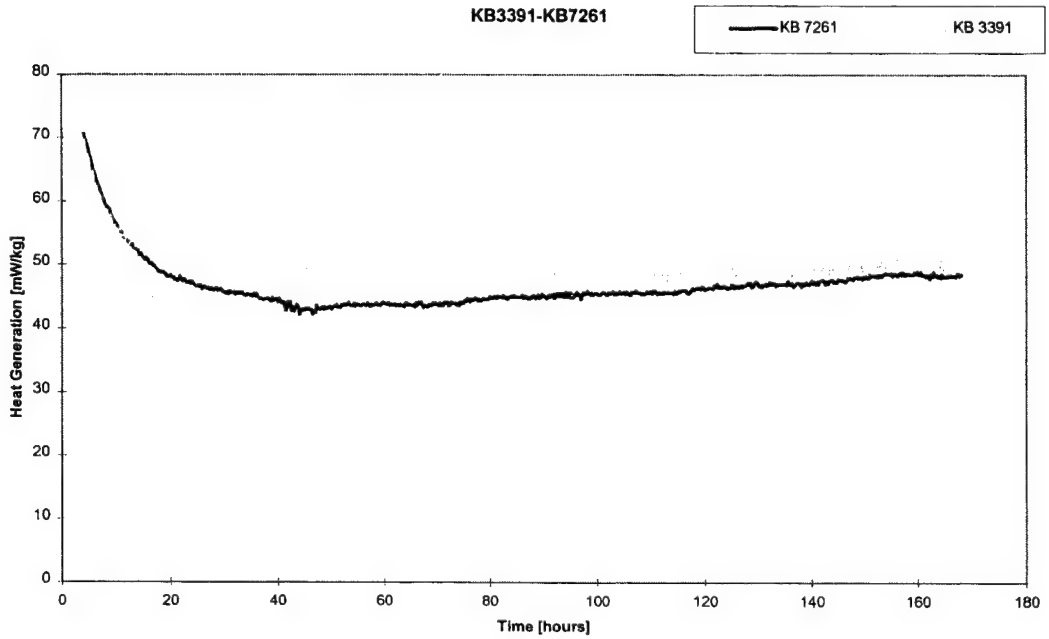

Figure 3: IST curve of propellant KB 3391 vs. KB 7261.

Let's first consider a propellant, which has been stored for 45 years in TNO magazines and the bunkers of the MoD. The IST-curve, obtained for the couple KB3391/KB7261, is graphically presented in Figure 3. The two curves have almost the same shape. So, it can be concluded, that the decomposition of the propellant is quite the same. If the decomposition (related to conversion) would be quite different, the graph would also have a different shape.

The second example, KB6479/KB7270, is presented in Figure 4 (production year 1981). There is a significant difference in magnitude but the shape of the curves is almost the same. Comparising propellant KB 7270 and the curve of KB 6479 produces over the whole measuring period about 15 mW/kg more.

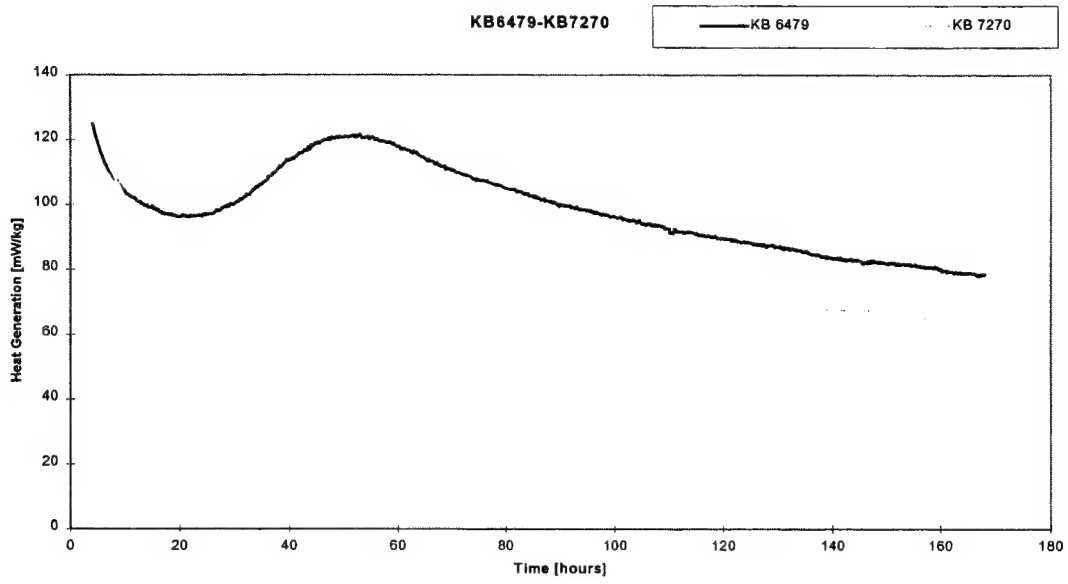

Figure 4: IST curve of propellant KB 6479 vs. KB 7270.

The difference depends on the reproducibility of the used apparatus. If the curve shows the same shape and the time to reach maximum values, is the same, the kinetic process is identical. If the period to reach the maximum, is shorter, there will be a larger conversion of the material. This results in an unstable gun-propellant. In fact the D_{344} and the decrease of the calorific value is of the same order for both propellants.

Figure 5 represents the influence of a storage period of 8 years. In fact the munition was stored under controlled conditions over the period of 8 years. The shape of the curve is the same as for the pair KB 6479/KB 7270. However the period in order to reach the maximum heat generation has shifted by about 8 hours for this propellant.
Although the difference in the maximum heat generation is being small and is within the accuracy of the equipment (~ 5 %). The shift could be due to the fact that KB 7274 has been stored at relatively lower temperature and lower humidity. The difference has almost no influence on the calculation of the safe diameter (D_{344}).

It has been observed that a higher relative humidity results in a shorter period to reach the maximum heat generation [4].

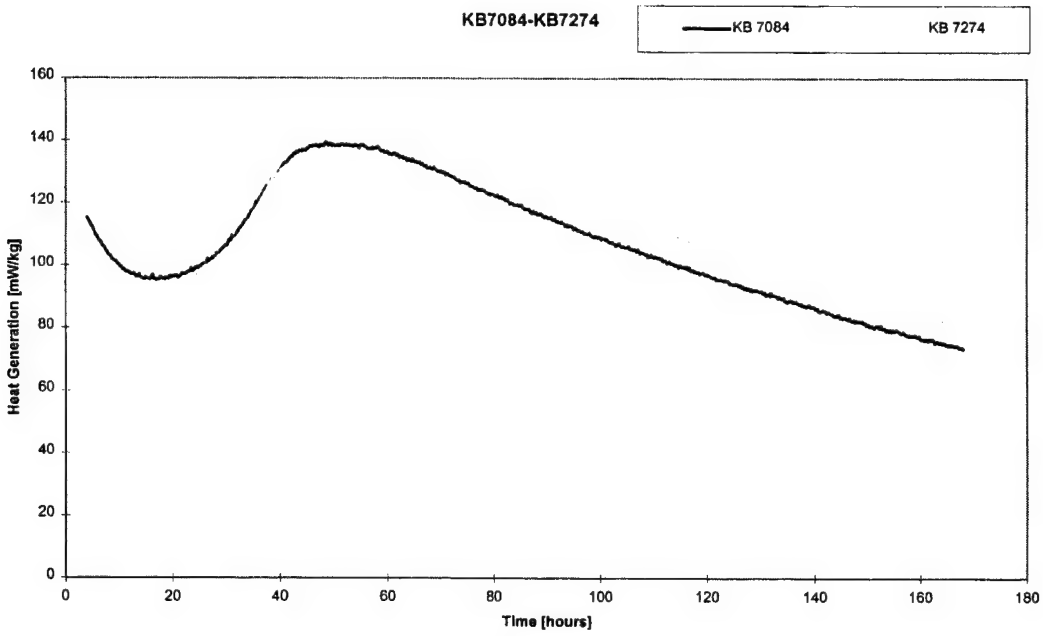

Figure 5: IST curve of propellant KB 7084 vs. KB 7274.

According to the results presented in table 3, one combination shows large differences namely KB 3977/KB 7263 as to the heat generation and the time of the maximum. In Figure 6, duplicate measurements for this propellant are presented.

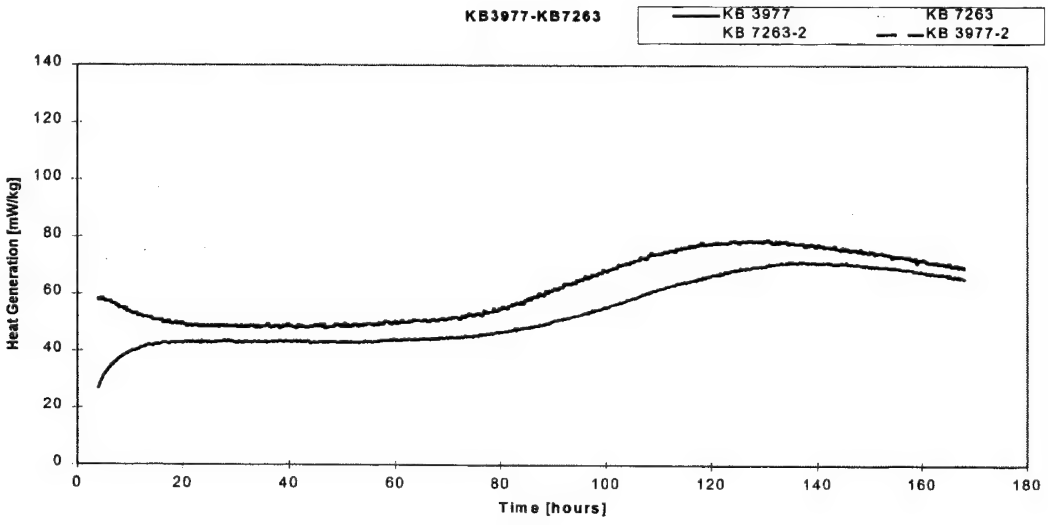

Figure 6 : IST curve of propellant KB 3977 vs. KB 7263.

However, in this case the way of storage is very important. This propellant, used in 155 mm charges, is stored in cartridge bags in metal containers. Consequently the decomposition products (nitrogen oxides) of the propellant can better diffuse. Also a reaction with the moisture might take place, forming nitric acid.
Those nitric acids act as a catalyst [4], if decomposition of the propellant continues. This might explain the higher heat generation and the shorter period for the propellants stored at the MoD.
The decomposition products can also effect the quality of the cartridge-bags. This has been observed in other investigations [9].
At this moment we are considering how to change the storage condition of 155 mm propellants for the surveillance testing.

Conclusion

According to the microcalorimetric investigations, the following remarks can be made;

- no significant influence of the different storage conditions can be measured by the used heat flow technique.
- the typical shapes from the IST-curves from the investigated samples (different storage place) do not differ significantly.
- the maximum heat generation and the calculated safe diameter are in the same order of magnitude for the articles.
- the only exception is the case with 155 mm ammunition. This munition is stored in cartridge bags.

References

[1] J.L.C. van Geel, The heat generation test for the determination of the self-ignition hazard and the ballistic stability of nitrate ester propellants, TNO-report, Rijswijk, 1971.

[2] J.L.C. van Geel, Self-ignition Hazard of Nitrate Ester Propellants, PhD thesis, Delft Technical University, 1969.

[3] H.P.J. Jongeneelen, The relation between the decrease in calorific value and in muzzle velocity, TNO-report, Rijswijk, 1971.

[4] R. Eerligh, W.P.C. de Klerk, B.J. v.d. Meer, Influence of relative humidity on ageing of propellants, 11th Symposium on Chemical Problems connected with the stability of explosives, Sweden, 1998.

[5] J.L.C. van Geel, J. Verhoeff, Heat generation measurements for the stability control of nitrate ester propellants, 4th Symposium on Chemical Problems connected with the stability of explosives, Sweden, 1976.

[6] R.B. Barendregt, Thermal investigations of unstable substances, including a comparison of different thermal analytical techniques, PhD thesis, Delft Technical University, 1981.

[7] A.G. Merzhanov, V.G. Abramov, Thermal explosion of explosives and propellants. A review, Propellants and explosives, 6, 130-148, 1981.
[8] W.P.C. de Klerk, Onderzoek naar de invloed van opslagcondities op de stabiliteitsbepaling van vuurwapenkruiten, TNO-report, Rijswijk, 1999 (in press).
[9] F.A.J.T. Kraak, Onderzoek oorzaak van het verteren van natuurzijden kardoeszakken, in aanraking met zwart buskruit, en met rookzwak buskruit, TNO-report, 1971.

Acknowledgement

The authors thanks the Dutch Ministry of Defense for financing this project, under contract number A98/KL/414.

MICROCALORIMETRY: A TECHNIQUE FOR DETERMINING PROPELLANT STABILITY.

by

R.G. Jeffrey[1], M. Elliot[1], D.J. Wood[1], P. Barnes[2] and N. Turner[2].

1. DERA WS3 Bishopton, Station Road, Bishopton, Renfrewshire, PA75NJ,UK

2. CESO (N), Block B, Ensleigh, Bath, BA1 5AB, UK

Abstract

DERA Bishopton carry out an in-service surveillance programme on behalf of Chief Environment and Safety Officer (Navy), CESO(N) to ensure that the safety and performance of Naval stores has not been compromised as a result of unusual storage conditions and /or excessive age. The techniques most commonly employed for estimation of propellant stability have been the traditional heat test methods, measurement of stabiliser depletion and more recently microcalorimetry.

The assessment of the stability of propellants using microcalorimetry indicates that heat output is strongly dependant on the microenvironment of the test material, and that careful control of the sample environment is required. To achieve this DERA have investigated a number of ways in preparing the propellant samples for test and controlling the humidity within the sample vial during the test. One specific aim was to attempt to emulate conditions (excluding temperature) that are experienced by the store under normal storage conditions.

The ageing of propellants at 80°C, the resultant degradation by such high temperature ageing and the time to autocatalytic decomposition are discussed, as well as propellants which have stability problems indicated by stabiliser loss under normal storage conditions.

1 Introduction

For many years DERA Bishopton has supported the in-service surveillance, ISS, programme of the UK Chief Environment and Safety Officer (Navy), CESO(N). The objective of this programme is to ensure that the safety and performance of Naval stores is not compromised as a result of storage conditions and /or excessive age. The primary techniques used in support of the programme have been traditional tests, such as the Abel Heat Test, and measurement of the residual stabiliser content. Use has also been made of accelerated ageing tests, such as the NATO Test (STANAG 4117)[1], and multi-temperature ageing trials. Both the latter tests and the measurement of residual stabiliser content assume the stability of propellant is related to the depletion rate of the stabiliser content. The Abel Heat Test and similar gas evolution tests monitor stability based on the evolution of gases such as oxides of nitrogen, NO_x, which are not reacted by the stabiliser. Acceptance that neither determination of residual stabiliser content or stabiliser depletion rate nor gas evolution rates necessarily measures or indicates true propellant stability has resulted in the increasing use of microcalorimetry to measure the rate of heat evolution during propellant ageing. In the UK use of microcalorimetry is still in its infancy as a tool to monitor the stability of in-service propellant and at present is used only to give added confidence and additional information as to how propellant are ageing.

Our experience to date has demonstrated that use of microcalorimetry to assess propellant stability is not straightforward and that great care needs to be taken in both the preparation of samples for analysis and the interpretation of the resultant data. In this paper we will discuss some of our key findings and conclusions. As an aid to this it is beneficial to consider the nature and range of propellants that we examine on behalf of CESO(N).

All microcalorimetry testing reported in this paper was undertaken using a four channel Thermal Activity Monitor (TAM) system from ThermoMetric Ltd. configured with Bomic software developed by Bofors, Sweden.

2 Propellant Types.

Propellants are designed to burn producing hot gas that is used to do work. The temperature of the gas and the rate at which it is generated are controlled by a combination of formulation and form. Fast burning propellants, such as those used in small arms, tend to be smaller grain and thin web whilst slower burning propellants, such as those used in rocket motors, tend to be larger grain with often a thick web. Figure 1 illustrates the range of propellant shapes and sizes examined in support of the CESO(N) ISS programme.

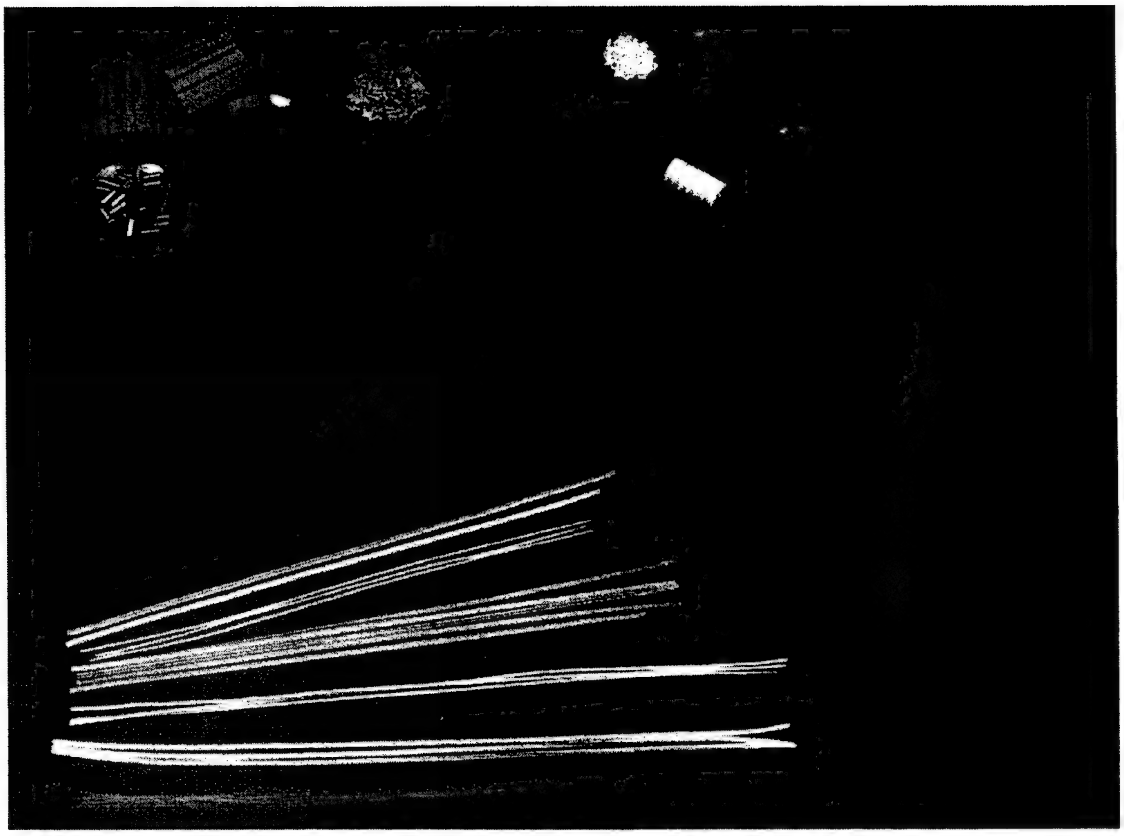

Figure 1 - Propellant Shapes and Sizes

Small arms powders are usually diphenylamine stabilised, nitrocellulose based and come in the form of ballpowders, flake and granular shapes. Preparation for testing by conventional techniques or by microcalorimetry is minimal. Samples are generally tested without any sample preparation. This allows the analyst to transfer the propellant directly from the store to the test apparatus, without changing the microenvironment within the propellant. This can be important as it is well documented that the microenvironment within the store, for example moisture content, can have a marked effect on reaction of the propellant stabiliser. Figure 2 illustrates the range of typical stabiliser degradation products found for diphenylamine.

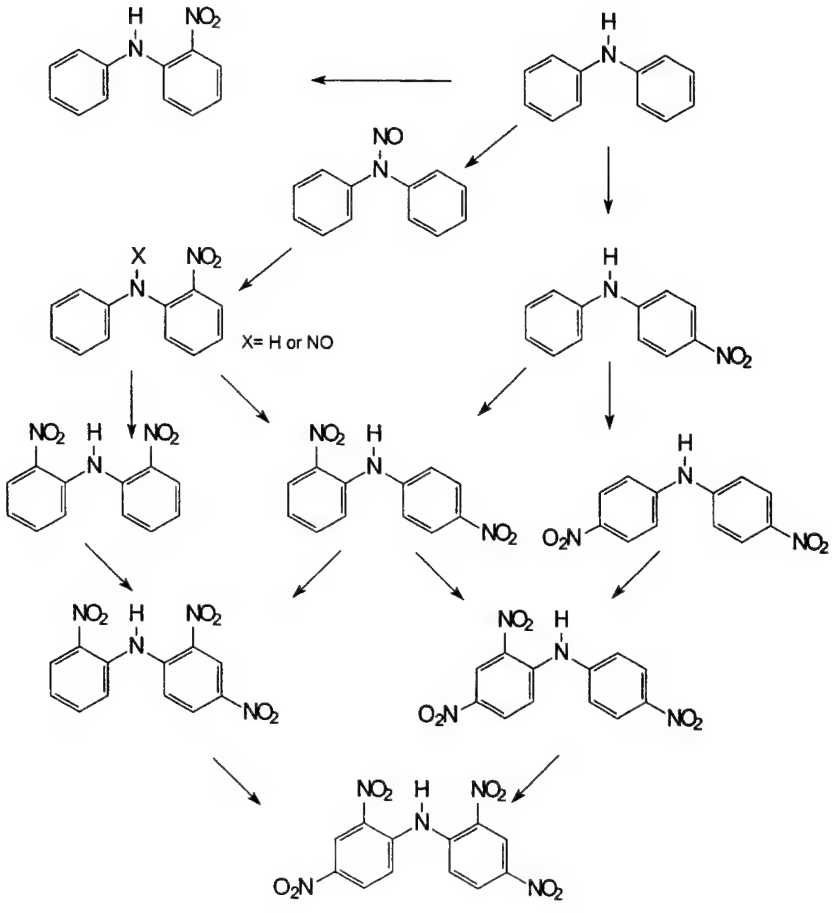

Figure 2 - Diphenylamine and its Degradation Products

The first stage of the stabiliser degradation reaction results in the production of N-nitrosodiphenylamine (N-NODPA). In UK practice this compound is considered as effective a stabiliser as diphenylamine. For sentencing purposes it is the sum of the residual diphenylamine and N-nitrosodiphenylamine content, expressed as diphenylamine, which is considered and reported as the Effective Stabiliser content. Although other degradation products can act as stabilisers they are not considered to be as effective as either diphenylamine or N-nitrosodiphenylamine and their contribution to propellant stability is ignored.

Ballpowders stabilised with diphenylamine can contain up to 15% nitroglycerine. These are generally found to fail high temperature ageing trials, such as the NATO test. This reflects the reactivity of nitroglycerine with the basic diphenylamine rather than any inherent instability of this type of ballpowder and has led to a relaxation in the test conditions for this type of propellant[2].

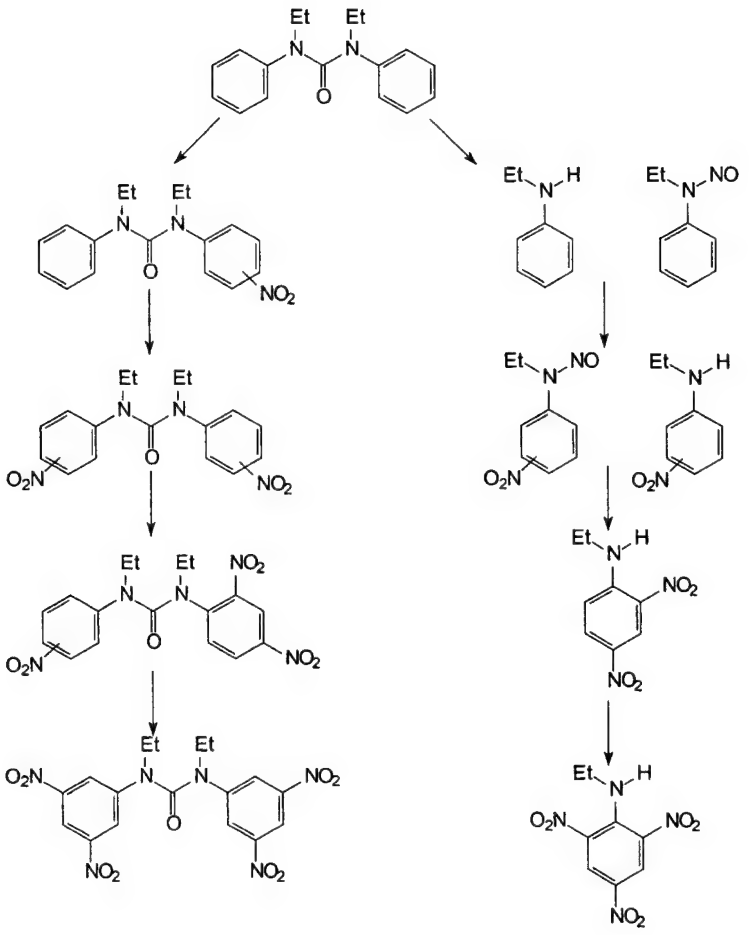

Figure 3 - Ethyl centralite and its Degradation Products

Many double and most triple and high energy propellants are stabilised with ethyl centralite. Within UK and many countries it is the stabiliser of choice for use in large calibre gun systems. Triple based propellants containing nitrocelluose, nitroglycerine and nitroguanidine can contain between approximately 1% to 7% ethyl centralite. The degradation of ethyl centralite can follow two distinct paths depending on the temperature of ageing and the concentration of the stabiliser. The typical degradation pathways for ethyl centralite are shown in figure 3. Only ethyl centralite is considered as an effective stabiliser for sentencing purposes.

Gases, produced by the breakdown of the propellant either from decomposition of the nitrate esters or, in the case of ethyl centralite, reaction

with the stabiliser, can result in cracking of large web rocket propellant motors. For this reason rocket motor propellant formulations employ more reactive stabilisers such as 2-nitrodiphenylamine (2NDPA), p-nitromethylaniline (pNMA) and resorcinol. Generally 2-nitrodiphenylamine is considered the effective stabiliser for sentencing purposes. Ageing studies indicate that there is no significant build up of N-nitroso-2NDPA, and that 2,4' dinitro-DPA is the first major degradation product. The degradation pathways are similar to those shown in figure 2 for diphenylamine.

Because of their physical size, gun and rocket propellants generally require sample pre-treatment prior to analysis. Generally this involves some form of sample size reduction process so as to ensure the portion of the sample selected for testing is representative of the bulk. The most common form of sample pre-treatment involves grinding or milling the propellant to produce a course powder form that can be blended and is suitable for chemical analysis by extraction techniques. The process of size reduction and grinding not only puts work into the propellant inducing localised heating and possible degradation but more importantly it allows release of trapped species, reintroduction of moisture air to the matrix of the propellant and fundamentally changes the microenvironment of the test material. This has major implications for any subsequent stability or ageing testing.

3 Types of Test Apparatus and Validation of Sample Size Reduction

TEST	Weight of Sample per Test(g)
Abel Heat Test	1.6
NATO test	20
Silver Vessel	70-80
Microcalorimetery	1-3

Table 1 – Sample size requirement for various ageing tests

Table 1 shows the range of sample sizes used in typical ageing tests. As can be seen microcalorimetry potentially uses the smallest sample size. This has advantages from a safety point of view but it must be demonstrated, so as to allow direct comparison, that the small sample size will not result in different ageing behaviour from that which would occur in ageing tests using larger propellant weights. It can also be argued that, particularly in the case of the small arms propellants, if the sample size is reduced an unrepresentative sample could be obtained resulting in a reduction in confidence of any result

obtained. Because of the cost of preparing sufficient sample for test, a programme of work was initiated to establish the effect of reducing the weight, and hence volume, of propellant used in testing of small arms propellant.

In UK, the NATO test is used to assign either a 5 or 10 year life extension to small arms propellants. In the case of standard 5.56mm calibre rounds, a nominal 60 rounds are require to be broken down to prepare sufficient sample, 20g, for a single analysis. As analysis is usually conducted in duplicate with duplicate determination, over 60 day and 120 day periods at 65.5°C, and analysis of the as received sample for initial stabiliser content a minimum of 82g of propellant is required per sample. The advantages of reducing the sample size for ageing by a factor 10 to 2g and for each analysis are therefore immediately obvious.

It can be argued that the dimensions of ageing vessels will effect the average temperature experienced by a sample and hence are of vital importance during accelerated ageing. The initial objective of the miniaturisation program for the NATO test was therefore to design and evaluate new ageing apparatus.

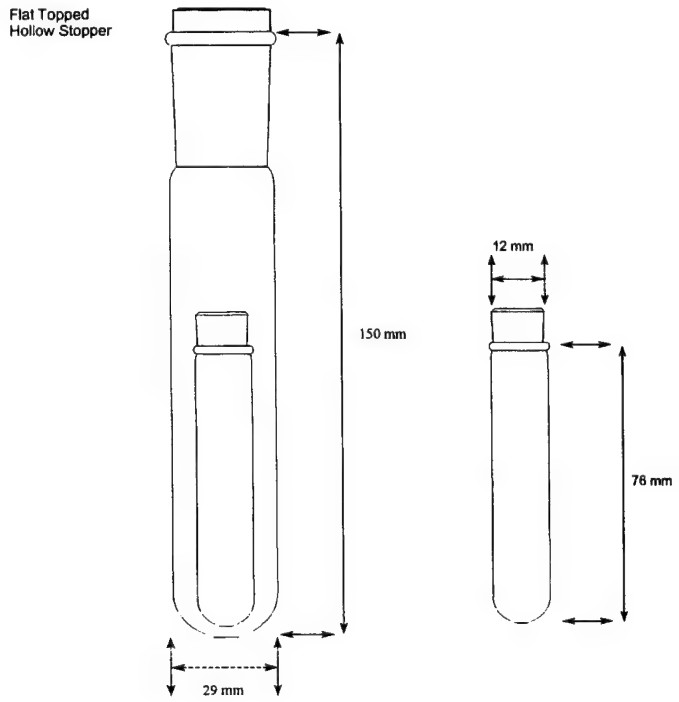

Figure 4 - Standard and Reduced Size NATO Tubes

Reducing the sample size by 10% to 2g will require a sample tube of approximately 10% the volume of a standard NATO tube (29mm x150mm). So as to minimise change it was decided to use tubes that maintained the

ratio of dimensions of the original NATO tube. Figure 4 shows the dimensions of the standard and reduced size tube used in the test. To allow use of existing block baths, the smaller tubes were inserted into a standard NATO Test tube with the void space between the tubes filled with either fine glass beads or sand. Experiment demonstrated that using this arrangement a uniform and constant temperature was obtained within the contents of the inner tube. Representative propellant samples were then subject to ageing in accordance with the standard NATO test conditions and time periods in both standard and reduced volume tubes. Results are summarised for the propellants studied in Tables 2 – 6.

Preparation details in all cases are:

(a) Standard NATO Test (20g ageing, 1g in 20cm^3 dichloromethane extraction).

(b) 0.5g extraction in 10cm^3 of dichloromethane

(c) 0.2g extraction in 4cm^3 of dichloromethane

Prep.	*As Received*	*60 Day NATO*	*60 Day Micro*	*% Stabiliser Drop(NATO)*	*% Stabiliser Drop(Micro)*
(a)1	0.85, 0.86	0.65, 0.65	-	24	-
(a)2	0.85, 0.85	0.65, 0.64	-	24	-
(b)1	0.90, 0.90	0.65, 0.64	0.64, 0.65	28	28
(b)2	0.90, 0.90	0.63, 0.63	0.62, 0.62	30	31
(c)1	0.89, 0.89	0.61, 0.61	0.64, 0.64	31	28
(c)2	0.89, 0.89	0.61, 0.62	0.64, 0.64	31	28

Table 2 - % Ethyl centralite in Powder 1, as received, 60 day NATO, and 60 day micro.

Prep.	*As Received*	*60 Day NATO*	*60 Day Micro*	*% Stabiliser Drop(NATO)*	*% Stabiliser Drop(Micro)*
(a)1	0.85, 0.85	0.61, 0.62	-	28	-
(a)2	0.84, 0.84	0.64, 0.64	-	24	-
(b)1	0.91, 0.91	0.63, 0.63	0.64, 0.64	31	30
(b)2	0.92, 0.91	0.63, 0.62	0.64, 0.65	32	30
(c)1	0.83, 0.83	0.59, 0.59	0.59, 0.59	29	29
(c)2	0.84, 0.84	0.59, 0.59	0.59, 0.60	30	29

Table 3 - % Ethyl centralite in Powder 2, as received, 60 day NATO, and 60 day micro.

Prep.	*As Received*	*60 Day NATO*	*60 Day Micro*	*% Stabiliser Drop(NATO)*	*% Stabiliser Drop(Micro)*
(a)1	1.04	0.80	-	23	-
(a)2	1.05	0.80	-	23	-
(b)1	1.04	0.81	0.77	22	26
(b)2	1.05	0.80	0.82	24	22
(c)1	1.05	0.79	0.81	25	23
(c)2	1.08	0.80	0.83	26	23

Table 4 - % Effective Stabiliser in Powder 3, as received, 60 day NATO, and 60 day micro.

Prep.	*As Received*	*60 Day NATO*	*60 Day Micro*	*% Stabiliser Drop(NATO)*	*% Stabiliser Drop(Micro)*
(a)1	0.92	0.40	-	57	-
(a)2	0.92	0.40	-	57	-
(b)1	0.92	0.32	0.28	67	70
(b)2	0.92	0.33	0.34	64	63
(c)1	0.95	0.31	0.33	67	65
(c)2	0.92	0.31	0.32	66	65

Table 5 - % Effective Stabiliser in Powder 4, as received, 60 day NATO, and 60 day micro.

Prep.	*As Received*	*60 Day NATO*	*60 Day Micro*	*% Stabiliser Drop(NATO)*	*% Stabiliser Drop(Micro)*
(a)1	1.75, 1.76	0.99, 0.99	-	44	-
(a)2	1.75, 1.74	1.00, 1.00	-	43	-
(b)1	1.73, 1.74	0.97, 0.97	0.98, 0.98	44	44
(b)2	1.74, 1.74	0.94, 0.96	1.02, 1.02	45	41
(c)1	1.72, 1.72	0.98, 0.97	1.03, 1.03	43	40
(c)2	1.71, 1.71	0.96, 0.97	1.06, 1.06	44	38

Table 6 - % Ethyl centralite in Powder 5, as received, 60 day NATO, and 60 day micro

Although there is some variation in the value of % stabiliser drop between tests the variation between standard and reduced volume, micro, tubes is not considered statistically significant. It therefore appears that in this case it is possible to reduce the size and volume of sample used for ageing purposes by a factor of 10 without compromising the result of any ageing study. This result would tend to suggest that it is possible to critically compare results obtained using smaller sample weights by microcalorimetry techniques with those obtained using standard tests.

A more stringent test of the reduced sample weight and volume is comparison of the time to autocatalytic breakdown of a propellant sample as measured in the microcalorimeter and the Silver Vessel. Figure 5 illustrates the difference in size and shape of the aged propellant bed contained in a Silver Vessel and a microcalorimeter tube. Again so as to allow use of existing block heating baths, microcalorimeter vials were contained in standard NATO Test tubes for ageing.

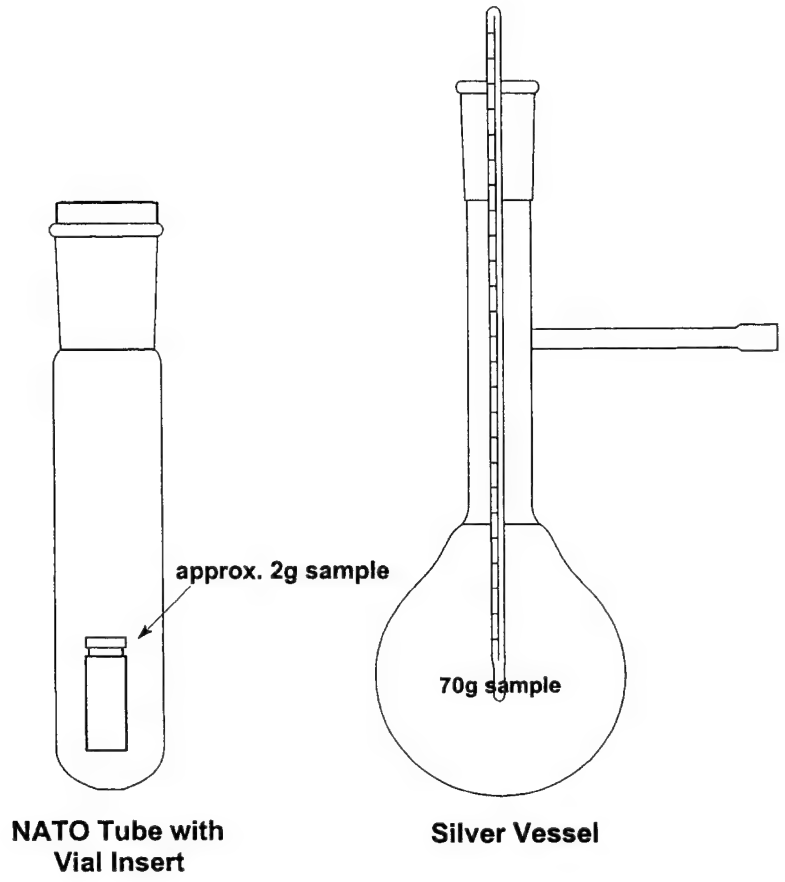

Figure 5 – Comparison of Shape and Size of Propellant Bed during Silver Vessel and Microcalorimetry Testing.

A reference propellant that had been well characterised by Silver Vessel tests and found to show onset of autocatalytic breakdown after approximately 40±2 days at 80°C was used for this test. The results for microcalorimetry are shown in figure 6.

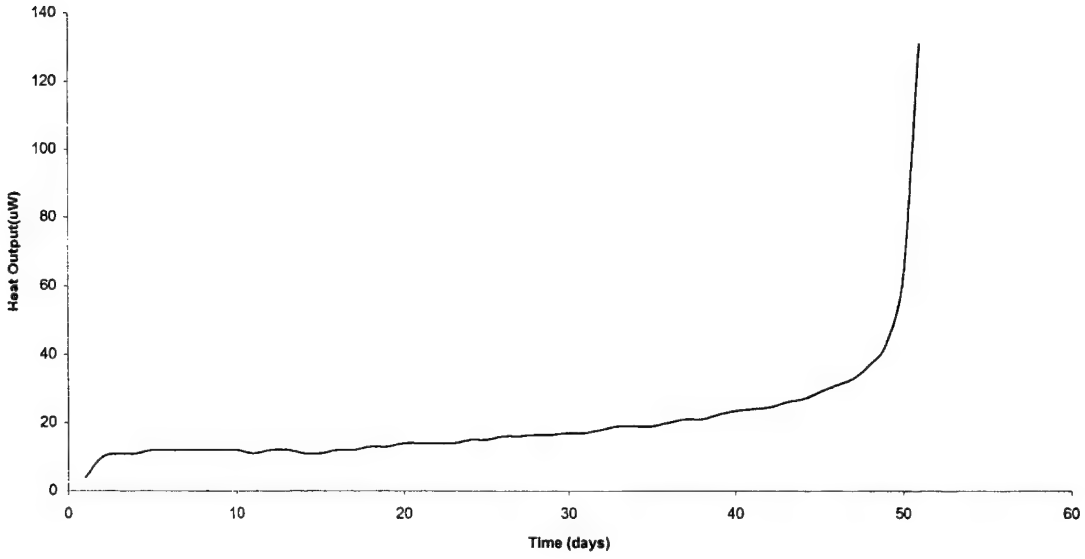

Figure 6 - Heat flow for the Silver Vessel Standard Propellant at 80°C

As can be seen the results for microcalorimetry indicate autocatalytic breakdown occurs after 50 days. This is significantly later than that determined by Silver Vessel testing. We believe this is due to the greater depth of the propellant bulk in the Silver Vessel test, compared to that in the microcalorimeter vial, resulting in different microclimates within the two propellant test beds. This is at odds with the findings for the reduced size NATO Test and shows that sample weight and volume can be critical. Any decision on sample size reduction for ageing tests must therefore be validated on a case by case basis.

Stabiliser consumption trials carried out concurrently with this work indicated that after 15 days at 80°C there is very little 2NDPA remaining. This is interesting as microcalorimetry shows the propellant is still stable after this time suggesting that initial stabiliser degradation products continue to act as effective stabilisers.

Analysis of the samples after removal from the microcalorimeter after 50 days heating showed that at the point of autocatalytic decomposition there was no detectable 2NDPA, N-NO-2NDPA or 2,4' DNDPA present in the material.

4 The Effect of Sample Grain Size

Of greater importance to the assessment of stability is the concern that sample preparation changes the nature of the propellant and so results in a different ageing assessment compared to that which occurs in the original propellant grain. This is of critical importance for the assessment of rocket propellant where propellant web is often large with potentially significant differences in the microenvironment between outer and inner parts of the grain. To establish the criticality of this the stability of a solid block and ground sample of a double based rocket motor stabilised with 2NDPA was determined by stabiliser depletion measurements and microcalorimetery.

Six NATO tubes were prepared for ageing at 80°C. Three tubes contained ground propellant and three contained a single solid block of propellant, which had been machined to fit into the NATO Test tube. Prior to undertaking the work it was demonstrated, using thermocouples placed into the solid block sample, that the time to reach 80°C throughout the test piece was only two hours. It was therefore considered that the different times to reach equilibrium between solid block and ground samples should have little effect on the overall test time or test result. Test results are shown in Table 7.

days @ 80°C	Block sample %2NDPA	Chopped sample %2NDPA
0	1.78	1.78
6	0.72	0.91
10	0.30	0.35
15	0.06	0.14

Table 7 - Effect of Grain Size on Stabiliser Depletion

As can be seen, results from the stabiliser depletion tests indicate that there is a difference for the solid and chopped samples with the block sample showing a higher rate of stabiliser loss.

Analysis by HPLC showed that during the ageing process 2NDPA degradation products were being formed and were increasing in concentration as the

propellant degraded. During the time scale of this study the main stabiliser depletion product was identified as 2,4'-dinitrodiphenylamine.

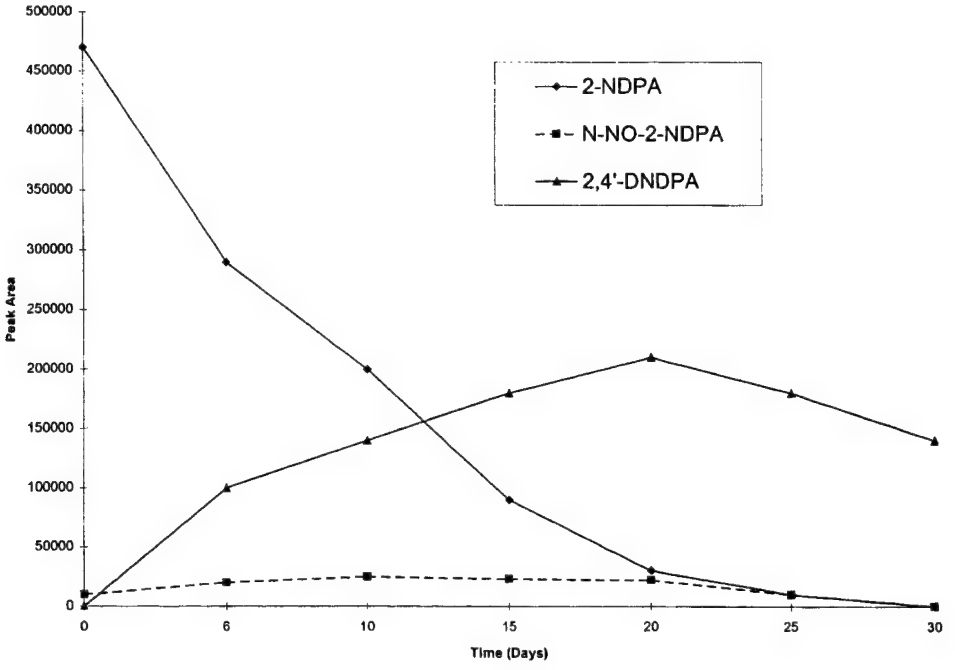

Figure 7 -2-NDPA Loss and build up of Degradation Products in Ground Propellant Sample

Figure 7 shows the concentration of 2,4'-dinitrodiphenylamine increases as the concentration of 2NDPA decreases. It also shows that the concentration of labile N-nitroso-2-nitrodiphenylamine (N-NO-2NDPA), considered to be the initial reaction product, does not increase to any great extent, most likely reflecting both its instability and reactivity. However it should also be noted that the stabiliser 2NDPA could reacted directly to give 2,4'-dinitrodiphenylamine without passage through N-NO-2NDPA as an intermediate.

The experiment was duplicated but using microcalorimetry. To keep the sample conditions similar to those used for the stabiliser consumption trial, a 1 gram solid block and a 1 gram ground sample were placed in vials and conditioned at 20°C and 50% relative humidity overnight. The sample vials

were then placed in the calorimeter at 80°C and their heat output measured by microcalorimetry.

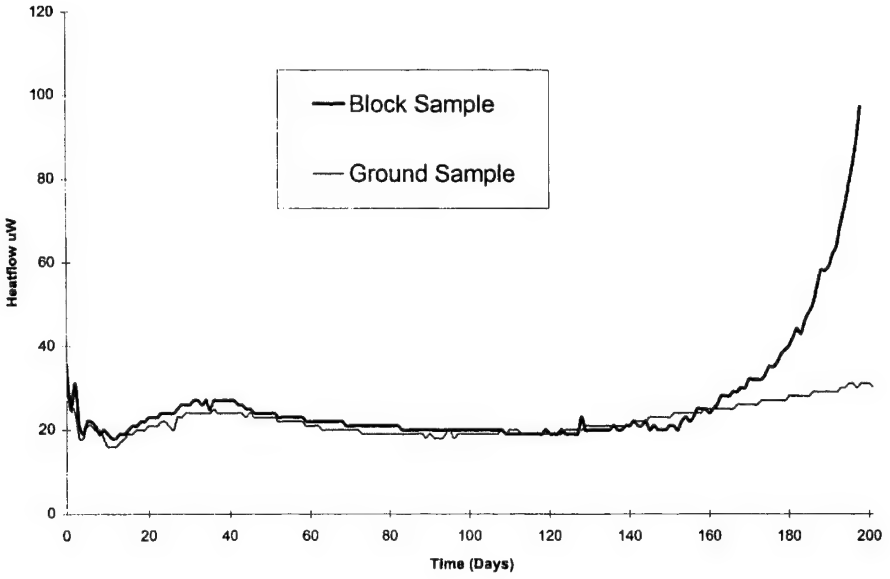

Figure 8 – Microcalorimetry of Ground and Block Propellant Samples

The results, figure 8, show a substantial drop in heat output during the first 15 days for all samples. This drop in heat output coincides with the depletion of 2NDPA. There is then a slight rise in output which eventually levels off to give a relatively steady output of 20μW. This relative stability, once all the primary stabiliser is consumed, we believe, demonstrates that the 2NDPA stabiliser degradation products are contributing to the stability of the propellant.

It is however more interesting to note that the solid block samples appear to undergo autocatalytic breakdown before the ground samples even though there was no overall difference in heat output prior to this stage. This result is in line with the findings for stabiliser depletion which showed that stabiliser depletion occurred at a higher rate in the solid block sample. We presume this result reflects the ease with which products of decomposition can be lost to the atmosphere within the vial from the finer grains of the chopped sample. In the solid block it is assumed that these breakdown products are retained in the bulk for longer giving rise to acceleration of the degradation process. This finding has significant implications for ageing studies of any large web propellant as it implies that assessment of ageing characteristics using

prepared or ground sample will always give an over optimistic assessment of stability.

5 The Effect and Control of Humidity in the Sample Vial.

Previous experiment had demonstrated that original humidity could have a marked effect on the heat output from propellant as measured by microcalorimetry. It had been shown that the heat output increased substantially with increasing humidity. It was therefore concluded that it was critical to control the humidity of samples either prior to or during testing.

Recent advances in technology have made it possible to control the intimate environment in the sample vial of the microcalorimeter by using a Flow through Cell. This should allow investigation of the effect of the atmospheric aspect of the microenvironment on propellant degradation.

A programme of work was undertaken, using a standard Thermometric Thermal Activity Monitor and one fitted with a flow through cell, to study the effect of atmosphere on heat output from single base, double base and high energy propellant samples, which had been artificially aged at a variety of temperatures in a stabiliser consumption trial.

It was initially planned that each type of propellant would be conditioned at three humidities and heated in the microcalorimeter at three different temperatures. One set of experiments would use the flow through cell to control humidity in the sample vial. The other would use small tubes containing saturated aqueous salt solutions insert into the sample vials as a means of controlling the humidity. To accommodate the volume of the small tube the sample weight for all tests was reduced to 0.5g. Tests were conducted at 60°C, 70°C and 80°C. Humidity was controlled in both cases using for 20% RH - KF, 30% RH - $MgCl_2$ and 50% RH - NaBr.

It was found that at 80°C the flow through cell could not control the humidity. As the propellant had already been aged and the objective was to measure the effect of atmosphere on heat output it was decided to attempt to conduct the test at lower temperatures. However at lower temperatures the heat output is lower and, coupled with the reduced sensitivity of the flow through cell arrangement, it was not possible to obtain meaningful data at lower temperatures. Use of the flow through cell for this study was, as a result, abandoned.

In work using the tubes inserted into the sample vials it was noted that after a few days the saturated aqueous salt solutions in the tubes changed colour from clear to deep orange in those vials containing the double and high energy propellant. This process did not occur for the single based propellant, which although they gave a positive heat output, showed no clear relationship

between heat output and humidity. Overall the data was poor and showed a marked lack of reproducibility with respect to heat output from all the propellants studied. For double and high energy propellants the results showed negative heat outputs with a suggestion that the lower heat output was associated with the higher humidity. These factors would suggest that considerable interaction has occurred between the humidity solutions and the propellant.

An essential pre-requisite of any humidity control technique, particularly for microcalorimetry, is that it is inert towards the propellant and any species resulting from the degradation of the propellant formulation. Clearly this is not the case when saturated salt solutions are used to control humidity within the sample vial. Therefore an alternative humidity control method was sought. Swedish Defence Method No. 120 utilises aqueous glycerol solutions to control sample humidity for the microcalorimeter analysis of propellant and explosive compositions. Use of such solutions was tried. However discoloration of the water/glycerol solutions in the tubes again occurred for both the double base (a yellow colour) and the high energy propellant (a brown colour) samples, indicating interaction between the solutions and the propellant. At the temperatures required to obtain measurable heat output, it is therefore evident that control of the humidity within the sample vial for double base and high energy propellant is not trivial. Perhaps the only viable solution is to precondition the sample prior to testing in the microcalorimeter. This does not however allow true measurement of the effect of sample atmosphere on heat output.

6 Conclusion.

It has been demonstrated that sample size and form can have a marked effect on the results of ageing tests.

It has been shown by microcalorimetry and ageing in NATO Test tubes that block and ground propellant samples, of the same nominal mass and shape, age at different rates. It is concluded that results obtained for ground samples are therefore likely to give an overly optimistic assessment of safe life as compared to that which will occur in the actual propellant grain. This effect will be more marked for larger web propellant, such as those used in rocket charges. The effect, we believe, is an intrinsic property of the propellant ageing process and not just a manifestation of the release of trapped species or additional work done on the propellant during the sample preparation and grinding process.

It has been shown that, for ground sample, the size of the propellant bed can also have a marked effect on ageing behaviour. The data here is, however, less conclusive. It has been demonstrated that reducing the sample size from 20 to 2 grams whilst maintaining the overall ratio of dimensions of the NATO

Test tube, has no significant effect on stabiliser depletion within the timescale and ageing environment of the NATO Test. However it has also been shown that monitoring the onset of autocatalytic breakdown using microcalorimetry, as opposed to Silver Vessel Testing, can increase the time to breakdown by 25%. These results imply that great care is needed when interpreting the results of any reduced scale testing particularly when comparing the results with those obtained or expected from a bulk test. They also show that it is necessary to demonstrate that any reduced scale testing gives comparable results to bulk testing or, at the very least, characterise and validate any bias that may occur.

Less success has been achieved with the experiments to characterise the effect of humidity on propellant ageing within the microcalorimeter. It has been found that the flow through cell arrangement on the Thermometric TAM is not capable of controlling sample environment at the temperatures necessary to obtain a meaningful signal. The alternative approach to the control of sample environment within the microcalorimeter vial, inclusion of tubes containing saturated salt solutions or glycerol/ water mixtures, has led to mixed results and is demonstrated as not suitable for double or triple based or high energy propellants. Although apparently capable of being used with single based propellants no clear relationship was evident in the limited work undertaken. It was concluded that the perhaps the only viable solution is to precondition the sample prior to testing in the microcalorimeter.

7 References.

1. Draft STANAG 4117 Explosives, stability testing procedures and requirements for propellants stabilised with diphenylamine, ethyl centralite or mixtures of both.

2. Draft STANAG 4541 Explosives, nitrocellulose based propellants containing nitroglycerine and stabilised with diphenylamine, stability test procedures and requirements.

THE APPLICATION OF MICROCALORIMETRY FOR OBTAINING THE CORRECT HEAT GENERATION RATES FOR PREDICTING THERMAL RUNAWAY IN NITROCELLULOSE BASED PROPELLANTS

Daniel S. Ellison and Anton Chin
Test & Evaluation Department
Ordnance Engineering Directorate
Crane Division, Naval Surface Warfare Center
Crane, Indiana 47522-5001 USA

NSWC Crane has been evaluating single and double based propellants since 1990 and has noticed that the early part of the heat flow curve always shows a sharp exothermic peak followed by a exponential decay which eventually starts to rise again. This seems to be an overshoot and relaxation process as the propellant reaches the test temperature.

It is known that the stabilizers are actively removing oxides of nitrogen which would account for reduced heat flow until all the primary stabilizers are gone. After which the heat rate begins to rise, as the secondary stabilizers react but not as effectively.

It is the purpose of this paper to provide data that the observed affect of initial decay in heat rate and rise may be in part related to the heat loss of the calorimeter measuring system. Data from measuring heat release as function of mass is examined. Calibration of calorimeters is considered in relation to the size of the calorimeter. Data from the TAM Thermal Activity Monitor, model 2777, using the 4 cc measuring cell and the 20 cc measuring cell is compared. Heat loss for these measuring cells are compared as to whether the data at the same isothermal temperature provide equivalent results.

INTRODUCTION

Predicting the possibility of thermal runaway depends using the correct Activation Energy parameters in the Arrhenius equation. Kinetic parameters always obtained from plotting heat flow as a function of time in an isothermal experiment. It is assumed that the temperature for data analysis is the isothermal bath temperature. If the sample is held isothermal then all the heat coming from the sample would be removed and none would be allowed to be stored in the sample. The net result would be zero and the measuring sensor (whether it was a peltier, thermocouple or other similar sensor) would report no heat flow. But it this is never the case! As the propellant ages the rate of heat release increases. In the calorimeter, the test sample is isolated from the bath by the design of the measuring system. In figure 1 we see the inside of the TAM calorimeter measuring system.

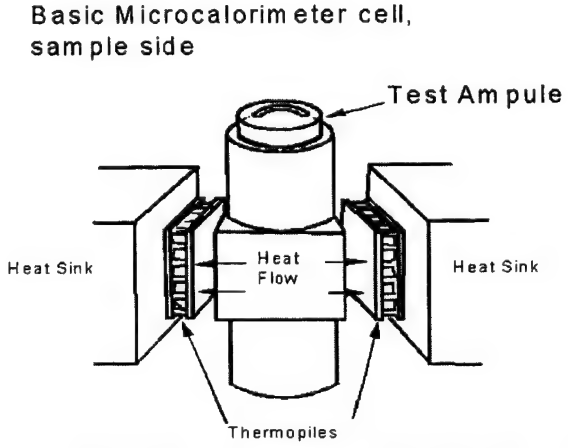

Figure 1. Heat Flow in TAM 4 cc measuring cell

The TAM, Model 2277, 4cc calorimeter is more complicated than it appears in Figure 1. A more detailed view of the calorimeter is shown in Figure 2. We see that the sample cell floats within the walls of a larger aluminum heat sink. The cell is thermally connected to this heat sink by the peltiers. The most direct path of heat loss from the sample is through the two peltier measuring sensors. From the cold side of the peltier the heat loss becomes dependent upon the thermal conductivity of the aluminum block and its steel cylinder cover (which isolates the aluminum cylinder from the water bath).

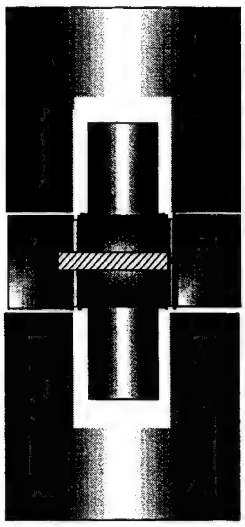

Figure 2. Closer view of TAM measuring Cell

From the point of view of the peltier thermopiles the sample container is on the hot side of the peltier, the isothermal environment is on the cold side of the Peltier. The industrial application of the Peltier utilizes this effect to provide cooling of the hot side by applying a DC voltage to the Peltier which pumps the heat from the hot side to the cold side. In a microcalorimeter, there is no applied DC voltage and the Peltier converts the difference of heat between the hot and cold side of the Peltier to a voltage signal which is measured as μwatts of power. In our case the sample chamber is warmer than the bath. The only heat loss to the environment is a function of radiant and/or conductive through the Peltier and the aluminum sample block. What does all this mean as far as obtaining kinetic data? **Why should the heat loss to the environment important?** After all the calorimeter was calibrated with a known power source using a calibration resistor and a constant current source. This should automatically correct the signal for this heat loss and give the right answer at any temperature.

My answer is that the calibration gives a result that is only true for an essentially infinite power source. The calibration fails when the source of the power from a chemical reaction. Energetic chemical reactions, which are usually encountered, are of two types: figure 3 where the reaction reaches its peak almost immediately, and figure 4 in which the reaction forms a "S" shape curve with the maximum at its inflection point. The heat output for these reactions are normalized as μwatts/gram when derived from microcalorimeters.

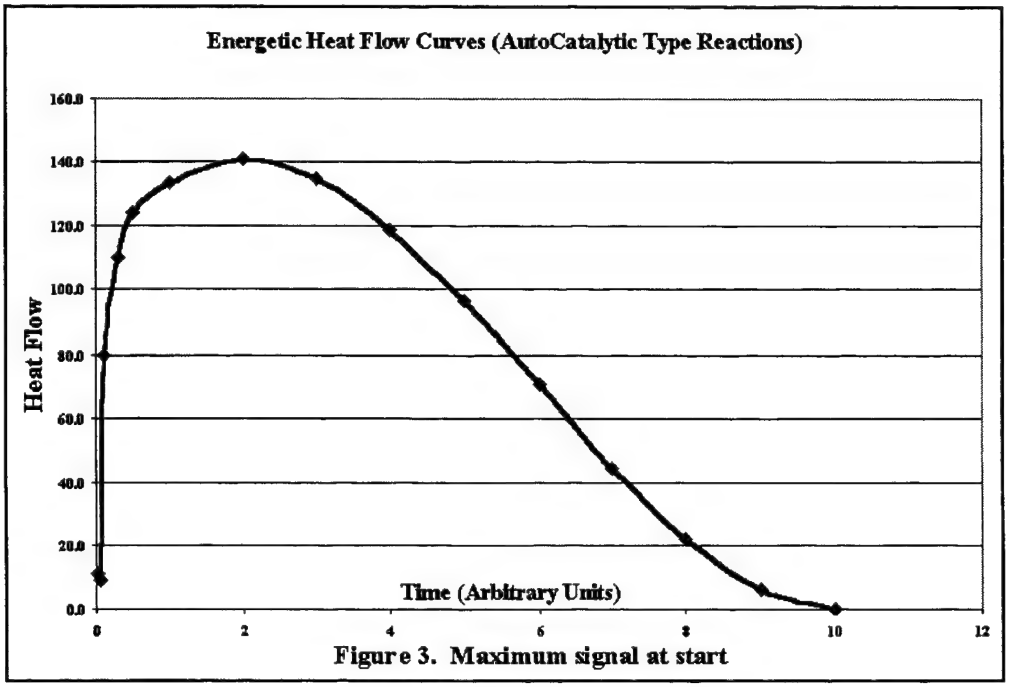

Figure 3. Maximum signal at start

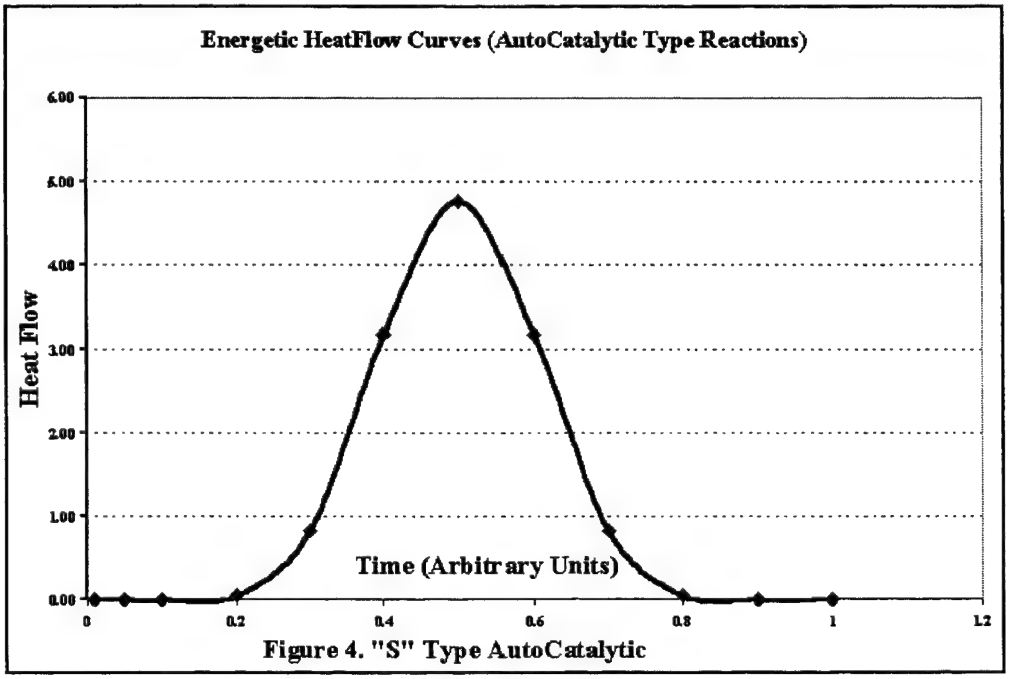

Figure 4. "S" Type AutoCatalytic

The heat flow that is shown in these curves (figures 3 and 4) is not totally representative of the thermal decomposition reaction. It must always be recognized that the energy from a decomposition reaction is a function of temperature of its environment. The higher the temperature the faster the rate. This statement may seem obvious to anyone experienced in thermal kinetics, but what is not so obvious is the fact that thermal decomposition rate for a sample is dependent on its **"control volume"**. The control volume is expressed in simple terms by the principle of conservation of energy, which controls the temperature of reaction:

[The rate at which energy of all forms enters the control volume]

+ [The rate at which energy is generated within the control volume itself]

= [The rate at which energy of all forms leaves the control volume]

+[The time rate of change of energy stored within the control volume] **[1]**

Or more generally presented as:

Rate (input) + Rate (generated) = Rate (out) + Rate (stored) **[2]**

The sample's net temperature is driving the decomposition reaction. The heat flow is accounted as follows:

(1) the bath temperature (65.5°C) (input)
(2) heat generated by the propellant, (generated)
(3) minus the amount of heat loss to the environment (out)
(4) the heat retained within the sample (stored)

Figure 5 is a plot of sample size for one and four grams. What you are observing is the differences in heat flow due to the amount of the sample in the 4 cc TAM measuring cell. A one-gram sample can not generate enough heat to overcome the heat loss due to the environment. The result is a drop in heat flow. When the size is increased to four grams, the maximum amount of this sample that could be placed in a TAM 4-cc stainless steel ampoule, the heat is enough to give the characteristic curve for an exothermic curve. But this mass is still not large enough to cause the sample to runaway.

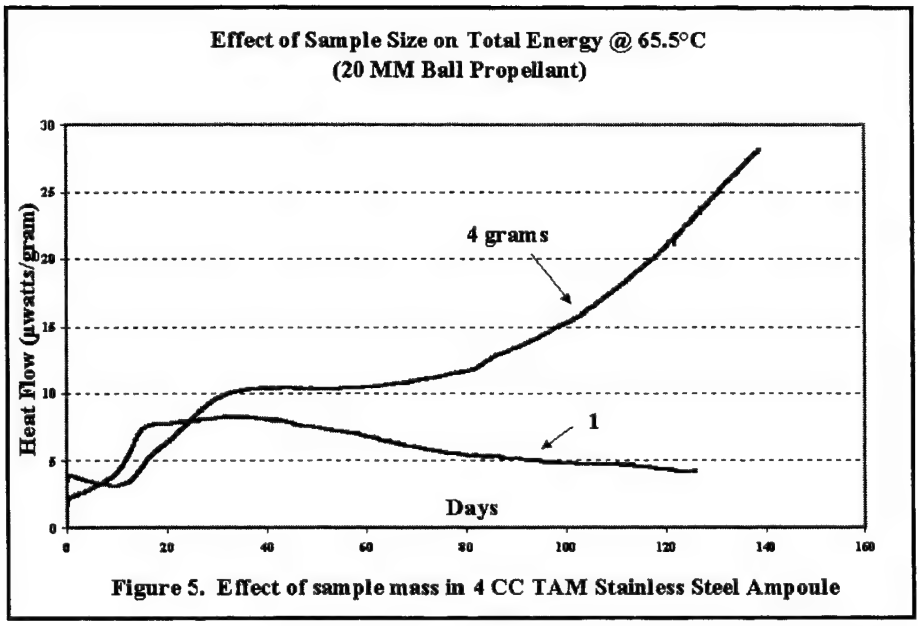

Figure 5. Effect of sample mass in 4 CC TAM Stainless Steel Ampoule

Does this effect extend to a larger calorimeter cell?

The Thermometric Model 2230, 20 cc internal volume, is shown in figure 6 based upon drawings provided with the manufacture's literature. The internal design of this larger cell is different from the 4 cc TAM measuring cell. The sample and reference sides of the cell each have four large peltier's. There is also more aluminum in the heat sink in the larger 20 cc measuring cell than the 4 cc measuring cell. This results in a faster responding cell for its size than the smaller 4 cc cell. The cell is calibrated in the same manner as the 4 cc measuring cell.

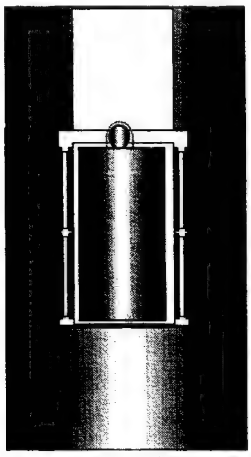
Figure 6. Larger 20 cc TAM measuring cell

Figure 7 shows the result of running two double base propellant samples at 65.5°C in the 4 cc and the 20 cc measuring cell. The large cell contains 15 gram of doublebase propellant. The small 4cc measuring cell contains 2.15 grams of the same propellant.

What becomes immediately obvious is the lack of self-heating due to the larger sample in the 20 cc cell which was observed with the 20 mm ball propellant. This may be the first indication that the 20 cc cell has a significantly larger heat loss than the 4 cc cell. The data at this point is preliminary and more work is planned to examine if this is due to the propellant or the measuring cell.

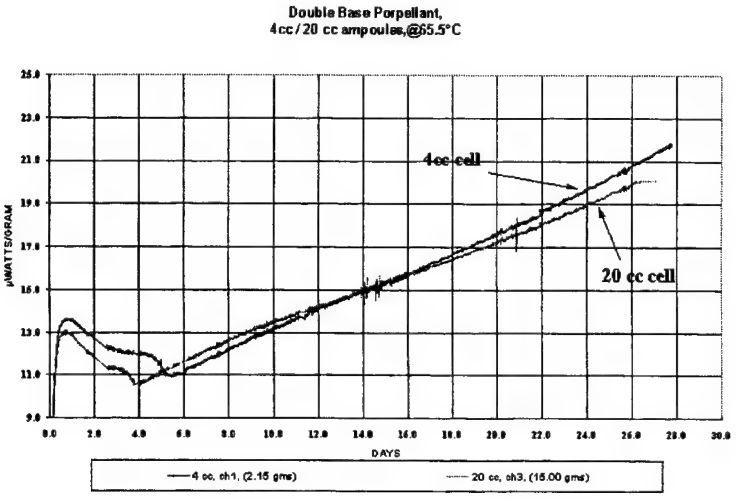

Figure 7. Comparing 4 cc and 20 cc measuring cells

CONCLUSIONS

NSWC Crane has been evaluating single and double based propellants since 1990 and has noticed that the early part of the heat flow curve always shows a sharp exothermic peak followed by a exponential decay which eventually starts to rise again. This seems to be an overshoot and relaxation process as the propellant reaches the test temperature.

It is known that the stabilizers are actively removing oxides of nitrogen which would account for reduced heat flow until all the primary stabilizers are gone. After which the heat rate begins to rise, as the secondary stabilizers react but not as effectively. Preliminary data from initial decay in heat rate and rise is related to the heat loss of the calorimeter measuring system shows that the heat loss of the individual calorimeter is an important factor which contributes to reducing the measured signal. Calibration of calorimeters was considered in relation to the size of the calorimeter. Data from the TAM Thermal Activity Monitor, model 2777, using the 201, 4 cc measuring cell and the 2230, 20 cc measuring cell was compared. The data suggests that the large cell may have a higher heat loss than the 4-cc cell, which may give different results due to sample size.

Future work will be a directed to extracting the true heat flow which will be independent of the calorimeter measuring system and corrected for sample size. This will allow for calculating more accurate thermal runaway conditions using small sample sizes.

HEAT CONDUCTION CALORIMETERS: PHYSICAL MODELS, AN APPROACH TO AN INCREASED ACCURACY

C.E. Auguet, J.L. Pelegrina[1], M. Rodriguez de Rivera[2], H. Tachoire[3] and V. Torra

CIRG-ETSECCPB-UPC, Campus Nord B-4, E-08034 Barcelona, Spain
E-mail: vtorra@etseccpb.upc.es, carlota@hal9000.upc.es
[1]Centro Atomico, 8400 S.C. de Bariloche, Argentina
[2]LAINCA-ETSII-ULPGC, Campus de Tafira, E-35017 Las Palmas de G.C., Spain
[3]Thermoch. Lab. UP & CTM UPR 7461 CNRS, F-13331 Marseille CEDEX 03, France

1.Introduction

Critical reading of the early papers in heat flux or conduction calorimeters visualizes the appearance of the intrinsic difficulties related with the inappropriateness of the used models (see [1] and references therein). In actual literature the main ideas established by Tian and Calvet are always used. *In fact, the detector system is not a perfectly "shielded" sphere nor a fixed fraction of global heat flux is detected and sensitivity (or transfer function) is position and contents dependent.* In the computer age, an increase of the complexity in used model seems the way to increase the accuracy of the instruments and to estimate the uncertainty.

In this work, the conduction calorimeters are modelized via the RC analogy. Using heat transfer equations, three types of improvements are suggested: The first one, an evaluation of the induced error realized via the used model. The influence of the position effect on the sensitivity and on the dynamics is analyzed. The second one, relates the construction of crucibles with multyshell protections optimizing the sensitivity changes. The third one is the identification via physical image (as outlined in ref. 2): found a RC analogy depicting the main effects of the experimental device. Two preliminary examples are provided: a standard calorimeter Picker type and a calorimetric analyzer developed in an INSTRON machine.

2. The early models: from 1920 to 1965

In Figure 1 (left) we can see an scheme of the conduction microcalorimeter designed by Albert Tian (about 1920-30). It was burried in a cylindrical hole placed in the underground of Provence University to prevent the base line fluctuations induced by daily room temperature fluctuations. Figure 1 (right) shows the RC model using the "modern" representation. Model includes only one heat capacity (C) and only one thermal coupling (P) with the external thermostat. The usual balance of heat power give the differential equation which relates the dissipated heat with the sensitivity and time constant reads,

$$W(t) = C \frac{dT}{dt} + P\ (T - T_o)$$

The output signal (or thermogram) relates the temperature difference via the Seebeck coefficient k_{Seeb}, using

$$s(t) = k_{Seeb}\ (T(t) - T_0)$$

The Tian device includes a complete description of the system. Tian establishes a "complete" link between thermogram or output s(t) and dissipation or input W(t) via two parameters: the time constant (τ) and the sensitivity (S). The representative formalism reads,

$$W(t) = (1/S)(\tau\ ds(t)/dt + s(t))$$

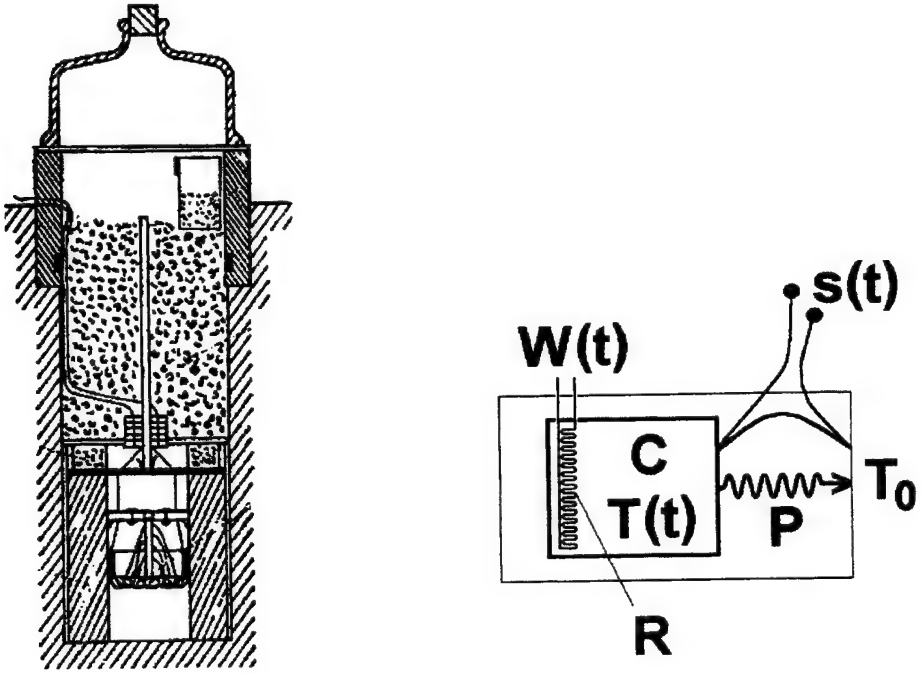

Figure 1. Left: Tian's calorimeter. Right: model.

The Tian representation assumes that the sensitivity is constant, it means that *the whole heat flux (or an invariant per cent) is detected:* if cell contents changes the coupling P remains invariant. *Tian developes a complete calorimetric system: constructs an experimental device, establish an elementary model* (appropriated to the available experimental devices) *and also, the suitable mathematical link between heat power and thermogram.*

In spring (or in fall) the external temperature evolution only permits measurements of several hours. To overcome these difficulties, Edouard Calvet outlined the classical differential microcalorimeter (near 1946) schematized in Figure 2. It consists of two identical an independent "Tian" device situated inside a common thermostat. In this way, both sides receive the same influence and the thermostat fluctuations are suppressed by a "hardware connection". The equipment (Figure 3) is adapted and progressively commertialized (DAM Co. aprox. 1960). This "basic" model is still used today.

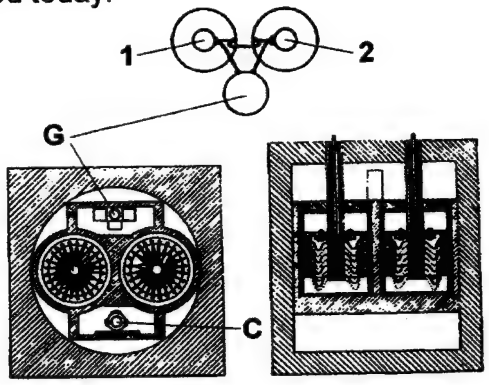

Figure 2. The classical differential equipment (≈ 1946): two "Tian" elements (1 and 2) inside the same thermostat; G) galvanometer; C) switch.

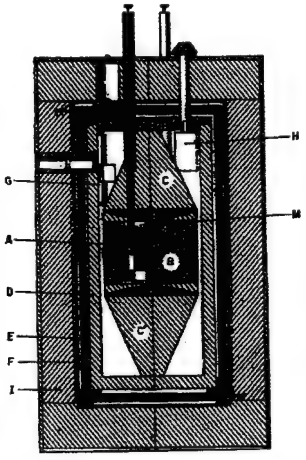

Figure 3. Calvet calorimeter (near 1960); external diameter around 60 cm, height 120 cm, available volume on the calorimetric cell 10 cm^3; A) calorimetric element; B) reference heat sink; C) and C' distribution of axial thermal perturbations (with thermal lenses); D and E) thermal multy-shells; F) heater; G) galvanometer; H) switch; I) low conductivity thermal protection; M) top of the calorimetric element with electrical links. (DAM Co. near 1960)

Calvet increases the complexity of the representative model *(for each non-differential element)*: "the impulsive curve is correctly represented by two exponentials ... [when the cell contents] is good conductor ... the impulsive curve is ... the sum of three exponentials" (1958). In our language, it means that we implicitelly assume that the system can be well represented with only two heat

capacities, so in the RC model we assign one of them to represent, for instance, the contents and the crucible. Figure 4 shows an scheme of the model with two elements. There is assumed the "perfect" differentiality and, also, that sensitivity is constant. The constant sensitivity is a permanent idea. It can be interesting to recall the statement said by E. Calvet, in a congress in Marseille at 1965: *"The same total area will always be obtained independently of the type of thermogram or the distortions occasioned by the variations of the position in the cell's interior, ... what changes is the form according to the position of the thermal source within the interior of the cell. The effect is important in thermokinetics but in calorimetry it is irrelevant.... " [3]*

In the older days the experimental set-up relates the calorimeter and auxiliary equipment, the model, and a description of the tools used in treatment.

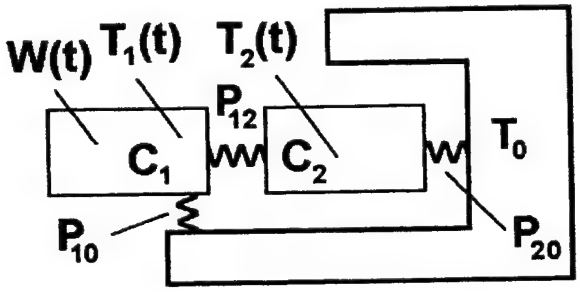

Figure 4. The "Calvet model" with two heat capacitites C_1 and C_2.

3. From 1965 to 1999: differences and similarities between the historical reasons and the scientific reasons

Critical reading of the literature reveals that at present the bases established by Tian and Calvet have not been highly modified or adapted. From the present literature we can find that:

1) Usually, unclear or oversimplified heat transfer is used in formalisms explaining the behavior of conduction calorimeters and derived equipments
2) Some confusionary terms are used in error evaluation and sometimes, reproducibility is used as accuracy .
3) It is still assumed that whole heat flux is detected or a constant fraction of it (as in Tian or Calvet working hypothesis).
4) It seems that software or "a mouse click" is a way to obtain excellent results [1].

Increase the accuracy of the equipment supposes a critical revision of the hypothesis used today. In particular, some of the older hypothesis "well established" are related with the used galvanometer and photographic paper. For

[1] "When analysing DSC curves software can easily convert a glitch due to electrical noise into a first-order phase transition and create a glass transition or a broad peak from the curvature of the sample baseline." [4]

instance, the differential systems solve a problem which today is, eventually, different. Is the oversimplified hardware base line correction the older approach? Is the software correction the expected improvement used in the third millennium? (see, for instance, ref. 5 and references therein). If the accuracy is the main target, the position of dissipation and of the crucible contents, need to be analyzed. Also, the fraction of detected heat flux need to be critically determined. An increase of the coherence between experimental systems and representative models seems the main tool to be used.

4. Mathematical formalism of conduction calorimeters via RC analogy

Three available posibilities are used in Fourier analysis: solution of three-dimensional differential equation via appropriate heat flux and temperature interphase condition, decomposition of the system in N discrete elements and a pure numeric description via finite elements analysis. The RC-analogy describes the experimental device via N heat capacities C_j and several the thermal couplings between elements P_{jk} and with the surroundings P_{jn}.. the system is represented by N differential linear equations as:

$$W_j = C_j \frac{dT_j}{dt} + \sum_{k \neq j} P_{jk}(T_j - T_k) + \sum_{n} P_{jn}(T_j - T_n^*) \quad ; \quad j = 1, 2, \ldots, N$$

If only one external temperature exists, this can be used as a new origin. The response (in Laplace coordinate) deduced via a convolution of dissipations W_{k+l} produced in *different positions* k + l reads,

$$T_m^{W_{k,\ k+1,\ \ldots,\ k+n}}(p) = \sum_{l=0}^{l=n} W_{k+l}(p)\, TF_{m,\,k+l}(p)$$

Each $TF_{m,k+l}$ is related to the temperature T_m associated to Dirac pulse dissipated in the k+l element ($W_{k+l}(\delta)$)

$$TF_{m,k}(p) = \frac{A_{m,k}(p)}{B(p)} = \frac{\sum_{j=0}^{M(m,k)} b_j(m,k)\, p^j}{\sum_{i=0}^{N} c_i\, p^i} = S_{m,k} \frac{\prod_{j=1}^{M(m,k)} (\tau_j^*(m,k)p + 1)}{\prod_{i=1}^{N} (\tau_i\, p + 1)} = \sum_{i=1}^{N} \frac{a_i(m,k)}{p + \omega_i}$$

with,

$$\tau_i = 1/\omega_i, \quad M(m,k) < N \quad \text{and} \quad S_{m,k} = \sum_{i=1}^{N} a_i(m,k)\, \tau_i$$

Using thermopairs as detectors, the thermogram or the output signal s(t) can be determined using and appropriate linear combination of the "warm and cold" junction temperatures :

$$s(p) = k_{Seeb.} \sum_{m,\,m'} \left(T_m(p) - T_{m'}(p) \right) \quad \overset{L^{-1}}{\Longrightarrow} \quad s(t) = k_{Seeb.} \sum_{m,\,m'} \left(T_m(t) - T_{m'}(t) \right)$$

In general, the thermogram includes the effect of several independent dissipations as in:

$$s^{W_{k,\,k+1,\,\ldots,\,k+n}}(p) = S_{k,\,\ldots,\,k+l,\,\ldots,\,k+n}(p) = \sum_{l=0}^{l=n} W_{k+l}(p)\, TF_{k+l}(p)$$

The thermogram is related with the independent dissipations via only one equation. The thermogram is univocaly related with the dissipations but the dissipations evaluation from only one equation is an ill defined problem! (only one equations and several unknown functions). This induces the classical approach: only one dissipation is used. For instance, if the dissipation appears only (or is supposed only) in the k^{th} element the previous equation reduces to:

$$s^{W_k}(p) = S_k(p) = W_k(p)\, TF_k(p)$$

with

$$\tau_i = 1/\omega_i \,,\ M(k) < N \ \text{ and } \ S_k = \sum a_i(k)\, \tau_i$$

If the sensitivity and the series of time constants and zeros are well known an eventual deconvolution can be obtained.

5. The models: a tool in accurated measurement

Three lines of analysis are briefly described. The first one, (evaluation of static and dynamic error), is related with the uncertainty on the dissipation position. The analysis is realized using the model (an injection calorimeter) established in reference 2. The second one is a theoretical approach and simulation. A way to increased accuracy via adapted multi-shell crucibles is achieved. In the third one, two preliminary examples of model preparation are presented. One of them is associated to a classical Picker system. Another connected to a calorimetric analyzer build in an INSTRON machine. Each particular situation needs an adaptation of the general formalisms. The standard invariant systems need to be adapted to open systems and/or to variable systems.

5.1. Static and dynamic uncertainty. An analysis via a Tian- Calvet injection calorimeter

The effect of position of dissipated heat on sensitivity is studied. For it, we have started from the values obtained for the model described in references 2 and 6 to represent the classical injection calorimeter of Calvet. In this model [2] only 6 heat capacities (Figure 5 A) are considered. The element 2 is assigned to the mixing cell (near 60 cm . We have broken down this heat capacity into four elements (numbers 2,7,8 and 9 in Figure 5 B). The analysis is accomplished via some asymmetries in couplings and in the inner thermal conductivity. The differential equations during injection are:

$$0 = C_1 \frac{dT_1}{dt} + \sum_{k \neq 1} P_{1k}(T_1 - T_k) + P_1(T_1 - T_0)$$

. . .

$$W = C_m \frac{dT_m}{dt} + \sum_{k \neq m} P_{mk}(T_m - T_k) + P_m(T_m - T_0) + \frac{dC_m}{dt}(T_m - T_0)$$

. . .

$$0 = C_N \frac{dT_N}{dt} + \sum_{k \neq N} P_{Nk}(T_N - T_k) + P_N(T_N - T_0)$$

The model includes the time evolution of heat capacity ($C_m = C_m(t)$) and the mass rate effect on the thermostat coupling ($P'_m = P_m + dC/dt$).

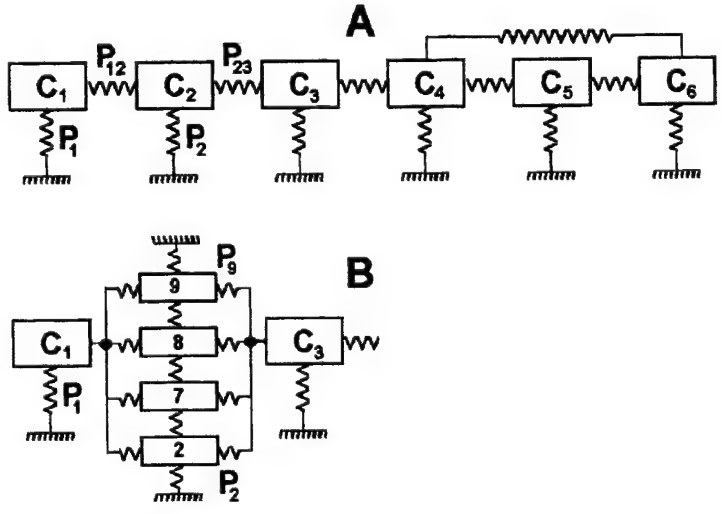

Figure 5. Heat capacities and couplings for a Calvet calorimeter. A: reference model. B: decomposition inside the cell.

The results for several different cases, compared with the initial values of sensitivity, do not overcome ± 1.5 %. An increased dynamic uncertainties are produced as we can see in Figure 6. In the initial part, the effect of "greater" frequencies creates a much more large uncertainty. The discontinuity associated to the initial steps uses the complete transference function (TF). As usual, the position effects (or the contents) induces big changes in the TF at higher frequencies. In the initial part, a greater difference on deconvoluted thermograms can be observed.

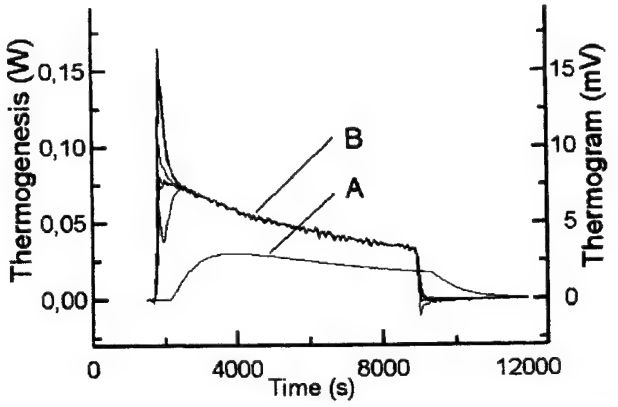

Figure 6. Thermogram (A) and several thermogenesis (B) related to different analized cases.

5.2. Models as a tool for new design

With the RC modelization we can prevent both, positional effect and the influence of the variation of cell contents. For it we have simulated three different configurations to place two different samples with radial simetry, one of them made on "brass" and the other on "non-convective water". We have compared the obtained values of the sensitivity for dissipation in two different places, in the inner part of the sample and in the external part. The three configurations (free, umbrella and onion) are shown in Figure 7. Table 1 shows the associated sensitivity evolution with contents and position. Onion structure reduces the practical uncertainty "to zero" and the umbrella approach is, also, very interesting. The dynamic effects at extremely lower frequencies are reduced. At relatively higher frequencies the dissipation against time is always affected (but always reduced in onion or umbrella) by the position and contents.

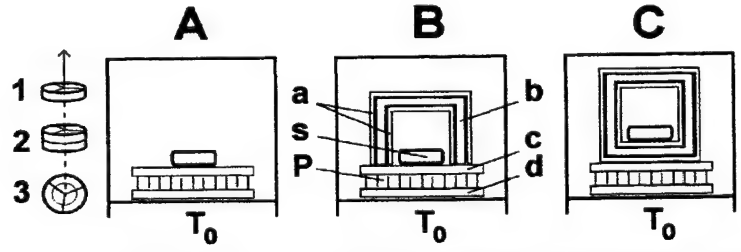

Figure 7. Analized models A) unprotected sample; B) umbrella; C) onion.

Table 1. Static effects: sensitivity comparison (via simulation) between unprotected, umbrella and onion (Si(p): porous silicon).

N	Protect.	Shell thick (mm)	Brass		Water		% max
			S_{int}	S_{ext}	S_{int}	S_{ext}	
11	- - - - - - -	- - - - - - -	104.16	104.15	99.20	98.11	5.0
26	Al Si(p) Al	0.1, 0.1, 0.1	104.36	104.35	103.85	103.66	0.5
38	Al Si Al	0.2, 0.2, 0.2	103.97	103.96	103.96	103.96	0.0

5.3. Identification via physical image: a Picker type calorimeter

In the steady state the output signal or thermogram is considered proportional to the mixing enthalpy. Figure 8 shows a scheme of the locked inner part of the device. In the scheme, five elements are specified. The element 1 includes the mixing cell and, eventually, a part of the inlet pipes. Element 2 corresponds to the central block. Close to the mixing chamber includes a resistor for Joule dissipation studies. Element 3 simulates the coil pipe. At higher flow rates some reaction takes place in this element. The elements 4 and 5 simulates, respectively, the warmer and colder junctions.

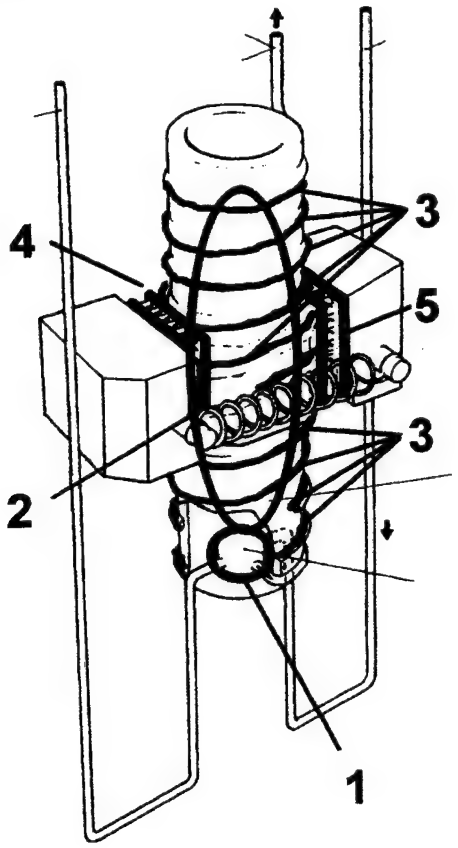

Figure 8. Suggested model for LKB 2277 204 (from ref. 7).

The differential equations reads,

$$\alpha_1 W_{mix} = C_1 \frac{dT_1}{dt} + \sum_{j \neq 1} P_{1j}(T_1 - T_j) + P_1(T_1 - T_0) + g_1(T_1 - T_0)$$

$$W_{Joule} = C_2 \frac{dT_2}{dt} + \sum_{j \neq 2} P_{2j}(T_2 - T_j) + P_2(T_2 - T_0)$$

$$\alpha_3 W_{mix} = C_3 \frac{dT_3}{dt} + \sum_{j \neq 3} P_{3j}(T_3 - T_j) + P_3(T_3 - T_0) + g_{13}(T_3 - T_1)$$

$$0 = C_4 \frac{dT_4}{dt} + \sum_{j \neq 4} P_{4j}(T_4 - T_j) + P_4(T_4 - T_0)$$

$$0 = C_5 \frac{dT_5}{dt} + \sum_{j \neq 5} P_{5j}(T_5 - T_j) + P_5(T_5 - T_0)$$

The model establishes a clear separation between the Joule (in 2) and the mixing reaction (in 1 and 3). The α_1 and α_3 coefficients are related to the prevailing dissipation inside the particular element. If injection rate is too high, it could remain some reaction outside ($\alpha_1 + \alpha_3 < 1$). g_1 and g_{13} are related to the flow rates and, also, to the thermomechanical properties of the used liquids. Their contribution represents the heat flux transferred by the liquids to the mixing chamber (1) and to the coil pipe (1-3). The sensitivity values are dependent on: the injection rate, the mixing liquids and the Joule dissipation. Figure 9 includes the comparison between calculated and experimental sensitivity against flow rate using Joule or hexane and cyclohexane mixture.

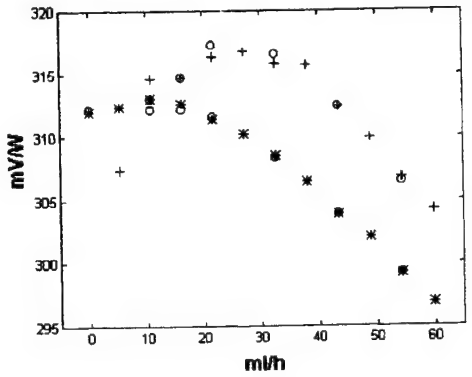

*Figure 9. Sensitivity against the volume rate $\Delta(V_1 + V_2)/\Delta t$, * * *: Joule effect; + + + hexane(1) + cyclohexane(2), o o o: calculated.*

5.4. Identification via physical image: calorimetric analyzer in a INSTRON machine

A Universal Testing Machine permits a quantitative evaluation of mechanical cycles. For instance, stress against strain at, usually, constant temperature is studied. The direct evaluation of dissipated heat in cycling or plastic deformation is an unsolved problem.

Figure 10 shows an INSTRON machine with an elementary non-differential conduction calorimeter. This device is primarily devoted to analyze the heat power dissipated in a stress induced martensitic transformation. Martensitic transformation is considered a first order solid-solid transformation, and can be induced decreasing the temperature or increasing the stress. Advancement of the transformation needs an auxiliary stress or undercooling associated to the dislocation concentration. Appropriate stress and crystallographic axis in single crystal can produce only one variant of martensite.

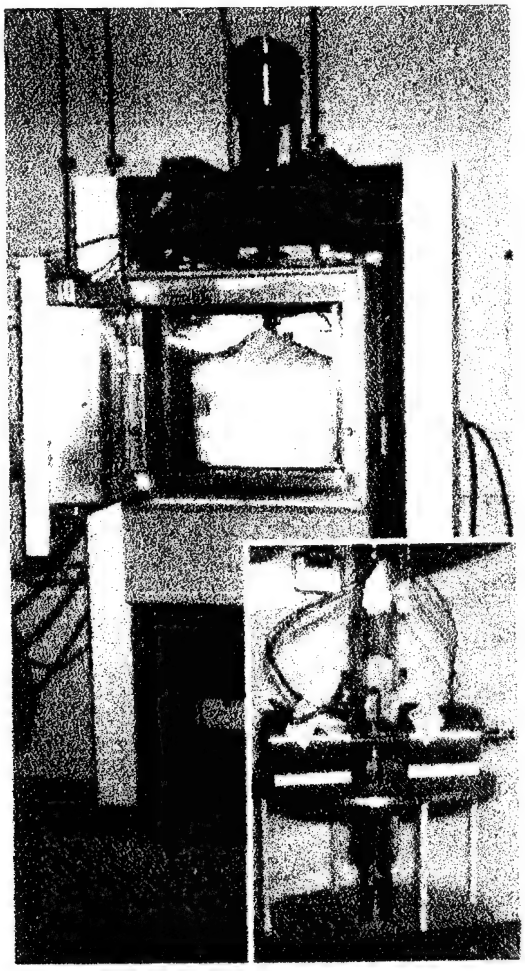

Figure 10. INSTRON machine. The thermal protection reduces the furnace and surroundings temperature perturbations. Bottom right: adapted calorimetetric analyzer [5].

See in Figure 11 a monovariant transformation (Cu-Zn-Al, single crystal alloy): the interface displacement is a function of the stress change (or, eventually, of the temperature change). As the phases are metastable (the quench process is always necessary) more or less relevant concentration of dislocation is always present. Pseudoelasticity or thermoelasticity always appear. The displacement of the single-interface, single-variant martensitic transformation is similar to other physico-chemical processes related to front reaction as, for instance, gas-solid reactions.

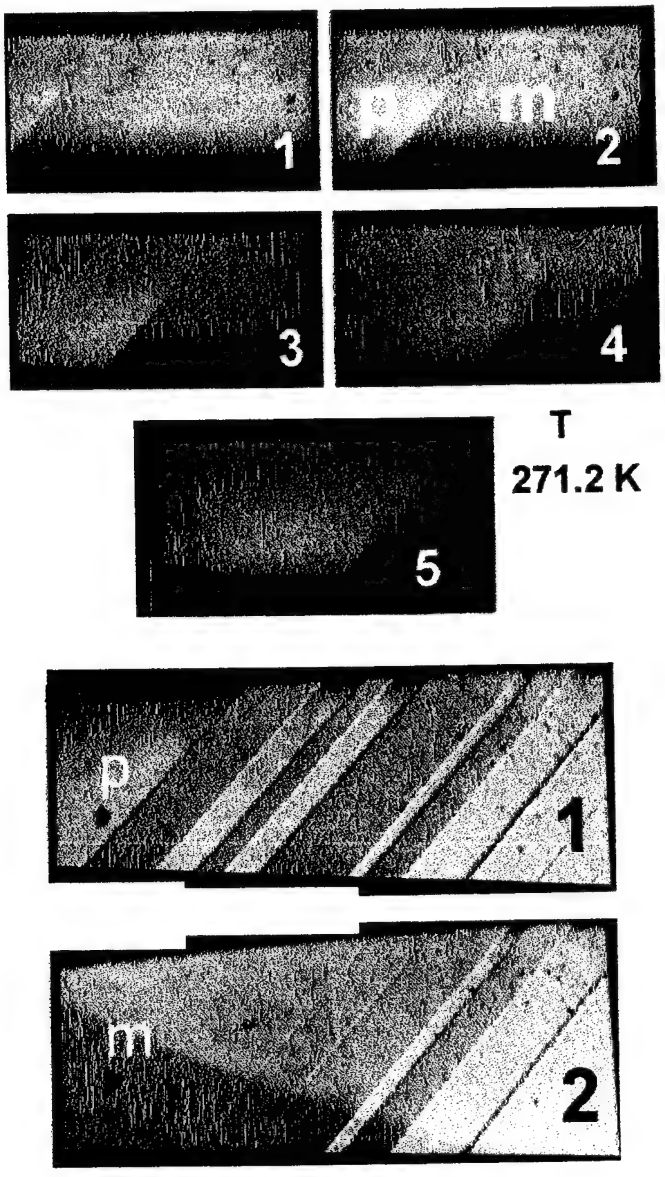

Figure 11. Single variant transformation in a martensitic transformation of Cu-Zn-Al single crystal alloy (observed length near 1 mm); p parent phase; m martensite phase. Top: single interface; 1,2,3,4, and 5 progressive displacement in unloading at constant temperature. Bottom: single variant transformation; 1 and 2 progressive loading.

Figure 12 shows a diagram of the experimental system and the associated RC model. Symmetries are more important (up to down, front to rear, and left to right) and reduces the complexity of the used model. Elements 1 to 7 represents the sample and the grips. The 8 to 12 are the warmed junctions and 13 to 17 the colder junctions.

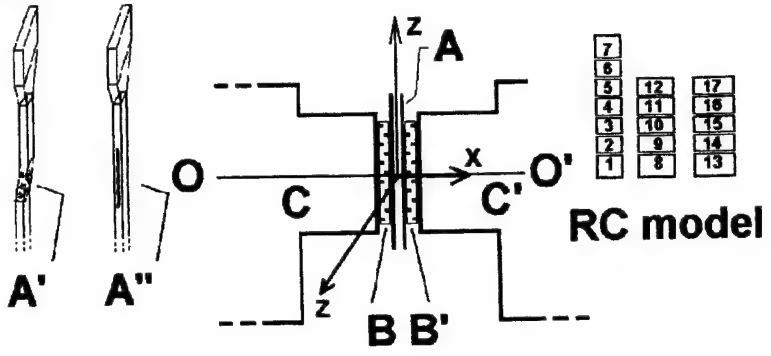

Figure 12. INSTRON. Left: Sample structure. A': transformation strain; A": hole (Joule effect analysis).Right: calorimetric analyzer. A: sample, B and B' MELCOR plates O-O' symmetry axis; C and C' reference thermal sink.

From the initial evaluation a preliminary set of parameters is established (see curve 1 in Figure 13). The automatic identification method permits a progressive approach via appropriate iteration (curves 2 and 3) to a satisfactory coincidence between experimental and calculated thermograms.

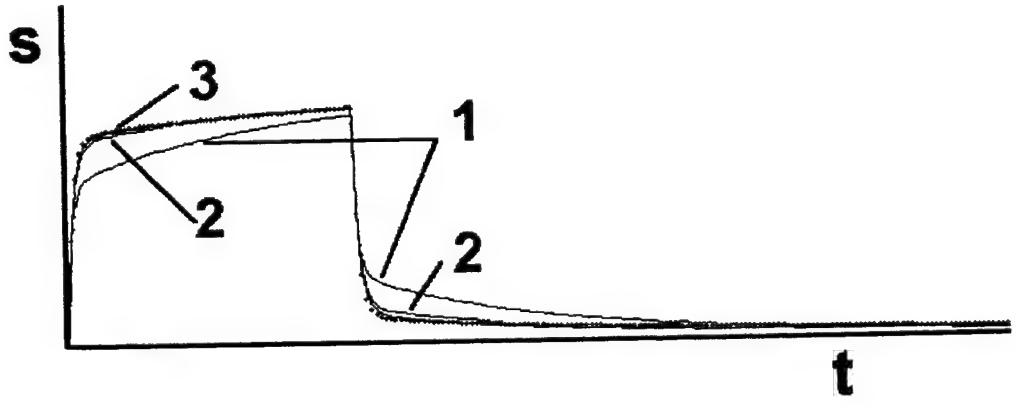

Figure 13. Approaching the model ++++ experimental. 1: initial parameters. 2 and 3: steps to the approach.

6. Conclusions

In the computer age some historical reasons need to be critically analyzed. For instance, the hypothesis based in experimental equipment on the fifties (the old models in heat transfert or the "imperishable" differential systems, ...)

The tratment via models seems the suitable tool for:

1) outline crucibles adapted to accurate measurements
2) evaluate the static and dynamic uncertainties
3) establish the physical image of experimental devices

Acknowledgements

Research realized in the frame of contracts NATO 920452 and ACI 1999 (UPC and C.A.B. Inst. Balseiro of S.C. de Bariloche, Argentina) of Generalitat of Catalonia. The cooperation between UPC and the Provence University is gratefully acknowledged.

References:

[1] V. Torra and H. Tachoire, J. Thermal Anal. 52 (1998) 663
M. Rodriguez de Rivera, H. Tachoire and V. Torra, "Older work and actual requirements in heat conduction calorimeters: physical models, a way to accurate measurements", Thermochim Acta submitted (1999)
[2] M. Rodriguez de Rivera, F. Socorro, J.P. Dubes, H. Tachoire and V. Torra, Thermochim. Acta 150 (1989) 11
[3] "Microcalorimétrie et Thermogenèse", n° 156, Éditions du CNRS, Paris 1967 (p. 329):
[4] "Thermal Analysis", 2nd edition, T. Hatakeyama, F.X. Quinn, Wiley, 1999
[5] J.L. Pelegrina, M. Sade, C. Auguet, V. Torra and A. Torralba, "Calorimetry under stress. A preliminary study in single crystalline Cu-Zn-Al shape memory alloys", J. Thermal Analysis and Calorimetry, 56 (1999) to be published
[6] F. Marco, M. Rodriguez de Rivera, J. Ortin, T. Serra, and V. Torra, Thermochim. Acta 107 (1986) 149
[7] Instruction Manual for 2277 Thermal Activity Monitor 1992 p 12 ThermoMetric AB, Sweden

DETERMINATION OF THE KINETIC DATA OF THE THERMAL DECOMPOSITION OF ENERGETIC PLASTICIZERS AND BINDERS BY ADIABATIC SELFHEATING

Manfred A. Bohn

Fraunhofer-Institut für Chemische Technologie, ICT
Postfach 1240, D-76318 Pfinztal-Berghausen, Germany
fax: +49-721-4640-111, e-mail: bo@ict.fhg.de

Abstract

The thermal decomposition behaviour of the following plasticizers and uncured binders (diols for PUR-type elastomer binders) was investigated in solutions of toluene (with 10 mass-% contents) by adiabatic selfheating with an 'Accelerating Rate Calorimeter' (ARC™): uncured GAP (poly-glycidylazide) from two manufacturers, PolyGLYN (poly-glycidylnitrate), mixture (58.8 / 41.2 in mass-%) N-Methyl-/ N-Ethyl-NENA (NENA = N-(2-nitratoethyl)-nitramine), DANPE (1,5-diazido-3-nitraza-pentane), GAPA (short chain GAP but with azido end groups), EGBAA (ethylene glycol-bis-(α-azidoacetate), octylazide (not for use in explosives), GAP-AA-2000 (normal GAP, but OH-end groups as esters of α-azidoacetic acid), GAP-AA-500 (short chain GAP, but OH-end groups as esters of α-azidoacetic acid). Three types of energetic groups are represented with these compounds: the organic nitric acid ester group, the nitramine group and the organic azido group. A closed measuring system was used. This prevents the solutions from evaporating and gives a good adiabaticity. The amount of the solution weighed-in was about 6g, the measuring cells used are made from titanium with one inch in diameter. All named energetic substances would deflagrate after a short period of controllable self heating with the weighed-in amount of energetic substance. The advantage of the investigation of the solutions is that the decomposition of the energetic substances can be followed in a fully controlled way. The characteristic data of the adiabatic selfheating are given. With the self heat rate curves one can distinguish the plasticizers and binders with respect to the decomposition temperature range, the heat generation and the heat generation rate. The Arrhenius parameters and the released heats of reaction have been determined from the self heat rate curves, which have been described well with reactions of first order. The self heat rate curves have been scaled to the thermal inertia equal to one, which corresponds to (1) the measurement on a solution without measuring cell and to (2) the measurement on the energetic substance alone without measuring cell. The procedures of the scaling and of the data evaluation are described. With the data

Paper presented at the 2nd International Workshop on 'Microcalorimetry of Energetic Materials', May 17-19, 1999, Otley/Leeds, Yorkshire, UK.

of the simulated situation 'energetic substance alone' the temperatures have been calculated for heat generation rates of 25µW/g and 50µW/g. For 25µW/g the predicted temperatures of Me/Et-NENA and PolyGLYN are 85°C and 90°C. The azido compounds have values above 100°C, whereby DANPE has the lowest temperature at 106°C and the investigated GAP binders have values of about 114°C.

1. Introduction

Energetic plasticizers and binders developed and used more recently contain the following energetic groups: nitric acid ester group, nitramine group, azido group. The basic objectives of developing energetic binders and plasticizers are: (1) increase of the thermal stability, (2) increase in energy content, (3) adjustment of the oxygen balance in a formulation, (4) improvement of the plasticizer functions in formulations: reducing the glass transition temperature and the brittle-ductile transition temperature, reducing migration and the so-called exudation, improving of other mechanical properties of the propellant matrix and (5) the improvement of the burning behaviour of the propellant. Apart from the additional energy of the azido group, it is also interesting because of its high gas production rate (nitrogen release). This can increase the burning rate and intensify the effect of the blast waves of high explosives. The nitric acid ester group is known for their low thermal stability, experienced in common blasting oils and nitrocellulose. This has not changed in the newer binders and plasticizers, which contain it as the energetic group. The advantage is the different decomposition behaviour of the polymeric backbone compared to the one of nitrocellulose. As known so far, the azido group do not induce an autocatalytic decomposition.

Comparative investigations with regard to the decomposition triggered by thermal energy classifies the substances investigated here in terms of their thermal stability and the energy released in amount and per time respectively. The method used was the adiabatic self heating of toluene solutions determined by an 'Accelerating Rate Calorimeter' (ARC™). The closed measuring system prevents evaporation. The advantage of performing the investigations using solutions is that the course of the decomposition reaction can be adjusted in its rate and therefore it can be measured in a controlled way and the reaction is more homogeneous. The energetic compounds alone in amounts used with the solutions would all deflagrate after a short controllable period of adiabatic self heating.

2. Apparatus

2.1 Principle of the method

A short description is presented here, a detailed one can be found in /1/. The main components of the 'Accelerating Rate Calorimeter' (ARC™) made by Columbia Scientific Industries, Austin, Texas, USA (recently taken over by Arthur D. Little Inc., Cambridge Massachusetts, USA) can be seen in Fig. 1.

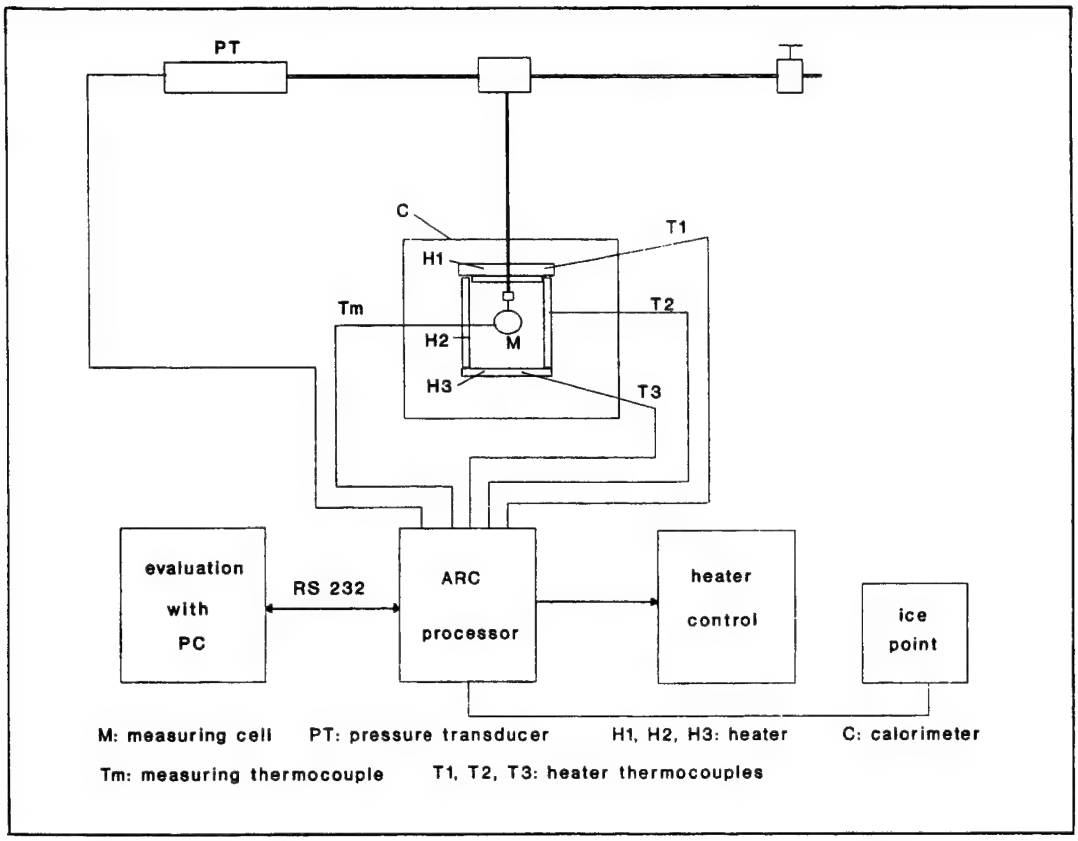

Fig. 1: Scheme of the 'Accelerating Rate Calorimeter' (ARC™).

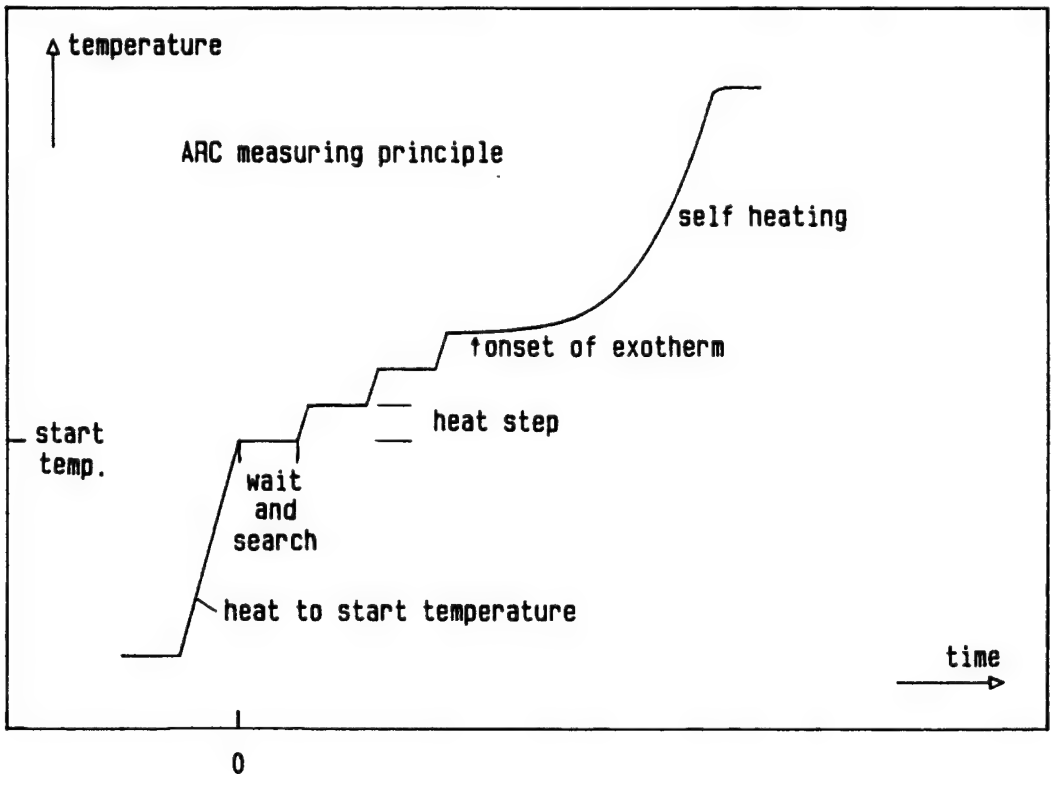

Fig. 2: ARC™ measuring principle of the measuring mode 'heat-wait-search'.

The heating block contains three separate heaters H1, H2 and H3 which can be regulated individually using the heating block thermocouples T1, T2 and T3. The measuring cell is positioned in the center of the heating block. The spherical measurement cells with a connecting stem can be made from titanium or stainless steel or tantalum or Hastelloy C 276 with a diameter of one inch or 0.5 inches. The measuring cell thermocouple Tm is fixed to the measuring cell using a clip. All thermocouples are sheathed and of type N (Nisil/Nicrosil). The measuring cell has a connection to the pressure transducer PT by a thin (1/16 inch) high pressure capillary tube. The measurements are made on the closed system, which makes possible the adiabaticity of the measurement system. The measurement signals are transmitted to the ARC™ processor, which executes the measuring program and controls the counter heating for the sample cell during the self heating of the sample. This counter heating generates a quasi-adiabatic environment. An electronic ice point device producing a zero centigrade bath is used as a temperature reference point for the thermocouples.

The course of the ARC™ measurement in the mode 'heat-wait-search' is shown in Fig. 2. The wait period serves to equilibrate the sample and the measuring cell with the environment after heating to the start temperature or after heating by one heat step. During the search period the processor checks whether the sample shows a self heating. To do this, the changes in temperature of the measuring cell are compared with a preset sensitivity parameter. If the temperature increase per unit time exceeds this preset level over a period of time, determined by another parameter, this is recognized as the start of the self heating and the device switches to the exotherm mode and the processor starts the counter heating. If this preset level is not exceeded during the search period, the sample is heated by a heat step and this in turn is followed by another wait and search period. This process is repeated until an exotherm has been found or until a preset end temperature has been reached.

Because of the higher sample amounts useable with the ARC™ compared to a DSC apparatus, the sensitivity of an ARC™ is higher by a factor of about 100 to 1000.

2.2 Taking the inert masses into consideration

During the exothermal decomposition, the sample also heats up the measuring cell itself. This means that the self heat rate is decreased by the so-called inert mass (means it show no own heat generation) of the measuring cell and other existing inert masses compared to a measurement without inert masses. To set up the heat balance equation, the increase in temperature at time t of the entire system 'measuring cell/sample' is called $\Delta T_{MS}(t)=T_{MS}(t)-T_{MS}(0)$ and that of the simulated measurement on the sample alone is called $\Delta T(t)=T(t)-T(0)$ with $T_{MS}(0)=T(0)$. During the self heating both temperature differences change with time. The heat balance equation given in eq.(1) takes into consideration the dependency on temperature of the specific heats and the decomposition of the sample during the course of the reaction.

$$\left(\sum_i m_i(R(t))\cdot C_i(T(t))\right)\cdot \Delta T(t) = \left(\sum_i m_i(R(t))\cdot C_i(T(t)) + m_M\cdot C_M(T(t)) + \sum_j m_j\cdot C_j(T(t))\right)\cdot \Delta T_{MS}(t) \quad (1)$$

The specific heats used are the ones at constant pressure, C_p, as the volume of the sample is not actually kept constant, this applies particularly to solids and liquids. The pressure is not constant either, however, any changes in pressure are small, often below 10 bar. C_v has to be used for gas reactions. R(t) is the reaction coordinate or equivalently named the degree of reaction conversion, which is used to determine the sample mass m_s (= m_i with i=1) and the masses of the reaction products m_i with i>1. The values with index M apply to the measuring cell, the sum expression over j includes additional thermally inert masses. Eq.(1) must be applied also before the onset of the measured exotherm, if there is already an appreciable decomposition.

In the case of an ARC™ measurement without sample and decomposition product analysis, the course of the reaction with regard to R(t) is unknown. But it is the point of interest in thermal analysis to get the information from the thermal data without the real chemical data on the composition of the sample. It is pointed out that this is not possible always. One has to check carefully the system under consideration, if thermal analysis is applicable in an unambiguous way.

To proceed with this method of thermal analysis, approximations are introduced. Only the sample mass m_s and the average specific heat C_s are used and similar approximations are made for the other terms. The dependency on temperature is also not taken into consideration, as $\Delta T_{MS}(t)$ is usually between 30°C and 70°C. The average value of C_s for organic substances is taken as 2.092 J/g/K. Eq.(2) is the simplified form of eq.(1).

$$m_S\cdot C_S\cdot \Delta T(t) = \left(m_S\cdot C_S + m_M\cdot C_M + \sum m_j\cdot C_j\right)\cdot \Delta T_{MS}(t) \quad (2)$$

which can be written as eq.(3) with the abbreviation ϕ given in eq.(4).

$$\Delta T(t) = \phi\cdot \Delta T_{MS}(t) \quad (3)$$

$$\phi = 1 + \frac{m_M C_M + \sum m_j C_j}{m_S C_S} \quad (4)$$

The quantity ϕ is called the thermal inertia of the system 'sample/measuring cell', in short named ϕ-factor. The ϕ-factor is used as a correction quantity, which means that the influence of the inert masses can be approximately eliminated /1/. A precise correction is possible using eq.(1) and all the necessary experimental information.

3. Evaluation and scaling of the adiabatic self heat rate curves

3.1 Types of the adiabatic self heat rate curves

Fig. 3 shows typical adiabatic self heat rate curves h(T) for different reactions. The adiabatic self heat rates h(T) shown in Fig. 3 and in the following figures are presented as lg(h[°C/min]) against 1/T [1/K]. On the abscissa the temperature values are indicated in °C. The Arrhenius parameters used to calculate the curves in Fig. 3 without the autocatalytic curve are the ones not in brackets given in Fig. 3. The onset temperature T_0 of the self heating is 150°C and its final temperature T_f = 250°C. The curves have been calculated for ϕ = 1, that means for a simulated measurement without measuring cell or for a measurement with negligible influence by inert masses.

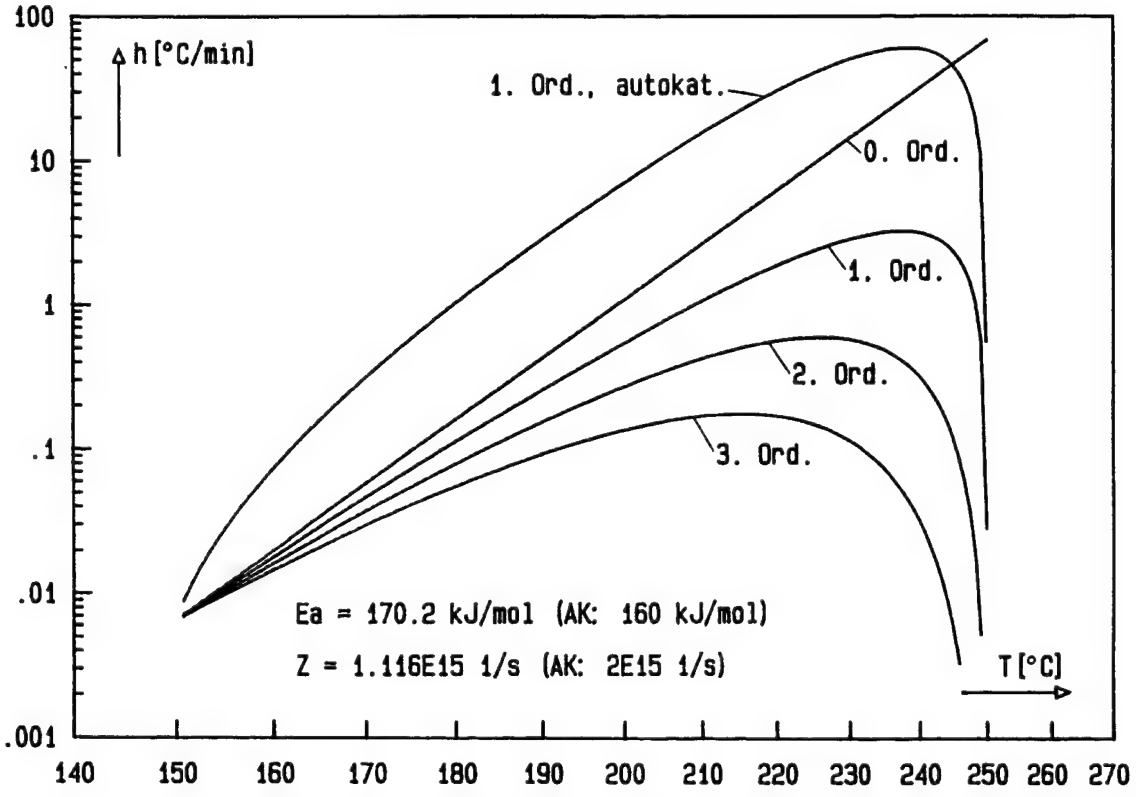

Fig. 3: Types of adiabatic self heat rate curves originating from decomposition reactions with different order n and of an autocatalytic reaction.

In the case of a reaction of zero order, h(T) results in a straight line, which ends at T_f because of the consumption of the substance. For reactions of first, second and third order, the h(T)-curves pass a maximum and then return to zero when they have reached T_f. The higher the reaction order n, the wider the range of the maximum of the curve. The h(T)-curves with $n \neq 0$ lie below the curve with $n = 0$. The curves clearly show that the order of reaction can be determined definitly. Fig. 3 also shows the course of h(T) for an autocatalytic reaction according to the

reaction scheme eq.(5) and to the kinetic expression eq.(6), with $\Delta H_{R,i}$ as reaction enthalpies. See also eq.(15) and eq.(16).

(5) $$A \xrightarrow{k_{A1}} B + Z \qquad \Delta H_{R,1}$$

$$A + B \xrightarrow{k_{A2}} 2\,B + Z \qquad \Delta H_{R,2}$$

(6) $$\frac{dA(T(t))}{dt} = -k_{A1}(T(t)) \cdot A(T(t)) - k_{A2}(T(t)) \cdot A(T(t)) \cdot B(T(t))$$

The primary decomposition of A with the reaction rate constant k_{A1} includes the formation of the autocatalyticly effective product B by a reaction of first order. The second decomposition reaction is the autocatalytic reaction. The reaction rate constant k_{A2} has the Arrhenius parameters given in brackets in Fig. 3, k_{A1} has the ones used for the other curves. Here B is not a catalyst in the common definition, in which it is not consumed and effects the reaction between two reactants by changing the activation parameters. Autocatalysis stands for the decomposition of the start substance in further reactions with its reactive decomposition products.

3.2 Determination of Arrhenius parameters from adiabatic self heating

To determine the Arrhenius parameters of the reaction rate constant k(T) of the decomposition reaction, the consumption of the substance as a function of temperature and time is the necessary information. If the decomposition of the substance A follows a defined reaction, the reaction rate constant can be determined from the self heat rate curve using the appropriate kinetic expression and balancing the substance consumption (= degree of reaction conversion) and the temperature increase, eq.(7). The increase in temperature is equivalent to the released heat Q_A by the decomposition reaction. The same approximations that are used in eq.(2) are used here too. In eq.(7) the terms '$m_K \cdot C_K$' (thermal masses) have been eliminated already. The onset quantity $Q_A(T(t_0))$ is normally set to zero. In eq.(7) the ΔT and the ΔT_{MS} are no functions of time.

(7) $$\frac{A(t,T)}{A(0)} = \frac{A(T(t))}{A(T(0))} = A_r(T(t)) = \frac{Q_A(T(t_f)) - Q_A(T(t))}{Q_A(T(t_f)) - Q_A(T(t_0))} = \frac{T_f - T(t)}{\Delta T} = \frac{T_{fMS} - T_{MS}(t)}{\Delta T_{MS}}$$

- $A(T(t))$ amount of sample substance A (concentration or mass) at time t at temperature T = f(t)
- $A(T(0))$ amount of substance A at T(0), the onset temperature of the adiabatic self heating. T(0) is also named T_0 or $T(t_0)$.
- $T(t)$ temperature of the sample alone at time t at condition $\phi = 1$
- $T_{MS}(t)$ temperature of the system 'sample/measuring cell' at time t at $\phi \neq 1$
- ΔT adiabatic temperature increase $\Delta T = T_f - T(0)$ of the sample alone at condition $\phi = 1$
- ΔT_{MS} adiabatic temperature increase $\Delta T_{MS} = T_{fMS} - T_{MS}(0)$ of the system

'sample/measuring' cell at $\phi \neq 1$

T_f final temperature of the adiabatic self heating of the sample alone at condition $\phi = 1$

T_{fMS} final temperature of the adiabatic self heating of the system 'sample/measuring cell' at condition $\phi \neq 1$

The differentiating of eq.(7) gives the eqn(8), where eq.(8-2) is the normalized form with $A_r(T(t)) = A(T(t)) / A(T(0))$.

$$\frac{dA(T(t))}{dt} = -\frac{A(T(0))}{\Delta T}\cdot\frac{dT(t)}{dt} = -\frac{A(T(0))}{\Delta T}\cdot h(T(t)) \quad = -\frac{A(T(0))}{\Delta T_{MS}}\cdot h(T_{MS}(t))$$

(8)

$$\frac{dA_r(T(t))}{dt} = -\frac{1}{\Delta T}\cdot h(T(t)) \quad = -\frac{1}{\Delta T_{MS}}\cdot h(T_{MS}(t))$$

The combination of eqn(8) with a reaction kinetic expression, here a reaction of order n shown in eq.(9) and in normalized form in eq.(10), gives eqn(11) for the adiabatic self heat rate $dT(t)/dt = h(T(t))$.

(9) $$\frac{dA(T(t))}{dt} = -k_n(T(t))\cdot A^n(T(t))$$

(10) $$\frac{dA_r(T(t))}{dt} = -k_{n,r}(T(t))\cdot A_r^n(T(t)) \qquad \text{with} \quad k_{n,r}(T(t)) = k_n(T(t))\cdot A^{n-1}(T(0))$$

$$h(T(t)) = k_{n,r}(T(t))\cdot\Delta T\cdot\left(\frac{T_f - T(t)}{\Delta T}\right)^n \qquad \text{with } \phi = 1$$

(11)

$$h(T_{MS}(t)) = k_{n,r}(T(t))\cdot\Delta T_{MS}\cdot\left(\frac{T_{fMS} - T_{MS}(t)}{\Delta T_{MS}}\right)^n \quad \text{with } \phi \neq 1$$

With eq.(11-2) the reaction rate constants $k_{n,r}(T)$ can be determined just by arithmetic operations on the measured adiabatic self heat rate h(T). Eq.(11-1) was used to calculate the curves in Fig. 3 with n = 1, 2, 3. Eq.(11-1) results in the following equations for the reaction orders n of value 0, 1 and 2.

- reaction of zero order

(12) $$h(T(t)) = k_{0,r}(T(t))\cdot\Delta T = \frac{k_0(T(t))}{A(T(0))}\cdot\Delta T$$

- reaction of first order

(13) $$h(T(t)) = k_{1,r}(T(t))\cdot(T_f - T(t)) = k_1(T(t))\cdot(T_f - T(t))$$

- reaction of second order

$$(14)\qquad h(T(t)) = k_{2,r}(T(t)) \cdot \frac{(T_f - T(t))^2}{\Delta T} = k_2(T(t)) \cdot \frac{A(T(0))}{\Delta T} \cdot (T_f - T(t))^2$$

In a reaction of first order, h(T) is explicitly independent of A(T(0)) but implicitly dependent on A(T(0)), because T_f increases with increasing amount A(T(0)). To calculate the autocatalytic self heating in Fig. 3, the reaction kinetic scheme according to eq.(5) was used as formulated in eq.(15), using B(T(t)) = A(T(0)) - A(T(t)).

$$(15)\qquad \frac{dA_r(T(t))}{dt} = -k_1(T(t)) \cdot A_r(T(t)) - k_2(T(t)) \cdot A_r(T(t)) \cdot (1 - A_r(T(t)))$$

$$\text{with } k_1(T(t)) = k_{A1}(T(t)) \text{ and } k_2(T(t)) = k_{A2}(T(t)) \cdot A(T(0))$$

Eq.(16) is gained by combining eq.(15) with eq.(8-2) and using eq.(7) to substitute $A_r(T(t))$. With eq.(16) the autocatalytic self heat rate curve in Fig. 3 was calculated. Eq.(16) is approximated.

$$(16)\qquad h(T(t)) = k_1(T(t)) \cdot (T_f - T(t)) + k_2(T(t)) \cdot (T_f - T(t)) \cdot \left(1 - \frac{T_f - T(t)}{\Delta T}\right)$$

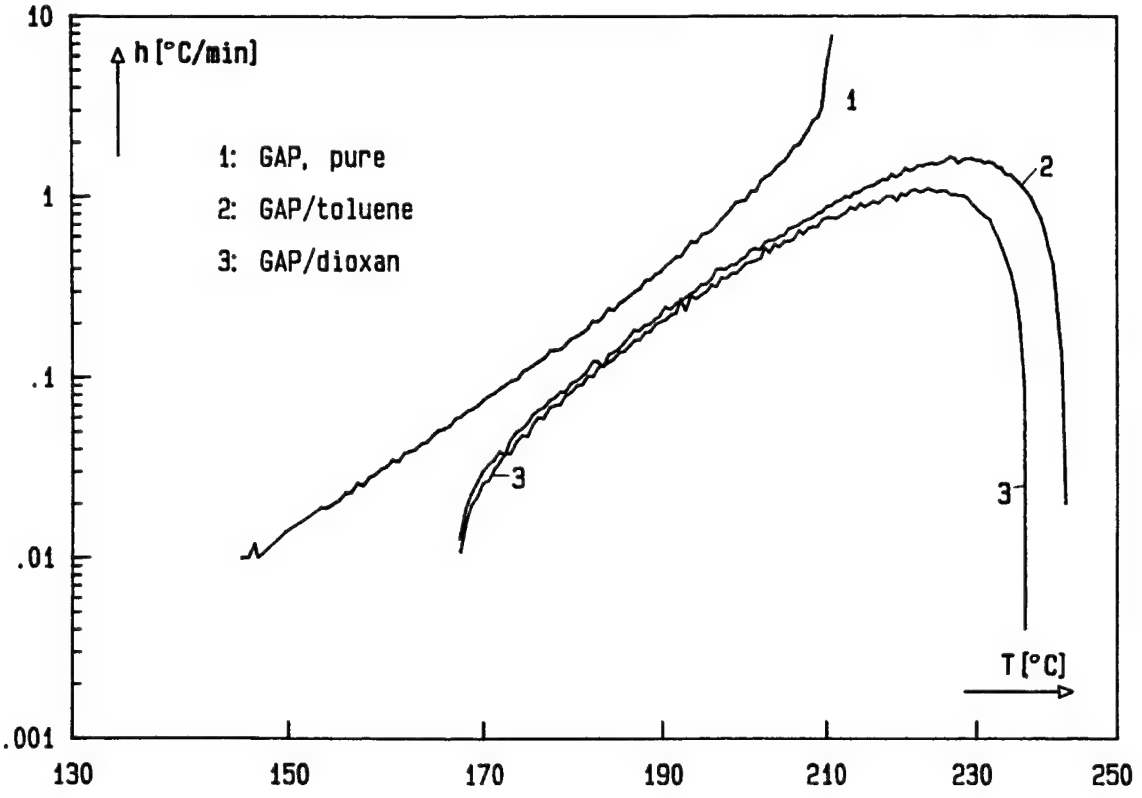

Fig. 4: Adiabatic self heat rates of uncured GAP and of uncured GAP dissolved in toluene and dioxan with 10 mass-% content.

3.3 Scaling of the experimental adiabatic self heat rate curves to $\phi = 1$

The scaling of the adiabatic self heat rate curves will be exemplified with the adiabatic self heating of non-cured GAP alone (ICT, batch 1 in Table 2) and the solution of this GAP in dioxan /2/.

3.3.1 Data used to show the scaling procedure

Fig. 4 shows the adiabatic self heat rates of GAP alone and GAP dissolved in toluene and in dioxan (about 10 mass-% of GAP in both solvents). The curves of the solutions have a defined final temperature T_{fMS}. GAP alone shows a transition to deflagration after the controllable part of the self heating as do other explosive substances /2/. The rate determining first reaction step of the GAP decomposition is assumed to be the formation of molecular nitrogen from the azido group, C-$\underline{N}$-N≡NI. This mechanistic model is supported by (1) the corresponding bond energy /3,4,5,6,7/, (2) the mass spectrometric investigation of nitrogen production /8/,

Table 1: Arrhenius parameters of the decomposition of GAP, determined by different methods.

method	ref.	m_s [mg]	T_0 [°C]	temp. range [°C]	Ea [kJ/mol]	Z [1/s]	lg(Z[1/s])
N_2-formation, mass spectrometry	/8/	~ 25	~ 120	140-170	176.6	n.m.	n.m.
DTA-measurements (heat rate to peak temp.)	/9/	n.m. (2)	~ 190	220-260	174.0	n.m.	n.m.
isothermal TGA	/10/	1.5-2.5	~ 170	180-205	164.9	$1.26 \cdot 10^{14}$	14.1
non-isothermal TGA	/10/	1.5-2.5	~ 170	180-220	164.9	$6.31 \cdot 10^{13}$	13.8
mass loss / FTIR	/10/	0.2-0.8	~ 240	240-260	177.0	$1 \cdot 10^{19}$	19.0
NH_3-formation / FTIR, [1]	/11/	n.m. (5)	~ 165	165-260	170.7	$3.548 \cdot 10^{15}$	15.55
isothermal TGA	/12/	~ 1	~ 170	170-240	135.7 [2]	$8.78 \cdot 10^{13}$	13.9
ARC, GAP / toluene	/2/	592	167	175-230	168.9	$7.814 \cdot 10^{14}$	14.89
ARC, GAP / dioxan	/2/	612	167	175-230	170.2	$1.116 \cdot 10^{15}$	15.05
CH_3-N_3	/13/	(120)	(155)	155-200	170.7	$2.85 \cdot 10^{14}$	14.455
C_2H_5-N_3	/14/	(100-600)	(187)	187-230	167.8	$3.30 \cdot 10^{14}$	14.519
n-propyl-N_3	/14/	(100-700)	(190)	190-226	164.9	$1.48 \cdot 10^{14}$	14.169
iso-propyl-N_3	/14/	(100-700)	(190)	190-223	161.1	$7.20 \cdot 10^{13}$	13.857

n.m. not mentioned in reference, values in brackets are estimated

[1] The monitored reaction sequence is probably the elimination of the acid HN_3 and the consecutive rate determining step of its decomposition into NH and N_2, which has a similar activation energy as the splitting reaction in C-$\underline{N}$-N≡NI. NH forms then NH_3 by H abstraction.

[2] The low activation energy may reflect the influence of evaporation.

(3) thermoanalytical investigations /9/ and previous investigations on alkylazides, see Table 1. The activation energy of the azido group decomposition or of the GAP decomposition should therefore be approximately equal to the bond energy of the RN-N_2 bond, which is given at 163.2 kJ/mol in /4/ and at 170 kJ/mol in /7/.

The activation energies determined from the ARC™ measurements agree well with the bond energy of the RN-N_2 bond and with the values stated in the literature listed in Table 1. The corresponding Arrhenius plots are shown in Fig. 5 and 6. The obtained correlation coefficients are with >0.999 high. The Arrhenius parameters determined from investigations of the unimolecular decomposition of the azido group of the gaseous azides methylazide and ethylazide /13,14/ represent the activation energy of the rate determining reaction step. The decrease in activation energy by increasing positive induction effect of the alkyl group indicates a stabilization of the nitrene functionality analogously to the stabilization of the radical functionality.

The consecutive stabilizing reactions of the nitrene formed by the loss of nitrogen in the C-N_3-group are very fast due to the high reactivity of the nitrene, which performs intramolecular and intermolecular insertion reactions in neighbouring chemical bonds. A polymerization by an imine functionality may also occur. It is also possible that the loss of nitrogen from the C-N_3-group and the insertion occur in a concerted or concomitant way /6/. The existence of intermolecular insertion reactions of GAP is supported by the following observations: (1) the formation of an unsolvable residue during the hydrolytic treatment of the cured GAP-binder and of GAP bonded propellants /15/, (2) the appearance and the increase of an unsoluble part with the ageing of uncured GAP and (3) the shift of the glass transition temperature determined by DMA with the ageing of the cured GAP-binder /16/.

3.3.2 Description of the scaling procedure

It will be shown that it is possible to scale the self heat rate curve of the GAP solution in such a way that it represents the self heating measured from GAP alone. This behaviour makes it possible to scale the measured data to $\phi = 1$ also, which means that no thermally inert mass is heated and therefore the adiabatic self heating of the energetic substance alone is simulated with the data of the measurements on the solutions. The scaling of the h(T)-data obtained from a solution of a decomposing substance was applied in /1/ also but not compared to the h(t)-data of the substance alone. Fig. 7 shows three sets of curves. The curve with a noise pattern in the middle is the measured adiabatic self heat rate of GAP/dioxan solution (10 mass-% GAP) with a ϕ-factor for the solution of value 1.25. The self heat rate curve h(T) calculated according to eq.(11) with $n = 1$ (which gives eq.(13)) and with $\phi = 1.25$ can be seen as the curve without a noise pattern. From the start temperature of 175°C on for the data evaluation, this calculated curve agree very well with the measured data. The calculated curve has been extrapolated down to 140°C. More concentrated solutions have lower experimental onset temperatures T_0.

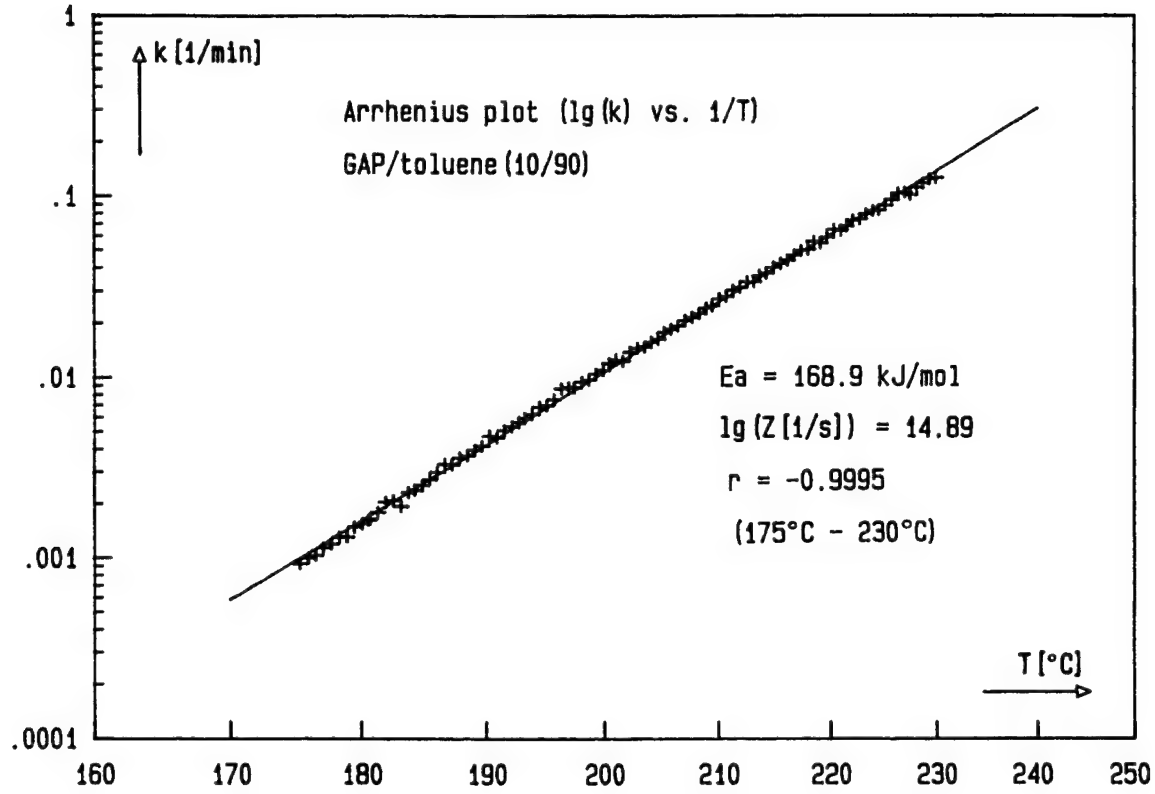

Fig. 5: Arrhenius plot of the GAP decomposition in toluene solution.

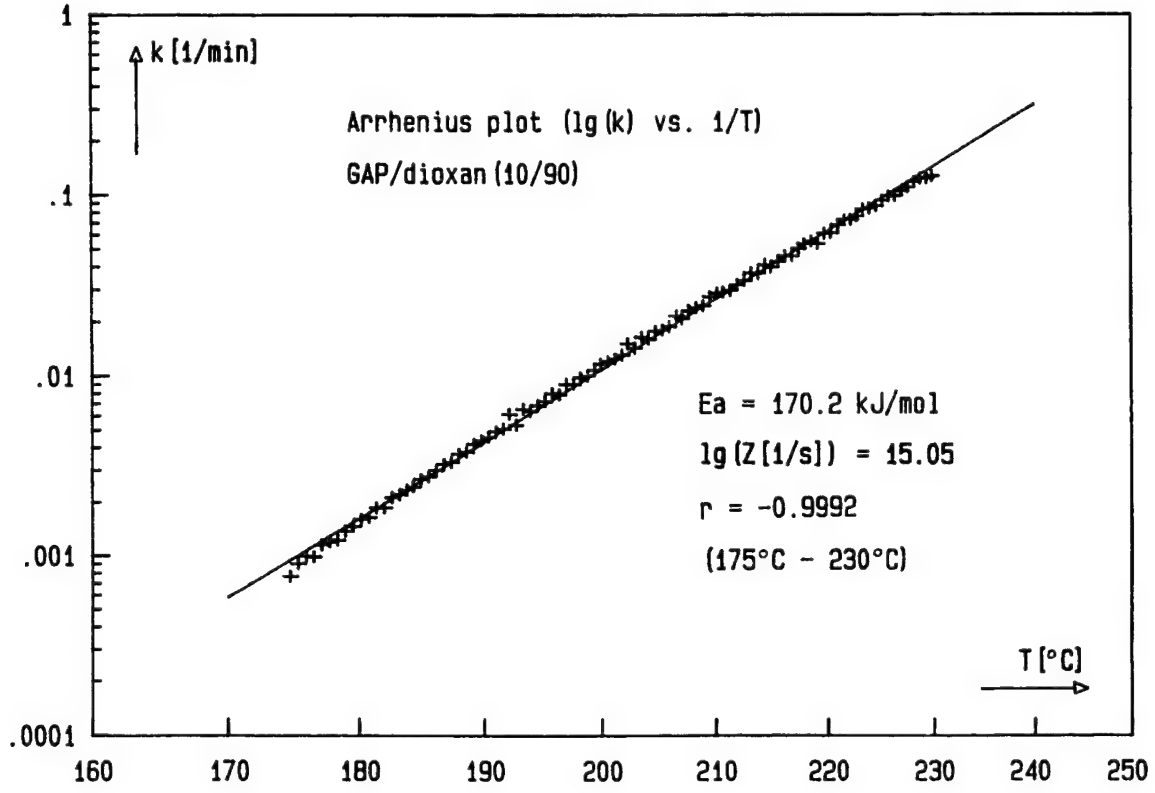

Fig. 6: Arrhenius plot of the GAP decomposition in dioxan solution.

Using eq.(11), h(T) can also be calculated for other ϕ-factors. With the factors ϕ_1 and ϕ_2, eq.(17) and eq.(18) are formulated for the entire measurement system, but omitting the index MS for reasons of better reading.

$$(17) \qquad h_1(T_1(t)) = k_{n,r}(T_1(t)) \cdot \Delta T_1 \cdot \left(\frac{T_{f1} - T_1(t)}{\Delta T_1} \right)^n \qquad \text{at } \phi_1$$

$$(18) \qquad h_2(T_2(t)) = k_{n,r}(T_2(t)) \cdot \Delta T_2 \cdot \left(\frac{T_{f2} - T_2(t)}{\Delta T_2} \right)^n \qquad \text{at } \phi_2$$

According to eq.(3), the following applies for the relation between the two temperature differences ΔT_i (exactly $\Delta T_{MS,i}$), the two final temperatures $T_{f,i}$ (exactly $T_{fMS,i}$) and the onset temperatures $T_i(0)$ (exactly $T_{MS,i}(0)$), eq.(19).

$$\Delta T = \phi_1 \cdot \Delta T_1 = \phi_2 \cdot \Delta T_2$$

$$(19) \qquad \phi_1 \cdot (T_{f1} - T_1(0)) = \phi_2 \cdot \Delta T_2$$

$$T_{f1} = \frac{\phi_2}{\phi_1} \Delta T_2 + T_1(0)$$

The temperature difference ΔT is the adiabatic temperature rise of the sample alone. Differences in the ϕ-factor result only by the different inert masses. Combining eq.(17) and eq.(19) the simulated self heat rate $h_1(T)$ can be calculated from the measured self heat rate $h_2(T)$ with eq.(20). The non-indexed temperature T(t) in eq.(20) and eq.(21) is the running variable.

$$(20) \qquad h_1(T(t)) = k_{n,r}(T(t)) \frac{\phi_2}{\phi_1} \Delta T_2 \left(\frac{\frac{\phi_2}{\phi_1} \Delta T_2 + T_1(0) - T_1(t)}{\frac{\phi_2}{\phi_1} \Delta T_2} \right)^n \qquad \text{with } T_1(t) \cong T(t)$$

To use eq.(20) the reaction rate constant is determined first from the experimental data that means from the $h_2(T)$-curve. Then the calculated data are scaled to other ϕ-factors according to eq.(20). The 'theoretical' self heat rate curves shown in Fig. 7 of virtual solutions of GAP with $\phi_1 = 1$ and $\phi_1 = 2$ have been calculated using eq.(20). The increase of the ϕ-factor from 1.25 to 2 reduces the measurable self heat rate considerably.

The experimental values itself can also be scaled to $\phi_1 = 1$. The appropriate equation is arrived at by dividing eq.(17) by eq.(18) and inserting the expressions from eq.(19), which results in eq.(21).

$$\frac{h_1(T(t))}{h_2(T(t))} = \frac{\phi_2}{\phi_1}\left(\frac{\frac{\phi_2}{\phi_1}\Delta T_2 + T_1(0) - T_1(t)}{T_{f2} - T_2(t)} \cdot \frac{1}{\frac{\phi_2}{\phi_1}}\right)^n$$

(21) with the following equalities and definition : $T_1(0) = T_2(0)$

$$T_1(t) = T_2(t) \cong T(t)$$

With eq.(21) the experimental curve $h_2(T)$ is scaled to $h_1(T)$ with the factor ϕ_1.

In Fig. 7 one can see the scaled experimental curve of the GAP/dioxan solution according to eq.(21) at $\phi_1 = 1$ as the curve with a noise pattern coinciding with the h(T)-curve calculated with eq.(20) for the condition $\phi_1 = 1$. Deviations occur when T(t) is greater than T_M, the temperature of the maximum of the experimental adiabatic self heat rate curve $h_2(T)$, as then $h_2(T)$ tends towards zero very quickly and a high scattering occurs in the experimental curve scaled to $\phi_1 = 1$. Non-existing measurements cannot be constructed so that the scaled experimental curve seems to be incomplete compared to the full theoretical curve at ϕ_1=1 and to the experimental curve at ϕ=1.25.

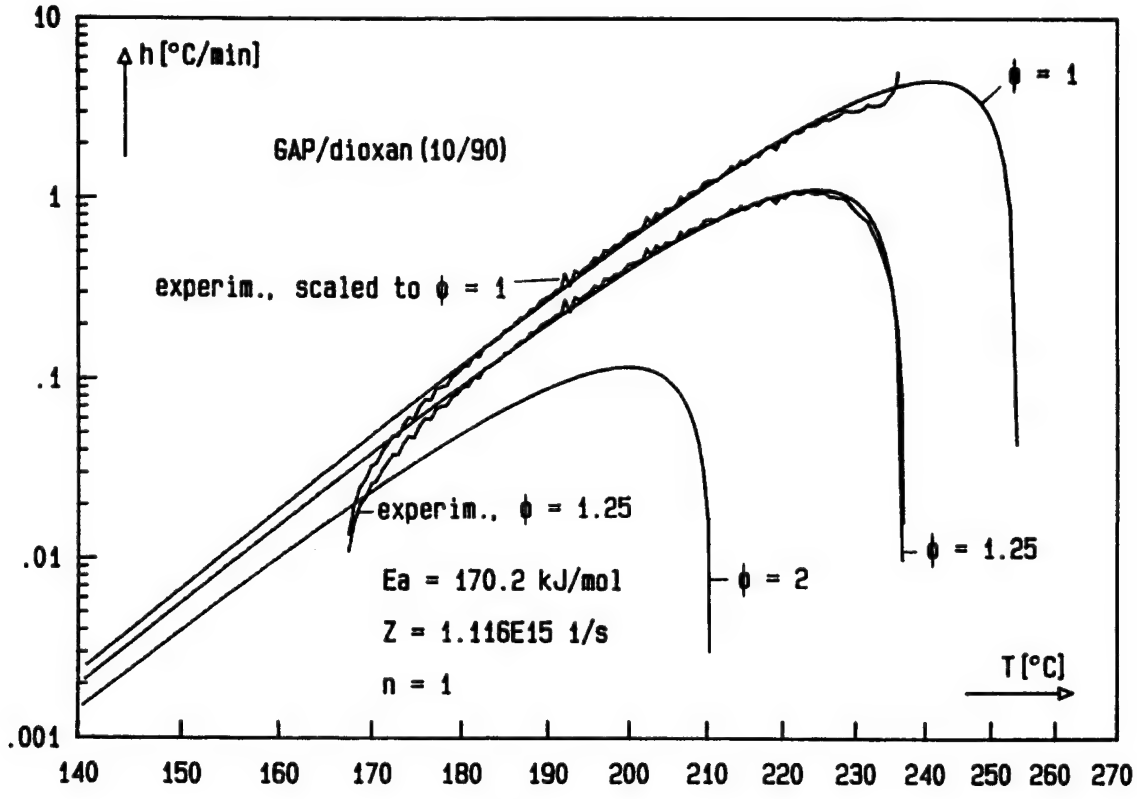

Fig. 7: Scaling of the adiabatic self heat rate of the GAP/dioxan solution to the ϕ-factors ϕ_1=1 and ϕ_1=2, smooth curves. The measured curve with ϕ=1.25 has a noise pattern. It is described also at ϕ=1.25, smooth curve. The experimental data have been scaled to ϕ_1=1 too, which is the curve with noise pattern on the scaled smooth curve with ϕ_1=1.

The adiabatic self heat rate curve of GAP alone, Fig. 4, has approximately the same slope in the middle part as the curves of the GAP solutions, which indicates at least a similar activation energy for the decomposition of GAP alone. The experimental ϕ-factor of the GAP solutions is 12.5 in relation to the weighed-in GAP. In contrast to the GAP solutions, pure GAP deflagrates under the measurement conditions stated at an experimental ϕ-factor of 6.2. Fig. 8 shows the theoretical h(T)-curves determined with the experimental curve of the GAP/dioxan solution as reference data and using eq.(20) with ϕ_1=12.5, ϕ_1=6.2 and ϕ_1=1. The curve with ϕ_1=1 is equivalent to a 'solution with 100% GAP', i.e. pure GAP without any thermally inert mass. The expression 'solution with 100% GAP' points to the fact that the decomposition takes place in the same way as it does in solution, that means homogeneous and without deflagration. The experimental data of the GAP/dioxan solution, now with reference to the GAP content of the solution, are described very well by eq.(20), as it was the case with the reference to the solution itself, see Fig. 7. The measured data of GAP alone with ϕ=6.2 are positioned well on the calculated h(T)-curve with ϕ_1 = 6.2 (using eq.(20)), and the measured data scaled to ϕ_1=1 are equally well described by the theoretical h(T)-curve 'solution with 100% GAP' with ϕ_1=1.

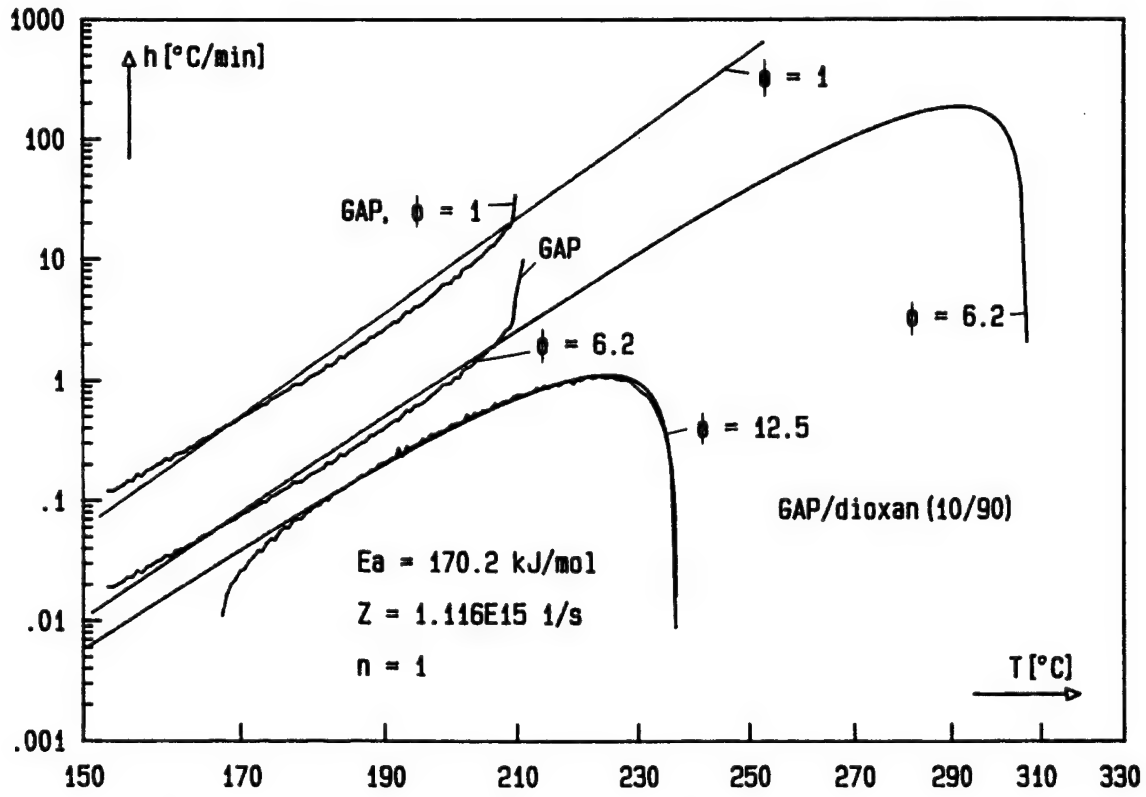

Fig. 8: Scaling of the adiabatic self heat rate of GAP dissolved in dioxan to ϕ_1=6.2 and ϕ_1=1, both curves are smooth. The solution type curve with a noise pattern is the experimental curve with a ϕ-factor equal to 12.5 with regard to the GAP content. It is also described at ϕ_1=12.5, smooth curve. The measured data of uncured GAP alone have ϕ=6.2 and are scaled to ϕ_1=1, these both curves have a noise pattern.

The deviation of the experimental GAP curve from the theoretical curve with ϕ_1=6.2 is explainable. Some of the GAP has been condensed in the vertical connection tube of the pressure capillary line to the pressure transducer, so the actual ϕ-factor has been increased somewhat during the measurement. This is expressed in the figure by a shift of the experimental GAP curve below the theoretical curve at increased temperatures. In the case of the solutions the vertical connection tube acts as a reflux condenser.

The conclusion is the measured data of GAP alone and the measured data of GAP in the dioxan solution agree well by the scaling with the associated ϕ-factors. This is the argument to use the experimental data of solutions of the energetic substances to get information on the decomposition behaviour of the energetic substances alone. The decomposition of the discussed binders and plasticizers in the propellant matrix can be assumed to be a homogeneous one, because with such substances the decomposition is statistically distributed in the propellant.

4. Substances investigated and measuring conditions

The adiabatic self heating was measured from the following plasticizers and uncured binders with an ARC™:

- mixture (58.8 / 41.2 in mass-%) N-methyl-/N-ethyl-NENA (Me/Et-NENA) from ICI / USA; NENA means N-(2-nitratoethyl)-nitramine
- DANPE, 1,5-diazido-3-nitraza-pentane, from Rocketdyne, USA
- GAPA, short chain GAP with N_3-end groups instead of OH, from Rocketdyne
- EGBAA (technical name A17), ethylene glycol-bis-(α-azidoacetate), from ICT
- Octylazide, from ICT, as model substance, not intended for use in explosives
- GAP-AA-2000, GAP with α-azidoacetic acid esterified OH-end groups, from ICT
- GAP-AA-500, as GAP-AA-2000, however short chains, from ICT
- uncured PolyGLYN, (also named PG in USA), poly-glycidylnitrate, from ICI / UK
- uncured GAP, poly-glycidylazide, from SNPE, France
- uncured GAP, poly-glycidylazide, from ICT

All substances were used as delivered. GAP and PolyGLYN are formally poly-(1,2-propylene glycol) or poly-(1,2-propylene oxide) with the energetic group attached to the lateral CH_3-group. Three types of energetic groups are represented with these compounds: the organic nitric acid ester group (NENA, PolyGLYN), the nitramine group (NENA, DANPE) and the organic azido group (in all but NENA and PolyGLYN). The substances were investigated as solutions in toluene p.A. grade with about 10 mass-% contents on the energetic substances.

The amount of weighed-in toluene solution was between 5.8g and 6.7g, which means an amount of energetic substance between 0.59g and 0.67g. Such amounts give a high measuring sensitivity with the ARC™. Together with the somewhat varying measurement cell masses, thermal inertia values between 1.21 and 1.27 for the solutions were determined as well as between 12.0 and 12.7 for the pure

energetic substances. Therefore the measurement conditions can be seen as identical for all substances in the meaning that the small differences in the experimental ϕ-factor do not change the course of the decomposition reactions. The measuring cells have been spherical containers made from titanium with one inch in diameter.

5. Results and discussion

Fig. 9 shows an overview of the measured adiabatic self heat rate curves of the substances investigated. Because of cross over in the curves, GAP-AA-500, GAP (ICT) and octylazide can be seen in Fig. 10 together with GAP (SNPE). No smoothing was applied to the data obtained from the ARC™. The figures give a first information on (1) the temperature range of the decomposition and (2) from the maximum values of the self heat rate curves and from their 'curve widths' (temperature range) qualitatively on the released energies. It was possible to describe the overall decomposition reaction for all substances with a reaction of first order. A significant secondary reaction was found in the case of Me/Et-NENA. The other substances did not show any or only negligible secondary reactions. Fig. 11 shows the entire adiabatic self heat rate curve for Me/Et-NENA. Presumably, the second reaction is the decomposition of the nitramine group in connection with the residual part of the already decomposed nitric acid ester group. In this case only the first reaction range has been evaluated, which is associated to the decomposition of the nitric acid ester group. The onset temperature of decomposition was between 159°C and 174°C for the azido compounds, in the case of the nitric acid ester groups it was 130°C for Me/Et-NENA and 146°C for PolyGLYN. In order to remove the remaining influences of differing sample amounts and differing ϕ-factors on the evaluation of the data, the self heat rate curves were normalized to ϕ=1 with regard to the energetic substance alone, see Table 2. If solutions are considered, they are normalized to ϕ=1 with regard to the solution and to the weighed-in amount of the energetic substance. Fig. 12 shows the self heat rate curves scaled to ϕ=1 in relation to the solution of some of the substances. In the main, the sequence of the curves in this h(T)-graph is the same as the one in the graph of the experimental curves, because of nearly the same experimental conditions. However, in the case of substances, which show a similar experimental adiabatic self heat rate, it is possible that the sequences are reversed by the normalization, for example in the case of GAPA compared to GAP-AA-2000.

The characteristic experimental data are listed in Table 2. T_0 and h_0 are the onset data of the adiabatic self heating, T_M and h_M are the values of the maximum of the h(T)-curve and T_f its final temperature. Further data are listed in Table 2 on the Arrhenius parameters for the overall decomposition reactions of first order, on the released energies and on the adiabatic self heatings at ϕ=1 with regard to the energetic substances, such as the associated temperatures predicted for given adiabatic self heat rates h. The activation energies are between 157 kJ/mol and 169.4 kJ/mol for azido compounds. Me/Et-NENA and PolyGLYN have activation energy values of 165.1 kJ/mol and 166.8 kJ/mol respectively. The correlation coefficients of all Arrhenius plots are higher than 0.99. The values of the Ea's lie in the

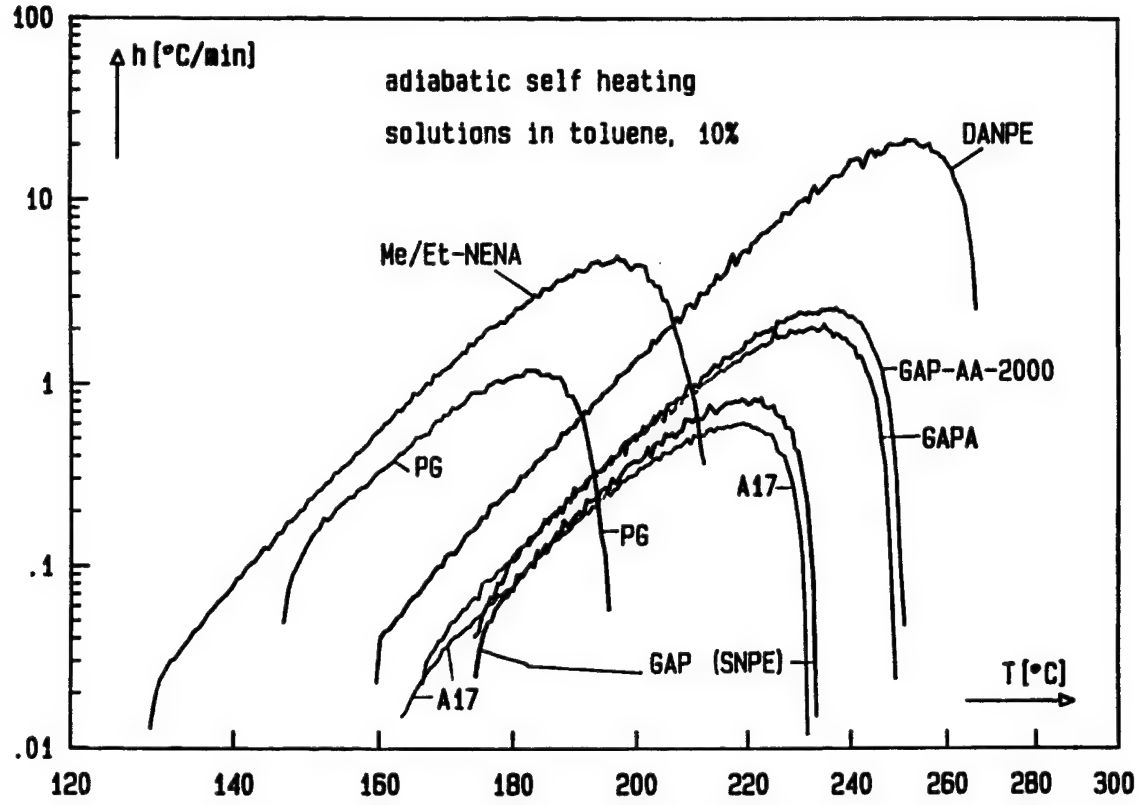

Fig. 9: Adiabatic selfheating of plasticizers and uncured binders, measured in solutions of toluene with 10 mass-% content, part 1.

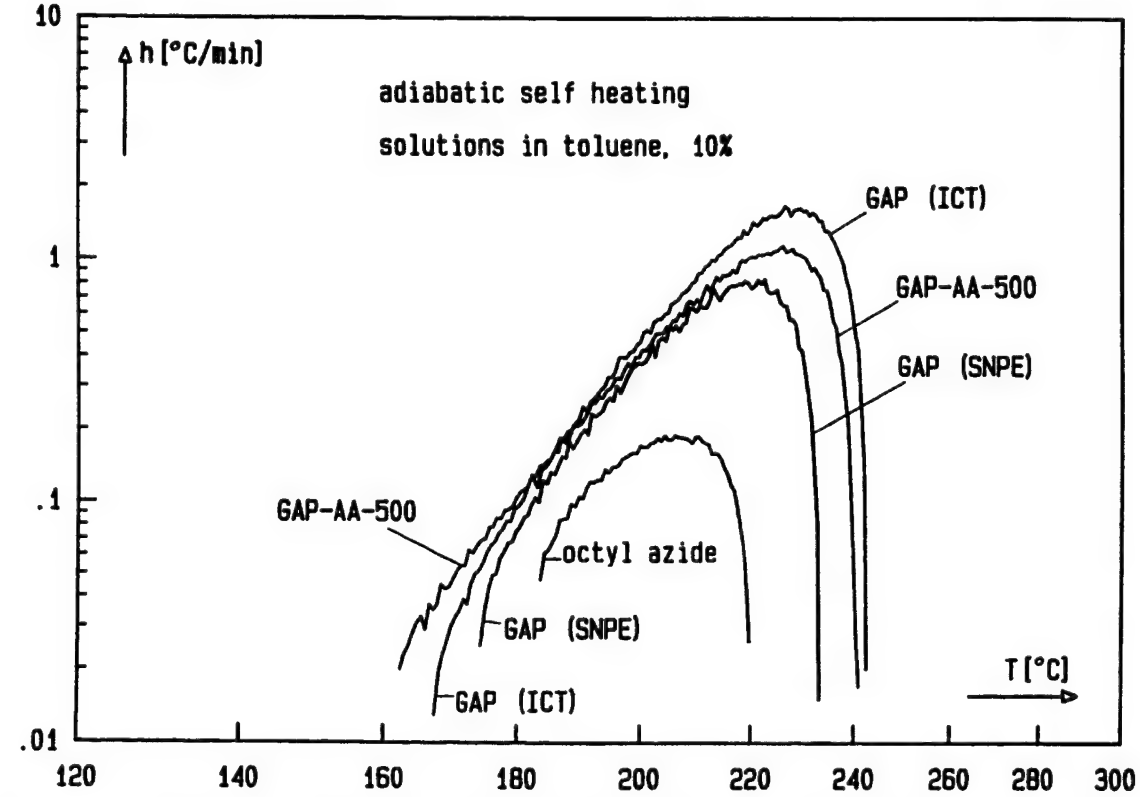

Fig. 10: Adiabatic selfheating of plasticizers and uncured binders, measured in solutions of toluene with 10 mass-% content, part 2.

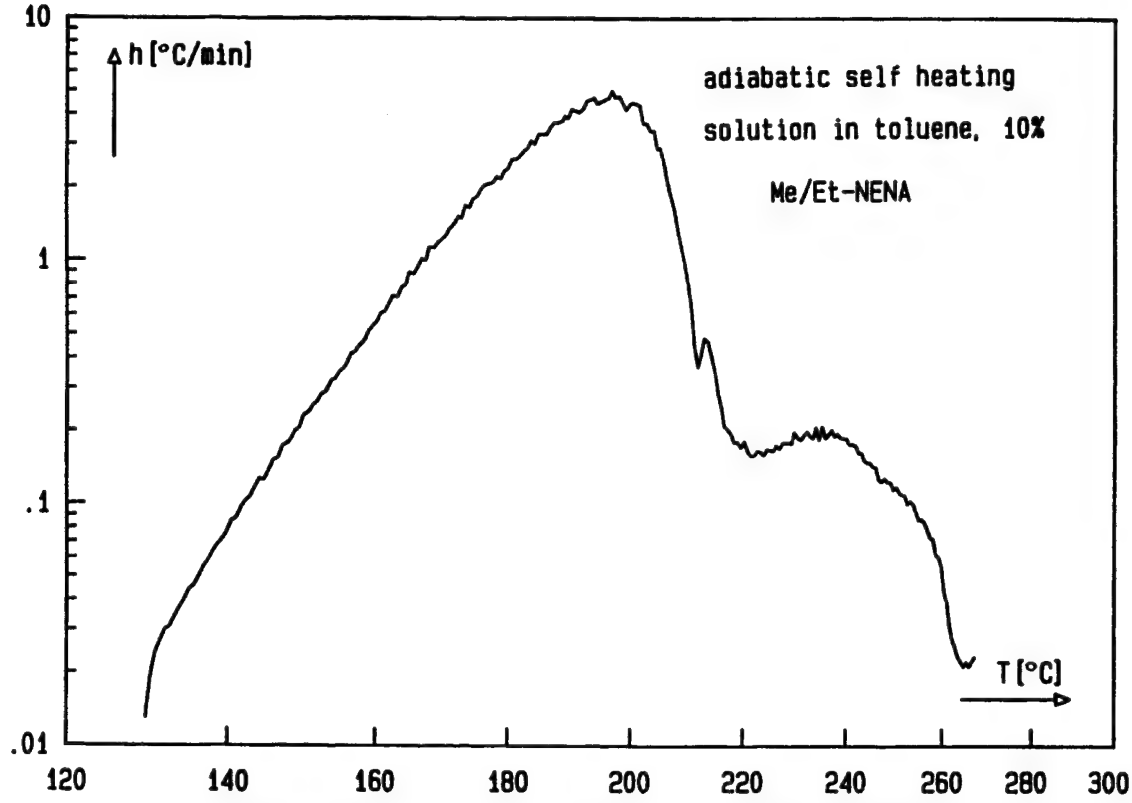

Fig. 11: Complete adiabatic self heat rate curve of Me-/Et-NENA, measured in solution of toluene with 10 mass-% content.

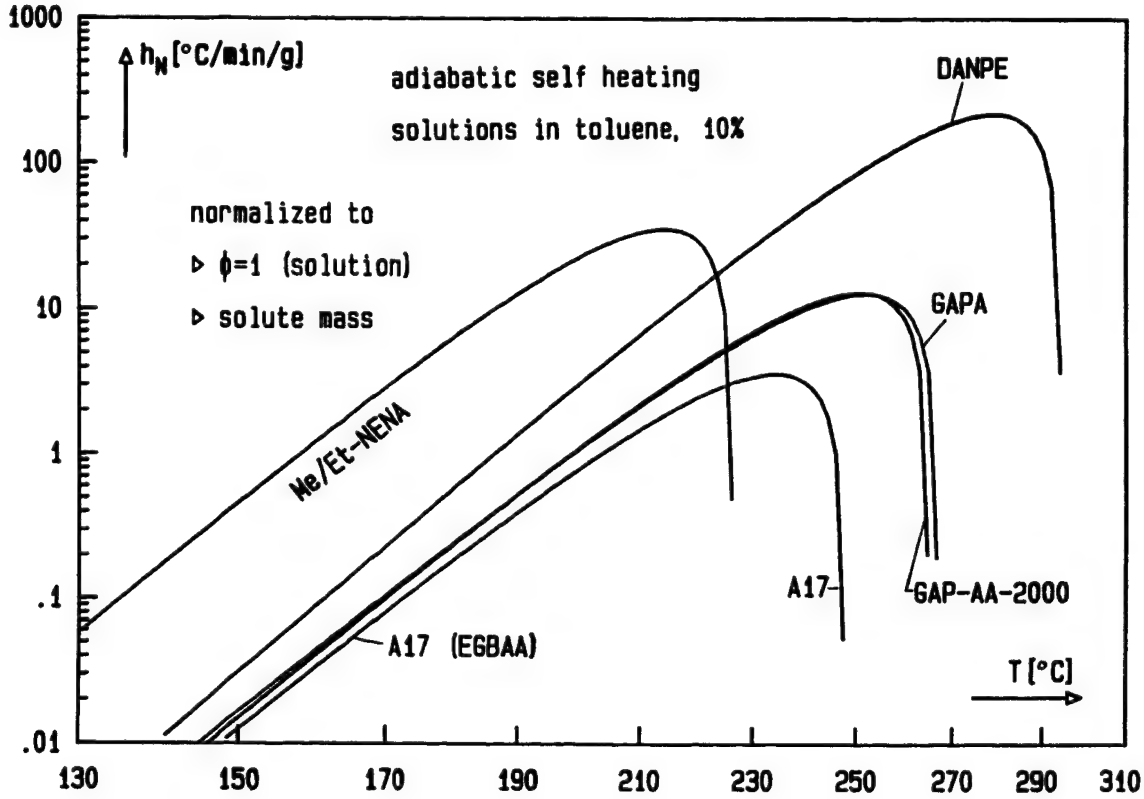

Fig. 12: Calculated adiabatic self heat rate curves of some of the investigated compounds, scaled to ϕ=1 and normalized to the amount of weighed-in energetic substance.

Table 2: Characteristic data of the adiabatic selfheating of plasticizers and binders from the measurments on their solutions in toluene, Arrhenius parameters of the decomposition, released heats Q_A and data for curves scaled to a thermal inertia $\phi = 1$ with regard to the energetic substances alone.

	GAP lot 1 ICT	GAP lot 2 ICT	GAP SNPE	EGBAA (A17) ICT	GAP-AA-2000 ICT	GAP-AA-500 ICT	Octyl-azide ICT	Me/Et-NENA ICI	PolyGlyn ICI	DANPE USA	GAPA USA
amount solution [g]	5.920	6.744	5.883	6.005	6.001	6.002	6.003	6.006	5.988	6.143	6.215
sample [g]	0.592	0.681	0.591	0.595	0.612	0.597	0.600	0.596	0.596	0.613	0.615
ϕ -solution	1.25	1.24	1.27	1.26	1.22	1.27	1.22	1.21	1.21	1.27	1.26
ϕ -sample	12.5	12.3	12.6	12.7	12.0	12.7	12.2	12.2	12.2	12.7	12.7
T_0 [°C]	167.4	169.9	174.3	161.4	174.1	162.3	177.6	129.6	146.7	159.0	166.3
h_0 [°C/min]	0.013	0.017	0.025	0.013	0.041	0.020	0.026	0.013	0.049	0.028	0.023
T_M [°C]	229.3	227.6	218.7	218.4	237.1	225.9	205.9	196.9 *)	183.4	251.4	234.7
h_M [°C/min]	1.63	1.55	0.82	0.598	2.62	1.14	0.188	5.00 *)	1.19	21.50	2.12
T_f [°C]	242.5	242.6	233.1	231.5	253.4	243.1	219.7	211.8 *)	205.5	266.4	249.1
	Arrhenius parameters and released heats Q_A calculated from the self heat rate curves										
Ea [kJ/mol]	168.9	167.7	169.4	162.2	162.4	154.6	157.0	165.1	166.8	167.3	157.9
Z [1/sec]	7.814E14	6.106E14	9.005E14	1.340E14	1.482E14	1.926E13	2.899E13	1.449E16	2.042E16	9.903E14	4.534E13
Q_A [J/g]	1995	1884	1573	1861	2000	2117	1074	2048 *)	1290	2822	2204
	predicted temperature in °C at a self heat rate h in °C/min, calculated for the energetic substance alone ($\phi = 1$)										
25 µW/g	114.3	113.6	115.7	112.5	111.7	107.6	116.0	85.0	89.6	106.1	115.7
50 µW/g	119.5	118.9	121.0	117.9	117.0	113.1	121.7	89.6	94.3	111.1	121.0
h=0.02	140.8	140.2	142.4	139.9	138.9	135.7	145.2	108.0	113.1	131.6	142.4
h=0.05	148.7	148.2	150.4	148.1	147.1	144.2	154.0	114.9	120.1	139.2	150.4
h=0.10	155.0	154.5	156.7	154.6	153.5	150.8	161.0	120.3	125.6	145.2	156.7
h=0.50	170.2	169.8	172.0	170.5	169.3	167.1	178.1	133.3	139.0	159.8	172.0
h=1.00	177.1	176.7	178.9	177.7	176.4	174.6	185.9	139.2	145.0	166.4	178.9

25µW/g ≡ 7.2 E-4 °C/min with C = 2.092 J/K/g *): total curve: Q_A = 3517 J/g, T_{M2} =234.6°C, h_{M2} =0.205°C/min, T_{f2} =263.5°C

range of the bond energy of the CN-NN bond (161 to 170 kJ/mol) of the azido group and of the CO-NO_2 bond (160 to 170 kJ/mol) of the nitric acid ester group. GAP-AA-500 and octylazide have somewhat lower activation energies. In the case of octylazide to one part this may be originating from the relatively small self heat rates measured. To the other part the lower activation energy of octylazide can be caused by the stabilizing effect of the n-octyl group (positive induction effect) for the nitrene functionality. The activation energy of the C-N_3-group decomposition is decreasing with increasing size of the alkyl group, see Table 3.

Table 3: Activation energies of the decomposition of some alkylazides /13,14/.

substance	methylazide	ethylazide	n-propylazide	iso-propylazide
Ea [kJ/mol]	170.7	167.8	164.9	161.1

The adiabatic heat generation rate can be determined from the adiabatic self heat rate curves. For this, the data of the specific heat as a function of temperature are required of the solvent, the reactants, the decomposition products and the measuring cell. In addition the respective masses of the substances involved are needed also. So far only little is known about the decomposition products. In a first approximation, the specific heat values are used as stated in section 2.2 to calculate the ϕ-factor. This results in the formulation of the heat generation rate dQ_A/dt of a decomposing substance A according to eq.(22).

$$(22)\qquad \frac{dQ_A(T(t))}{dt} = C_S \cdot m_S \cdot \frac{dT(t)}{dt} + C_{LM} \cdot m_{LM} \cdot \frac{dT(t)}{dt} + C_M \cdot m_M \cdot \frac{dT(t)}{dt}$$

Q_A released heat from the decomposition of substance A in dimension of energy. In Table 2 Q_A is given normalized to the weighed-in amount of the energetic substance. This normalization is not included in eq.(22).
C_i specific heat of substance i in dimension of energy/mass/Kelvin
m_i mass of substance i
dT/dt self heat rate measured of the system 'energetic substance - solvent - measurement cell'
Index S: means the energetic substance or sample
Index LM: means the solvent
Index M: means the measuring cell

Using the enthalpy of reaction ($-\Delta H_{R,A}$) for the decomposition of the substance A according to a reaction of the first order, the heat generation rate dQ_A/dt is given also by eq.(23), where A(T(t)) is in mol, $M_A(T(t))$ is the actual mass of A and m_A is the molar mass of A.

$$(23)\qquad \frac{dQ_A(T(t))}{dt} = -\frac{dA(T(t))}{dt}\cdot(-\Delta H_{R,A}) = -\frac{dM_A(T(t))}{dt}\cdot\frac{1}{m_A}\cdot(-\Delta H_{R,A})$$
$$= (-\Delta H_{R,A})\cdot k_1(T(t))\cdot A(T(t_0))\cdot \exp(-k_1(T(t))\cdot t)$$

Figs. 13 and 14 show the dQ_A/dt curves calculated using eq.(22) for the plasticizers GAPA and A17 (EGBAA) as examples, once as a function of temperature (used as 1/T with T in Kelvin on the abscissa but indicated in °C) and once as a function of

the experimental self heat time. The different reaction rates can be recognized in the time representation. The A17 reacts considerably slower than GAPA as the increase in temperature is slower. By integrating the heat generation rate as a function of time, one arrives at the heat Q_A generated, which is 2204 J/g for GAPA and 1861 J/g for A17. Table 2 contains all the Q_A-values and also shows the extrapolated temperatures at which a heat generation rate of 25µW/g and 50µW/g would be measured. Me/Et-NENA and PolyGLYN have the lowest temperature values, they are 85°C and 89.6°C for 25µW/g. The values of the compounds with azido groups are all significantly greater than 100°C. DANPE has a relatively low value at 106.1°C, the values for the GAP samples are about 114°C. Fig. 15 shows the adiabatic self heat rate as function of the normalized self heat time. The experimental self heat time values were normalized using the respective ϕ-factor in relation to the weighed-in energetic substance. For a number of the substances investigated the adiabatic self heat rates can be seen in the time period from the times corresponding to h=0.05°C/min to the times corresponding to their maximums at h_M. The scaling with the ϕ-factor gives the approximate time ranges of the decomposition reaction of the energetic substances alone.

The presented data evaluation includes the approximations described in section 2.2. The obtained kinetic data for the decomposition reactions agree with literature data and with the results of other measuring methods. The conclusion is the approximations made for the evaluation of the ARC™ data seem not to influence it. This means the adiabatic selfheating can be used as a method of thermal analysis to assess the energetic substances with regard to (1) the decomposition

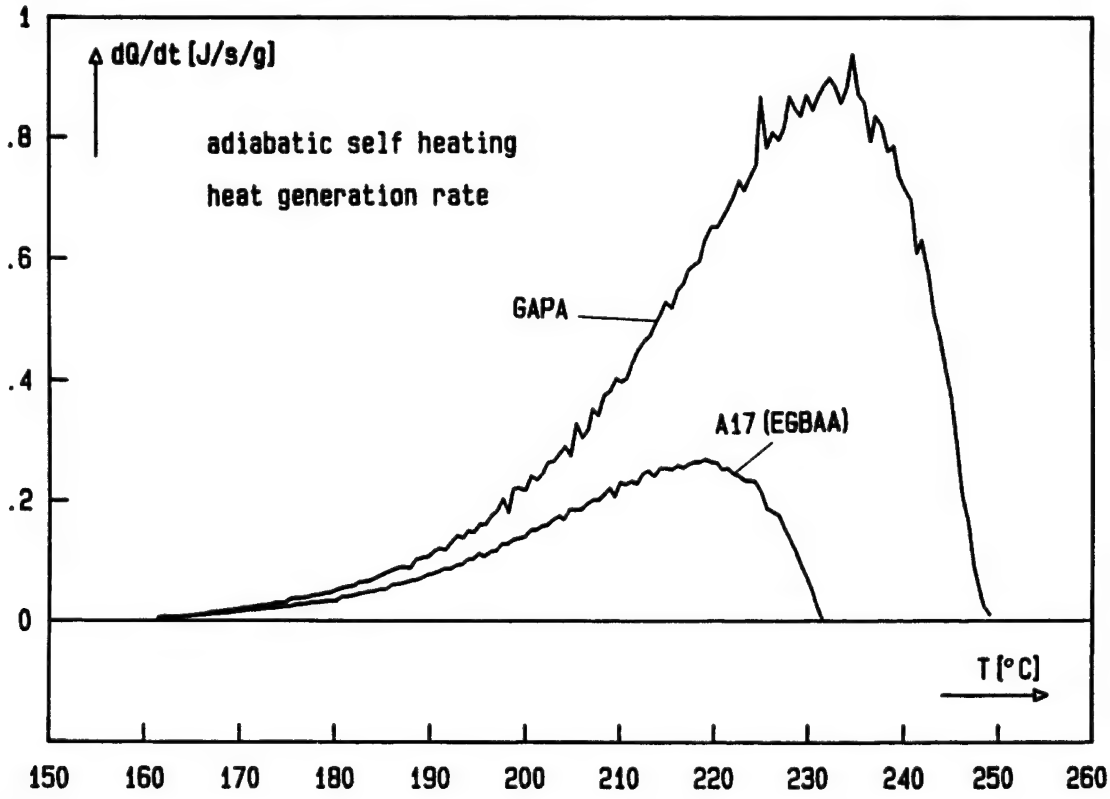

Fig. 13: Adiabatic heat generation rates of the plasticizers GAPA and EGBAA (A17) as function of the temperature reached by the selfheating.

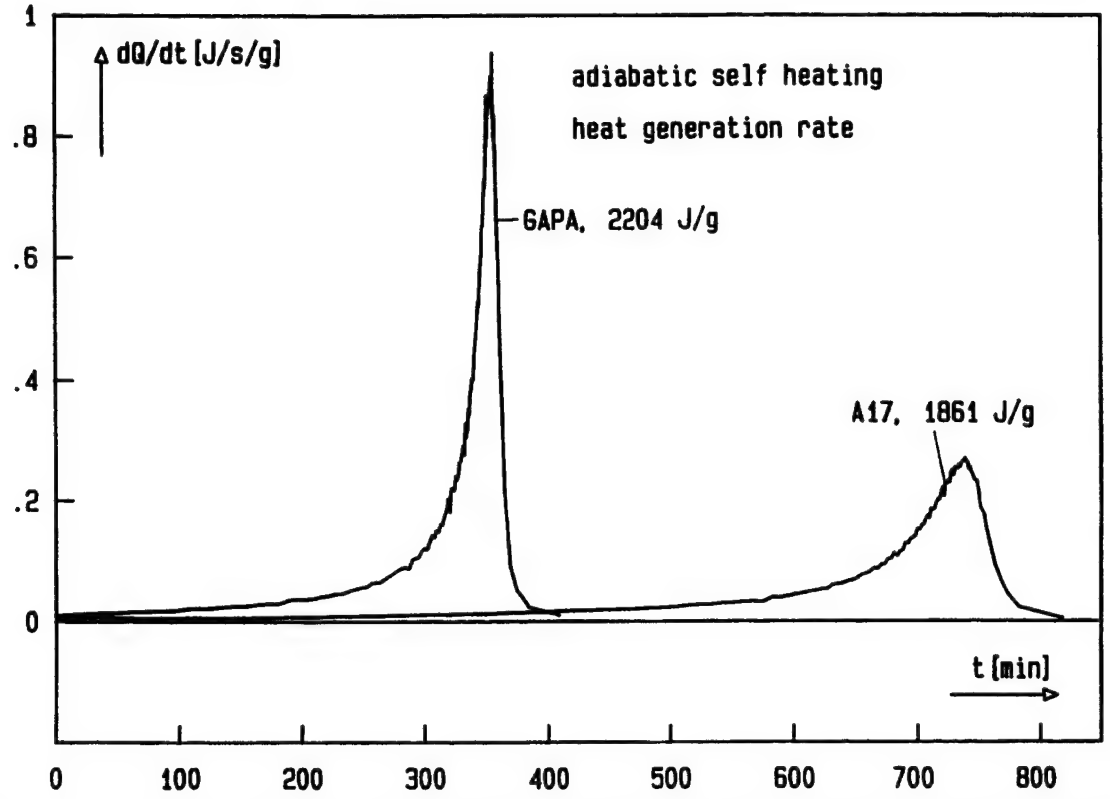

Fig. 14: Adiabatic heat generation rates of the plasticizers GAPA and EGBAA (A17) as function of the self heat time.

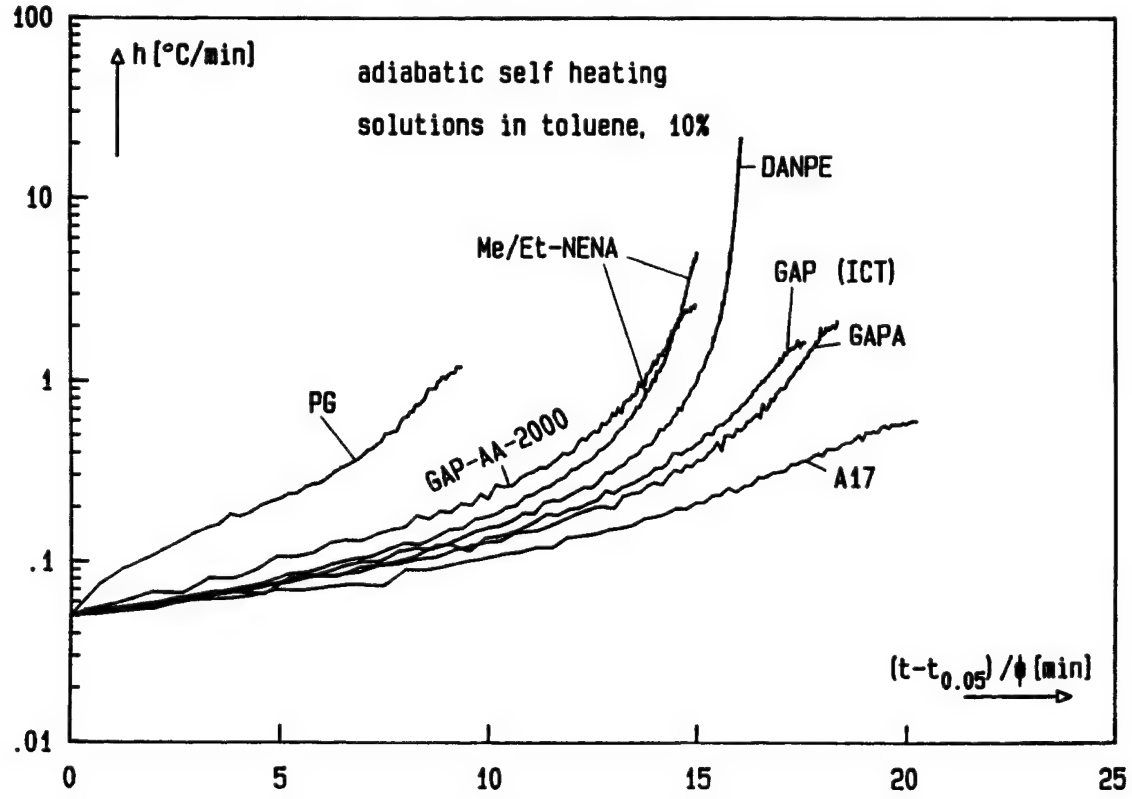

Fig. 15: Adiabatic self heat rates of some of the investigated compounds as function of the self heat time, normalized with the corresponding ϕ-factor related to the energetic substance alone. The curves are shown from h=0.05°C/min on up to the maximums h_M of the h(T)-curves.

temperature range, (2) the Arrhenius parameters obtained from the adiabatic self heat rate curves, (3) the heat generation and (4) the heat generation rate. The last two quantities contain a systematic error because of the approximations in the specific heats, but they are useable for comparative purpose.

6. Summary

The adiabatic self heat rates of more recent plasticizers and non-cured binders with azido groups, nitramine groups and nitric acid ester groups were measured with an ARC™ in toluene solutions of the energetic substances with contents of about 10 mass-%. The following substances were investigated: (1) mixture (58.8 / 41.2 in mass-%) N-methyl-/N-ethyl-NENA, (2) DANPE, 1,5-diazido-3-nitraza-pentane, (3) GAPA, short chain GAP with N_3-end groups instead of OH-end groups, (4), EGBAA (A17), ethylene glycol-bis-(α-azidoacetate), (5) octylazide, (only model substance, not intended for use in explosives), (6) GAP-AA-2000, GAP with α-azidoacetic acid esterified OH-end groups, (7) GAP-AA-500, as GAP-AA-2000, however short chains, (8) uncured PolyGLYN, poly-glycidylnitrate, (9) uncured GAP, poly-glycidylazide, one manufacturer, (10) uncured GAP, poly-glycidylazide, another manufacturer.

Using weighed-in amounts of energetic substance between 0.59g and 0.67g a high measurement sensitivity was achieved with the ARC™. As the measurements were made in a closed measuring system, the results were not falsified by evaporation. The investigations in solutions make a controlled observation of the decomposition reactions possible. The energetic substances alone would deflagrate after a short time period of controllable selfheating. The onset temperatures of decomposition were determined to be between 159°C and 174°C for compounds with azido groups. They have the values of 130°C and 146°C for Me/Et-NENA and PolyGLYN, which contain nitric acid ester groups. With the data measured one can classify the substances according to the decomposition temperature range, the energy released (heat generation Q_A) and the rate of the energy release (heat generation rate dQ_A/dt). It was possible to apply a reaction of first order to all investigated substances for the main decomposition range. A definite secondary reaction was observed only in the case of Me/Et-NENA. The activation energies are between 157 kJ/mol and 169.4 kJ/mol for the compounds with azido groups. Me/Et-NENA and PolyGLYN show activation energies of 165.1 kJ/mol and 166.8 kJ/mol respectively. The values are in the range of the bond energy of the CN-NN bond (161 to 170 kJ/mol) of the azido group and of the $CO-NO_2$ bond (160 to 170 kJ/mol) of the nitric acid ester group. With the examples uncured GAP alone and uncured GAP dissolved in dioxan, it was shown that the measured adiabatic self heat rate of the solution can be scaled to those of the energetic substance alone. The procedures to do this have been described. From the adiabatic self heat rates scaled to $\phi=1$ with respect to the energetic substance, temperatures were extrapolated for which a heat generation rate of 25µW/g and 50µW/g is to be expected. Me/Et-NENA and PolyGLYN have the lowest temperature values, they are 85°C and 89.6°C for 25µW/g. The corresponding values of the compounds with azido groups are all significantly higher than 100°C. DANPE has a relatively low value at 106.1°C, the values for the GAP samples are about 114°C.

7. Literature

/1/ D. I. Townsend, J. C. Tou, Thermochim. Acta 37, 1 (1980).

/2/ M.A. Bohn, F. Volk
"Adiabatische Selbstaufheizung bei Treib- und Explosivstoffen"
Paper 8 in Proceed. 24th Internat. Annual Conference of ICT, 1993.
Fraunhofer-Institut für Chemische Technologie, ICT.

/3/ Saul Patai (Ed.)
"The Chemistry of the Azido Group"
Interscience Publishers, Wiley, 1971.

/4/ A. Treinin, chapter 1 in /3/

/5/ Eric F.V. Scriven (Ed.)
"Azides and Nitrenes"
Academic Press, London, Orlando (USA), 1984.

/6/ E.P. Kyba, chapter 1 in /5/

/7/ H. Bock, R. Dammel
"Die Pyrolyse von Aziden in der Gasphase"
Angew. Chemie 99, 518-540 (1987).

/8/ M. Farber, S. P. Harris, R. D. Srivastava, Combust. Flame 55, 203 (1984).

/9/ N. Kubota, T. Sonobe, Propell. Expl. Pyrotech. 13, 172 (1988).

/10/ J. K. Chen, T. B. Brill, Combust. Flame 87, 157 (1991).

/11/ H. Krause, A. Pfeil
"FTIR-Untersuchungen an Pyrolyseprodukten von GAP"
Paper 8 in Proceed. 21st Internat. Annual Conference of ICT, 1990.
Fraunhofer-Institut für Chemische Technologie, ICT.

/12/ Y. Oyumi, Propell. Expl. Pyrotech. 17, 226 (1992).

/13/ M. S. O'Dell, B. de Darwent, Can. J. Chem. 48, 1140 (1970).

/14/ G. Geiseler, W. König, Z. Phys. Chem. 227, 81 (1964).

/15/ M.A. Bohn, R. Schweppe, W. Weisweiler
"Recovering of components from plastic bonded propellants"
Waste Management 17, 175-185 (1997).

/16/ M.A. Bohn, P. Elsner
"Torsions-DMA-Glasübergang der Binderelastomere GAP-N100 und HTPB-IPDI als Funktion der Alterung"
Paper 120 in Proceed. 27th Internat. Annual Conference of ICT, 1996.
Fraunhofer-Institut für Chemische Technologie, ICT.

Self ignition modelling method based on microcalorimetry measurements

A. FABRE, J. BATAILLET.
DGA/ETBS Route de Guerry, Carrefour Zéro Nord, BP 712, 18015 Bourges Cedex (France).

ABSTRACT

The decomposition of nitric ester-based gun propellants is accompanied by a release of heat which can be measured by means of microcalorimetry and which can be hazardous enough to cause self ignition. Indeed, the gun propellant is a non heat conductive material, so there is competition between heat production and heat evacuation, competition which ends either in temperature equilibrium or ignition (1).

There are two possible ways for determining the ignition risk :

- the self-ignition test, which consists in maintaining a gun propellant charge at constant temperature until it ignites or until a temperature plateau is obtained,
- simulating the heat released by the gun propellant charge.

This communication is divided into 4 parts :

- self ignition test (experimental part)
- self ignition model
- microcalorimetry measurements
- examples (comparison between model and experience).

It gives the description of the self ignition test and facilities. It briefly presents the modelling calculation method of the phenomenom. Experimental results are compared with those obtained by modelling from microcalorimetry tests.

RESUME

La décomposition des esters nitriques des poudres propulsives est accompagnée d'une libération de chaleur qui peut être mesurée au moyen de la microcalorimétrie et qui peut s'avérer suffisamment dangereuse pour provoquer l'autoinflammation. En effet, la poudre propulsive est un matériau non conducteur aussi, il y a compétition entre la production et l'évacuation de chaleur qui aboutit soit à un équilibre thermique soit à une autoinflammation (1).

Il existe deux voies possibles de détermination du risque d'autoinflammation :

- l'épreuve d'autoinflammation, qui consiste à maintenir un lit de poudre propulsive à température constante jusqu'à l'autoinflammation ou jusqu'à l'obtention d'un plateau de température,
- la simulation de la chaleur libérée par la poudre propulsive.

Cette communication est divisée en 4 parties :

- l'essai d'autoinflammation (partie expérimentale),
- le modèle de simulation de l'autoinflammation,
- les mesures de microcalorimétrie,
- les exemples (comparaison entre le modèle et l'expérience).

Elle donne la description de l'essai d'autoinflammation. Elle présente brièvement les modalités de calcul de modélisation de ce phénomène. Des résultats expérimentaux sont comparés avec ceux obtenus par modélisation à partir des essais de microcalorimétrie.

1 - SELF-IGNITION TRIAL

The term "self-ignition" refers to the spontaneous inflammation of gun propellant at constant temperature.

The compass of this trial includes the simple or double base propellant with nitro-cellulose, which degrade according to an exothermal mechanism. A process liable to lead to hazardous situations, in the event of spontaneous gun propellant self-ignition.

The purpose of the trial detailed in this document is to study the behaviour of the gun propellant in the calibre of the ammunition in which it is used. This test is performed in detonation cells with calibres ranging from 12.7 mm to 150 mm. In this document, the trial is described as it is conducted with 30 mm and 105 mm calibres.

1.1 - Instrumented cartridges

Test procedure definition implies that the only pyrotechnic product subject to the trial must be gun propellant. Therefore, with the 30 mm calibre (Figures 1 and 2) a case equipped with an inert initiator, on which is fitted an inert shell, which features a thermocouple to measure the temperature at the gun propellant's centre. With the 105 mm calibre, a case closed by an aluminium cap, which is stuck on it, is equipped with 4 thermocouples located near the priming system (Figures 3 and 4).

The thermocouples which are used (chromel-alumel) allow measuring temperatures within a range from 20 to 200 °C.

The cases contain either ca. 45 g of gun propellant, for the 30 x 113, or ca. 92 g for the 30 x 150, according to the type of 30 mm calibre. Furthermore, according to the type of 105 mm calibre, the cases contain up to ca. 4.7 kg of propellant for the 150 F1.

1.2 - Heating blocks

Once the cartridges are instrumented and prepared, as detailed above, they are respectively placed in 30 mm (Figure 5) and 105 mm (Figure 6) heating blocks. Each heating block features heating rings, a thermocouple and a temperature control thermocouple.

The 30 mm rounds are equipped with inert crimped shells. Even in the event that gun propellant degradation does not lead to self-ignition, a discharge of gas takes place, thus putting the 30 mm cases under pressure. Therefore, for safety reasons, a pneumatic drill is placed above the heating blocks. The purpose of this drill is to make an opening through a hole located in the heating block, upon trial completion. Therefore, once the process is completed the pressure can be released before the operator intervenes.

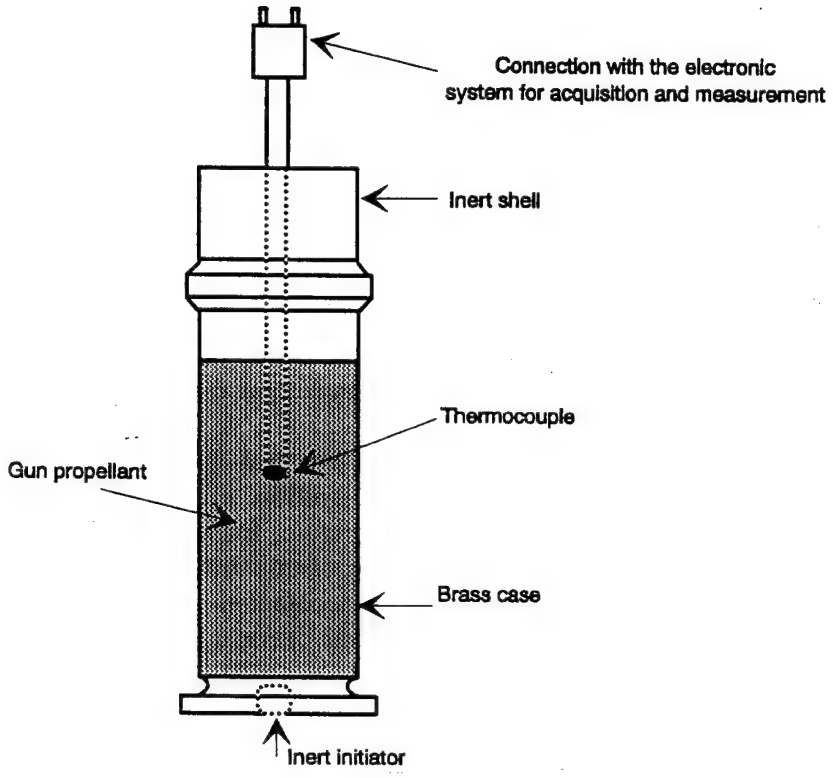

Figure 1 : calibre 30 mm

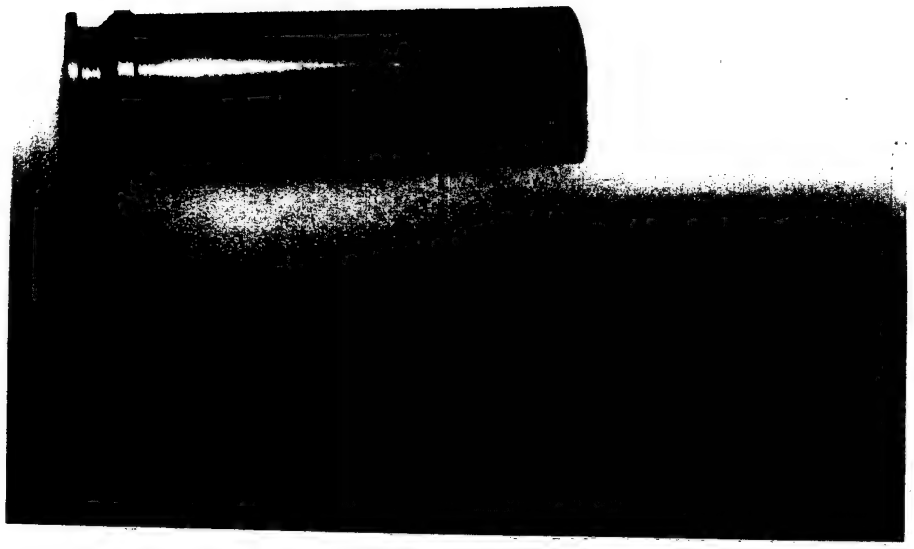

Figure 2 : case and shell with its thermocouple for 30 mm

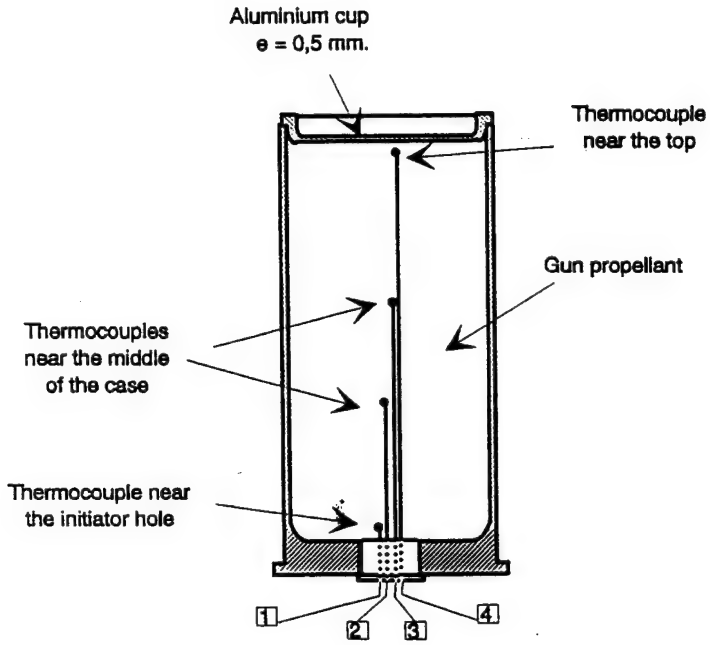

Figure 3 : calibre 105 mm

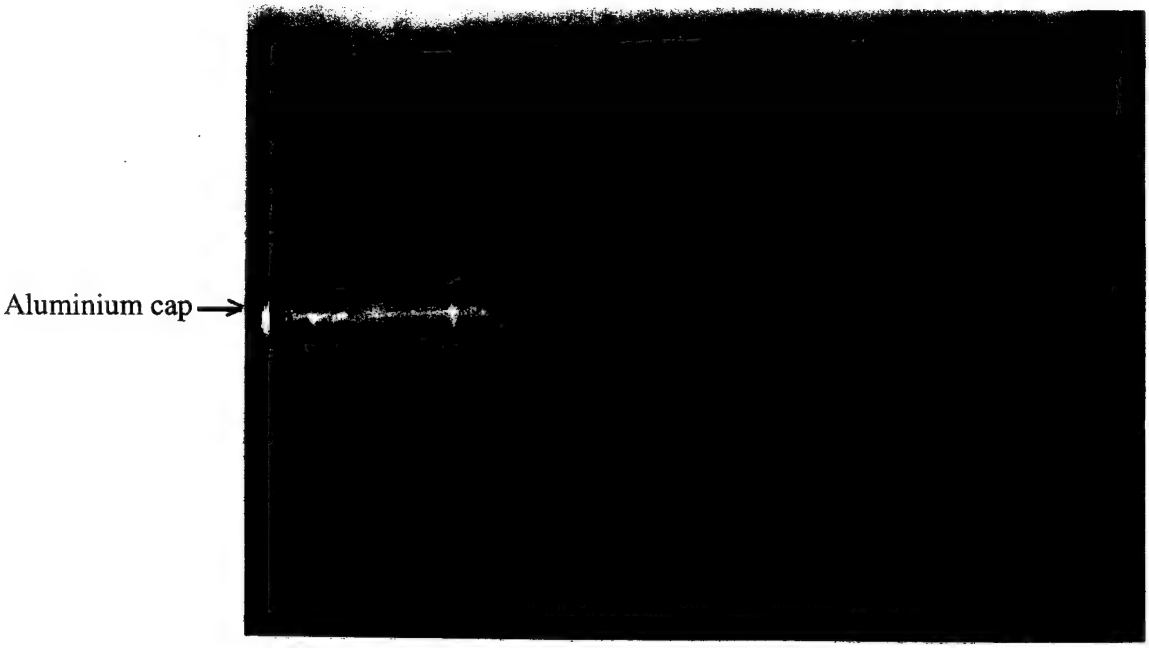

Figure 4 : case and thermocouples for 105 mm

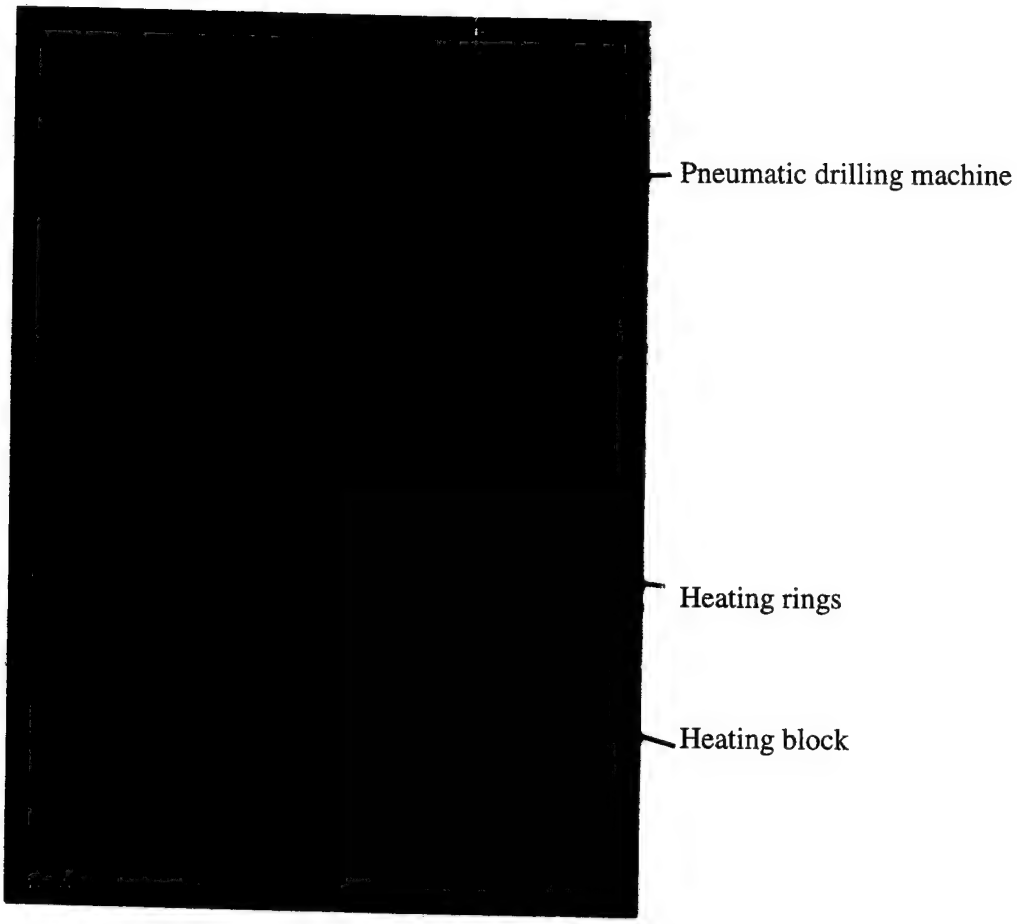

Figure 5 : heating block and pneumatic drilling machine for 30 mm

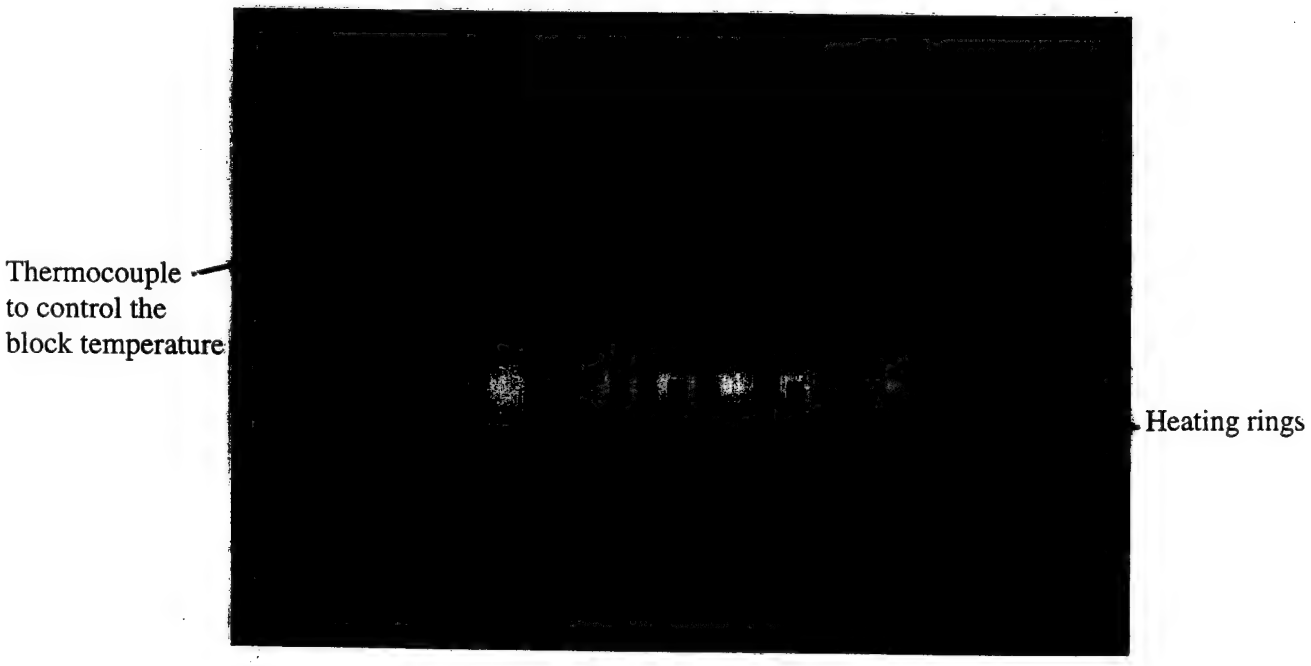

Figure 6 : heating block used for 105 mm

1.3 - Test procedure and result analysis

An instrumented cartridge is placed in a block, which was previously placed under constant temperature, ranging between 100 and 170 °C.

The recorded temperatures correspond to the heating block and the bed of propellant. The recordings are similar to those provided in Figure 7.

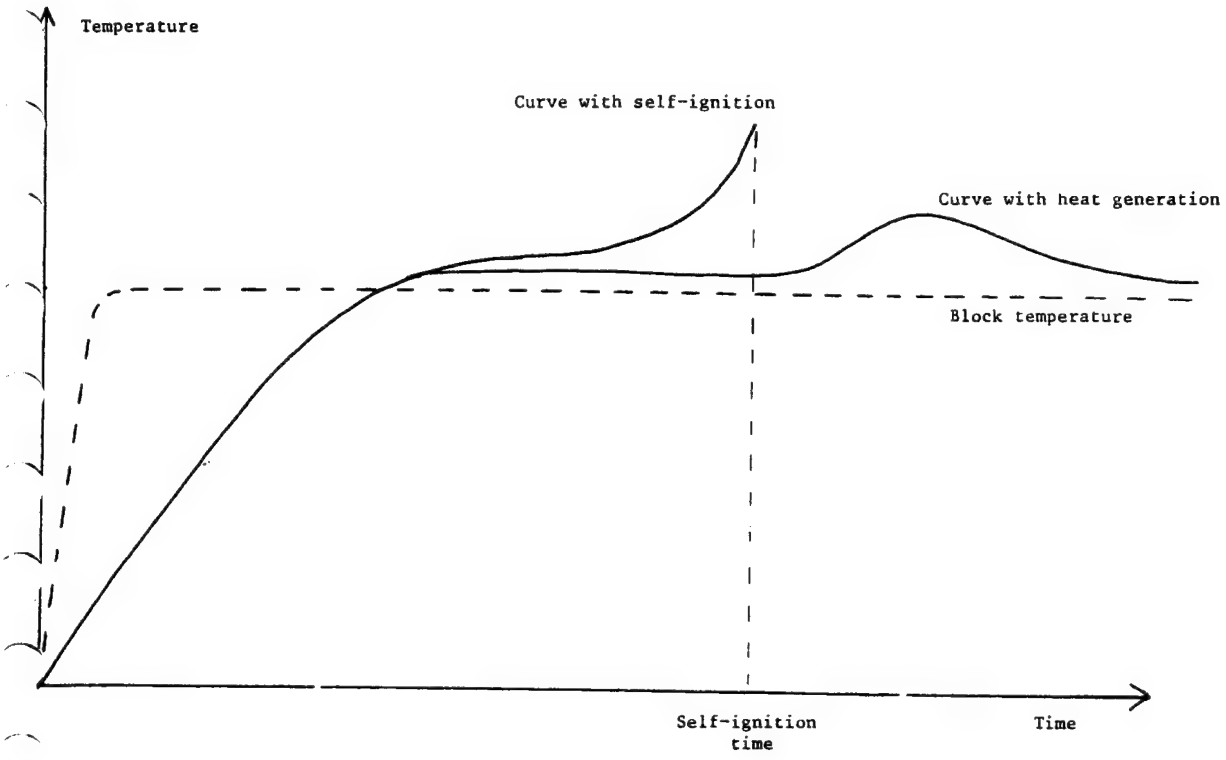

Figure 7

Two types of curves should be noted:

- a heat production curve. In this case, slow gun propellant decomposition leads to heat production, which results in a temperature increase. At the end of the decomposition process, the temperature tends to come back to that of the block.

- a curve with self-ignition. In this case, the prompt propellant decomposition auto-catalyses the nitro-cellulose's degradation and triggers a self-ignition process.

4 to 5 trials were performed with miscellaneous cartridges. The recordings in Figure 7 provide couples of values (bloc temperature, time required before self-ignition). These couples of values are plotted on a graph similar to that of Figure 8.

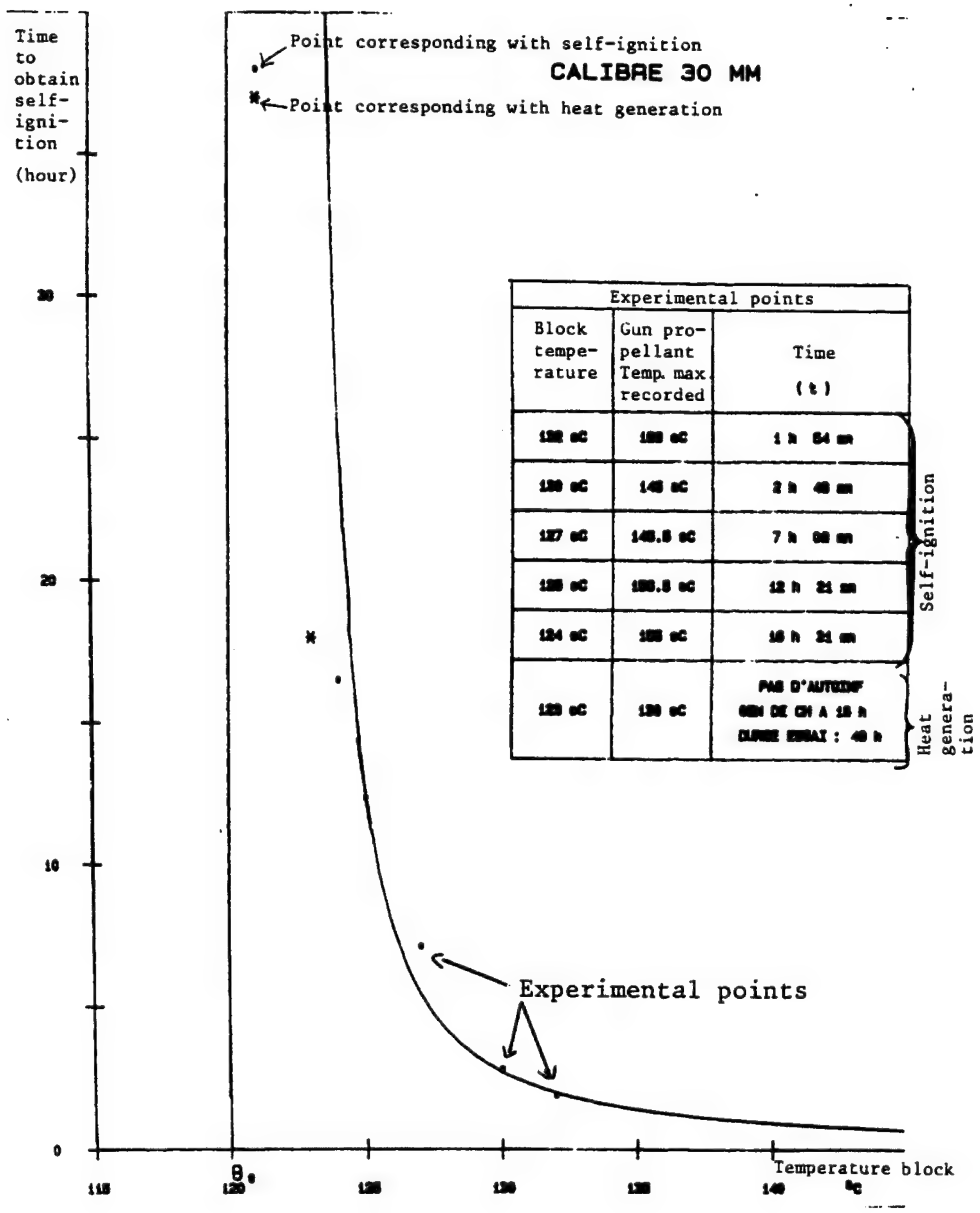

Figure 8

The logarithmic law curve, whose asymptote corresponds to the no-self-ignition temperature θ_0, is drawn according to the experimental points. The no-self-ignition temperature corresponds to the limit temperature in excess of which no self-ignition occurs. A value, which will be established based on the modelling result.

2 - MICROCALORIMETRY

The results obtained for activation energy measurement correspond to the decomposition phenomena of a propellant placed under isothermal conditions.

The studied gun propellants are:

Simple base propellants with 19 holes:
- B.19T (1.34),
- LB.19T (1.5),
- B.19T (2.0)L,
- B.19T (1.6),

Simple base propellant with 7 holes:
- B.7T (0.3),

Double base ball powder :
- GB.Sp (0.7),
- GB.Se (0.35),

Double base chaff propellants:
- GB.Pa (0.15).

2.1 - Principle

The microcalorimetry tests were performed at 50 °C, 80°C, and 105 °C.

By applying the Arrhenius law we managed to determine the activation energies, according to the following formula :

$$Q = Ae^{-\frac{E}{RT}}$$

$$\ln(Q) = \ln(A) - \frac{E}{RT}$$

The $\ln(Q) = f\left(\frac{1}{T}\right)$ curve is a section with a $p = -\frac{E}{R}$ slope and an ordinate at the origin of ln(A), hence: E = -pR.

2.2 - Results

The microcalorimetry tests were performed at temperatures of 50, 80 and, 105 C with Calvet MS 70 and MS 80 type Setaram microcalorimeters.
These three temperatures were chosen in order to have three sufficiently distant points, to obtain significant measurement deviations.

In this piece of work, we suppose that the reaction or processes do not change at these temperatures, in-spite of the general aspect of the microcalorimetry activation energy determination curves (see Figure 9).

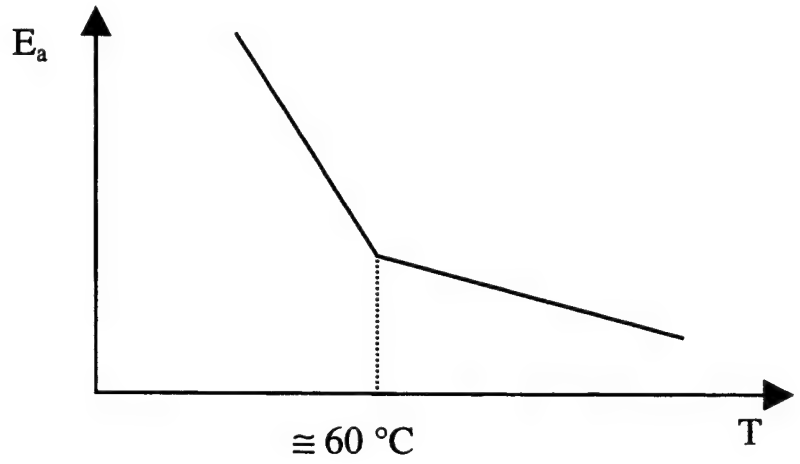

Figure 9

We will see that this assumption is acceptable compared to the modelling results' expected accuracy.

Microcalorimetry results are gathered together in table 1.

GUN PROPELLANT	50 °C at 45 hr P in mW/kg	80 °C at 45 hr P in mW/kg	105 °C at 45 hr P in mW/kg
B.19T (1.34)	1.45	16.55	947.3
LB.19T (1.5)	9.00	33.68	599.2
B.19T (2.0)L	22.79	45.58	504.4
B.19T (1.6)	4.68	13.70	619.5
B.7T (0.3) (2)	1,700	/	/
GB.Sp (0.7)	/	9.1	2,394.10
GB.Se (0.35)	/	10	629.4
GB.Pa (0.15)	6.59 (at 60 °C)	81.61	/

Table 1

Tests at 50 and 80 °C were mostly performed with ca. 75 grams in closed cells (ca. 60 g for the B.19T (1.6) at 80 °C and ca. 60 g for the LB.19T (1.5) at 50°C). Tests at 105°C were mainly performed with ca. 30 grams in open cells (ca. 75 g for the B.19T (1.34)).

2.3 - Activation energy results

Tables from 2 to 5 provide the $T, \frac{1}{T}$, P (released power) and In (P) values for several studied propellants.

T (°C)	50	80	105
$\frac{1}{T}(K^{-1})$	3.09×10^{-3}	2.83×10^{-3}	2.645×10^{-3}
P (mW/kg)	4.68	13.70	619.5
LnP	1.543	2.617	6.429

Table 2 (B.19T (1.6))

T (°C)	50	80	105
$\frac{1}{T}(K^{-1})$	3.096×10^{-3}	2.83×10^{-3}	2.645×10^{-3}
P (mW/kg)	1.45	16.55	947.3
LnP	0.371	2.806	6.85

Table 3 (B.19T (1.34))

T (°C)	50	80	105
$\frac{1}{T}(K^{-1})$	3.09×10^{-3}	2.83×10^{-3}	2.645×10^{-3}
P (mW/kg)	9	33.68	599.2
LnP	2.197	3.517	6.395

Table 4 (LB.19T (1.5))

T (°C)	50	80	105
$\frac{1}{T}(K^{-1})$	3.09×10^{-3}	2.83×10^{-3}	2.645×10^{-3}
P (mW/kg)	22.79	45.58	504.4
LnP	3.126	3.819	6.223

Table 5 (B.19T (2.0)L)

The Figure 10 shows the $\ln(P) = f\left(\frac{1}{T}\right)$ curves obtained with three measurement points for several gun propellants.

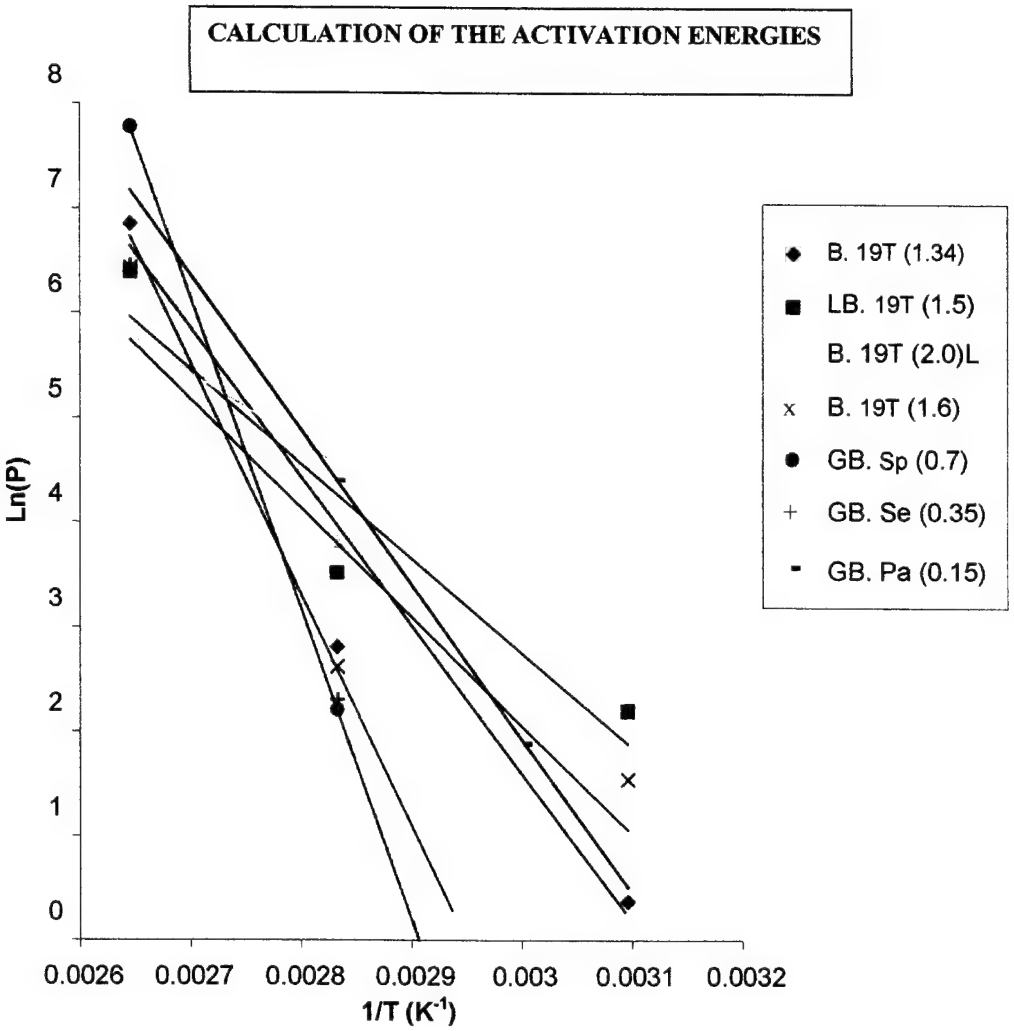

Figure 10

Table 6 provides results as regards the activation energy (E) for each propellant.

Propellant	E (cal/mode)
B.19T (1.6)	20,926
B.19T (1.34)	27,813
LB.19T (1.50)	18,177
B.19T (2.0) L.	13,270
B.7T (0.3)	22,000
GB.Sp(0.7)	58,064
GB.Se (0.35)	43,636
GB.Pa (0.15)	30,000

Table 6

The activation energy E ranges from 13,270 cal/mole for the B.19T (2.0)L. propellant and 58,064 cal/mole for the GB.Sp (0.7) propellant.

These values will be used for modelling calculations as regards the self-ignition behaviour of these gun propellants.

3. NO-SELF-IGNITION TEMPERATURE MODELLING

The mathematical model (3), developed by the ETBS, supposes that the evolution of the temperature T curve at a point within the propellant's cylinder is ruled by two phenomena : heat conduction and internal heat production by chemical reaction. The formula at the partial derived, which describes this evolution according to the time "t" is as follows:

$$\frac{\partial T}{\partial t} = a\Delta T + \phi(T) \text{ with a } = \frac{\lambda}{\rho C_p}$$

where λ refers to the thermal conductivity ($W.m^{-1}K^{-1}$),
Cp refers to the specific heat ($J.kg^{-1}K^{-1}$),
ρ refers to the mass per unit volume (kg/m^3).

The gun propellant cylinder is supposed homogeneous and isotropic, all these parameters are constant.

The $a\Delta T$ term refers to the temperature variation caused by heat transfers due to conduction. It expresses heat transfer from high temperatures to low temperatures, in accordance with the Fourier law. The diffusivity "a" is a factor of the heat transfer's speed.

The $\phi(T)$ term, caused by the internal heat generation due to chemical reaction, is supposed constant. We assume that the heat generation complies with the law according to which the quantity of heat "q" produced, per time and weight unit, at a given temperature T, is defined according to the following formula:

$$q = Q_e^{-E/RT} \text{ with } Q = q_0 e^{-E/RT_0}$$

where q_0 refers to the quantity of heat produced at the temperature T_0. The q_0 value is experimentally defined. The value of the activation energy E is assumed constant in the calculation.

The final formula is an increasing function of T, expressed as follows:

$$\Phi(T) = \frac{q_0}{C_p} \frac{E}{e^{\frac{R(T-T0)}{RT0}}}$$

The calculation assumptions are as follows (4):

- the load, with a cylindrical shape, has a length of more than 3 times the diameter, it is therefore possible to suppose an infinite length,
- the environment is isotropic,
- the released heat varies with the temperature in accordance with the Arrhenius law,
- the wall's temperature is constant,
- the activation energy, specific heat and thermal conductivity are constant.

The calculation parameters to be introduced are:
- activation energy,
- specific heat,
- thermal-conductivity,
- bulk density,
- cylinder diameter,
- initial gun propellant temperature (T0),
  wall's temperature (T1),
- the measurement temperatures and the released power (microcalorimetry).

Initially, gun propellant temperature is uniform and equal to T_0 in all points. The wall is at the outside temperature T_1. As the load is cylindrical, the calculation is performed according to a radius divided into 100 equal sections for each section, the thermal evolution is calculated over a given lapse of time. The heat balance allows calculating temperature variation in the considered section. Then, the same calculation is performed for the next section, and so on, until the border is reached. We consider that self-ignition occurs, only if a section exceeds the temperature of 200 °C.
These time and self-ignition temperature values are used in order to define the no-self-ignition temperature from a curve similar to that in Figure 8.

4 - EXAMPLES (COMPARISON BETWEEN MODEL AND EXPERIMENT)

Table 7 provides results obtained by modelling (5), grounded on microcalorimetry measurements, compared to self-ignition experiment results. This table includes the activation energy values, as well as the calculated and measured no-self-ignition temperatures.

Gun propellant	Calibre (mm)	E (cal/mode)	No-self-ignition calculated temperature (θ_0^*) (°C)	No-self-ignition measured temperature (θ_0) (°C)
B.19T (1.6)	105	20,926	93	102.3
B.19T (1.34)	105	27,813	89.4	89.9
LB.19T (1.50)	105	18,177	92.9	114
B.19T (2.0) L.	105	13,270	100.1	110.4
B.7T (0.3)	30	22,000	67	63
GB.Sp(0.7) *	30	58,064	110	108.1
GB.Se (0.35) *	30	43,636	119.5	121.3
GB.Pa (0.15) *	30	30,000	118	119.2

Table 7

*: These gun propellants for small calibres or mortars were tested with a 30 mm calibre to study their thermal behaviour. The tests were performed in 30 mm as the laboratory did not have the appropriate calibre facilities, when the trials were performed. Activation energies were calculated between 80 and 105° C for the GB.Sp (0.7) and GB.Se (0.35) gun propellants, on the one hand, and between 60 and 80 for the GB.Pa (0.15) gun propellant, on the other hand.

5 - CONCLUSION

The mean error is of 9 % for the largest deviations, which is an acceptable result, considering the achieved accuracy in the determination of the activation energy by microcalorimetry (ca. 10 % for low releases), as well as the repeatability and accuracy of the self-ignition tests (ca. 2 to 6 % according to the case).

However, if the activation energy measurements in microcalorimetry are performed at temperatures included between 80 and 105 °C (i.e. in the vicinity of the gun propellant's self-ignition values), results can be improved.

It would be interesting to take up this study grounded on the obtained TAM microcalorimeter measurement results for weights from 3 to 13 grams (13 g in open cells for safety reasons) to check that results match. The TAM microcalorimeter, which has a more flexible operation, would allow us to perform easier measurements in-spite of the maximum temperature, limited to + 89°C.

REFERENCES

(1) - LEVEQUE M., Calculating the amount of heat evolved by a powder charge, rapport interne ETBS.

(2) - BATAILLET J., FABRE A., Comparaison des résultats expérimentaux avec les calculs de simulation en autoinflammation sur la poudre B.7T (0.32). Rapport interne ETBS RE 3780 du 07/04/93.

(3) – RUNFOLA, VANDERWIND, Modèle de simulation numérique des phénomènes d'autoinflammation. Rapport interne ETBS, 26 Août 1983.

(4) - BATAILLET J., FABRE A., Calculs de simulation du phénomène d'autoinflammation. Rapport interne ETBS RE 3747 du 11/12/92.

(5) - CRETI L., FABRE A., Modélisation de l'autoinflammation à partir des mesures de microcalorimétrie – Comparaison avec les résultats expérimentaux – Etude de l'influence de l'énergie d'activation et de la puissance dégagée. Rapport interne ETBS NT 57/94 du 13/09/94.

A STUDY OF THERMAL STABILITY AND PERFORMANCE OF ENERGETIC MATERIALS USE HEAT FLOW CALORIMETRY

Anton Chin and Daniel S. Ellison
Test & Evaluation Department
Ordnance Engineering Directorate
Crane Division, Naval Surface Warfare Center
Crane, Indiana 47522-5001 USA

ABSTRACT

In a recent study of thermal stability and safe storage life of various energetic compositions, we found that, in addition to the shelf life information, the heat flow curve also shows indications of performance behavior. Based on the preliminary microcalorimetric results, it was found that after all the stabilizer is nearly consumed (depleted), the magnitude and slope of the heat flow curve becomes an important guideline for predicting the performance of the propellant. At this time we name this portion of the microcalorimetric curve "Performance Region". It should be noted that the physical nature of heat flow (μj/s) released from the microcalorimeter can be considered as a very slow burning. In the performance region, if the heat flow is below the normal magnitude, especially after the effective stabilizers are completely depleted, the rate of energy released per second may be too slow to meet the performance requirement. A standard will have to be used to determine what will be the normal heat flow (threshold) for a good performer.

I. INTRODUCTION AND BACKGROUND

Microcalorimetry has been in use since the early 1980's in many areas of chemical reactivity [1]. Crane Division, Naval Surface Warfare Center (Crane) has been developing methods and techniques starting in 1988 for use with a broad range of propellants and explosives [2-5].

This investigation is based upon a previous investigation of the precursor casting powder used in a specific type of double base propellant (composition grain A from device A) [6]. An indication of homogeneity problems was found in the casting powder using a combination of heat flow microcalorimetry (HFMC) and high-pressure liquid chromatography (HPLC). Any anomalies encountered in the casting powder may be applicable to the propellant in its final form

This effort was designed to characterize the double base propellant (grain A) thermally and determine if there is a relationship with the heat flow of the propellant and "low performers". When the double base propellant composition is fired, energy in the propellant is released rapidly. This energy comes from the thermal decomposition of the nitrocellulose/nitroglycerin composition. The temperatures in the burning propellant are high but before that condition can be reached the propellant has to thermally decompose. When the propellant composition is functioned, the temperature rise is instantaneous. The thermal path should be related to how well the propellant grain performs. The microcalorimeter measures the rate of heat released as the propellant thermally decomposes. The microcalorimeter is like a camera taking a snap shot of the first seconds of the ignition process. The heat release is measured under isothermal temperatures where the path to the next stage of decomposition can be detected.

Supporting data about the molecular weight changes are provided by Gel Permeation Chromatography on selected samples aged in the microcalorimeter.

II. EXPERIMENTAL

A. Sample Preparation:

Double base propellant samples are listed in Table I showing sample number, grain location and amount received. All samples were from one contractor. Solid samples approximately 0.25 inch square and 2 inches long were prepared from sample # 30297, 30655 and 03129. Sample # 03129 was made from grain B (propellant composition from device B). The grain B propellant, a naturally aged but still good, was used as reference in this investigation to compare against the grain A and grain C propellants.

Table I. Sampling			
Propellant Grain*	**Sample #**	**Grain Location**	**Weight (Grams)**
A	30655	Center	465
A	30655	Misc. (3" pieces)	49
C	30297	Misc. (3" pieces)	49
C	30297	Center	454
C	30297	Edge near CA	464
B	3129	Center	499
B	3129	Edge near CA	489
B	3129	Misc. (3" pieces)	69

*Grain A and Grain C are double base propellants from the same devices of different age. Grain B is similar composition except in different configuration (device).

B. Instrumentation and Test Parameters:

1. Microcalorimetry:

The ThermoMetric Model 2277 Microcalorimeters (Thermal Activity Monitor -TAM) was used in the analysis. Figure 1 shows the TAM model is equipped with 4 ampoule calorimeters of differential types with a sample and a reference heat detector for effective suppression of thermal noise. The propellant samples (~2 to 4 g each) were loaded in an orientation as close as possible to that of the actual devices. All the propellant samples were loaded at a relative humidity (RH) of 30% or less at 70± 0.5 °F room temperature. The experiments were carried out at 80°C. There was no special preconditioning of the samples carried out before loading, so the original characteristics of the propellants could be retained.

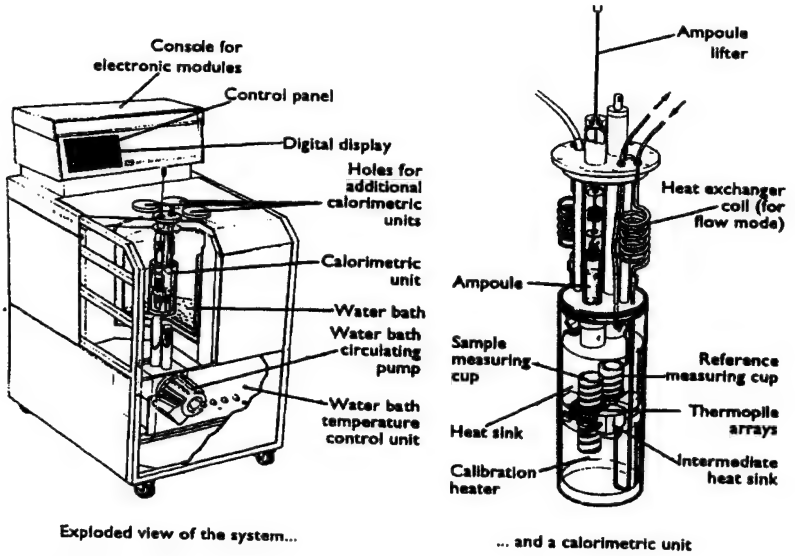

Figure 1. View of a Commercial Microcalorimeter Used in Evaluating the Energetic Materials.

2. Gel Permeation Chromatography:

The propellant samples were dissolved (approximately 100 milligrams (mg) of propellant in 100 milliliters (mL) of tetrahydrofuran (THF) stabilized with butylated hydroxytoluene). The samples were sonicated in a luke-warm water bath for approximately 2 hours and were allowed to stand overnight before analyzing. The volumetric flasks were wrapped in aluminum foil to prevent degradation due to light. Calibration standards were prepared from polystyrene standards of varying molecular weights dissolved in stabilized THF for molecular weight calibration.

A Water 150-C gel permeation chromatograph equipped with a refractive index detector was used for analysis. Three Waters styragel 7.8 x 300 mm columns with molecular weight ranges of $5x10^4$ - $4x10^6$; $5x10^4$ - $4x10^6$; $5x10^2$ - $3x10^4$ were used. The temperature was set at 35° C for both the column and injector compartment. Chromatography conditions were: flow rate 1.0 mL/minute, injection volume 200 µL, detector sensitivity -256, scale factor 40. Run time per sample was 45 minutes.

3. Ion Chromatography:

EPA Method 300.1 was used for ion analysis. A waters liquid chromatograph equipped with a Waters Model 590 HPLC pump and Waters Model 430 Conductivity Detector was used for analysis. Data was processed with a Waters Model 740 Data Module. Samples were loaded into a Shimadzu Model SIL-9A Auto Injector. A small volume of sample, typically 100 microliters, is introduced into the ion chromatograph. The anions of interest are separated and measured, using a system comprised of a guard column, separator column, suppressor device, and conductivity detector. The standard is added to a known volume of reagent water and analyzed with procedures used for samples.

III. Data Analysis

A. Microcalorimetry shows potential for a performance indicator

Figure 2 shows the first 35 days of microcalorimeter heat flow data for the three solid samples # 03129, # 30655 and # 30297. Previous work on 20 mm gun propellant has already shown that the heat flow directly relates to stability [6]. It is proposed now that heat flow is also the first indicator for lower performance later. This is illustrated in figure 3, which contains two heat flow curves. One is a hypothetical "low performer" and the other is a "good performer". For some unknown reasons, either through manufacture or natural aging the NC in the "low performer" is not as stable as the NC in the "good performer". This is reflected as a higher initial heat rate. This high heat rate means that NC is breaking down at a faster rate for the " low performer" than the "good performer". From a molecular weight point of view, this can be understood by using GPC. Figure 4 shows actual average molecular weight changes as # 30297 samples were aged in the microcalorimeter. Figure 5 is an extrapolation of what to expect if all grain A and grain B propellant samples were evaluated in the same way.

This is provided to show how GPC supporting data in combination with microcalorimetry would provide a better indication of the propellant condition than one depending on microcalorimetry alone.

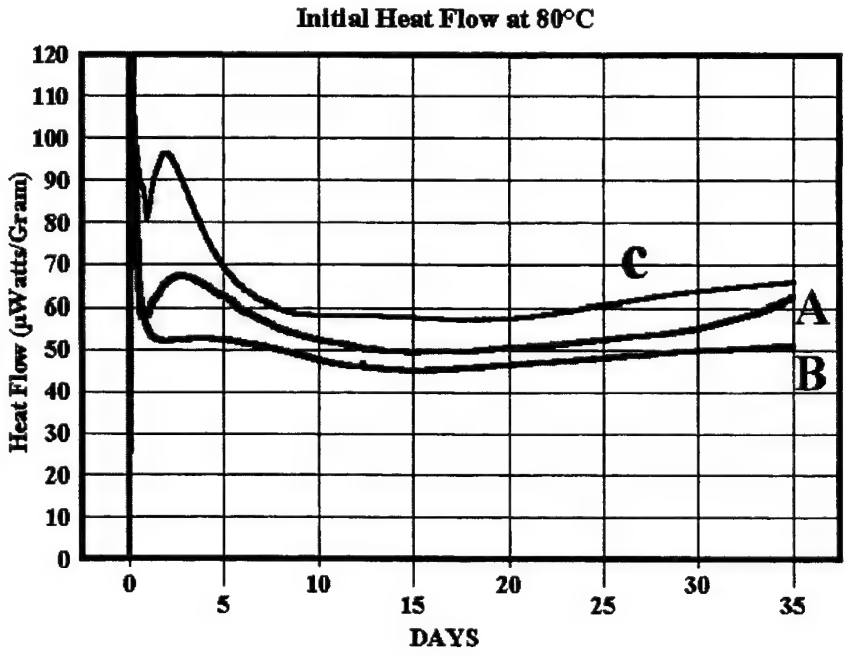

Figure 2. Initial heat flow for Grain A and B Double Base propellant. C is Same as Grain A Except for Different Aging Time.

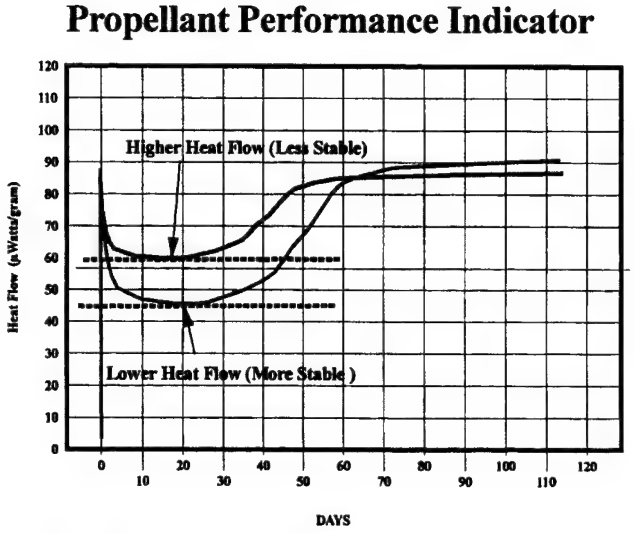

Figure 3. Hypothetical microcalorimetry curves for Grain A Double Base Propellant showing how higher heat rates resulting from different NC.

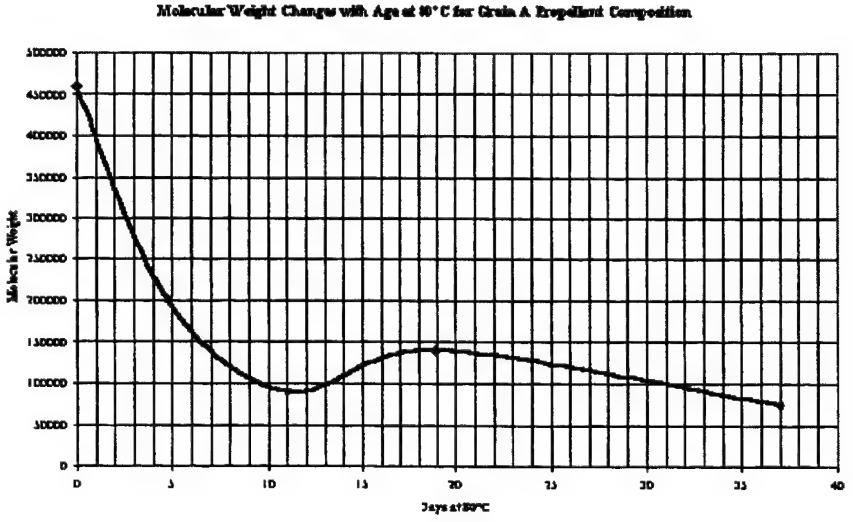

Figure 4. Gel Permeation data from samples that were aged in the microcalorimeter showing the decrease in molecular weight.

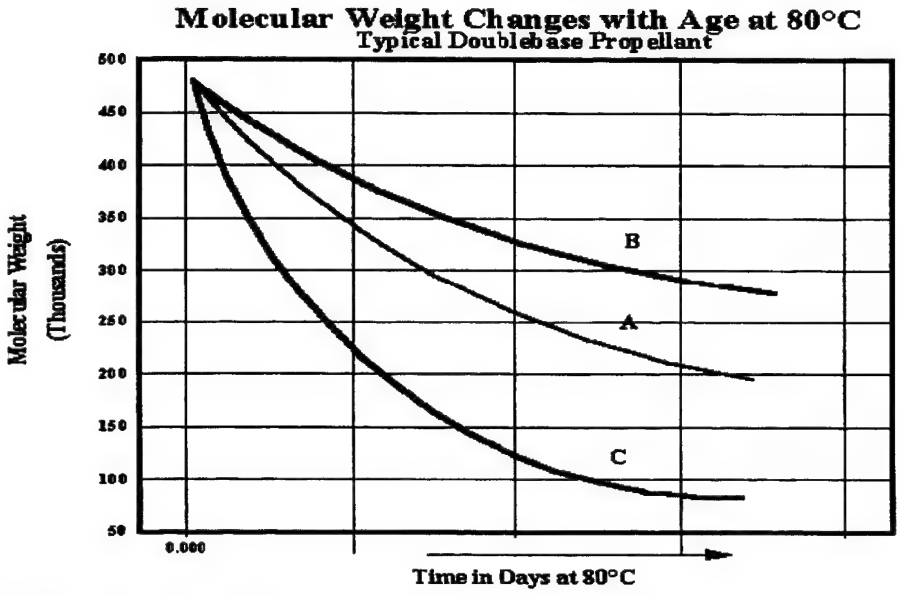

Figure 5. Projections what to expect if the NC is degrading at different rates.

B. How much of the decomposition has occurred before the performance indicator becomes apparent?

The total amount of energy released after 120 days of aging at 80°C for the grain A propellant is approximately 180 calories/gram. Heat of explosion on the grain A propellant has been reported at about 950 to 990 calories/gram. Therefore the microcalorimeter data represents about 18% of the decomposition of the grain A composition. Figure 6 shows the heat flow data from the grain B propellant for 120 days. As it ages at 80°C, one can see the effects of stabilizers during the first 10 to 30 days, which are important to storage. After the stabilizers are consumed, the propellant starts to release its energy with large amounts of gas, which serves the purpose of its design. One is in a sense is looking at the early part of ignition of the propellant stretched out over days instead of microseconds.

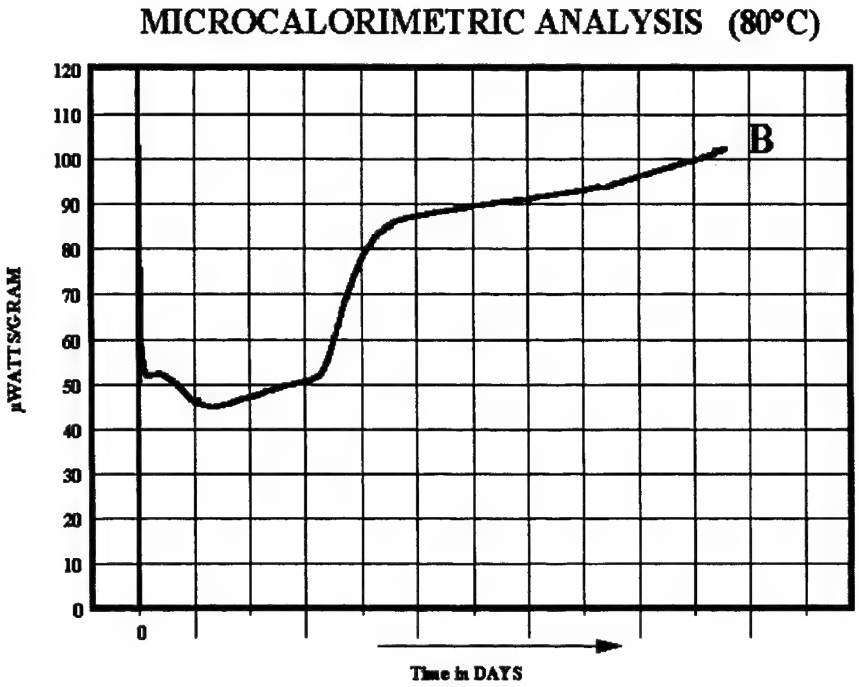

Figure 6. Heat flow microcalorimetry curve for Grain B Double Base Propellant- a "good performer".

C. Comparing Heat Curves for the Grain A, Grain C and Grain B Double Base Propellant Samples

At this point one can use the heat flow curves for evaluating the propellant. Figure 7 shows the three gas generators evaluated. # 03129 is the grain B sample that was designated a "good performer". The heat flow curve for # 30655 is very close to the heat flow curve for # 03129. Sample # 30297 heat flow curve is higher at the beginning for the reasons stated earlier. But later into the decomposition the curve is noticeably lower than the others. This is because the NC in # 30297 was initially more degraded than the other two. It would be expected at this point that if GPC analysis were done at 120 days for all three samples, # 30297 would be lower than any of the others. The December 1998 IPT meeting suggests that # 30297 may be a suspect "low performer".

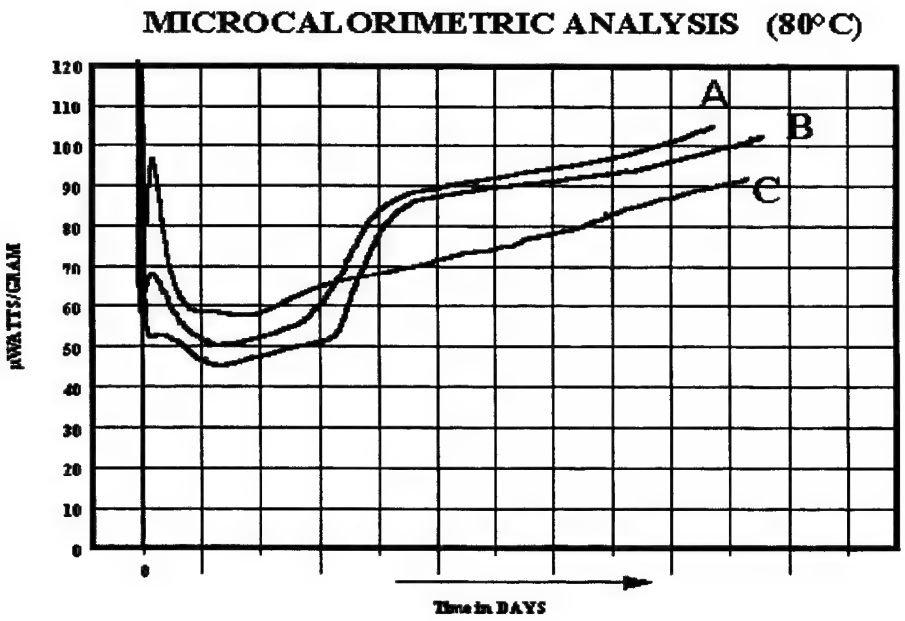

Figure 7. Comparison of heat flow curves for the Grain A (# 30655) and Grain C (#30297) Double Base Propellants with the "good performer" Grain B # 03129.

D. Looking at the starting product (the precursor casting powder), how will it affect the final performance of the final double base propellant grain?

Previous work on the precursor casting powder also included microcalorimeter heat flow data on the powder used in the grain C double base propellant. Figure 8 overlays all data for the double base propellant grain and precursor casting powders. Based on the technical discussions previously presented, the relative position of the heat flow curves for the casting powders would be an indicator for future performance.

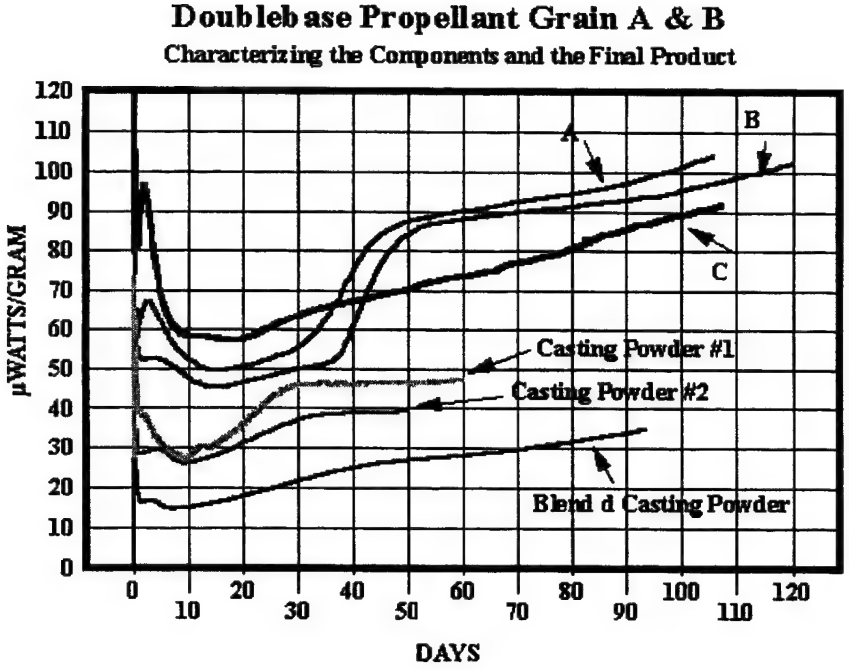

Figure 8. Characterizing the both the precursor casting powder and the resulting duble base propellant grain.

IV CONCLUSIONS

The propellant from # 30297 starts out with a higher heat rate than the reference propellant grain B # 03129 and propellant grain A # 30655 samples. Based upon previous experience, this suggests the quality of NC in this propellant will result in low performance. More known poor performers would have to be evaluated to provide increased confidence.

V RECOMMENDATIONS

- Identify and perform microcalorimetry on known 'low performers".
- Fully characterize (baseline) the grain A and grain C propellants with microcalorimetry at three temperatures to allow prediction of service life. This would be supported with HPLC and GPC testing.
- Develop a sampling technique to perform a quick NDT microcalorimetry test (once the baselines are established) to screen the gas generators)

VI REFERENCES

1. T. Lindblom, P. E. Lagerkvist, L. G. Svensson, "Comparison and Evaluation of Modem Analytical Methods Used for Stability Testing of a Single Base Propellant", 7th Symp. On Chemical Problems Connected with the Stability of Explosives, Sweden, p-247 (1985).

2. A. Chin, R. G. Shortridge, and B. R. Hubble, "Microcalorimetric Study of the Aging Reactions of Atomic Magnesium Powder", NWSCC/RDTR-92/003. Naval Surface Warfare Center, Crane Division, Crane, IN 47522 (1992).

3. A. Chin and D. S. Ellison, "New Microcalorimetric Approaches in Shelf Life Technology", Proceedings of the 1993 Predictive Technology Symposium, 22-24 June, Orlando, FL (1994).

4. A. Chin and D. S. Ellison, "The Applicability of Microcalorimetry as an Effective Surveillance Technique for Stored Munitions", and references therein. ADPA Symposium on Energetic Materials Technology, Orlando, Florida, 21-24 March 1994. P-399.

5. A. Chin and D. S. Ellison, "20 MM Gum Propellant Safety Service Life Study Using Microcalorimetry/HPLC Correlation Diagram". 1997 International Workshop on Microcalorimetry, Leeds, UK, April 7 – 9 (1997).

6. A. Chin and D.S. Ellison, "Microcalorimetric/HPLC Analysis of Blend 222 Casting Powder", Test and Evaluation Department, Ordnance Engineering Directorate, Crane Division, Naval Surface Warfare Center, Crane, IN 47522 (1998)

ABSTRACT

Recent Developments in Heat Flow Calorimetry (HFC) and Large Scale Sampling Systems

James A. Wilson and Daniel S Ellison
Test and Evaluation Department
Naval Surface Warfare Center, Crane Division
300 Highway 361
Crane IN 47522

With increasing workload and the need for testing larger sized samples, the Naval Surface Warfare Center at Crane Division is developing an automated sampling system and a 14 pound sized ampoule system to meet our new emerging requirements. The automatic sampling system, with thirty six 4 ml ampoule capacity, is built using the TAM Model 2277 microcalorimeter as the core of this new test system. This system will load and unload samples automatically and will continue testing without human over sight for extended periods of time.

The large sample calorimeter has been manufactured with a 5 x 5 x 12" ampoule that is capable of hold up to 14 pounds of energetic material. Calorimetric Scientific Corporation in Utah built the system. This large system was designed to test actual end items (life size) devices such as 20 and 25 mm ammunition cartridges, fuzes, thermal batteries and Cartridge Actuated Devices (CADs), to name just a few. The system will also be used for measuring the heat flow rates of material that exhibit very low levels of heat flow per gram.

Both systems are current at Crane and should be completely operational by late summer or early fall of 1999.

Recent Developments in Heat Flow Calorimetry (HFC) and Large Scale Sampling Systems

BACKGROUND

With in the US Navy weapon arena, the use of Heat Flow Calorimetry (HFC) to augment the traditional Service Life program of energetic / one-shot components has gone up dramatically over the last two years. Many of the sponsors have seen great benefits which can be derived from the integration of HFC into the service life program for their weapon components. These include the early detection of chemical instability, long range prediction on performance, early identification of potential safety problems, and models for optimizing stockpile utilization. As a result of the initial success of the HFC, a number of new potential sponsors have come to us seeking assistance with their service life problems. This should be and is a very rewarding consequence of long effort, however, like most success stories - - there is a catch. The increased demand for our HFC services has caused our facilities to be more than fully occupied. For a time we were able to keep up with our increased demand by rotating samples between the HFC cell and a controlled temperature chambers set to the same temperature as the HFC. By collecting data for at least a day and then removing the ampoule for two to four days, the resultant "doted line" usually provides all of the information needed. This works very well for material on which we have historical data and can be sure of the fundamental trace we expect to obtain. Obviously, new material with no historical basis is not a good candidate for this process.

The ability to increase the HFC laboratory through put using this process of cycling in and out of the HFC has some very real and fixed limitations. Our facility and number of Calorimeters is limited. We normally have only six or seven HFCs on line and working at any one time. On the average, 50% of the cells are occupied with items that cannot be cycled. This leaves us with the other half of our capacity to work with. Although we have thus far been able to satisfy our sponsors, we have been working on the margins and any significant increase in demand will result in failure to meet our obligations. Obviously this would be an unacceptable situation for both our sponsors and Crane.

When analyzing our future problems, there is one obvious solution - - buy more HFCs. The problems with this option are two fold: 1. Our sponsors have already purchased eleven HFC and would not look with favor procuring five or six more, (2) we currently operate with minimal overhead and personnel costs and the acquisition of many more HFCs would have a detrimental action for the cost of this program.

CAPACITY SOLUTION

Since it was not feasible to make a significant increase to our current number of HFCs, some other solution was needed. The obvious alternative was to obtain or modify a single HFC that could automatically test a large number of samples at the same time. Do entirely to cost divers, most possibilities were rapidly set aside. After much debating, it was decided that our best alternative would be to design a HFC with auto sampling capability. In order to

assure that the final product would satisfy our requirements, a list of essential system attributes was developed. The following is the list developed:

1. The system must be capable of at least 36 samples.
2. The design must use "off-the-shelf" components as much as possible.
3. The system must be capable of working for long periods without human over sight.
4. The system must have software and hardware which will provide automatic shut off capability in the event of extreme exothermic reaction.
5. The system must have direct and consistent correlation with other HFCs in lab.

Based on the above design criteria, it was decides that a TAM model # 2277 would be used as the core HFC device. This would be a single cell unit identical to a number of the other HFCs used in our laboratory. This would assure data consistency and correlation. The auto-sampling unit would sit on top of the TAM and would be a separate sub-system. All HFC measurements would be taken by the standard TAM circuitry and stored in a work station computer.

Off-the-shelf Components

36 Sample Carousel

Standard TAM

The major engineering problem faced during the design and fabrication of this auto-sampling HFC was maintaining the temperature of all the samples at the same temperature as that of the HFC water bath. The key to this problem is the sample carousel itself. It is

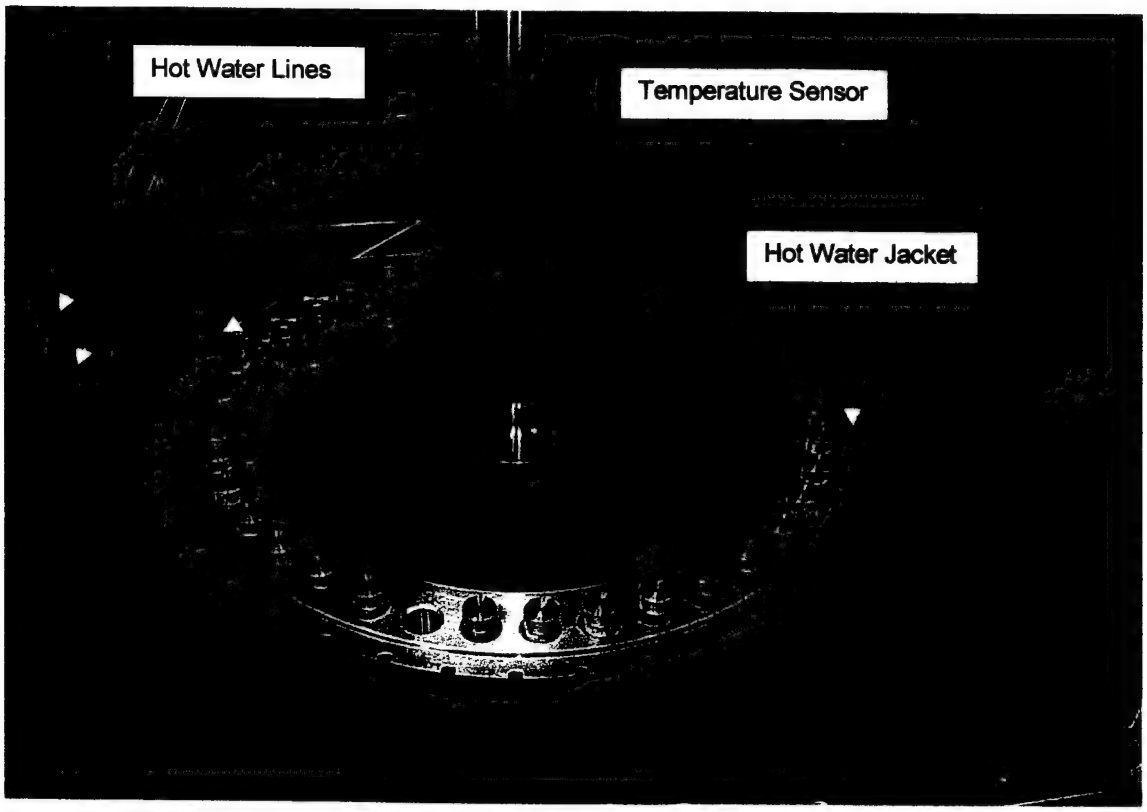

essential that the carousel be maintained at the identical temperature as that of the HFC bath. Our design incorporated a hot water jacket which surrounds the aluminum portion of the carousel. The temperature of the water jacket is monitored by a temperature sensor mounted directly into the carousel jacket. Through experimentation the delta temperature needed to maintain the proper carousel temperature was found to be approximately 102% of the selected HFC temperature. Obviously this is a factor that is unique to this configuration and should not be considered as a constant.

During the development of the carousel there were a number of design changes made. Our initial design was an all aluminum unit with a fairly large surface area. We found that this design resulted in excessive heat loss from the carousel and made it very difficult to maintain temperature stability. During re-design the amount of aluminum in the out portion of the

carousel was reduced and the entire center portion of the aluminum was replaced with a heavy duty Phenolic. The combination of these changes dramatically reduced the carousel heat loss problem.

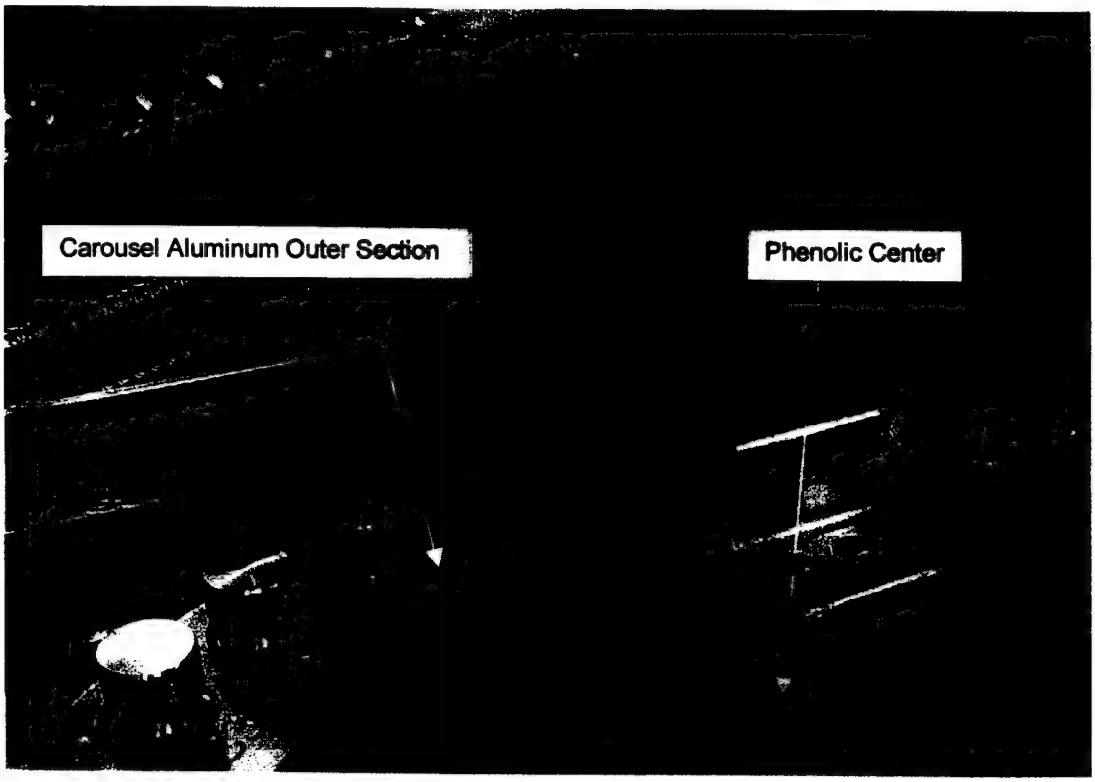

Although there are still a number of design and software problems to be overcome, preliminary results have shown that the concept is very viable and should lead to significant cost reductions to a number of our traditional sponsors.

OTHER PROBLEMS

While automation seems to be the best solution for the increased HFC workload for items such as propellant, explosives and some pyro comps, other energetic materials are not easily evaluated by conventional HFCs. This would include such items as thermal batteries, composite rocket propellant and those items that would be destroyed during the breakdown process. Because of these limitations and the desire to bring HFC technology to all the energetic items for which we have service life responsibility, it became apparent that a HFC with a much larger cell size was needed. The actual size of the cell was determined by the largest item that we realistically intended to evaluate within the next few years. The item selected was a missile thermal battery which required a cell size of 5 inches by 5 inches by 12 inches. The cells themselves were to be a square cell versus the traditional round cell. We required this device to detect heat flow at the 200-microwatt level and to do this over a temperature range of 25°C to 100°C. The contract for this device was issued to Calorimetry Sciences Corporation in Utah.

When compared to other HFCs this unit is rather formidable.

This unit is currently undergoing calibration testing and it is hoped to be completely operational by the fall of 1999. Once this initial calibration / validation phase is completed, this unit will be used to accomplish tasks which are not possible with any other technology. One of the first tasks will be to determine if there is any self ignition potential for 20 mm gun ammunition propellant. A fixture has been designed that will hold up to seven rounds of ammunition. This loaded fixture will be placed into the end-item calorimeter which will be set at 80 degrees C. If the propellant follows the same pattern as that revealed in twenty gram sample testing, we would expect to see the HFC trace peak out at approximately 30 days. The trace would then fall off rapidly and eventually go into thermal oscillations. If this vision become reality, it would then be very safe to state that the propellant in the 20 mm round configuration would have no self ignition potential. This would eliminate the requirements for never ending chemical stability testing and make more funding available for increased shock and thermal sensitivity testing which has been ignored due to lack of funding. Other devices that will be evaluated by this system include items such as 20 and 25mm ammunition cartridges, fuzes, thermal batteries and Cartridge Actuated Devices.

Low level reaction material such as composite rocket motor propellant will also be evaluated by using pounds of propellant rather than grams. The larger sample size provides a much larger heat flow profile and makes detection far easier.

Novel methods of characterisation of adsorbents by Flow Adsorption Microcalorimetry (FMC)

A. J. Groszek
MICROSCAL Limited, 79 Southern Row, London W10 5AL, U.K.

Introduction

The flow adsorption microcalorimeter has been applied to the study of a wide range of interactions at liquid–solid and at gas–solid interfaces and a review of this work has been published [1].

Much work has been carried out in recent years on the determinations of differential heats of adsorption of basic and acidic probes on catalyst supports, such as aluminas and zeolites, in an effort to characterise the strengths of the active sites. Recent examples of this work include that of Parillo and Gorte [2], Gervasini and Auroux [3], and Auroux, Muscas, Coster, and Fripiat [4]. In all this work the heats of adsorption were determined under static conditions on evacuated adsorbents.

The present paper describes some current microcalorimetric studies of microporous adsorbents and catalysts carried out under *flow–through conditions*, whereby the adsorbents are first saturated with a carrier gas, such as nitrogen, and then the carrier is exchanged for a mixture of a probe and the carrier. The heats determined in this way are the heats of displacement of the carrier by the probe.

Differential heats of adsorption are determined at increasing surface coverage and the rate of heat evolution and adsorption are determined simultaneously, the latter being measured by down stream detectors of the type used in chromatographic separations.

The use of Microscal flow–through adsorption microcalorimetry has permitted the calorimetric determinations to be carried out at the pressure at which the carrier gas is passed through the adsorbent bed, which is usually atmospheric pressure. The choice of carrier gas is made in such a way as to come as closely as possible to the conditions under which the adsorbents are used in practice. The rates of adsorption of the probes and the accompanying heat evolution could then be followed directly as they enter and pass through the adsorbent bed.

This paper is concerned with determinations of the differential heats of displacement of nitrogen by ammonia on an active carbon and on a zeolite, representing microporous solids with hydrophobic and hydrophilic properties respectively. The work is focused on the determination of surface acidity.

Experimental

Adsorbents: Zeolite, Mordenite in the acid form (MH) prepared by calcination of NH_4^+ exchanged material.

Active carbon Chemviron BPL – a well known commercial material having an N_2 BET surface area of 1000 m^2g^{-1}. The surface sites having hydrophobic properties constituted 95% of the total surface and 5·4% of the carbon surface was polar as previously determined [5].

The adsorbents were used as received. Their surfaces were purged with N_2 at the temperature at which the adsorption experiments were carried out: 25°C for the BPL carbon, and 208°C for the MH zeolite. The purging was conducted for 20 hours with the N_2 flow fixed at 60 ml per hour. The purging removed adsorbed air, CO_2, and water as was clearly shown by negative heat effects due to the displacement of these gases and vapours by the carrier gas. A Microscal Mark 4Vms flow adsorption microcalorimeter (model FMC–4110) fitted with a thermal conductivity detector was used to carry out the simultaneous determination of the rates of adsorption and the accompanying heats of adsorption, as recently described in [1].

An important feature of the calorimeter is the small volume of the adsorption cell (170 µl) which, when completely filled, contained about 0·1 g of the adsorbent. For experiments with NH_3, which produced very large amounts of heat during the displacement of N_2, the adsorbents may be 'diluted' with quartz sand, the volume of the sand / catalyst mixture being adjusted so as to completely fill the adsorption cell. In the present work about 100 mg of MH zeolite and 72 mg of BPL carbon (weighed to 0·1 mg) were sealed in the adsorption cell. A sketch of the cell filled with the adsorbent with a centrally placed calibration stem is shown in Figure 1.

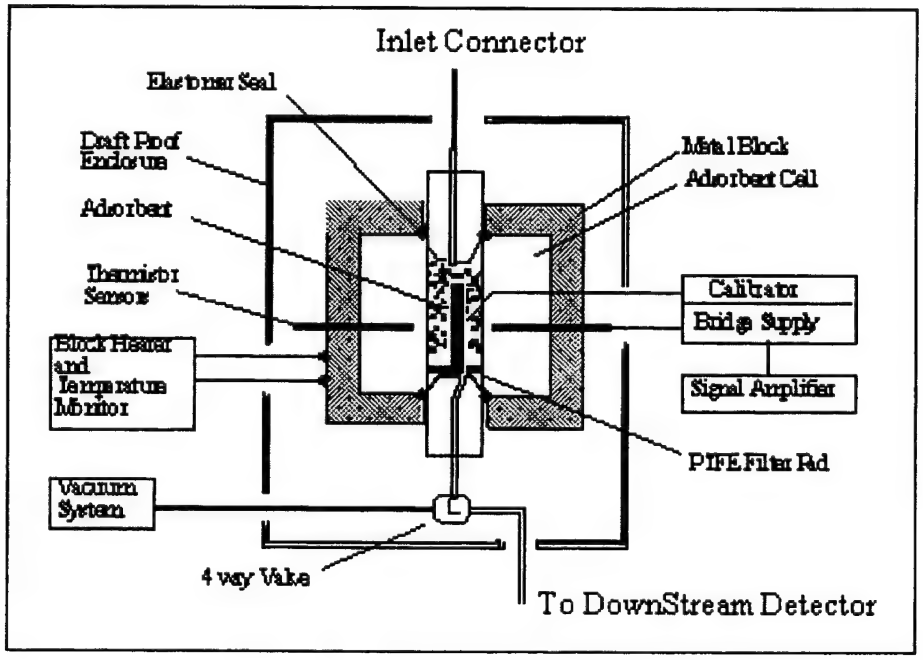

Figure 1 – FMC cell schematic

Gases could be percolated through the cell with a very small pressure drop (less than 50 mbar) and the heat effects calibrated in–situ. Blank experiments were conducted with the cell filled

with pure quartz sand. The latter did produce very small heats of N_2 displacement and NH_3 adsorption which were subtracted from the much larger heat effects produced by the preferential adsorption of NH_3 by the catalysts. The blank experiments were also used to fix accurately the time at which the adsorption process commenced in the cell containing the adsorbent. This permitted an accurate determination of any retention times produced during adsorption and the total amount of adsorption that takes place during equilibration of the adsorbent with the probe during the adsorption process involving displacement of N_2 by NH_3. Furthermore, the blank experiments permitted a good matching of the heat evolution curves and the probe adsorption curves resulting in accurate determinations of the integral and differential molar heats of adsorption.

Typical results obtained in this way are shown in Figure 2 for adsorption of 5% vol NH_3 on 0·072 g of BPL carbon from an N_2 carrier.

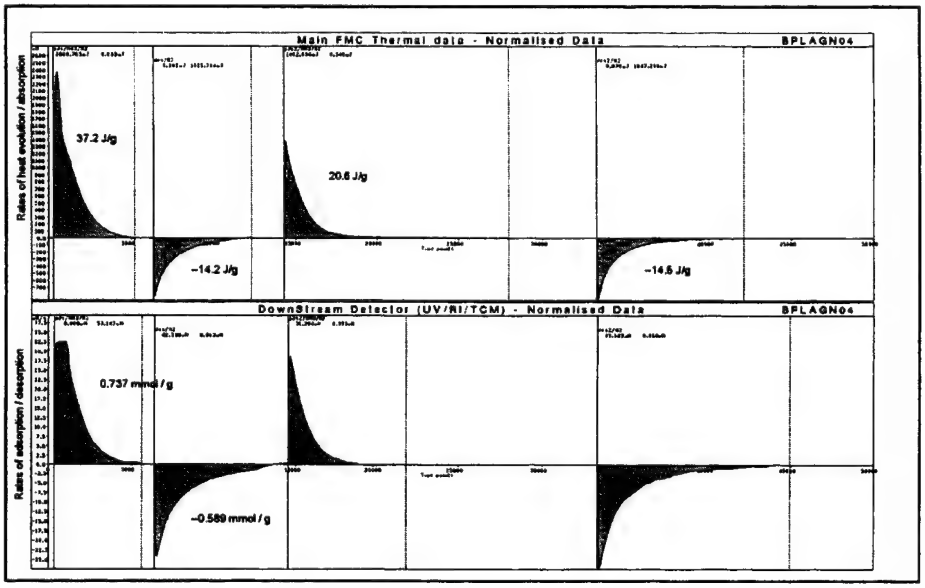

Figure 2 – Rates of adsorption of NH_3 from N_2 on 72 mg of BPL carbon at 25°C

The Figure shows two adsorption / desorption cycles and the corresponding rates of heat evolution and adsorption, completed in 12½ hours. The difference in the total heat evolution between the first and second cycles is taken as the heat of irreversible adsorption. The corresponding amount of irreversible adsorption is shown by the data in the second channel, the lower set of peaks, recording the total amount of adsorption occurring during the percolation of the NH_3 / N_2 mixture through 0·072 g of BPL carbon at 25°C. Details of this experiment and similar experiments with the MH zeolite are discussed below. It should be noted that the peaks represent the rates of heat evolution or absorption and the rates of adsorption / desorption and, therefore, indicate the kinetics of the probe mass transfer. The areas under the peaks are the integral quantities.

Results and Discussion

Table 1 gives the integral heats of adsorption of NH_3 on BPL carbon and on MH zeolite at 25°C and 208°C respectively. These integral heats combine reversible and irreversible adsorption. To obtain an estimate of the irreversible heats of adsorption, two adsorption / desorption cycles have to be carried out, as shown in Figure 2, and the heats and amounts of adsorption for the second cycle subtracted from the corresponding results for the first cycle. The molar irreversible heats obtained by dividing the irreversible heats and mass transfers are listed in the last column of Table 1.

Table 1 – Integral heats of adsorption of NH_3 – Two adsorption / desorption cycles

	Heats of Adsorption, J g^{-1}		Reversibility	Integral Heat of Irreversible Adsorption
Sample	First Cycle	Second Cycle	%	kJ mol^{-1}
MH zeolite	184·3	72·3	39·2	156
BPL carbon	37·2	20·6	55·4	89

As can be seen the heats of adsorption are lower for the BPL carbon, but the integral molar irreversible heats for the MH zeolite and the BPL carbon are much higher for the MH zeolite than for the BPL carbon. In addition, the adsorption reversibility is relatively high for the carbon reflecting the overall lower heats of NH_3 adsorption on this adsorbent.

The rates of adsorption and heat evolution shown in Figure 2 show striking differences between the first and second adsorption cycles. In the first cycle the rate of adsorption remains constant for eight minutes of NH_3 passage at its maximum level of 33 nmol per second, but the rate of heat evolution during that time drops from a maximum of 2·4 μJ per second to 1·3 μJ per second indicating that NH_3 is being adsorbed on successively weaker acid sites during that period.

In fact the first adsorption cycle represents a mixture of irreversible adsorption and reversible adsorption, and clearly the proportion of irreversible adsorption increases as the adsorption process continues. For the second adsorption cycle both the heat evolution and the amounts of adsorption are predominantly reversible. The irreversible part of the adsorption can be obtained, therefore, by subtracting the heat evolution and the amounts of adsorption obtained during the second cycle from the corresponding values recorded for the first cycle.

The heats and amounts of irreversible adsorption obtained in this way can be related and the resulting differential heats of adsorption plotted against increasing surface coverage by the irreversibly adsorbed NH_3. Figures 3 and 4 represent the variations of the differential molar heats for BPL carbon and MH zeolite respectively against surface coverage by irreversibly adsorbed NH_3.

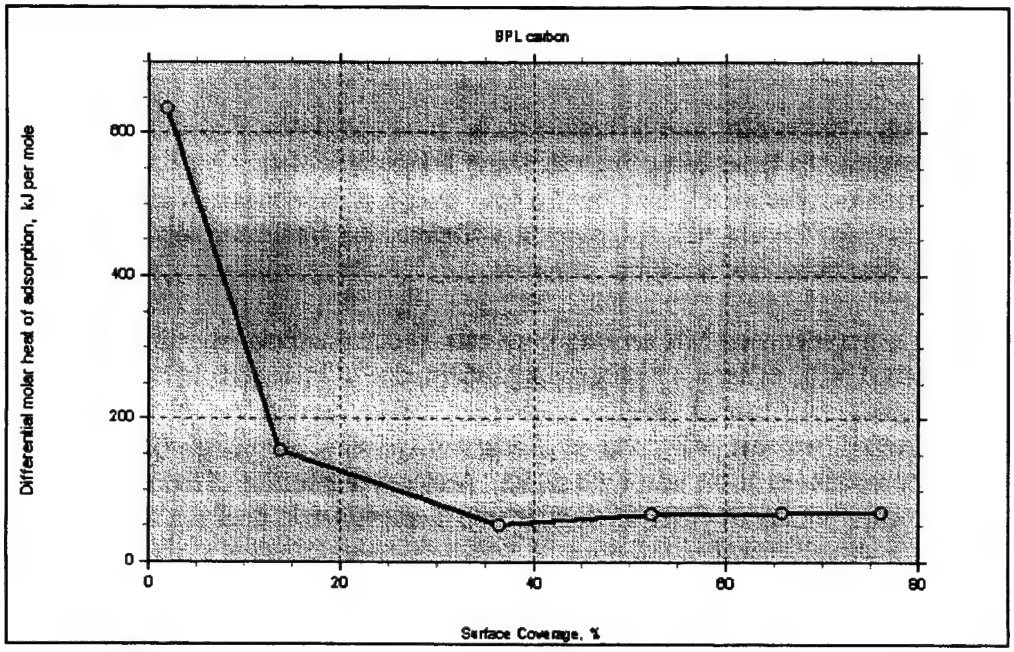

Figure 3 – Differential molar heat of irreversible adsorption of NH_3 on BPL carbon.
(Total irreversible adsorption – 208 μmol g^{-1})

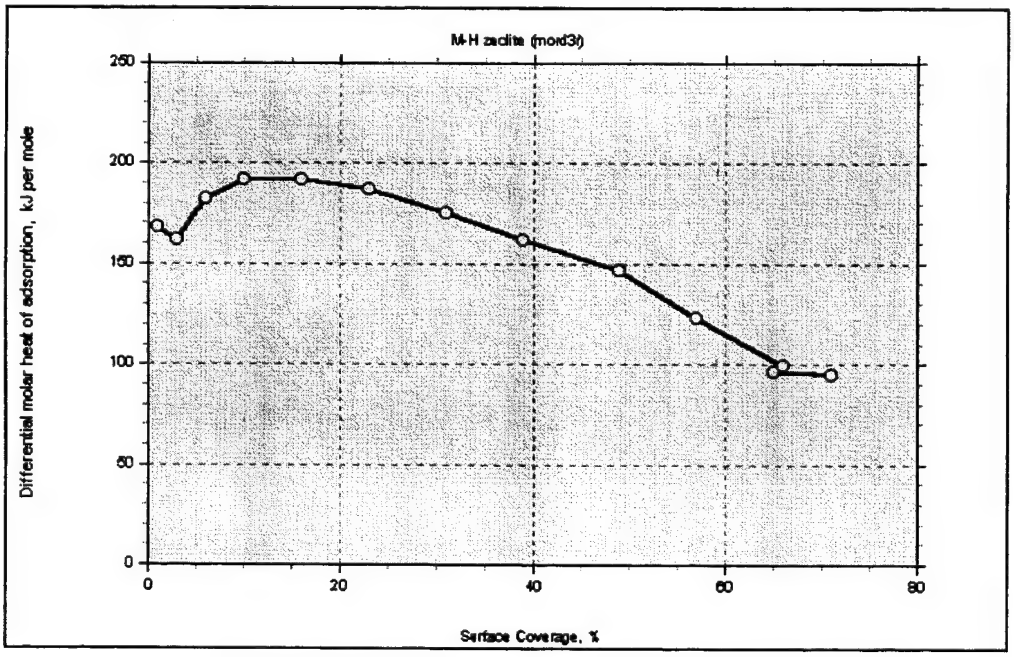

Figure 4 – Differential molar heat of irreversible adsorption of NH_3 on MH zeolite.
(Total irreversible adsorption – 868 μmol g^{-1})

It is very clear that the molar heats for MH zeolite and BPL carbon decrease gradually with the surface coverage and for MH zeolite reach levels similar to those found by static experimentation (by Parillo et al [2]), i.e. 150 kJ per mol at a surface coverage of 50%.

The molar heats for the BPL carbon are relatively high at low surface coverage but they become much lower than the heats obtained for MH zeolite at coverages above 20%.

For both adsorbents there is a marked difference in the rates and heats of adsorption between the first and second cycles, the latter being predominantly reversible. In the first cycle the rates of heat evolution are initially relatively low and for MH zeolite reach a maximum value after 1500 seconds of NH_3 flow (of 5% vol NH_3 / N_2 mixture), whereas the maximum rate for the second cycles is reached after about 300 seconds.

Pulse adsorption experiments on MH zeolites have clearly demonstrated mobility of the irreversibly adsorbed NH_3, as shown by the peak profiles, due to injections of three 5 μmol quantities of NH_3 and one 10 μmol quantity of NH_3 into the N_2 carrier. As shown in Figure 5 the injections produce positive heat peaks and very little desorption of the injected NH_3, but there may be some decomposition of the adsorbed probe. A closer inspection of these adsorption peaks shows that after injection of NH_3 is stopped, the heat evolution does not stop immediately, as it does during in situ electrical calibrations, in which the heat evolution stops almost immediately after the calibrator is switched off. In contrast, the heat evolution caused by the adsorption of NH_3 continues at a high level for some 60 seconds after the injection is stopped, indicating that the initially adsorbed probe, which does not leave the adsorbent bed (i.e. is irreversibly adsorbed) diffuses through the sample with the generation of high heat of N_2 displacement. The 10 μmol NH_3 injection produces a peak with two maxima and a long tail but very little desorption. The molar heats of adsorption for the four pulses increase from 72 kJ mol^{-1} to 111 kJ mol^{-1}.

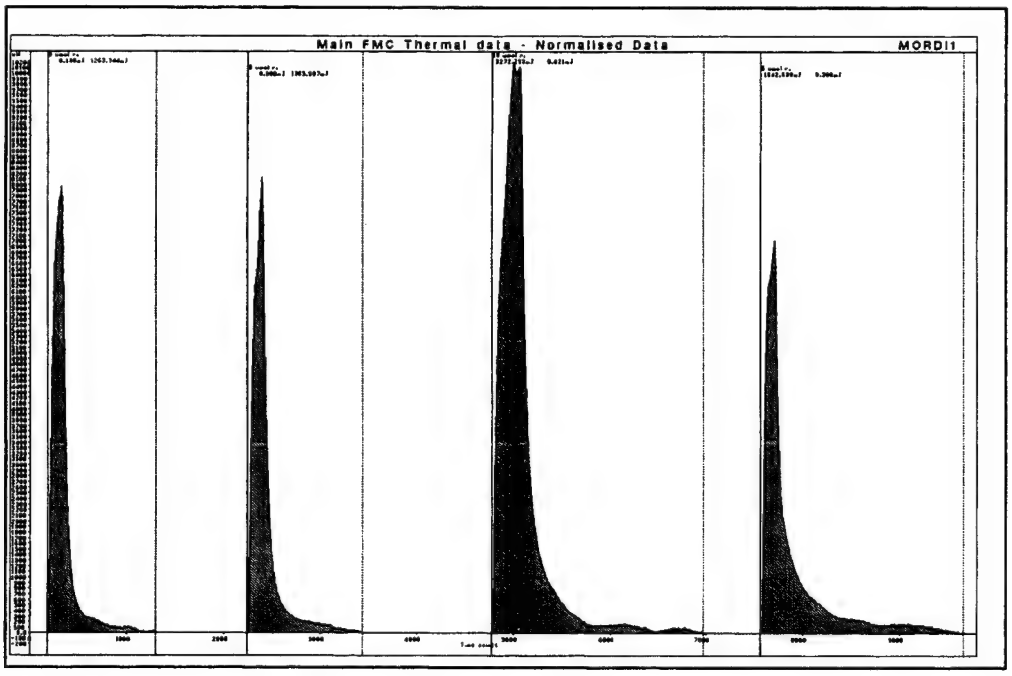

Figure 5 – Pulse adsorption of NH_3 from N_2 on MH zeolite at 208°C
(A series of injections of 5% NH_3 into an N_2 carrier flowing through 103 mg of MH zeolite at 208°C. There is no indication of desorption, but there may be some decomposition of the adsorbed NH_3 as suggested by the long tails of the third and fourth injections.)

It seems, therefore, that there is mobility in the strongly adsorbed NH_3, which in the presence of N_2 carrier passes from less active to more active sites which may initially be less accessible. The heat of adsorption increases after the initial stages of irreversible adsorption suggesting that pore filling phenomena may be playing a role in the adsorption process.

There is a marked difference between the results of static experiments as reported by Parillo and Gorte [2] and the present work which indicates significant differences in the differential heats of irreversible NH_3 adsorption with coverage in the range in which the statically obtained results remain constant around 150 kJ mol^{-1}. It is possible, of course, that the difference is due to the different nature of the MH zeolite sample used in the present work and the work reported by Parillo and Gorte. Further experimentation with the use of static and flow–through methods using identical samples would clarify this point. It is very interesting, however, that the heats of NH_3 adsorption in the presence of N_2 reached values which were significantly in excess of those reported by the above mentioned authors in spite of the fact that their MH zeolite samples were heated to 500°C before the *static* adsorption experiments were carried out. The samples used in the present work were merely purged with N_2 at 208°C before the preferential adsorption of NH_3 was determined under *flow conditions*. This raises the possibility that some of the active sites in MH zeolite samples are destroyed by the heating treatment at 500°C. Clearly further work in this area would be desirable.

Conclusions

The rates of heat evolution and adsorption occurring during interaction of NH_3 with MH zeolite and on BPL carbon show that the process is strongly influenced by acid site accessibility. The irreversibly adsorbed ammonia is mobile and in the presence of N_2 tends to occupy the strongest surface sites long after the supply of NH_3 is cut off.

The adsorption appears to occur initially on the most accessible, but not necessarily the most energetic, acid sites and most of this adsorption is irreversible.

It should be noted that the adsorption experiments carried out from nitrogen as a carrier gas, using flow adsorption microcalorimetry, produces higher heats of adsorption than those determined previously by static calorimetry on similar adsorbents heat treated to 500°C and evacuated before the commencement of NH_3 adsorption. This suggests that NH_3 adsorbed on evacuated surfaces is less strongly adsorbed than that adsorbed from N_2, which further suggests that the acidity of the evacuated materials is relatively low.

Simultaneous determination of the rates of heat evolution and mass transfer during the flow experiments reveals new information on surface heterogeneity of adsorbents which exist at atmospheric pressures of nitrogen. It is expected that the presence of other constituents in the carrier gas (such as water) would strongly affect the strength of acidity and the accessibility of the acid sites to basic probes. This information is clearly of crucial importance in the understanding of catalytic performance of the adsorbents in industrial practice.

References

1. Groszek, A. J. "Advances in characterization of adsorbents by flow adsorption microcalorimetry", *Studies in Surface Sciences and Catalysis*, **120A**, Adsorption and its applications in Industry and Environmental Protection – 1 Applications in industry, ed. A. Dąbrowski, 1999, pp. 143 – 175

2. Parillo, D. J. and Gorte, R. J. "Characterization of Acidity in H–ZSM–5, H–ZSM–12, H–Mordenite, and H–Y Using Microcalorimetry", *J. Phys. Chem.*, **97**, 1993, pp. 8786–8792

3. Gervasini, A. and Auroux, A. *J. Phys. Chem.*, **97**, 1993, pp. 2628–2639

4. Auroux, A., Muscas, M., Coster, D. J. and Fripiat, J. J. *Catalysis Letters*, **28**, 1994, pp. 179–186

5. Partyka, S. and Groszek, A. J. "Measurements of Hydrophobic and Hydrophilic Surface Sites by Flow Microcalorimetry", *Langmuir*, **9**, 1993, pp. 2721–2725

An Absolute Calibration Method For Microcalorimeters

P F Bunyan

Defence Evaluation and Research Agency, Fort Halstead, Sevenoaks, Kent, TN14 7BP (UK).

INTRODUCTION AND BACKGROUND

An Isothermal microcalorimeter, the Thermal Activity Monitor (TAM), has been used in this laboratory to study a variety of heat generating reactions of energetic materials since 1986 [1,2]. The operating principles of this instrument are described in reference 3. Until recently, the integral, internal, electric calibration heater supplied with unit has been the sole means of calibrating the instrument for power. While the accuracy of the instrument specified by the suppliers was considered adequate for these investigations, there has, until recently, been no convenient, independent, absolute way of checking that the selected power is still a true description of the energy applied to the detectors. It would therefore be possible for the internal calibration to become invalid, e.g. due to a change in the resistance of the heater itself, its electrical connectors, or a malfunction in the heater power supply, without the operator's knowledge. This would result in systematic errors in reported heat flow data when the calorimeter was used experimentally.

Internal calibration relies on generating heat from a resistance wire coil which is located in close proximity to the sample ampoule, although obviously not in precisely the same place. As the heater is not coincident with the sample and the heat flow detecting Peltier element cannot surround either heat source entirely, it is possible that the proportion of heat loss from each type of heat source (i.e. from the calibration heater, or due to a chemical reaction occurring inside an ampoule) which actually flows through the detector will differ and further errors could result. For this reason, the instrument operating manual suggests applying an approximate correction factor of about 4%, or, preferably, using an alternative method of calibration [4].

The problem of finding a suitable reaction that can be used for isothermal calorimeter calibration was discussed at the previous Workshop in this series and the need for more convenient, safe, universal and absolute calibration methods was highlighted [5]. The calibration requirements imposed by the need for laboratories to achieve ISO 9000 and NAMUS certification also make finding solutions to this requirement a priority.

An external method of chemical calibration which utilizes the heat generation during the hydrolysis of triacetin in an imidazole/acetic acid buffer located inside a sample ampoule has been described by Wadsö and Chen [6]. In order to know the true heat generated by such a reaction at a given time, it is essential to have a full description of the enthalpy changes, the temperature dependence of rate and the mechanism of the reaction. Even if these are known, the concentration and purity of all reactants must be carefully controlled and the reaction must not be influenced by the ampoule construction material. Consequently, the method is a demanding task for the analyst.

A second external means of calibrating the calorimeter has been suggested, using a radioactive material of known activity [5]. An americium probe has been used for this purpose in Sweden for more than a decade. However, problems of licensing, toxicity, transport and availability make this procedure unattractive in most cases [5,7].

The manufacturers of the thermal activity monitor have recently introduced an external electric heater. With the aid of a good calibrated multimeter, the exact amount of heat formed in the stainless steel ampoule can be deduced [8].

This paper describes the development and assessment of an alternative method for calibrating isothermal microcalorimeters using a well characterized, physico-thermal property of a stable, pure material of known mass, located in the same position that will be used for experimental samples.

THEORY

In order to deduce a valid calibration factor, it is essential to generate an accurately known amount of heat energy within an ampoule identical to those which will be used to study heat generating processes from thermally reactive samples. The energy produced must be capable of being determined using values of absolute quantities which can be measures accurately and independently.

Calibration Using Electric Heaters

Both the internal calibration device supplied with the TAM and the independent external calibration device rely on heating a resistance coil, located close to, or at, the intended site of the sample to be analyzed, electrically.

The manufactures supply a data acquisition and instrument control computer program with their external electric heater. This will carry out a calibration experiment and subsequently process the data to check the accuracy of the internal calibration and calculate a correction factor. The program requires that the voltage across the resistor and its resistance are measured manually and then input by the operator through the keyboard. Alternatively, if an accurately measured voltage is applied across the resistor and its resistance is known, the resulting power dissipated within the ampoule may be calculated directly as follows.

SKETCH

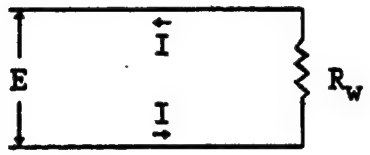

Where: R_W = Resistance of wire in ampoule (Ω)
E = Applied voltage (Volts)
I = Current (Amps)

From Ohm's law $I = E/R_W$ 1

And from the power law $q = I^2 . R_W$ 2

Where: q = Power generated within the ampoule (Watts)

Substituting equation 1 into equation 2

$$q = (E/R_W)^2 . R_W$$

Calibration Using Specific Heat Standard Material

A method to determine the specific heat of reactive materials, which relied on measuring the area under the recorded signal imbalance curve when the temperature of the TAM thermostat bath was altered, was described previously [9]. If the total area under the imbalance curve given by an accurately weighed sample of known specific heat is recorded during a temperature step, it is possible to calibrate the TAM for power by following the inverse procedure:

For a temperature step experiment in a calorimeter which has previously been calibrated using the internal electric heater.

$$C_{P(app)} = \frac{Q}{M_{CAL} \times T_{STEP}}$$

Where: $C_{P(app)}$ = Apparent specific heat of calibration material

Q = Total heat generation/consumption following temperature change indicated by internally calibrated calorimeter.

M_{CAL} = Mass of calibration sample employed

T_{STEP} = Temperature change experienced by system

Then correction factor to be applied to heat generation data = $\frac{C_{P(true)}}{C_{P(app)}}$

Where : $C_{P(true)}$ = Correct C_P of calibrant at the test temperature - as reported in the literature [11].

EXPERIMENTATION AND RESULTS

Two microcalorimeter cylinders, A and B, were investigated. These were installed in the thermostatted waterbath of the same calorimeter unit. All experiments were conducted between 76 and 77°C.

Equipment and Materials

A Thermometric 2277 microcalorimeter "Thermal Activity Monitor" (TAM) was used for this work. This calorimeter was purchased in 1986 and has been in continuous use since then. It is still using its original amplifiers, detectors and electronics. The specifications of the calorimeter, with regard to signal to noise ratio and long term drift, quoted at the time [4] were slightly inferior to those reported now for a new 2277 calorimeter [10].

Temperature step calibration experiments used an alumina specific heat calibration sample (α-Al_2O_3, Mettler-Toledo accessory 29801) contained in 5cm^3 stainless steel ampoules. The temperature in the sample detection region of each TAM cylinder was measured using a calibrated Hewlett Packard 2804A digital quartz thermometer (serial no. 02296/calibration certificate no. 35756T), which is accurate to better than 1/1000 °C. Samples were weighed on a Mettler AE163 analytical balance (serial no. D48019/calibration certificate no. E002148).

External electric calibration was performed using a Thermometric 4ml external calibration heater (Thermometric accessory 2611). Resistance and applied voltage were both measured using the Keithley 196 system DVM (serial no. 381016/calibration certificate no. 23717), which meets the accuracy, precision and 4 wire resistor reading requirements of the external calibration heater [8].

Electric Calibration

Internal

The instrument was calibrated, at the sensitivity range under investigation, internally using the thermal activity monitor's integral electric heater, as recommended by the manufacturers, prior to each type of external calibration [10].

External

Following internal calibration, the external calibration ampoule and matched blank ampoule were lowered into the detection regions of the calorimeter's sample and reference wells respectively. The system was allowed to equilibrate until a constant, zero signal was observed. After measuring the resistance of the heater, a voltage was applied by using the TAM's own power supply. When the resulting positive heat flow signal had settled to a constant rate, this apparent rate was recorded. The applied voltage was measured and used to calculate the true rate of heat generation within the calibration ampoule. Results are summarized in table 1.

Specific Heat Calibration Method

In order to utilize the dynamic range of the detector more efficiently and improve signal to noise ratio, the reference ampoule was ballasted at all times with approximately half the mass of alumina which would eventually be used for the calibration temperature step experiment - i.e. the ampoules were intentionally not of equal thermal capacity.

Following internal calibration, the pair of stainless steel ampoules were lowered into the detection region of the calorimeter and the system was allowed to equilibrate until a constant, zero signal was observed. The temperature of the calorimeter thermostat was recorded by a digital quartz thermometer probe located in an adjacent analytical cylinder. The operating temperature of the calorimeter was then either raised or lowered by approximately 1°C by altering the TAM's thermostat decade resistor settings manually. The resulting blank imbalance peak was recorded until the signal returned to zero. The final temperature of the system was then recorded using the quartz thermometer probe. This indicated that the true temperature variation experienced by the ampoules was actually 0.997°C in each case. The sample ampoule was removed from the calorimeter and an accurately weighed alumina calibration sample placed in it. The ampoule was returned to the calorimeter and a calibration temperature step experiment was performed using identical conditions to those employed for the earlier blank experiment. The total thermal activity due to the calibration sample could then be found by adding the areas under each imbalance peak together. The appearance of the resulting thermal activity curves obtained from cylinder A at ranges of 300 and 3000µW are illustrated in figures 1 and 2. The curves obtained from cylinder B resembled these and are not shown. Results are summarized in table 2.

DISCUSSION

Results obtained with both the external electric heater and temperature step method are broadly in agreement with regard to the magnitude of the systematic calibration error introduced by employing internal calibration. Since the two approaches rely on determining entirely different, absolute quantities, this is consistent with the view that both methods can be considered valid calibration procedures.

At low sensitivity (3000μW), both approaches indicate that a correction factor of .983 ± 0.003 should be applied to experimental results obtained after internal calibration. At higher sensitivity (300μW), the electric heater method indicates a very similar correction factor to that obtained at low sensitivity (0.987), while the temperature step method suggests that a gain of 0.965 is required.

The necessary corrections required to correct the internal calibration are therefore quite small; still less than the estimated error of 4% given when the calorimeter was purchased [4]. Considering that this calorimeter is over a decade old and is in continuous use at elevated temperature, it would appear that the longevity, stability and robustness of the original calibration system has been good. An annual external calibration check would therefore appear adequate for most quality assurance purposes.

The age of the instrument used for this study, the fact that it is used at elevated temperature and is not located in a constant temperature environment may account for the slight discrepancy in factors indicated by the two external methods at the more sensitive range. As the temperature step approach requires sample and reference ampoules to be poorly thermally balanced, this would exacerbate the effects of these environmental factors on the signal noise and drift characteristics and variability might be reduced if the calorimeter was relocated in a constant temperature room, or if a new calorimeter was employed.

In general, the temperature step approach utilizes materials and equipment that a thermal analysis laboratory would normally be equipped with anyway for unrelated, general experimental tasks; the calibration material used for this work is chemically inert, readily available as an inexpensive pure substance and is re-useable. All laboratories should have an analytical balance with a valid traceable calibration. However, an accurate, high precision, calibrated thermometer is essential.

When calibrating one analytical cylinder electrically, it would be possible to carry out isothermal microcalorimetry experiments in adjacent analytical cylinders. In contrast, most experiments would be interrupted during a temperature step calibration, except in the case of experiments to determine unknown thermal capacities, which can apply similar temperature step methodology [9].

A variety of different ampoules may be used in this type of calorimeter, such as glass ampoules, which are sealed with a crimped rubber lined lid. More sophisticated sample containers, with gas or liquid flow through tubing connections, titration, mechanical stirring and relative humidity control facilities, are also employed for specific experimental situations. It is not clear to what extent the different geometry, sample positions, construction materials and connecting tubing would alter the proportion of the total heat evolved during an experiment which passes across the heat flow detecting Peltier element compared to heat produced by a calibration device located in a dissimilar ampoule. It would be possible to investigate this possibility by manufacturing a version of each type of sample container with an electric heater located in the same position normally occupied by the sample. The development and construction of these ampoules would be a demanding engineering task, which would result in additional expense. Alternatively, it should be possible to achieve a similar result by doing a temperature step calibration within the same sample containers which will be used for experiments, without the need to construct or purchase any additional equipment.

CONCLUSIONS

An external calibration method suitable for use with isothermal microcalorimeters has been described which requires knowing only the mass of a pure, well-characterized, chemically stable material and the initial and final experimental temperatures. These absolute quantities can be determined accurately using calibrated instruments commonly available in an analytical laboratory.

Results obtained in stainless steel ampoules using the method show good agreement with those obtained using an external electrically heated calibration device, which relies on the measurement of entirely different, absolute quantities. This suggests that both methods are valid, absolute calibration procedures.

REFERENCES

1 P F Bunyan, Thermochimica Acta, 207 (1992), 147.
2 P F Bunyan and A V Cunliffe, Thermochimica Acta, 276 (1996), 131.
3 J Suurkuusk and I Wadsö, Chemica Scripta, 20 (1982) 155.
4 LKB 2277 Bioactivity Monitor Instruction Manual - No. 90 01 2963, LKB-Produkter AB, February 1985.
5 Proc. of TTCP Open Workshop on the Microcalorimetry of Energetic Materials - Final Discussion Section Lead by Dr P Laye, Leeds, UK, 7-9th April 1997.
6 I Wadsö and A T Chen, J. Biochem. Biophys. Methods., 6, No 4 (1982) 297.
7 J Suurkuusk, Proc of TTCP Open Workshop on the Microcalorimetry of Energetic Materials, Leeds, UK, 7-9th April 1997, Paper Z1-1.
8 Thermometric Technical Instruction Manual, Validation and Performance Service for TAM V1.0, Thermometric AB, November 1996.
9 P F Bunyan, Thermochim. Acta, 130 (1988) 335.
10 Thermometric 2277 Thermal Activity Monitor instruction manual, Thermometric AB, 1995.
11 D C Ginnings and G T Furukawa, J. Am. Chem. Soc., 75 (1953) 522.

TABLE 1 ***Calibration Using External Electric Heater***

Cylinder identity	Amplifier Sensitivity - as set with internal electric calibration heater/μW (full scale)	Nominal power selected through Digitam Software /μW	Resistance of external calibration heater/Ω	Voltage across external calibration heater/mV	Calculated heat generation rate /μW	Indicated heat generation rate/μW	Required correction factor to be applied to an experiment calibrated internally
A	300	300	49.2559	121.08	297.6	301.5	0.987
B	3000	3000	49.2579	381.8	2959	3010	0.983
A	3000	3000	49.2536	382.2	2966	3015	0.984
B	300	300	49.2706	120.89	296.6	300.2	0.988

TABLE 2 ***Calibration By Temperature Step Method***

Cylinder identity	Amplifier Sensitivity - as set using internal electric calibratio heater /μW full scale	Mass of Alumina calibration Standard /g	Temperature - Rise or Fall - /°C	Integral of ballasted blank experiment /mJ	Integral of calibration experiment /mJ	Total Heat evolved or consumed by alumina calibration sample /mJ	Apparent C_p indicated for alumina /J g^{-1} K^{-1}	Required correction factor needed, (given true C_p of alumina is 0.8717 J g^{-1} K^{-1} [11])
A	300	1.6667	R (0.997)	882	628	1510	0.9087	0.959
B	3000	6.4926	R (0.997)	1695	4053	5748	0.8879	0.982
A	300	1.6667	F (0.997)	881	631	1512	0.9099	0.958
B	3000	6.4926	F (0.997)	1701	4044	5745	0.8875	0.982
A	3000	6.4926	R (0.997)	2076	3673	5749	0.8881	0.982
B	300	1.6667	R (0.997)	529	967	1496	0.9002	0.968
A	3000	6.4926	F (0.997)	2081	3674	5755	0.8891	0.980
B	300	1.6667	F (0.997)	529	968	1497	0.9009	0.968

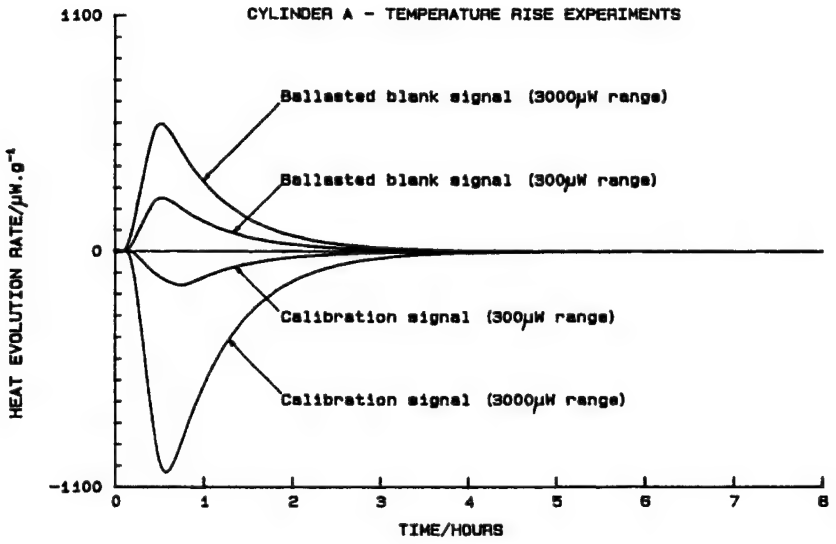

FIG 1 *Thermal activity curves resulting from temperature rise calibration experiments performed in cylinder A*

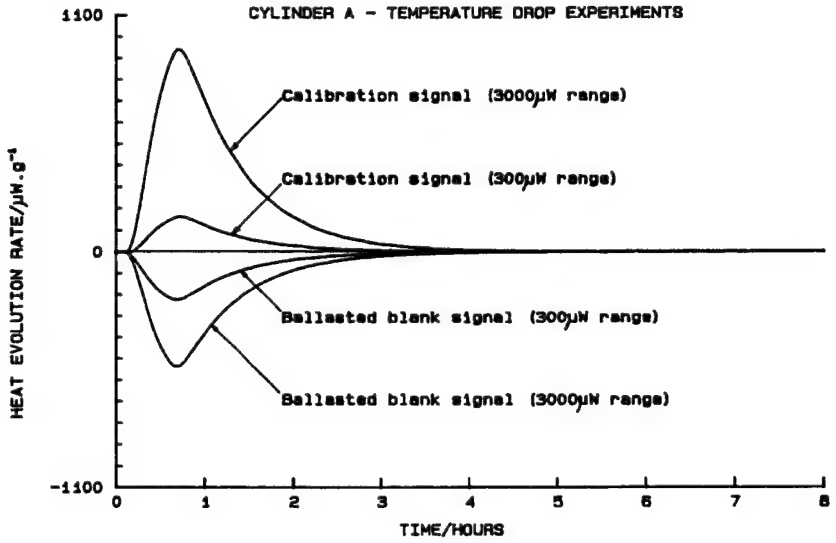

FIG 2 *Thermal activity curves resulting from temperature drop calibration experiments performed in cylinder A*

USE OF RH PERFUSION AMPOULE IN TAM AT ELEVATED TEMPERATURES

Mark A. Phipps[1] and Jaak Suurkuusk[2]

1. Thermometric Ltd, 10 Dalby Court, Gadbrook Business Park, Northwich, Cheshire, CW9 7TN, UK
2. Thermometric AB, Spjutvägen 5A, S-175 61 Järfälla, Sweden

Introduction

Feedback from a number of laboratories indicates that users of the RH Perfusion system have identified some specific difficulties when operating at elevated temperatures. Condensation in the sample ampoule and at the flow outlet has caused significant problems. In addition, long-term experiments have been difficult because of the premature emptying of the humidifiers.

The Thermometric R&D laboratory has addressed these problems and has resolved the difficulties by the introduction of a simple modification kit and some recommendations on operating procedure.

Tables of recommended flow rates and Flow Switch settings are given below. In addition the introduction of the Mass Flow Controller has contributed greatly to standardisation and overall ease of use of the RH systems.

Condensation in the sample ampoule

After removing the RH Perfusion system from the calorimetric unit at the end of a run at high temperature, it has been reported that the sample remaining in the ampoule is often saturated with water. This is normally caused by condensation of the saturated gas in the ampoule and main tube due to the sudden drop in temperature as the vessel is removed from the calorimetric unit. This problem can be overcome by programming the Flow Switch to run zero RH for about 15 minutes at the end of the experiment to thoroughly flush the system with dry gas.

Condensation at the flow outlet

When operating the RH perfusion system at elevated temperatures some users have reported that condensation of liquid occurs at the flow outlet. This effect has been overcome by a modification kit consisting of a new narrow bore perfusion shaft for the dry air line to replace the existing perfusion shaft.

The tube is made of stainless steel and has a bore throughout its length similar to the tip of the existing gas inlet to the ampoule. The narrower bore of the new perfusion shaft increases the efficiency of heat exchange. It reduces the surface area in contact with the outward flow, thus preventing the formation of condensation. The kit, which is simple to install in the laboratory, fits both 4ml and 20ml systems. It is delivered with full installation instructions. Ordering information can be found at the end of this information sheet.

Condensation at the flow outlet is also significantly reduced by use of a lower flow rate as described in the following paragraph.

Long-term experiments

Extended experiments at elevated temperatures have often failed because the humidifier vessels have dried out before the experiment has been completed. This problem can be overcome by operating at a reduced flow rate through the system. The table below shows that when operating at elevated temperatures the flow rate can be significantly reduced while still maintaining the same flow rate of water molecules.

When using high flow rates at higher temperatures there is a significant excess of water in the gas flow. The use of lower flow rates reduces the possibility of condensation problems occurring during the run.

Temp. in °C	**Flow rate in ml/hr at 25°C**				
	10	50	100	150	200
	Corresponding flow rate in ml/hr				
25	10.0	50.0	100.0	150.0	200.0
40	5.0	25.1	50.3	75.4	100.6
50	2.8	14.0	28.0	42.0	55.9
60	1.6	8.1	16.3	24.4	32.5
70	1.0	4.9	9.9	14.8	19.8
80	0.7	3.3	6.6	9.9	13.2
90	0.5	2.3	4.5	6.8	9.0

Table 1. Flow rate as a function of the operating temperature, giving the same water availability as at 25°C

Mass Flow Controller

When the RH Perfusion system was originally marketed, a peristaltic pump was the only available mechanism for the introduction of the gas flow. In 1998 the Mass Flow Controller

became available. This accessory uses a gas supply from a cylinder through a conventional gas regulator to produce a very precise and constant flow of gas. It is factory-calibrated for use with nitrogen gas and a correction factor should be used if any other gas is used. The flow rate from the device is controlled through the Digitam Software and becomes a part of the standard Experimental Method.

RH Correction Table

For operation at elevated temperatures, a correction equation[Ref 1] can be used to calculate the Flow Switch setting which will produce the required RH in the sample ampoule.

$$RH_{in} = \frac{1}{\left[1 - \left(\frac{P_{w,sat}}{P_0} \times (1 - RH_{set})\right)\right]} \times RH_{set}$$

where, RH_{in} is the required RH in the sample ampoule
RH_{set} is the fraction of the gas directed to the humidifier by the Flow Switch
$P_{w,sat}$ is the vapour pressure of water
P_0 is the back pressure of the system

Using this equation, it is possible to calculate the Flow Switch setting which will produce the required RH in the ampoule. These settings are given in Table 2 below.

Temp °C	$P_{w,sat}$ torr	Required RH% (RH_{in})					
		0	20	40	60	80	100
		Flow Switch Setting (RH_{set})					
20	18	0	19.6	39.4	59.4	79.6	100
30	27	0	19.4	39.1	59.1	79.4	100
40	48	0	19.0	38.5	58.4	78.9	100
50	86	0	18.2	37.2	57.1	78.0	100
60	148	0	16.8	34.9	54.7	76.3	100
70	243	0	14.5	31.2	50.5	73.1	100
80	365	0	11.5	25.7	43.8	67.5	100

Table 2. Flow Switch settings for obtaining the required RH at elevated operating temperatures

References

1. The derivation of the RH Correction Equation, Appendix to Technical Note 04, Thermometric AB, April 1999

Appendix

Assumptions and definitions

1. In the following presentation the Mass Flow Controller is used to maintain the constant flow of moles of dry gas.

$$\frac{dn_o}{dt} = \text{constant}$$

2. There are no significant drops in pressure in the system. This means that the total pressure in all parts of the flow system is equal to P_0, the external atmospheric pressure. This assumption is valid since the flow rates are very small.

3. The general gas law is valid.

$$P_x = n_x \times R \times \frac{T}{V}, \text{ where}$$

P_x is the partial pressure of the gas,
n_x is the number of moles of gas in the total volume V
R is the gas constant,
T is the temperature in Kelvin

By rearranging the equation and taking the first derivative of the gas law, the following relationship is obtained:

$$f = \frac{dV}{dt} = \frac{RT}{P_x} \times \frac{dn_x}{dt}, \text{ where}$$

f is the total volume flow rate in volume units per second

$\frac{dn_x}{dt}$ is the mass flow of the gas.

This is the relationship between the mass flow and the volume flow of a gas at constant total pressure and temperature.

4. RH_{set} is the fraction of the gas supply which is directed by the Flow Switch to the humidifier. When entering the RH_{set} value into the equation, divide the %RH value selected in the Digitam software by 100. For example, if the %RH programmed is 60%, enter 0.6 in the equation.

Step 1

The mass flow, $\frac{dn_0}{dt}$, from the Mass Flow Controller enters the Flow Switch where it is divided on a time basis to either enter the humidifier or to pass directly to the ampoule. The sum of the two resulting mass flows must be equal to $\frac{dn_0}{dt}$.

$$\frac{dn_o}{dt} = \frac{dn_1}{dt} + \frac{dn_2}{dt} = \text{constant(mol/sec)} \qquad \textbf{Equation 1}$$

$$\frac{dn_1}{dt} = \frac{dn_o}{dt} \times RH_{set} \text{ mol/sec} \qquad \textbf{Equation 2}$$

$$\frac{dn_2}{dt} = \frac{dn_o}{dt} \times (1 - RH_{set}) \text{ mol/sec} \qquad \textbf{Equation 3}$$

The total number of moles per second of gas, ($\frac{dn_{in}}{dt}$), entering the sample ampoule is equal to the sum of the two mass flows, ($\frac{dn_0}{dt}$), plus the number of water molecules entering the gas from the humidifier, ($\frac{dn_w}{dt}$). That is

$$\frac{dn_{in}}{dt} = \frac{dn_0}{dt} + \frac{dn_w}{dt} \text{ mol/sec} \qquad \textbf{Equation 4}$$

Step 2

The volume flow rate of carrier gas in litres per second entering the Flow Switch from the Mass Flow Controller is

$$f_0 = \frac{RT}{P_0} \times \frac{dn_0}{dt} \text{ l/sec} \qquad \textbf{Equation 5}$$

The pressure of the carrier gas is equal to the back pressure, P_0, (atmospheric).

Step 3

The following equations describe the volume flow rates for the carrier gas leaving the Flow Switch. The volume flow rate entering the humidifier is

$$f_1 = f_0 \times RH_{set} \qquad \textbf{Equation 6}$$

The volume flow rate passing directly into the ampoule, that is the dry gas is

$$f_2 = f_0 \times (1 - RH_{set}) \qquad \textbf{Equation 7}$$

Step 4

This must be explained in several stages.

The partial pressure of water in the humidifier is assumed to be the saturation pressure, $P_{w,sat}$, corresponding to 100% RH. The total pressure in the humidifier is equal to atmospheric pressure, P_0. This pressure, P_0, is made up of the partial pressure of carrier gas, P_1, plus the partial pressure of water. That is

$$P_0 = P_1 + P_{w,sat} \qquad \textbf{Equation 8}$$

The volume flow rate leaving the humidifier is greater than the flow entering the humidifier. This is because of the added water molecules in the carrier gas. The total pressure is constant and there is no accumulation of carrier gas. As the carrier gas and the water molecules are leaving the humidifier at the same volume flow rate, this flow rate can be expressed by the differential gas equation for both the mass flow of water and the mass flow of the carrier gas. Hence the outgoing volume flow rate, f_3, from the humidifier can be expressed as

$$f_3 = \frac{RT}{P_{w,sat}} \times \frac{dn_w}{dt} \ , \qquad \textbf{Equation 9}$$

or,

$$f_3 = \frac{RT}{P_1} \times \frac{dn_1}{dt} \qquad \textbf{Equation 10}$$

$$= \frac{RT}{(P_0 - P_{w,sat})} \times RH_{set} \times \frac{dn_0}{dt} \qquad \textbf{Equation 11}$$

By combining the above equations 9 and 11 expressing the outgoing flow rate, the following description for the mass flow of water is obtained

$$\frac{dn_w}{dt} = \frac{P_{w,sat}}{\left(P_0 - P_{w,sat}\right)} \times RH_{set} \times \frac{dn_0}{dt} \qquad \textbf{Equation 12}$$

Substitution of $\frac{dn_0}{dt} = \frac{P_0}{RT} \times f_0$ from Equation 5 into the above equation and with rearrangement gives

$$\frac{dn_w}{dt} = \frac{P_{w,sat}}{RT} \times \frac{P_0}{\left(P_0 - P_{w,sat}\right)} \times RH_{set} \times f_0 \qquad \textbf{Equation 13}$$

Step 5

As shown in Equation 4, the mass flow of molecules into the sample ampoule is

$$\frac{dn_{in}}{dt} = \frac{dn_0}{dt} + \frac{dn_w}{dt}$$

By using Equations 5 and 13 in the above equation and with rearrangement, the following expression for the mass flow is obtained.

$$\frac{dn_{in}}{dt} = \frac{P_0}{RT} \times f_0 \times \left[1 + \left(\frac{P_{w,sat}}{\left(P_0 - P_{w,sat}\right)} \times RH_{set}\right)\right] \qquad \textbf{Equation 14}$$

Step 6

The volume flow rate into the sample ampoule is

$$f_{in} = \frac{RT}{P_0} \times \frac{dn_{in}}{dt} \qquad \textbf{Equation 15}$$

By incorporating Equation 14 into Equation 15

$$f_{in} = f_o \times \left[1 + \left(\frac{P_{w,sat}}{(P_0 - P_{w,sat})} \times RH_{set}\right)\right] \qquad \textbf{Equation 16}$$

Step 7

The mass flow of water into the sample ampoule can be expressed by the actual partial pressure of water and the volume flow rate.

$$\frac{dn_w}{dt} = \frac{P_{w,in}}{RT} \times f_{in} \qquad \textbf{Equation 17}$$

By substituting Equation 16 for f_{in} in Equation 17, the expression for the partial pressure of water entering the sample ampoule is obtained.

$$P_{w,in} = \frac{RT}{f_0 \times \left[1 + \left(\frac{P_{w,sat}}{(P_0 - P_{w,sat})} \times RH_{set}\right)\right]} \times \frac{dn_w}{dt} \qquad \textbf{Equation 18}$$

Furthermore, by replacing $\frac{dn_w}{dt}$ in Equation 18 with the calculation taken from Equation 13 and with rearrangement, an equation for the partial pressure of water as a function of the RH_{set} is obtained.

$$P_{w,in} = P_{w,sat} \times \frac{1}{\left[1 - \left(\frac{P_{w,sat}}{P_0} \times (1 - RH_{set})\right)\right]} \times RH_{set} \qquad \textbf{Equation 19}$$

Step 8

The definition of the RH of the gas entering the sample ampoule is

$$RH_{in} = \frac{P_{w,in}}{P_{w,sat}} \qquad \textbf{Equation 20}$$

Step 9

Using Equations 19 and 20, the RH Correction Equation is obtained.

$$RH_{in} = \frac{1}{\left[1 - \left(\frac{P_{w,sat}}{P_0} \times \left(1 - RH_{set}\right)\right)\right]} \times RH_{set} \qquad \textbf{Equation 21}$$

MICROCALORIMETRIC METHOD TO DETERMINE THE CORROSION RATE OF LIQUID PROPELLANT AND METAL CONTAINER

Anton Chin, Daniel S. Ellison, Harry A. Farmer and Daniel R. Crowley
Test & Evaluation Department
Ordnance Engineering Directorate
Crane Division, Naval Surface Warfare Center
Crane, Indiana 47522-5001 USA

ABSTRACT

In our last paper presented at the 1st International Workshop on Microcalorimetry at Leeds, UK, we reported the design and development of a special metal ampoule which would fit the detector of the TAM Model 2277 microcalorimeter. The ampoule, made by machining the same alloy metal used for the actual container (17-7 PH stainless steel), was used to determine the compatibility, corrosion rate and safe storage life of metal containers containing liquid propellant IRFNA (Inhibited Red Fuming Nitric Acid).

The compatibility and corrosion rate between the metal and IRFNA were evaluated between 25, 30, 35, 40. 45 and 50°C. The corrosion rate as a function of these temperatures were determined. The safe storage life of the metal container was determined by pressure burst test at 20,000 psi.

In this paper, we will report the modification of the design of the test apparatus and methods used to determine the corrosion rate and the safe storage life of the container.

I. INTRODUCTION AND BACKGROUND

Liquid propulsion system containing IRFNA (Inhibited Red Fuming Nitric Acid) and MAF-4 (Hydrazine Derivatives) are widely used in the training missiles. Due to the corrosive nature of these ingredients, these system may possess high potential explosion hazard. A spontaneous explosion of one of the IRFNA container was reported during storage in a tropical country in Southeast Asia. Preliminary results from failure analysis indicated that the major cause for the explosion was probably due to the over-pressure from the IRFNA tank. In order to accurately simulate the accident at laboratory scale, a special sample cell was designed to fit the detector of TAM Model 2277 Microcalorimeter. The complete sample cell assembly, including inner cell for holding the sample and outer cell for protecting the microcalorimeter detector in case the inner cell cracks, was made at NSWC, Crane [1]. Both inner and outer cells were made by machining the same alloy metal used for the actual container (17-7 PH). The detailed design and methods of testing were reported in the Proceeding of the 1st International Workshop on the Microcalorimetry of Energetic Materials, 1987 [2].

The objective of this project is to determine if the shelf life of the training missile could be extended to a minimum five years or more at normal storage conditions by determining the compatibility and corrosion rate between the liquid fuel/oxidizer and the PH 17-7 alloy container. A three-way real time temperature, pressure, and degradation rate correlation table will be established to predict the shelf life of the fuel/oxidizer container system at various storage temperatures. The need for an extension of shelf life is due to the two year shelf life restriction which is presently in effect for the training missile due to the early incident. A scientific method was required to extend the shelf life and meet the realistic production or operational requirements of the program.

II. EXPERIMENTAL

1. Sample Identification.

a. Twelve test cell ampoules made from PH 17-7 stainless steel, four from each of the three groups of heat treated and welded test cell ampoules were subjected to a visual inspection, heat flow calorimetry, SEM tests, optical metallography, stress analysis and hydro burst tests. All samples used in the shelf life study are identified below.

b. Four plates from standard PH 17-7 stainless steel were supplied by Raytheon.

c. A 500ml sample of IRFNA (inhibited red fuming nitric acid) oxidizer in an inert container was provided by Raytheon.

d. A premixed 500ml sample of MAF-4 fuel containing 60% 1, 1-dimethylhydrazine, and 40% diethylenetriamine in an inert container was provided by Beechcraft (Raytheon).

2. Evaluation Process.

In this evaluation four plates approximately 1" x 1" x .063" of sheet metal from standard PH 17-7 tank material were provided by Raytheon. The first two plates were from plain tank metal which were used as models to calibrate the surface condition of the test cells made at NSWC Crane. The other two plates were two separate pieces of 1" x 0.5" x .063" tank metal welded together by a electron beam and were used in the controlled experiments. Before shipment to NSWC Crane all 4 metal plates were heat treated using the same process as the full size storage tanks.

All of the test cell ampoules used for this evaluation were machined at NSWC Crane from the same alloy metal block PH 17-7 stainless steel from Allegheny Ludlum) to the dimensions as illustrated in Figures 1a - 1c. The proportion of dimensions of the small scale sample cell was made as close as possible to that of the actual storage tanks.

After completion, the test cell ampoules were sent to Beechcraft for heat treatment and electron beam welding according to manufacturer's specification.

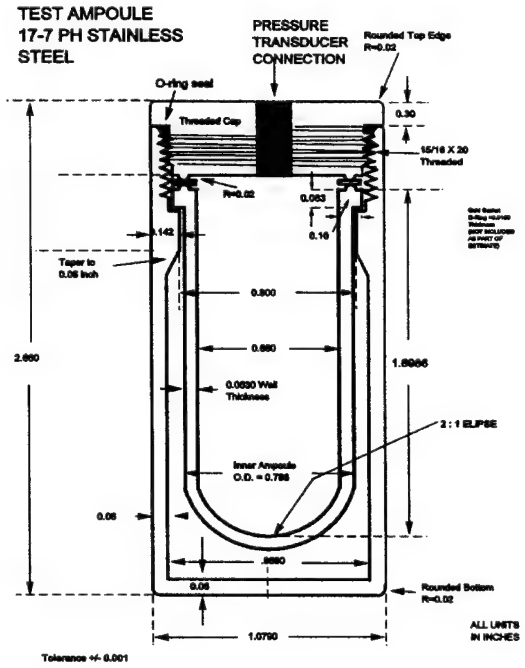

Figure 1a: Overall View of Microcalorimeter Test Cell for Corrosion Rate and Shelf Life Analysis of AQM-37 Fuel/Oxidizer Tank.

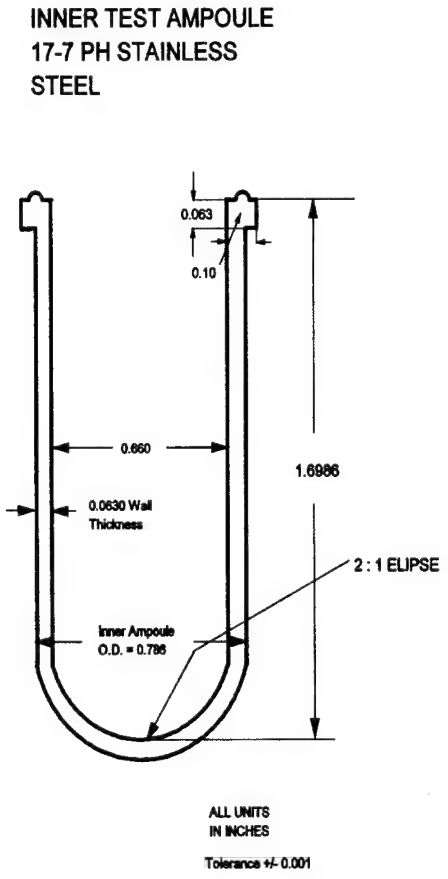

Figure 1b: The Dimensions of Inner Sample Cell for Oxidizer or Fuel.

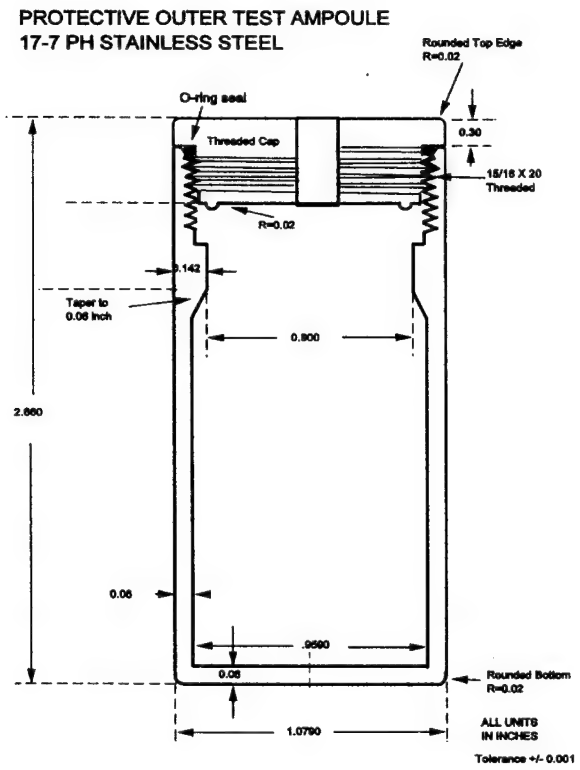

Figure 1c: The Dimensions of Outer Protecting Cell. The Purpose of This Cell is to Protect the Microcalorimeter Detector in Case the Inner Sample Cell Burst.

The small scale test sample cells were delivered to Beechcraft in three groups of four each. This was performed to determine if the heat treating and welding process were consistent for each of the three groups.

Samples of both the Fuel and Oxidizer were evaluated. Test cell ampoules were filled with both the IRFNA and MAF-4 samples to a point that the volume of ullage to sample ratio is proportional to the storage tanks. In addition some test cell samples were overfilled above the ullage level.

A. Microcalorimetry - Thermometric (TAM Model 2277). Isothermal microcalorimeter was used for the analysis. Measuring the heat flow of an energetic system (i.e. metal + acid) at different temperatures will establish the database for tabulating the accelerating factors. Accelerating factor is defined as the ratio of rate of reaction (k_2/K_1) or degradation (corrosion, etc.) at any two different temperatures (T_2 and T_1). The

accelerating factor by far is the most important single number for providing guidelines for an accurate and successful accelerating aging test. To conduct the accelerated aging test at the highest temperature, without compromising safety and/or changing the course of degradation mechanism, microcalorimetry is the best method to achieve the longest aging equivalent within the shortest possible time. Initial tests were conducted at 25, 30, 35, 40, 45 and 50°C. Different temperatures may be used depending upon the initial results. In general, the basic kinetic approach to determine the shelf life of the corrosion process follows the guidelines (a) Define the end of induction time. (b) Establish critical properties at zero aging time. This requires historical information and database analysis. (c) Obtain heat flow (μW) as function of temperature. (d) Identify limiting reactions (Reagents) which control the major aging and degradation processes (rate determine step). (e) Develop a quantitative model for properties as a function of time. (f) Determine orders of reaction and rate constants for property changes. (g) Fit rate constants to the Arrhenius Equation and determine the activation energy and accelerating factors of the corrosion process in a temperature interval between the natural storage and test temperatures. (h) Define critical property value (end of service life) of the item under test by calculating the maximum acceptable heat flow for the prevailing storage conditions (temperature, material quantity, etc.), using standard models for thermal runaway reactions. (i) Time to reach critical property value at various temperatures (Service life or shelf life) will then be determined.

B. Scanning Electron Microscopy (SEM)Test: An Amray Model 3200S, ECO SEM was used to perform this test. The SEM provides qualitative information on the corrosion by-product during the testing. The morphology information provided by the SEM will allow insight into the growth rate and method of corrosion.

C. Leco Neophot Optical Metallograph (LNOM): The LNOM test was performed on a cross-sectioned sample of the corroded material. The sample was polished and etched in accordance with ASTM procedures. The depth of pitting and corrosion mode, intergranular or transgranular, can show the potential failure mode of the material due to corrosion.

D. Stress Analysis-Hydro-burst Test: A stress analysis and hydro-burst test was performed on the test cells ampoules after exposure to aging. When two pressure cylinders of different size are subjected to the same internal pressure, the distribution of radial and tangential stress to the vessel wall is a function of the ratio of radius to wall thickness. In order to compensate for the differences, high pressures have to be applied to the smaller cell. A computer stress study was conducted to compensate for the difference before the actual hydro-burst test took place. Since the data from the hydro-burst test of the smaller container has to be compensated for by using higher pressure (>20,000 psia), therefore an higher deviation is expected.

E. Three-way Correlation Diagram of Corrosion rate, Temperature and Pressure Charts: Table (1) is by far the most important information for the responsible safety officer (RSO) to overview the entire relationship of degradation rate as a function of temperature and pressure over a known period of time. In a normal or emergency

situation, the RSO will be able to know the exact safety condition of the tank and make a quick judgement.

F. Aging Trend and Shelf Life: Based on the information from these tests the shelf life within the test temperature range (i.e. 25, 30, 35, 40 and 45°C) can be determined. Shelf life beyond this region has to be extrapolated by an Arrhenius Plot (Ln rate vs. reciprocal of test temperatures). The training missile APML and RSO will determine the final safety margin of extension for shelf life.

There are some limitations involved and some questions may arise about the microcalorimetric data being truly representative of the data from testing the actual storage tank and fuel/oxidizer. The answer is positive for the following three reasons: a) corrosion rate is measured in the unit of depth of corrosion per time (mm/year) which is independent of size, shape, and total surface area of the container: b) the test cell is nearly a true replica since it was made of the same material as the actual tank and later heat treated according to the manufacturer's specification; c) all theories and test methods are based on science and existing procedures.

III. TEST RESULTS

The following paragraphs present the overall test results of all test parameters.

1. **Visual Inspection**. All test samples were subjected to an incoming visual inspection. The inspection revealed that no damage had occurred during shipment and no other defects were observed.

2. **Electron Microscope Inspection.** All twelve samples were subjected to inspection prior to thermal analysis and no major defects were revealed.

3. **Microcalorimetry Analysis of IRFNA.** Twelve samples were subjected to microcalorimetry tests. During the tests the temperature and pressure was monitored and the output data from the test samples was recorded by the Microcalorimetry Test Set. Before the actual data was taken, the sample container was preleached 3 times with IRFNA to assure the surface of the PH 17-7 metal was passivated. The IRFNA was then filled to a point where the volume ratio between IRFNA and ullage are proportional to that of the actual IRFNA container in the training missile. After the pressure transducer was connected, the sample cell was inserted into the micro calorimeter for heat flow measurement after temperature equilibrium was reached. Three micro calorimeters (TAM Model 2277) were used in the analysis. During the test, the temperature and pressure output data from the test samples were recorded by the TAM micro calorimeter. The TAM micro calorimeters are equipped with 4 measuring cells with a sample and a reference heat detector for effective suppression of thermal noise. The measuring cells are all in a constant temperature controlled water bath. The baseline stability over 8 hours at 25 °C is within ± 0.05 μW in static mode, and ± 0.5 μW in liquid flow mode. The sample capacity was in between 4 to 25 ml. The TAM

was used to perform the tests between 25 and 50 °C. Based on the data all twelve samples exceeded minimum safety specifications. A typical micro calorimetric heat flow chart is shown in Figure 2 and the rate of corrosion as function of temperature and pressure are shown in Table 1. The comparison of corrosion rate and pressure build up in the IRENA sample cell can be seen in Figures 3 and 4.

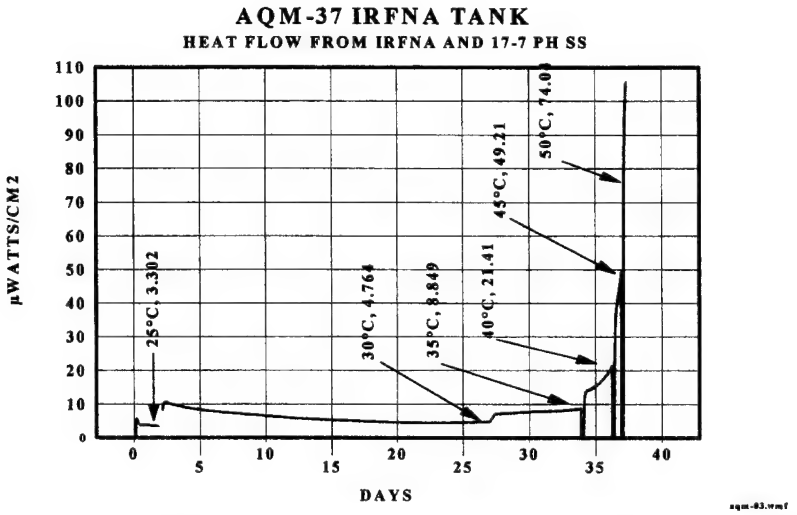

Figure 2. Microcalorimetric Heat Flow Analysis of IRFNA and PH 17-7 Steel at 25, 30, 35, 40, 45 and 50°C.

Table 1. MICROCALORIMETRIC ANALYSIS OF REACTION OF IRENA WITH PH17-7 STAINLESS STEEL

TEST TEMPERATURE (°C)	STEADY STATE HEAT FLOW (μW/cm^2)	CORROSION RATE mm/year	%per year	PRESSURE (PSI)
25	3.302	0.0165	1.031	3.6
30	4.764	0.0238	1.488	6.0
35	8.849	0.0443	2.769	13
40	21.41	0.1071	6.693	20
45	49.21	0.2461	15.38	56
50	74.04	0.3702	23.13	76

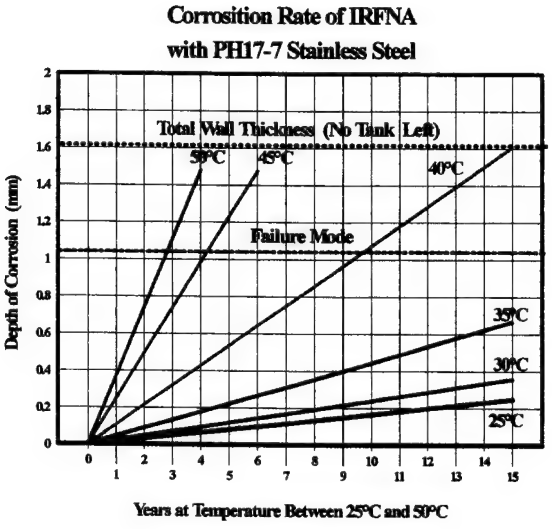

Figure 3: Corrosion Rate

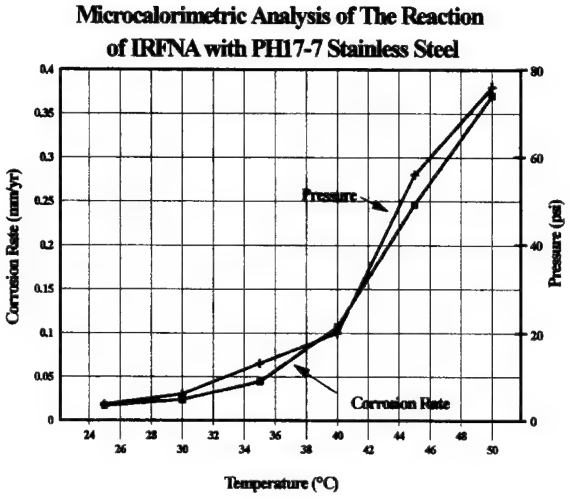

Figure 4: Pressure

4. Micro calorimetry Analysis of MAF-4

The MAF-4 tests were conducted in the same way the IRENA was tested. During the tests the temperature was monitored and the output data from the test samples was recorded by the Micro calorimetry Test Set. Before the actual data was taken, the sample container was preleached 3 times with MAF-4 to assure the surface of the PH17-7 metal was passivated. The MAF-4 was then filled to a point where the volume ratio between MAF-4 and ullage are proportional to that of the actual MAF-4 container in the training missile. After the sample cell was inserted into the micro calorimeter for heat flow measurements temperature equilibrium was reached. Three micro calorimeters (TAM Model 2277) were used in the analysis. During the test, the temperature data from the test samples were recorded by the TAM micro calorimeter. A typical MAF-4 micro calorimetric heat flow chart and rate of corrosion as function of temperature is shown in Figure 5. The thermal data collected from the Micro calorimetry test conducted on the MAF-4 indicated the heat flow rate were below 2 μ watts at 40°C. A heat flow of 2 μ watts is generally used as the criteria to determine the thermal safety of energetic materials.

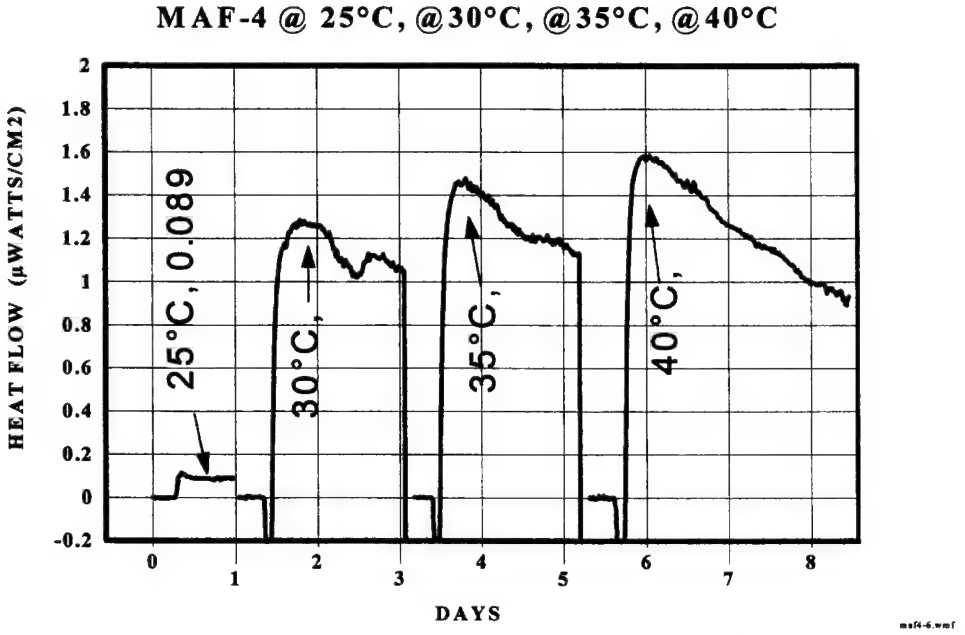

Figure 5: Microcalorimetry Analysis on MAF-4

This means that the test data indicated the corrosion rate for the MAF-4 was considered low. Overall, the test results indicated the MAF-4 storage tanks should meet the minimum five year shelf life requirement without jeopardizing safety. If shelf life beyond five years is required additional testing should be conducted.

5. Stress Analysis and Hydro Burst Test

A stress analysis was conducted to determine the amount of pressure that should be applied to the small scale test cell ampoules. The analysis determined that 20,000 PSI would be required to equal the same amount of hydrostatic pressure used for the pressure proof test of the actual propellant tank by the manufacturer. Hydro burst tests were performed after accelerated aging and stress analysis of the test samples. All of the Hydro bursts test were conducted by NSWC 's Calibration laboratory.

The Micro calorimetry data from the IRENA tests determined that the rate of corrosion/year was equal to 0.016 millimeters at 25°C, 0.16 millimeters for 10 years and 0.24 millimeters for 15 years. (See Table 1) A large amount of time is consumed for the corrosion rate to etch the same amount of material from the test cell ampoules, therefore,

a decision was made to machine away part of the material from the outside of the test cell amploules. This would provide a verification of the calculated corrosion rates. The calculated corrosion rates (Table 1) determined the amount of material that was machined from the test cell ampoules.

Based on the results of stress analysis the test cell ampoules used to conduct the accelerated aging tests were pressurized to 20,000 PSI for 30 minutes. After passing the 20,000 PSI test the pressure on the test cell ampoules was increased to 22,500 PSI for 1 hour. All of the test cell ampoules withstood the 20,000 PSI test without burst, however, minor deformation of the test cell ampoules began when temperatures reached 35°C.

While machining one of the test cell ampoules for testing at 40°C, which is equal to 10 years of exposure to corrosion, a defect was observed. The defect, as shown in Figure 6, indicates this void was in the test cell ampoule before it was machined. It appears that the defect was caused by the electron beam welding process. This may indicate that the welding process used on the PH 17-7 stainless steel material should be monitored more closely. However, it should be noted that the PH 17-7 stainless steel used to manufacture the test cell ampoules was manufactured from a single piece of stainless steel while the storage tanks used by the training target missile is composed of three separate pieces of PH 17-7 stainless steel. It is not known at this time how this difference may affect the performance of the storage tanks. Perhaps the use of ultrasound may be more helpful to determine if voids or air bubbles are occurring during the welding process. After machining the test cell ampoules Hydro Burst tests were performed at ambient temperature for each of the temperatures shown in Figure 7. Beginning at 25°C which is equal to a corrosion rate of 10 years and also at a corrosion rate of 15 years. Hydro burst tests without ullage were repeated at the 10 and 15 year age equivalent at 30°C and 35°C with no burst. The burst occurred at 40°C test (10 years age equivalent). Testing at 40°C for 15 years was unnecessary because the corrosion rate is greater than 100%.

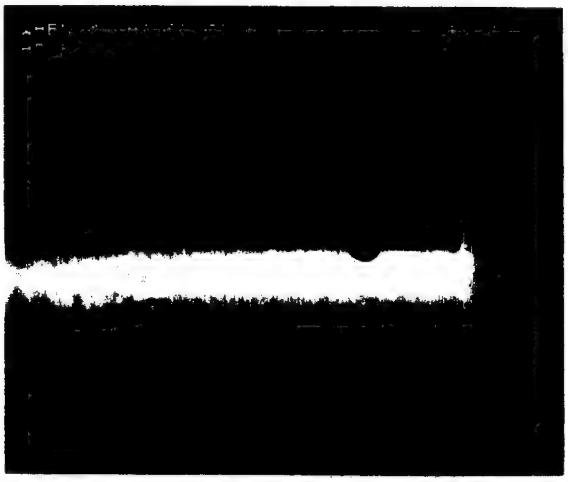

Figure 6: 10 years @ 40°C

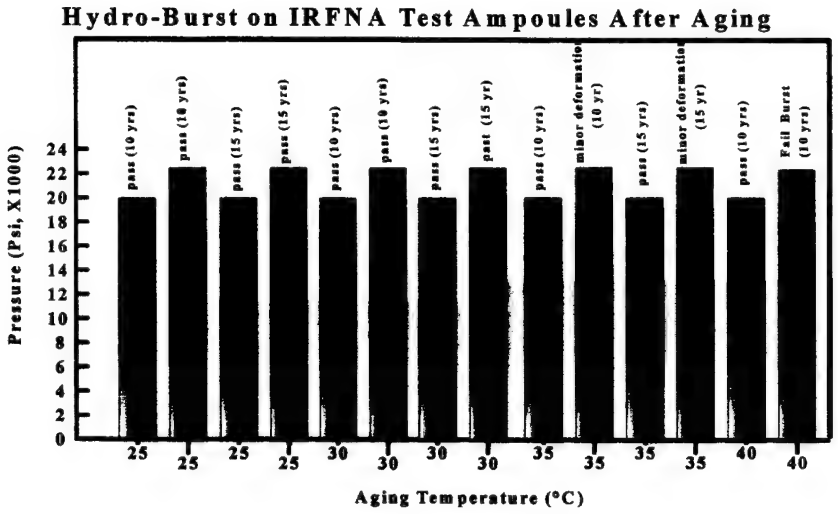

Figure 7: Hydro Burst on IRFNA Test Ampoules After Aging

To determine when burst would occur, one of the test cell ampoules, shown in Figure 8, was machined to equal 40°C at 10 years. The ampoule developed a rupture when the pressure within the test cell ampoule reached only 4,500 PSI. The rupture, as indicated by the small hole along the bottom, occurred at the closed end of the test cell ampoule. The ruptured hole appears next to the intersection of the electron beam welds.

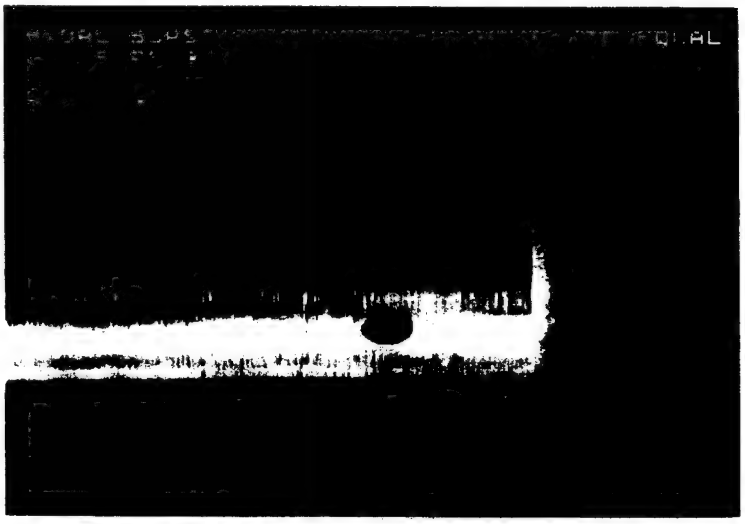

Figure 8: Burst @ 4,500 PSI

One of the

40°C 10 year equivalent test cell ampoules, after being exposed to 20,000 PSI for 30 minutes, burst when the pressure was increased to 22,300 PSI (see Figures 9 and 10). This proved that the test cell ampoules may withstand the pressure and corrosion tests up to 40°C at 10 years aging equivalent corrosion before burst would occur.

Figure 9: Burst @ 22,300 PSI

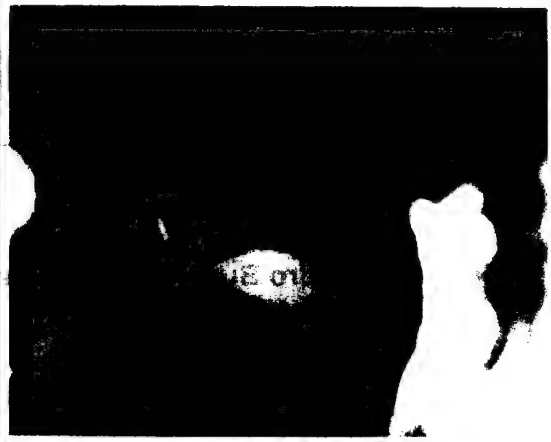

Figure 10: Inside View of Burst

The hydro burst test was considered the final proof the PH 17-7 stainless steel storage tanks used for both the IRENA oxidizer and MAF-4 fuel could withstand both the corrosion and pressure at 25°C. Based on these test results the PH 17-7 stainless steel storage tanks will meet the necessary requirements needed to extend the shelf-life to meet the five years required. However, current hydro burst data indicates that the IRENA can meet a maximum shelf life of 7 years at 25°C and 5 years at 30°C.

6. Metallographic Microstructure Analysis of Cold-rolled Stainless Steel

A sample of the PH 17-7 cold-rolled stainless steel used in the storage tanks was sent to NSWC Crane Code 4052 for Metallographic Microstructure Analysis. The samples were evaluated to determine its microstructual identification, cold-rolling characteristics and presence of corrosion as a zero time point for future identification. The evaluation was performed by cutting the samples on a metallographic cut-off saw to enable it to be potted as two separate samples. Potting and preparing the metallographic samples in this way enabled the pieces at locations ninety degrees to one another to be examined for the purpose of seeing the cold-rolling affects to the microstructure and any corrosion in both these zero time and future samples.

The results indicated the samples were a 301 stainless steel which is a match for the material specified as PH 17-7 stainless. It was also determined that the sample had been cold-rolled. These characteristics were determined by the grain structure when etched. Representative photomicrographs were taken of the grain structure . The grain structure indicates no presence of corrosion development at the time zero point.

IV. DISCUSSIONS

Twelve samples from three groups of four were subjected to heat flow calorimetry tests and the data indicated the IRENA and MAF-4 samples were thermally stable with minimal degradation at ambient temperatures. Testing of both the IRENA and MAF-4 samples showed no significant variation due to age. Equilibrium occurs rather early once the test cell ampoules are filled. Then the temperature and time in storage determines the corrosion rate.

This was the first time these samples were exposed to Micro calorimetry tests. The reaction rate observed were within the regions expected. The test temperatures were constant at 25°C to 50°C, however, normal temperatures will be variable depending on the location and length of storage. Overall, the data from all of the tests indicate the IRENA and MAF-4 shelf life should meet the minimum five year shelf life requirements at ambient temperature.

V. CONCLUSIONS

From the evaluation results the following conclusions have been reached. The PH 17-7 stainless steel test cell ampoules which were used to determine the corrosion rates were manufactured by NSWC Crane. The test cell ampoules were heat treated and welded by Raytheon Corporation in Wichita, Kansas, to simulate the fuel tank construction.

Thermal analysis tests support the finding that the fuel and oxidizer are thermally stable at ambient temperature. However, as temperatures increase in the IRENA, the degradation increases dramatically. Thermal analysis data, from IRENA ,indicated the rate of degradation and pressure dramatically increased with temperatures above 45°C. Therefore, if the storage temperature is above 45°C , the pressure increases and becomes a safety factor.

Three different groups of PH 17-7 heat treated and welded samples were evaluated and no significant difference in the heat treating and welding process was observed.

The current quality of the IRENA and MAF-4 container system are satisfactory for in-service use if stored at temperatures below 30°C. Therefore, handling or storage safety is not considered a hazard provided standard handling instructions are observed.

The shelf life of the IRENA and MAF-4 container system should meet the minimum five year requirement provided the materials used meet the weapon specification. The current hydro burst data indicates that the IRENA can meet a maximum shelf life of 7 years at 25°C and 5 years at 30°C.

VI. RECOMMENDATIONS

Based on the test results and an analysis of data the following recommendations are made.

The IRENA and MAF-4 storage tanks should be retained as Serviceable, if stored below 30°C. Storage tanks should not be stored at temperatures above 35°C for prolonged periods to prevent degradation from corrosion and over-pressurization. Temperatures above 30°C should be monitored and recorded closely to ensure safety is not jeopardized.

Future evaluations should include both older and newer production samples of fuel and storage tanks to ensure a sample that is representative of the stockpile. The next shelf life study should be in FY-2001 to monitor the stockpile for aging trends to determine if the safety and serviceability of the fuel/oxidizer container system is continuing to meet specifications.

VII. REFERENCES

1. Naval Surface Warfare Center, 300 Highway 361, Crane. Indiana 47522

2. A. Chin, D. S. Ellison, D. R. Crowley and H. A. Farmer, "Micro calorimetric Criteria For Evaluation of Corrosive Liquid Propellant on Metal Containers". **Proceeding of the 1st International Workshop on the Micro calorimetry of Energetic Materials (7-9 April 1997, Leeds, United Kingdom), and references therein.** Published by Defense Research Agency (DRUMS), WX3 Pyrotechnics Group, Electro-optic Warfare department, Fort Halstead, Sevenoaks, Kent TN14 7BP, United Kingdom.

A NEW DIFFUSION CONTROLLED CALIBRATION AND TEST DEVICE FOR MICROCALORIMETERS

Lars Wadsö[1], Vitaly Kocherbitov[2]

1. Building Materials, Lund University, Sweden (Lars.Wadso@byggtek.lth.se)
2. Physical Chemistry 1, Lund University, Sweden (at leave from Department of Chemical Thermodynamics and Kinetics, S.-Petersburg University, Russia)

1 Abstract

Calibration of microcalorimeters is normally done by electrical or chemical calibration or with radioactive calibration devices. We have developed a fourth type of calibration device that consists of an ampoule with two small chambers connected by a thin tube. In each of the chambers we place chemical systems with constant - but different - vapor pressures (e.g. saturated salt solutions, water, drying agents). A diffusive flow of vapor will than take place from high to low vapor pressure. The flow rate is governed by the geometry of the thin tube. The thermal power generated is proportional to the vapor pressure difference and the sum of the enthalpies of the vaporization and condensation processes in the two chemical systems.

2 Introduction

The calibration and testing of microcalorimeters is an important issue. The quality of a measurement cannot be ascertained if an instrument is not calibrated at regular intervals and also tested at shorter intervals to make sure that it is still functioning as it did when it was calibrated. It is advantageous to calibrate and test calorimeters with devices and procedures that generate heat in the same way as the experiments being performed. It is therefore good to have a number of different types of calibration equipment for different purposes.

Today there are basically three methods used to calibrate microcalorimeters: electrical, radioactive and chemical calibration. Here a fourth physical method is described: diffusion-controlled vaporization-condensation.

3 Nomenclature

a	(water) activity	1
D	diffusion coefficient with vapor pressure as potential	mol/m/s/Pa
ΔH	overall enthalpy of calibration vessel (Eq. 2)	J/mol(water)
$\Delta_1 H$, $\Delta_2 H$	enthalpies of condensation of water into systems	J/mol(water)
K	transport coefficient of ampoule	mol/s/Pa
ℓ	tube length	m
p_{sat}	saturation vapor pressure of water	Pa
P	thermal power	W
q_m	mass flow rate	mol/s
r	tube radius	m

indices

1	vaporization (high activity) chamber
2	condensation (low activity) chamber

4 Experimental method

In the present method the thermal power for calibration is produced by a vaporization-condensation process. The rate of this process is governed by diffusion through a thin tube that connects two small chambers in a calorimetric ampoule. The chambers are charged with systems with different vapor pressures; preferably systems whose vapor pressures do not change when water is added or removed.

Figure 1 shows a schematic cross section of the calibration ampoule used in the present experiments. It has an outer diameter of 13.85 mm. Each of the two chambers has a diameter of approx. 12 mm and a height of 16 mm. The seals are made of teflon and the three parts are screwed together. The diffusion tube has a length of 18 mm and an inner radius of 0.32 ± 0.02 mm.

The calorimeter, which was built at Division of Thermochemistry at Lund University (calorimeter C in Bäckman et al. [1]) is similar to a Thermometric microcalorimeter, but each ampoule is surrounded by 16 thermocouple plates. All tests have been conducted with the microcalorimeter in a TAM thermostated bath (Thermometric, Järfälla, Sweden).

During the experiments a 20 μW radioactive Am^{241}-sample was used to generate a constant thermal power. Baselines taken with an empty steel ampoule were close to 0 μW.

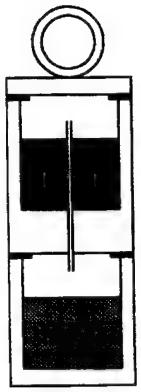

Figure 1: A schematic drawing of the calibration ampoule.

5 Theory of method

The thermal power produced by the calibration ampoule is given by the following general equation:

$$P = q_m \Delta H \tag{1}$$

Here, ΔH (J/mol) is the overall enthalpy of the vaporization-condensation process:

$$\Delta H = \Delta H_2 - \Delta H_1 \tag{2}$$

Here, $\Delta_1 H$ and $\Delta_2 H$ are defined as the enthalpies of condensation of water vapor into the respective systems.

Diffusion of vapor through the system is governed by Ficks law:

$$q_m = K p_{\mathrm{sat}} (a_1 - a_2) \tag{3}$$

Here, K is the vapor conductivity coefficient that is mainly governed by the tube geometry:

$$K \approx D \frac{\pi r^2}{\ell} \tag{4}$$

At 25°C $D = 10.1 \cdot 10^{-9}$ mol/m/s/Pa. For the present device $K \approx 180 \cdot 10^{-15} \pm 20 \cdot 10^{-15}$ mol/s/Pa. We have made computer simulations that show that more than 96% of the diffusion resistance is in the tube; i.e. less than 4% is in the chambers.

There are two primary criteria for choosing chemical systems for the calibration device:

- constant equilibrium water activity.
- constant enthalpy of condensation.

A number of different chemical systems may, at least in theory, be used in the two chambers:

1. Water will give $a = 1$ and $\Delta H_1 = \Delta_{\text{vap}} H$.
2. Some drying agents will give $a = 0$ and at the same time have a constant ΔH_2 over a certain capacity range. We have used 5 Å molecular sieves in the present study.
3. A saturated salt solution will give constant a and constant ΔH_1 (or ΔH_2). Enthalpies may be calculated from the enthalpy of formation of solution, the number of waters in the highest hydrated form of the salt, and the molar ratio of water in the saturated solution of the salt.
4. Liquids - like mixtures of sulfuric acid and water or glycerol and water - may also be used. For such systems both activity and enthalpy are concentration dependent and these dependencies must be known as they will influence the thermal power of the calibration device. In such cases the thermal power may not be constant, but the change will be small and predictable.

The calibration ampoule is charged with a pair of chemical systems from the above list. In theory a very large number of systems may be used, but for practical purposes the useful combinations are quite limited. The main limitations are the following:

- Each of the systems must under practical conditions behave as if under equilibrium conditions.
- The two systems must have a high enough water activity difference (Eq. 3).
- The two systems must have a high enough difference in condensation enthalpy (Eq. 2).

The combination of the activity difference and the enthalpy difference (second and third points above) is what gives the resulting thermal power. The present calibration ampoule has a narrow diffusion tube and therefore gives low flow rates. Enthalpy changes (ΔH) in systems consisting of two saturated salt solutions (or water and a saturated salt solution) are usually quite low. Because of this, the thermal power of the present calibration ampoule charged with such systems was only in the order of 1 μW.

The mass flow rate is very low in the present device. In the experiments presented in this paper the flow rate was less than 1 nmol/s, i.e. it will take more than three months for the water level in the vaporization chamber to decrease by 1 mm.

The time during which the thermal power is constant (or well known) may be calculated from a knowledge of the limiting capacity of the chemical systems:

$$t = \frac{\min(c_1, c_2)}{q_m} \tag{5}$$

Here, c is the number of moles that a system can take up or give away without loosing its wanted properties and $\min$ signifies the lowest of the c-values.

6 Materials

The following materials were used in the present experiments:

- 5 Å molecular sieves that were dried at 350°C for several days prior to use.
- Sulfuric acid (97 mass-% as measured with a Paar densitometer). The acid was placed in a thin-walled glass vessel to prevent reactions with the steel.
- Millipore (MQ) water.

The radioactive calibration sample was placed in a stainless steel ampoule of similar size as the calibration ampoule.

7 Results

Figure 2 shows the results of tests of the calibration ampoule done with the systems given in Table 1.

	bottom	top
1	5 Å molecular sieves	water
2	water	5 Å molecular sieves
3	sulphuric acid	water
4	20 μW radioactive sample (Am^{241})	

Table 1: The systems with which the calibration ampoule was charged during the present measurements.

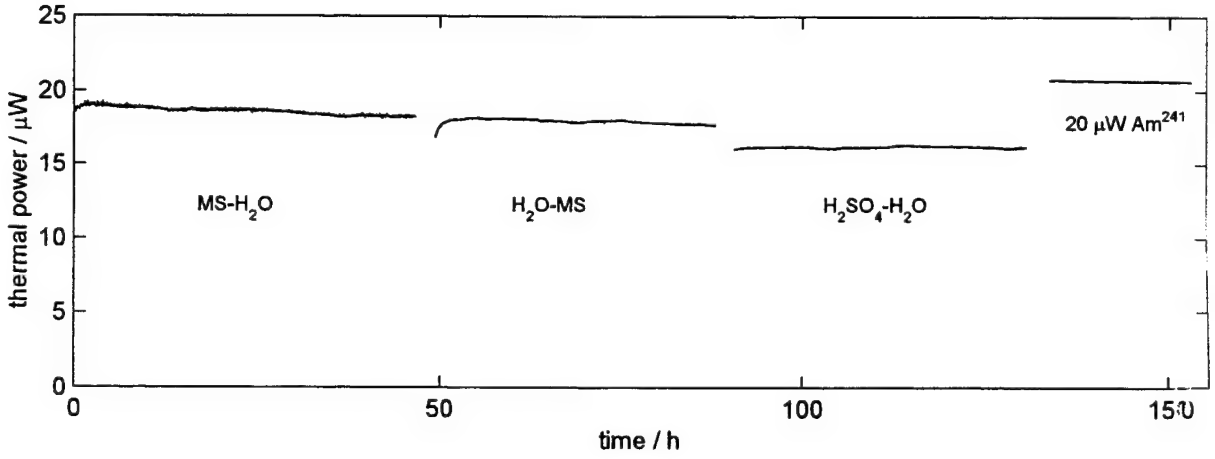

Figure 2: A series of three measurements made with the calibration ampoule (shown in Fig. 1) and one measurement with a radioactive calibration sample. The thermal power scale is only approximate as no absolute calibration was done during the present study.

8 Discussion

In the present experiments sulfuric acid and water gave the most constant thermal power. During the 40 h experiment seen in Fig. 2 the thermal power was constant within less than $\pm 1\%$. The result is was not so good for molecular sieves and water that gave a slightly decreasing thermal power. Note, however, that almost the same thermal powers were obtained when the molecular sieves and the water were interchanged.

In this paper we present a new method for calibrating microcalorimeters. Potential advantages with this method are:

- One calibration vessel may be charged with different combinations of saturated salt solutions, drying agents or liquids to give a wide range of thermal powers.
- The substances used are easy to handle in a laboratory.
- It is easy to charge a vessel and start a calibration.
- Not only exothermic, but also endothermic thermal powers may be produced (at least in theory).
- Once charged, a calibration vessel may produce a constant thermal power for quite long periods of time.

We have noted two problems with the present device:

- The thermal powers sometimes have a slope (in most cases giving a decreasing signal). The measurements with water and molecular sieves shown in Fig. 2 is an example of this. We suggest this is caused by changes in the properties of some of the chemical systems during the experiments, but there may also be other factors that play a role in this.
- In all heat conduction calorimeters part of the heat produced in the ampoule does not pass through the heat flow sensors, but is lost through other conduction paths. In the present device an exothermic thermal power and an endothermic thermal power are generated in different parts of the ampoule. The lost fraction of the heat will not necessarily be the same for these two heat sources. The result may be that the device will generate different thermal powers in calorimeters with different heat loss paths. We

believe we have this problem to some extent with the present device, but it is certainly possible to design a vessel in which this problem will be eliminated.

The thermal power from the present type of vessel is difficult to calculate from geometric data as the tube diameter cannot be measured with high enough accuracy. Therefore, each calibration ampoule will probably have to be calibrated in a calibrated calorimeter and then used to calibrate or test other calorimeters. It is not known what accuracy and precision an optimized device of this type will have.

The main use of the device will be similar to the use of radioactive calibration sources; as a simple way to generate constant thermal powers. It has the advantage over radioactive sources in that it contains only compounds that can be handled without problem in any laboratory. The charging of a vessel takes approx. 5 minutes.

The ampoule is inserted like any other calorimetric insertion vessel. However, care must be taken so that the vessel is not tilted or shaken. If a drop of liquid or a grain of drying agent clogs the diffusion tube the result will not be correct. The output of the device will be temperature dependent; mainly because the saturation vapor pressures is temperature dependent.

9 Conclusions

A new diffusion controlled calibration device for microcalorimeters is presented. Charged with common laboratory substances it produces constant thermal powers for long periods of time.

10 References

1. Bäckman, P., Bastos, M, Hallén, D., Lönnbro, P and Wadsö, I., J. Biochem. Biophys. Methods 28 (1994) 85-100.

MICROCALORIMETRY AND DSC STUDY OF THE COMPATIBILITY OF ENERGETIC MATERIALS

By Albert S. Tompa and William F. Bryant, Jr.

Indian Head Division Naval Surface Warfare Center
101 Strauss Avenue, Indian Head, MD 20640-5035

Abstract:

Isothermal microcalorimetry (IMC) analyses at 55 to 75°C and DSC analyses at decomposition temperatures (180 to 300°C) were in agreement regarding compatibility. Studies included accelerated aging of cyclotetramethylene tetranitramine (HMX) and CH-6 (>97% RDX), coating of HTPB propellant with two sealants (A, B), and reaction kinetics between cyclotrimethylenetrinitramine (RDX) and organic salt (ammonium benzoate). IMC heat flow measurements indicated that aging conditions did not affect HMX and CH-6. DSC rates of reaction at 200°C were similar and thus indicated no reaction. DSC onset of reaction and IMC heat flow measurements showed that one sealant (A) had an interaction with the HTPB propellant while the other did not. When the sealants were combined their reaction with HTPB decreased as the amount of sealant (B) increased. Reruns of HTPB with sealants A and sealants A+B after three weeks at room temperature showed that there was still an additional reaction of ~9%. IMC and DSC kinetic analyses were carried out on HTPB propellant + sealant A admixture. IMC gave a value of 5 kcal/mol for the reaction in the 55 to 75°C region while DSC measured the decomposition reaction where the activation energy was lowered from 48 kcal/mol for the propellant to 43 kcal/mol for the admixture. DSC kinetic study of RDX + organic salt showed a shift of the RDX peak temperature from 217°C (neat RDX) to 180°C (admixture). The activation energy for decomposition of the admixture was 25 kcal/mol. Literature values for neat RDX was 47 kcal/mol. Thus DSC kinetic data indicated that the admixture was incompatible at elevated temperature. An IMC kinetic study at temperatures from 65 to 77°C for this admixture gave a value of 33 kcal/mole. The reaction mechanism in the DSC and IMC experiments may be different since in the former case it involves a reaction between a gas (NH_3) and a liquid (RDX) while in the latter case it involves a gas (NH_3) and solid RDX which is a much slower reaction as also reflected in the higher activation energy.

Introduction:

Compatibility studies of energetic materials by DSC and TG have been carried out in our laboratory (1-7) for several years. In order to detect any interaction between the ingredients, the temperature had to be raised to about 50°C of the decomposition peak temperature. The heat flow sensitivity scale in DSC was at least 100 milliwatts (mW) per gram. The major advantages of the isothermal microcalorimetry (IMC) method are (a) the heat flow sensitivity scale is now in the microwatts (μW) and nanowatts (nW) region, (b) a large sample mass up to 30 grams depending upon the sensitivity of the sample (c)

temperature measurements in the 40 to 70°C region, (d) kinetic studies in this temperature region may result in more realistic service life predictions for propellants because you would not have to be concerned upon changes in mechanism as when you extrapolate from high temperature DSC measurements to temperatures in the 40 to 70°C region and (e) accurate constant temperature experiments may be performed. In the present study good agreement was observed in the conclusions drawn from DSC and IMC experiments on compatibility of energetic materials.

Experimental:

DSC experiments were carried out with a TA Instruments Model 2910 DSC module and a 3100 Thermal Analyzer. Sample masses varied from 0.5 to 3 mg and were placed in aluminum sample pans. Admixture ratios were 1:1. The variable heating rate method employed heating rates of 0.5, 1, 2, 5, 10 and 20°C/min in a nitrogen atmosphere. The instrument was calibrated with indium.

A Calorimetry Science Corporation (CSC) 4400 IMC and two 4500 INC instruments were employed. The instruments were calibrated according to the manufacturer procedure. The IMC was held at 55 to 75°C with sample masses of ~ 5 grams hydroxyl terminated polybutadiene (HTPB) propellant and ~ 0.4 to ~ 0.9 grams of sealants. Sealant A (major ingredient lead peroxide) and sealant B (major ingredient polysulfide) were mixed in ratios of 1:1 and 1:10 (A:B). The ~ 5 grams HTPB propellant was cut into ~ 25 slices and coated with the sealant (s) and then placed inside a 30 ml glass bottle. Later it was found to be more efficient to put the liquid sealant inside the bottle and then add propellant to it and mix the ingredients together. Since sealant A was the reactive ingredient whenever it was used the Joule value was normalized to a constant value of sealant A (i.e. 0.6 gram). The bottles were capped. INC experiments were carried out at three temperatures namely 65.7, 70.7, and 76.8°C. Sample masses varied from 0.1 to 0.4 grams and were placed in 2 ml glass vials and capped. Samples included cyclotetramethylene tetranitramine (HMX), cyclotrimethylenetrinitramine (RDX), CH-6 whose major ingredient (>97%) is RDX, and ammonium benzoate (AB). Admixtures of RDX and AB were prepared in molar ratios of 2:1, 1:1, and 1:2 and since AB was the reactive ingredient the enthalpy values are reported as Joules/gram AB.

Before any sample is run in the microcalorimetry it is run in the DSC and TG instruments at 5°C/min in order to see where the decomposition temperatures occurred. Then the samples are run for 20 hours at 80°C to see if any exothermic events and weight loss occurred. The magnitude (i.e., mW/g / %wt loss) of the interaction if any would determine whether the samples would be run in the microcalorimeter and under what conditions (i.e., sample mass and temperature).

Discussion:

1. Aging of HMX and CH-6 (> 97% RDX) Accelerated

Samples of HMX and CH-6 were aged at 50% RH/ 40°C/1 mo. DSC kinetic analyses employing a variable heating rate method (8) were carried out in a sealed and

open sample pan and the results compared to isothermal nanocalorimetry analysis at 70°C for 100 hours. Figures 1 and 2 for unaged HMX in an open pan and for aged HMX in sealed pans, respectively, showed differences in the peak shape, rate and enthalpy of reactions while peak maximum were within ± 1°C. Higher values were observed when the decomposition gases were confined. Similar observations were noted for CH-6. Rate constants for decomposition at 200°C were calculated and they were similar for aged and unaged samples namely 0.0002 ± 0.0001 min $^{-1}$ for HMX and 0.005 ± 0.001 min $^{-1}$ for CH-6. Thus aged and unaged samples were the same and accelerated aging did not have any effect.

Microcalorimetry analyses of unaged/aged samples showed heat flow values in microwatts were close to zero which indicated that no reaction occurred in the aged samples. The INC and DSC data were in agreement.

2. HTPB Propellant Coated with Sealants:

HTPB is a hydroxylterminated polybutadiene polymer cross-linked with an epoxide with fillers such as oxidizer (major ingredient), fuel, plasticizer, etc. The propellant is coated with a mixture of sealants. Namely, sealant A (major ingredient is lead peroxide) and sealant B (major ingredient is a polysulfide). In a 30 ml bottle neat propellant (~5 grams) and sealants (~ 0.6 grams) were run and then combinations of propellant with sealants were carried out at isothermal temperatures of 55 to 75°C for at least 100 hours. DSC analyses in open sample pans in a nitrogen atmosphere were also done.

The sealants had transitions in the same temperature region where the decomposition of the oxidizer occurred. DSC curve of the propellant is shown in Figure 3. Addition of sealant A to HTPB showed the onset of decomposition to be shifted to a much lower temperature (~130°C) which indicated an interaction between them. With sealant B the reaction was insignificant.

Microcalorimetry curves of neat propellant, neat sealant B and propellant + sealant B had heat flow values near zero which indicated no reaction was occurring in these samples. The IMC curve in microwatts for sealant A is presented in Figure 4, the decrease in microwatts from ~750 to ~50 with time was typical for an n^{th} order reaction. Integration of this curve is shown in Figure 5 where a plot of Joules versus time gradually is leveling off after 75 hours at 70°C.

Integral plots (Joules versus time) were obtained for admixtures of sealants A+B, HTPB + sealant A, and HTPB + sealants A+B (1:1), respectively. The data are presented in Table 1 and plotted as a bar graph in Figure 6. It is evident that the admixture of HTPB propellant and sealant A is incompatible because the enthalpy of reaction for the admixture is greater that the sum of the reactants i.e., 64 Joules >33 Joules (sealant A) + 0 Joules (HTPB). The greater the difference, the greater the degree of incompatibility. Compatibility of energetic materials by microcalorimetry has been expressed by two equations namely.

$$C_{ab}=\frac{2\,E_{ab}}{E_a+E_b} \quad (1) \text{ and } C_{ab}=\frac{2E_{ab}-(E_a+E_b)}{2} \quad (2)$$

Where E is the energy evolved in Joules/gram, C is the compatibility and the subscripts a and b refer to the individual components and the subscript ab refers to the mixture of a and b. In equation (1) [9] if C $\leq$2 then mixture is compatible and if C> 3 then it is incompatible. In our case Cab = (2 x 64)/(0+33) = 3.9 J/g and the admixture is incompatible. With equation [10]

$$C_{ab}=\frac{2 \times 64-(0+33)}{2}=47.5 \text{ J/g}$$

Therefore the compatibility of HTPB propellant with sealant A was found to be 47.5 J/g.

The higher the number the greater the degree of incompatibility. When the admixture is HTPB + AB (1:10) then E_{ab} = -3 (Table 2), A:B (1:10) = -4, and HTPB =0.

$$C_{ab}=\frac{2 \times (-3)}{0+(-4)}=1.5$$ and the admixture is compatible.

Three samples of HTPB + sealant were rerun after being at room temperature for three weeks. The integral plot of the rerun sample Figure (7) showed an enthalpy value of about 6 compared to a value of 52 in the initial run. The rerun data are also given in Table 1 and plotted as a bar graph in Figure (8) in comparison to the initial run. It appears that the reaction between the propellant and sealant was about 90% completed in the initial run. The ratio of sealant in the IMC and DSC work was 1:1 (A:B). In actual practice the ratio is 1:10 (A:B). Since sealant B does not react with HTPB at 70°C/70 hrs the 1:10 ratio of A:B would be expected to have only minimal reaction due to dilution by sealant B in the admixture. IMC data for HTPB with sealant in 1:10 ratios (A+B) are given in Table 2 and confirmed expectation of minimal reaction.

An IMC kinetic study was made of the HTPB propellant + sealant A at temperature from 55 to 75°C. The kinetic plot is displayed in Figure 9. Activation energy of 5 kcal/mol was calculated for the reaction. This low value indicated that perhaps the diffusion reaction involved a free radical attack on the unsaturated linkage and an abstraction of the allylic hydrogen from the HTPB binder by the lead peroxide in sealant A. A DSC variable heating rate kinetic study was also carried out on this admixture. However, this was done in the decomposition region (> 200°C) of the propellant. A decrease in the activation energy for the second peak (major peak, see Figure 3) from 48

to 43 kcal/mol was found. This resulted in a 30-fold increase in the rate of reaction at 200°C in the admixture. DSC was not sensitive enough to measure the actual reaction between the ingredients in the admixtures.

3. Cyclotrimethylenetrinitramine (RDX) + Ammonium Benzoate (AB):

Ammonium Benzoate (AB) is the salt of a weak acid and a weak base. When heated it can liberate ammonia, which may react slowly with solid RDX to form nitrous acid and eventually destabilize RDX. RDX decomposes readily in the presence of strong bases (NaOH). The compatibility of RDX + AB was investigated by dynamic DSC and IMC. A DSC curve of AB in nitrogen in an uncrimped pan with an aligned cover showed the melting endotherm at 190°C that was in agreement with that reported in the Merck Index. The melting endothem is depended upon the sample confinement. In an open pan it was observed in 150°C region and in a sealed pan in the 210°C region. This variance is due to the liberation of ammonium gas when the sample melts. RDX decomposition curve at 2°C/min is shown in Figure (10). It exhibits an HMX phase transition endotherm at 189°C followed by melt of RDX at 199°C immediately followed by exothermic decomposition with a major peak at 217°C. Admixtures of RDX + AB in molar ratios of 2:1, 1:1, and 1:2 were prepared. The curves were similar and had a peak maximum at 180 $\pm$ 0.5°C, and a typical curve is presented in Figure 11 for 1:1 mixture in a sealed pan.

The large shift in peak temperature from 217°C for neat RDX to 180°C for RDX in the admixture was an indication of a large degree of incompatibility in this admixture in this temperature region. It may also be noted that the peak shape of the exothermic decomposition curve is much narrower in the admixture and also that it has a much higher rate of reaction at the peak maximum (15.8 versus 4.6 Watts/gram). These are additional indications of incompatibility.

DSC kinetic analysis employing a variable heating rate method was carried out on RDX + AB admixture. A straight line plot was observed and the activation was calculated from the slope of the line. It was found to be 25.0 kcal/mol. Now the activation energy for RDX decomposition is well known and given as 47.1 kcal/mol (11). This large shift in activation energies to a much lower value in the admixture indicated that a reaction occurred in the admixture and that it was incompatible in this temperature region (~150 to ~200°C).

Microcalorimetry data were obtained at 65.7, 70.7, and 76.8°C. The enthalpy values increased with time and temperature and the values after 100 hours are presented in Table 3. An Arrhenius plot of the IMC data assuming a first order reaction gave an activation energy of 33 kcal/mol. DSC kinetics gave a value of 25 kcal/mol. If the reaction mechanism were the same in the two experiments then similar activation energies would be expected with differences in frequency factors because of the differences in reaction temperatures in the experiments. However, there may be small differences in the reaction mechanism since in the DSC experiment the reaction is between a gas (NH_3) and solid/liquid RDX while in IMC it is between a gas (NH_3) and solid RDX. The latter reaction would be expected to be much slower than the former and

this is shown by the differences in activation energies with a larger value for the latter reaction. A rerun of the 70.7°C reaction after a delay of four weeks at room temperature resulted in an integral curve with a higher enthalpy of reaction which indicated that the reaction was continuing even at room temperature.

Conclusions:

Compatibility determination of energetic materials in different temperature regions by DSC and IMC were in good agreement. Differences in the activation energies by DSC and IMC for the HTPB propellant and sealant A were due to different reactions being measured (i.e., free radical and decompositions). Differences in the activation energies for the reaction between an organic nitramine and an organic salt may be due to differences in the physical state of the nitramine i.e., a liquid by high temperature DSC measurement and a solid by IMC in 65 to 77°C region.

References:

1. A. S. Tompa, Thermochimica Acta, 77 (1984) 133.
2. A. S. Tompa, R. F. Boswell, and F. M. Gallant, CPIA Publ. 545(1990) 71.
3. R. F. Boswell and A. S. Tompa, CPIA Publ. 588 (1992) 97.
4. R. F. Boswell and A. S. Tompa, CPIA Publ. 597 (1993) 301
5. R. F. Boswell and A. S. Tompa, CPIA Publ. 625 (1995) 11.
6. A. S. Tompa, P. F. Boswell, P. Desear, and M. K. Ibrahim,CPIA Publ. 647 (1997) 355
7. R. F. Boswell and A. S. Tompa, Proceedings of the Workshop on Microcalorimetry of Energetic Materials, April 1997, Leeds, United Kingdom.
8. ASTM E698-84
9. S. Wilker, G. Pantel, V. Ticmanis and P. Guillaume, Proceedings of the Workshop on Microcalorimetry of Energetic Materials April 1997, Leeds, United Kingdom.
10. T. Jernelov, P. Lagerkvist, P. Sjoberg, and K. Nyberg, Green Energetic Materials Environmental DEA Meeting between the United States and Sweden, China Lake, CA, January 1998.
11. R. N. Rogers, Thermochimica Acta, 11 (1975) 131.

TABLE 1

Microcalorimetry Data after 70 hours at 70°C
for the HTPB Propellant and Sealants A and B

Mass in Grams				Energy Enthalpy
HTPB	A	B	A+B[1]	Joules/0.6 grams (A)
3.0				0
		0.834		-3.3
		0.91		-2.2
5.171		0.9066		-3.3
5.055		0.8155		-3.6
3.02	0.53			60
5.01 [2]	0.622			66
	0.559			38
	0.498			28
			0.8531	37
	0.784	0.756		42
			0.855	31
5.1825			0.910	52
5.076	0.420	0.412		56
5.127 [2]	0.5299	0.5324		52

Rerun [3] after 3 weeks at Room Temperature

Mass in Grams				Energy Enthalpy
HTPB	A	B	A+B	Joules/0.6 grams (A)
5.01 [2]	0.622			7
5.1825			0.910	6
5.076	0.420	0.412		4

Where:

[1] = Ratio of A:B is 1:1.

[2] Sample covered with 20 grams of sea sand.

[3] Appears about $9 \pm 2\%$ additional reaction.

TABLE 2

MICROCALORIMETRY DATA FOR HTPB PROPELLANT
WITH SEALANTS A AND B IN THE RATIO OF 1:10

Mass in Grams			Energy Enthalpy
HTPB	A	A+B	Joules/0.6 grams (A)
5.64	0.637		64
5.159	0.698		67
		0.989	- 4[(1)]
5.064		0.985	-3[(1)]
5.183		0.985	-3[(1)]

[(1)] Energy value based on total mass of A+B.

TABLE 3

IMC Kinetic Data [1] After 100 Hours for
RDX + Ammonium Benzoate (AB)

Temperature, °C	65.7	70.7	76.8
Joules/gram AB	5.0	14.2	24.3
Log Joules/gram, AB	0.70	1.05	1.39
10^3/K	2.952	2.910	2.859

(1) Ea = 33 kcal/mole assuming a first order reaction.

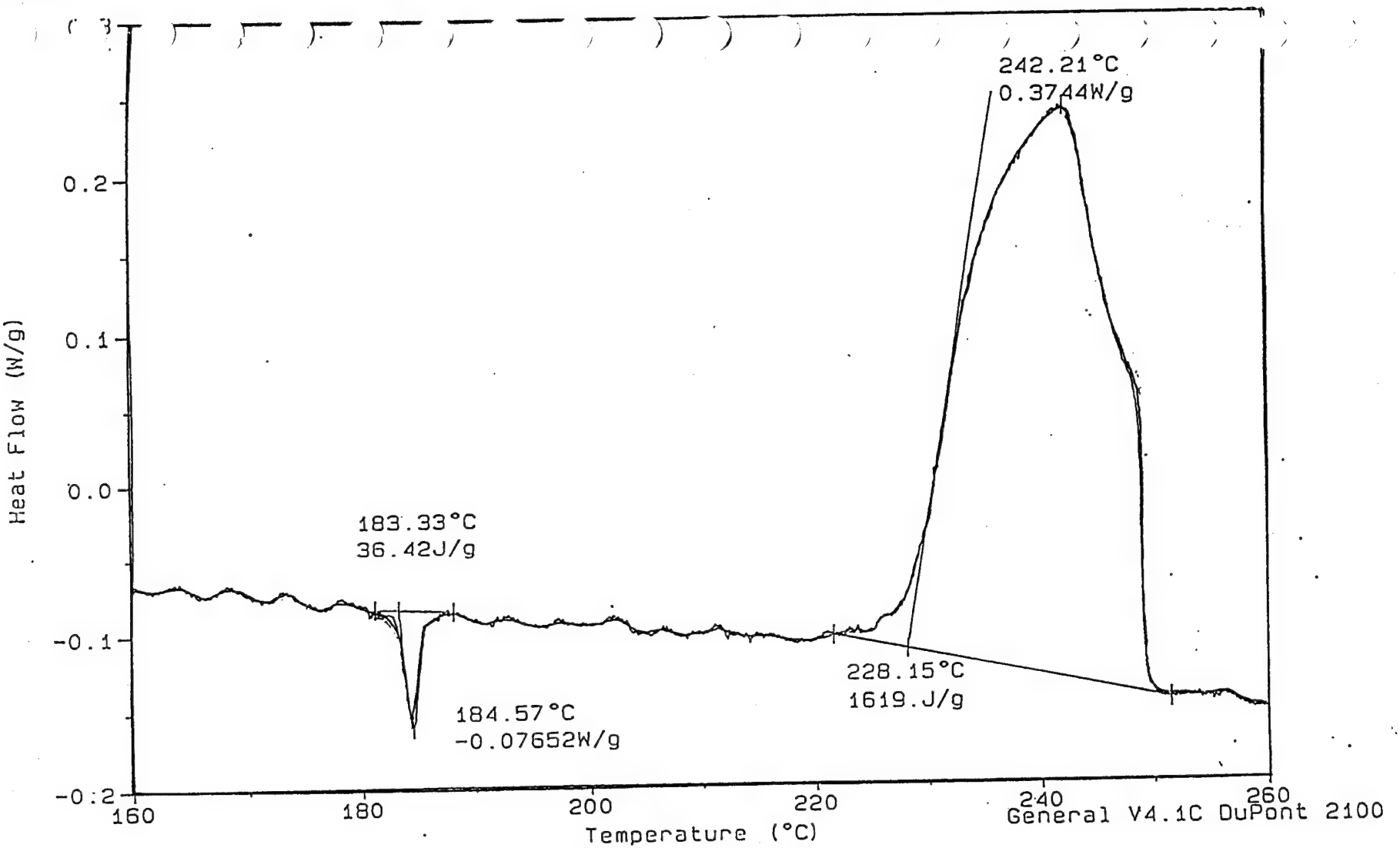

Figure 1. DSC curve of unaged HMX in an open pan at 0.2°C/min..

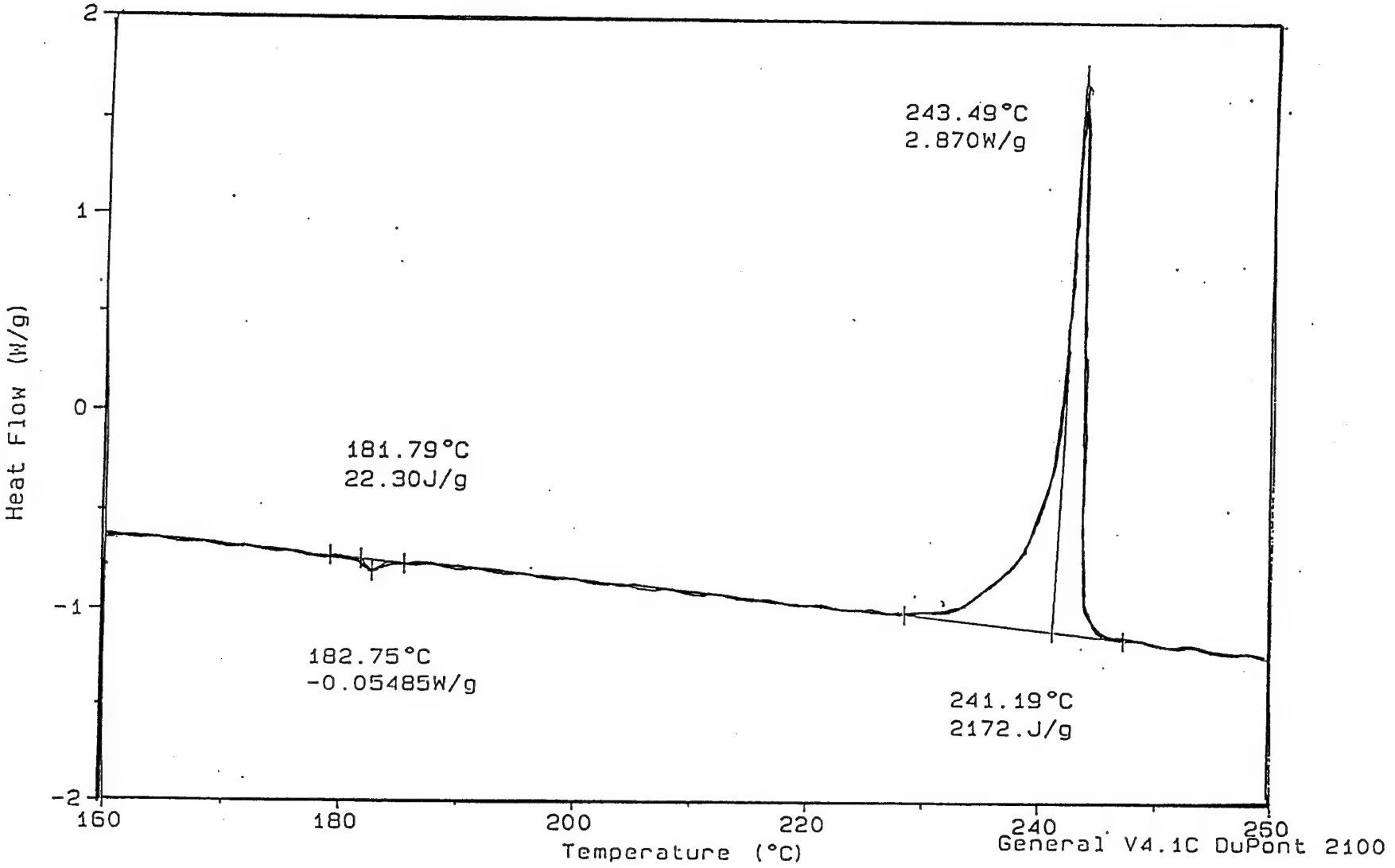

Figure 2. DSC curve of aged HMX in a sealed pan at 0.2°C/min.

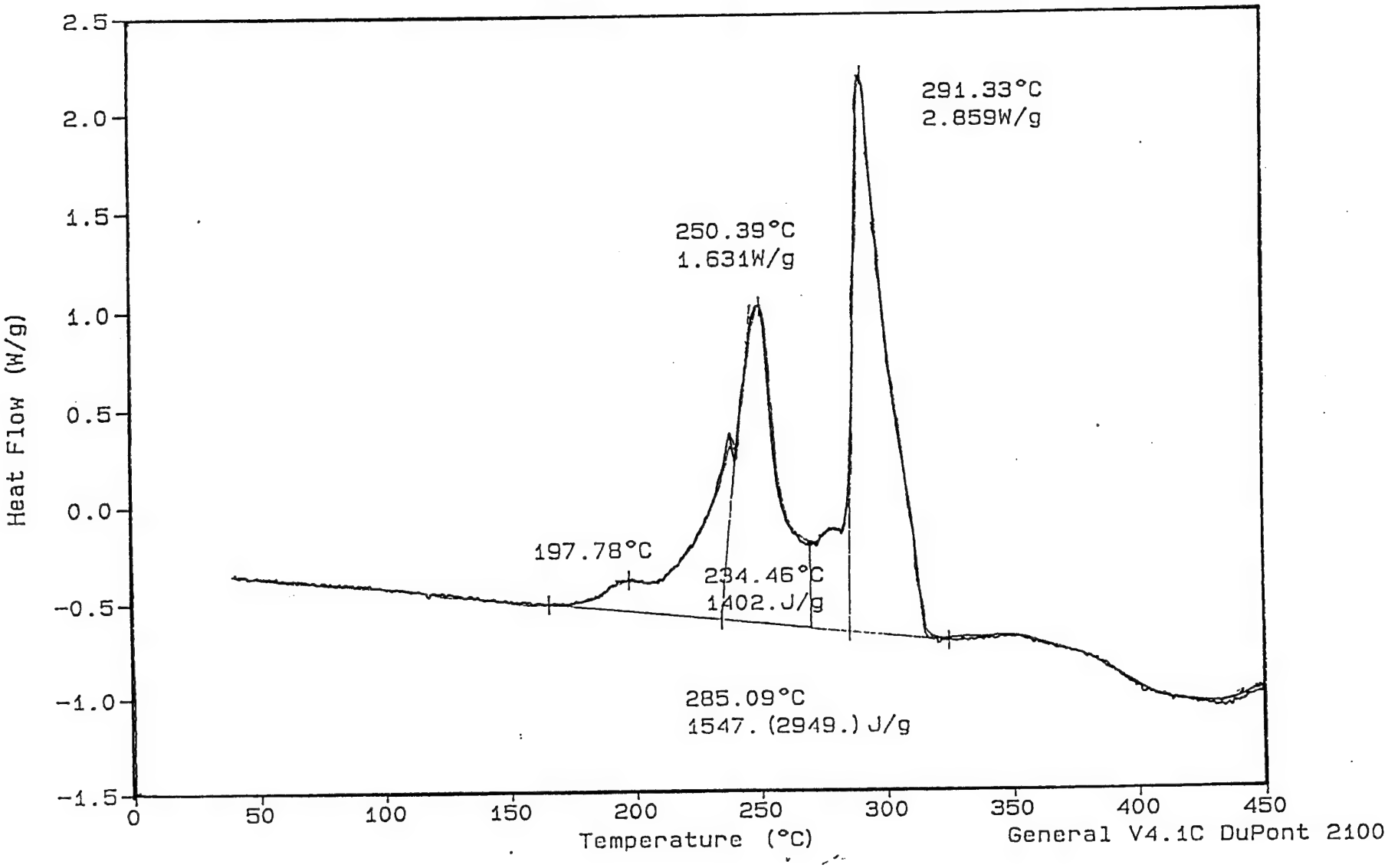

Figure 3. DSC curve of HTPB Propellant in sealed pan at 2°C/min.

Q13

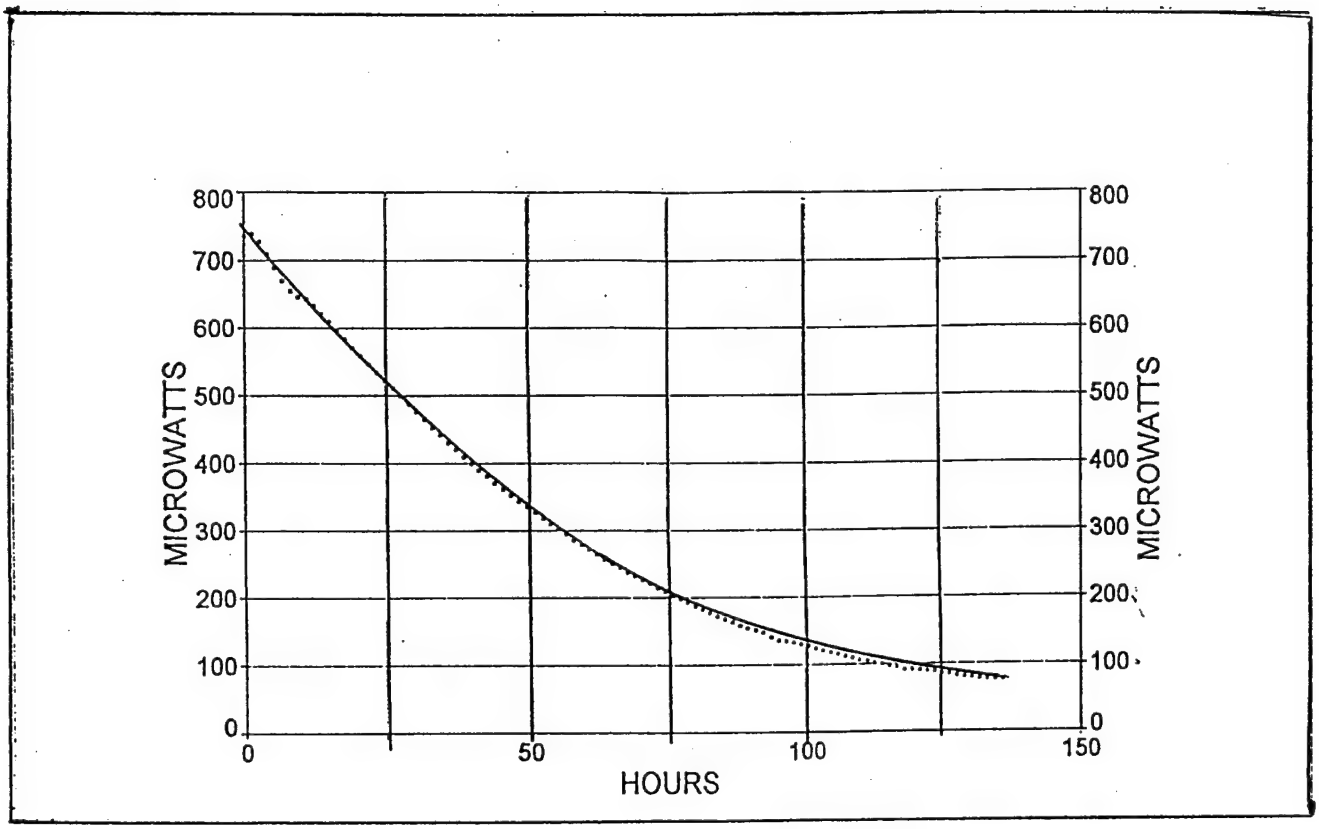

Figure 4. IMC curve in a microwatts of sealant #A at 70°C.

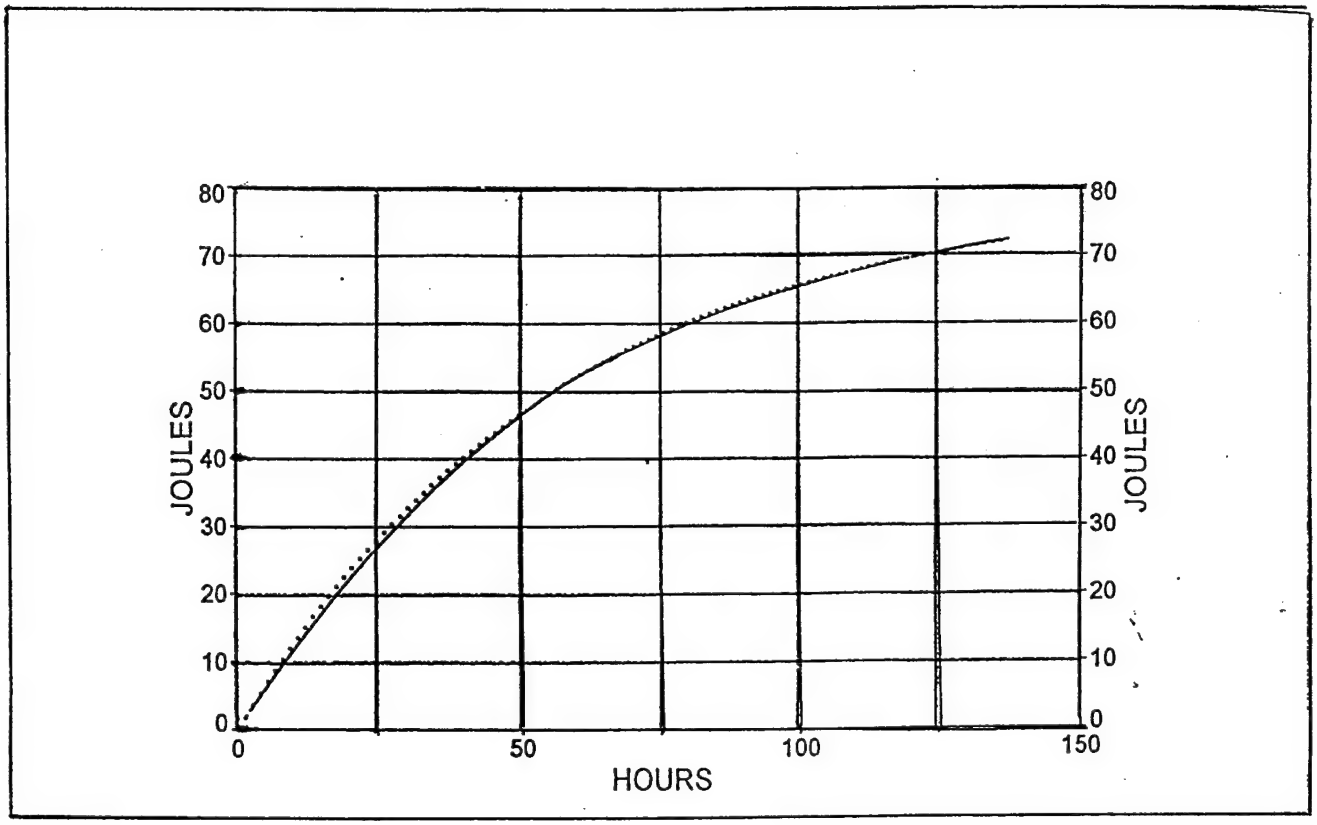

Figure 5. IMC curve in Joules of Sealant #A in 70°C.

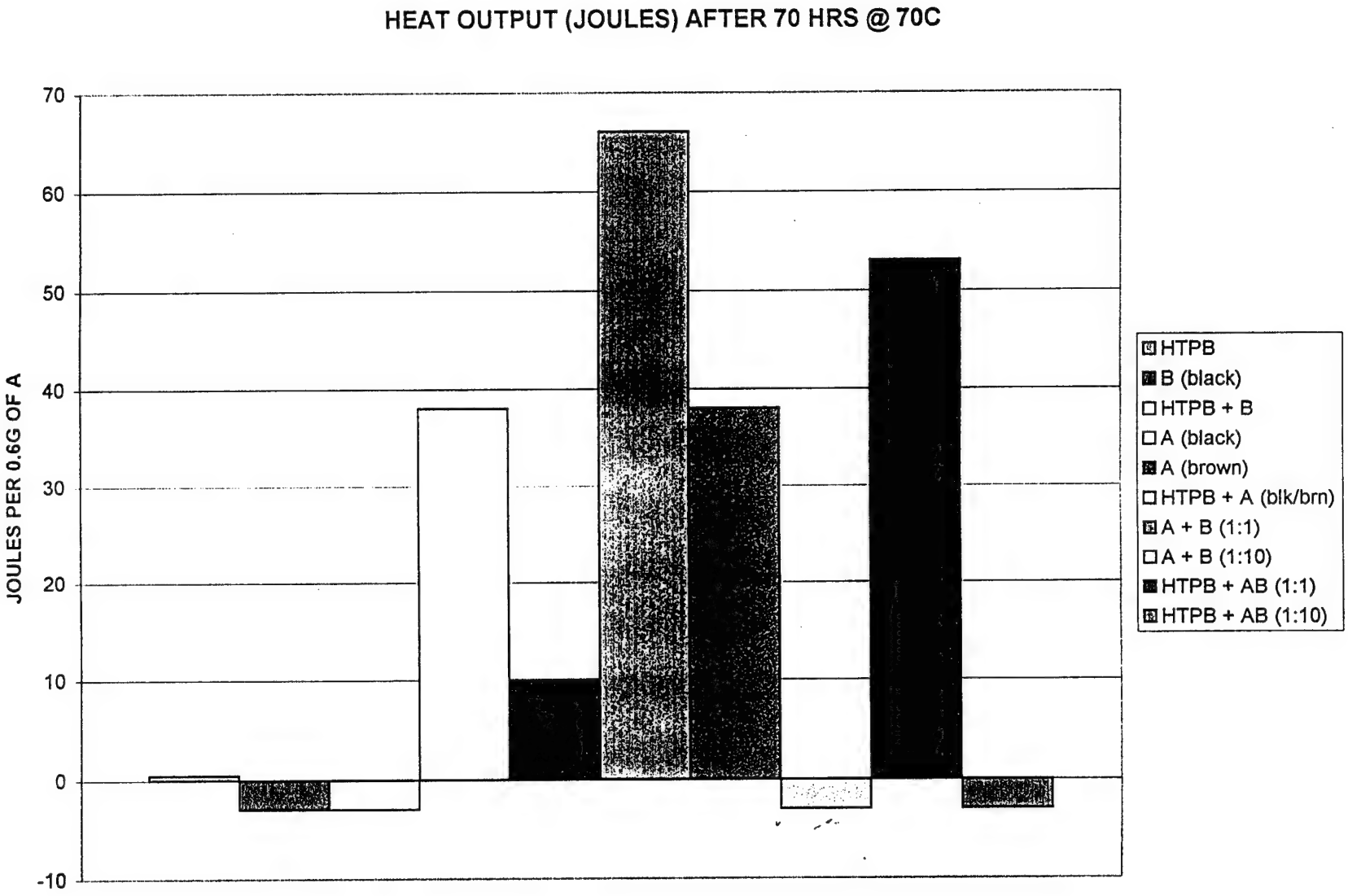

Figure 6. IMC bar graph plot of HTPB propellant and sealants at 70°C.

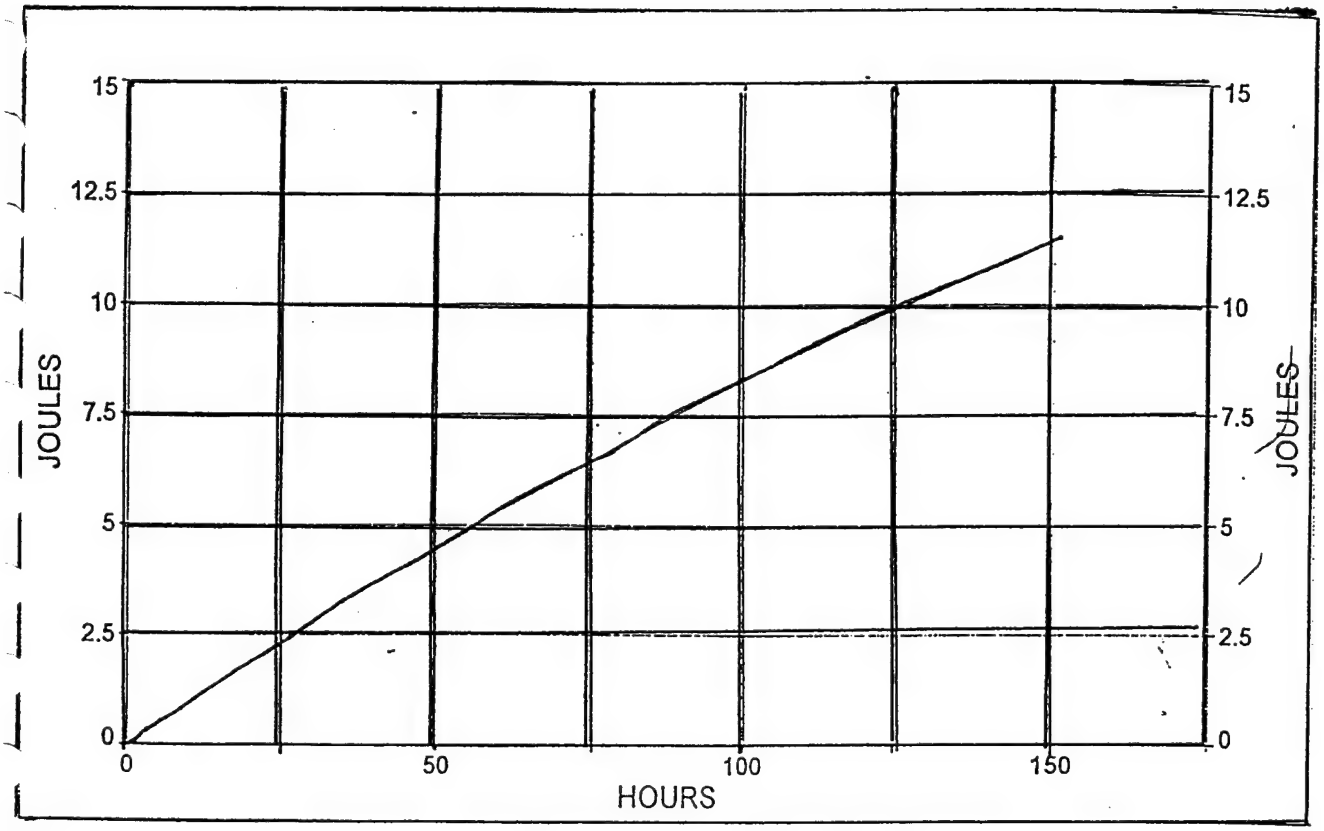

Figure 7. IMC curve in Joules of rerun HTPB Propellant + sealants AB (1:1) at 70°C.

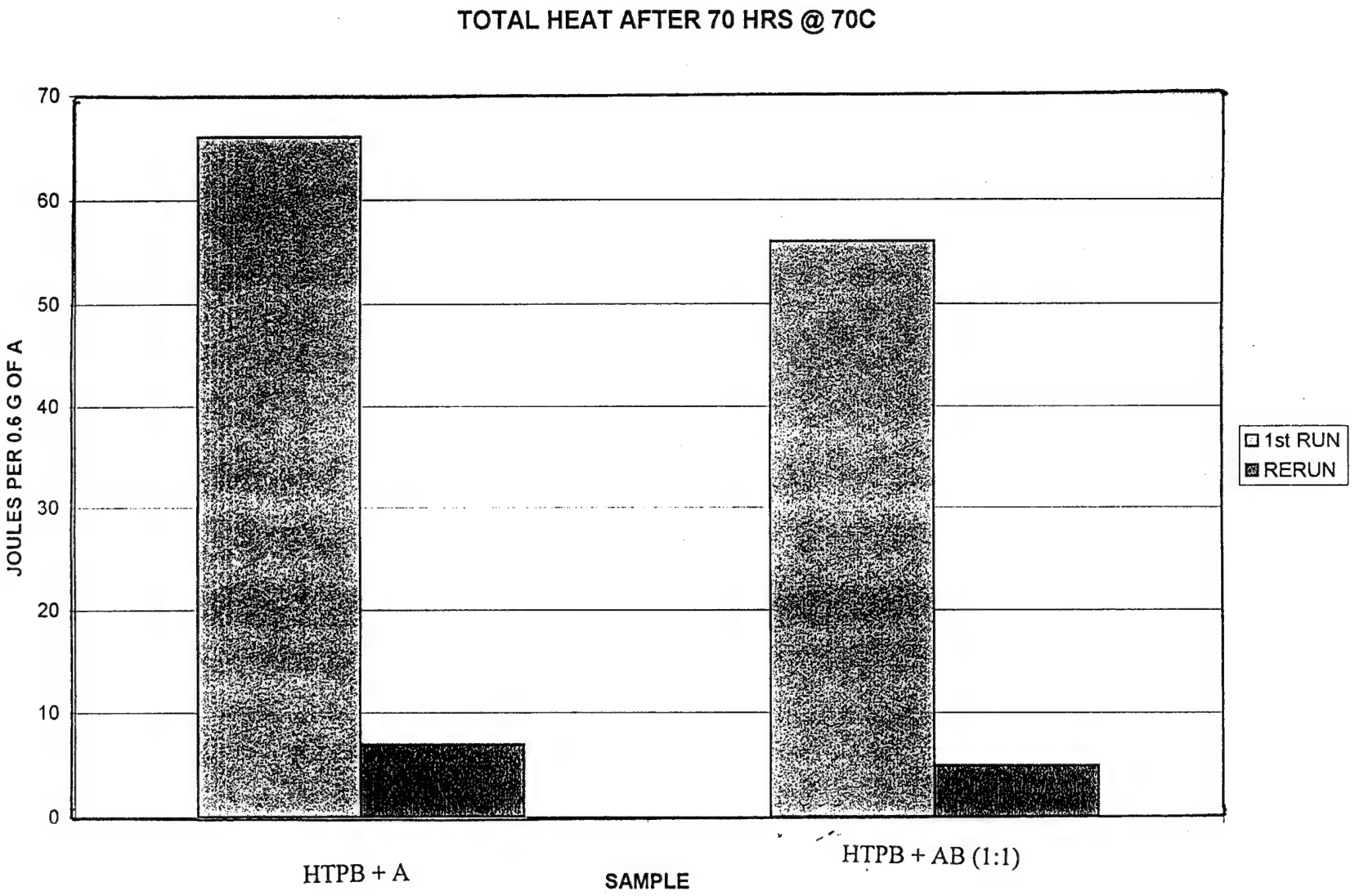

Figure 8. IMC bar graph of initial and rerun of HTPB propellant and sealants A and AB (1:1) at 70°C.

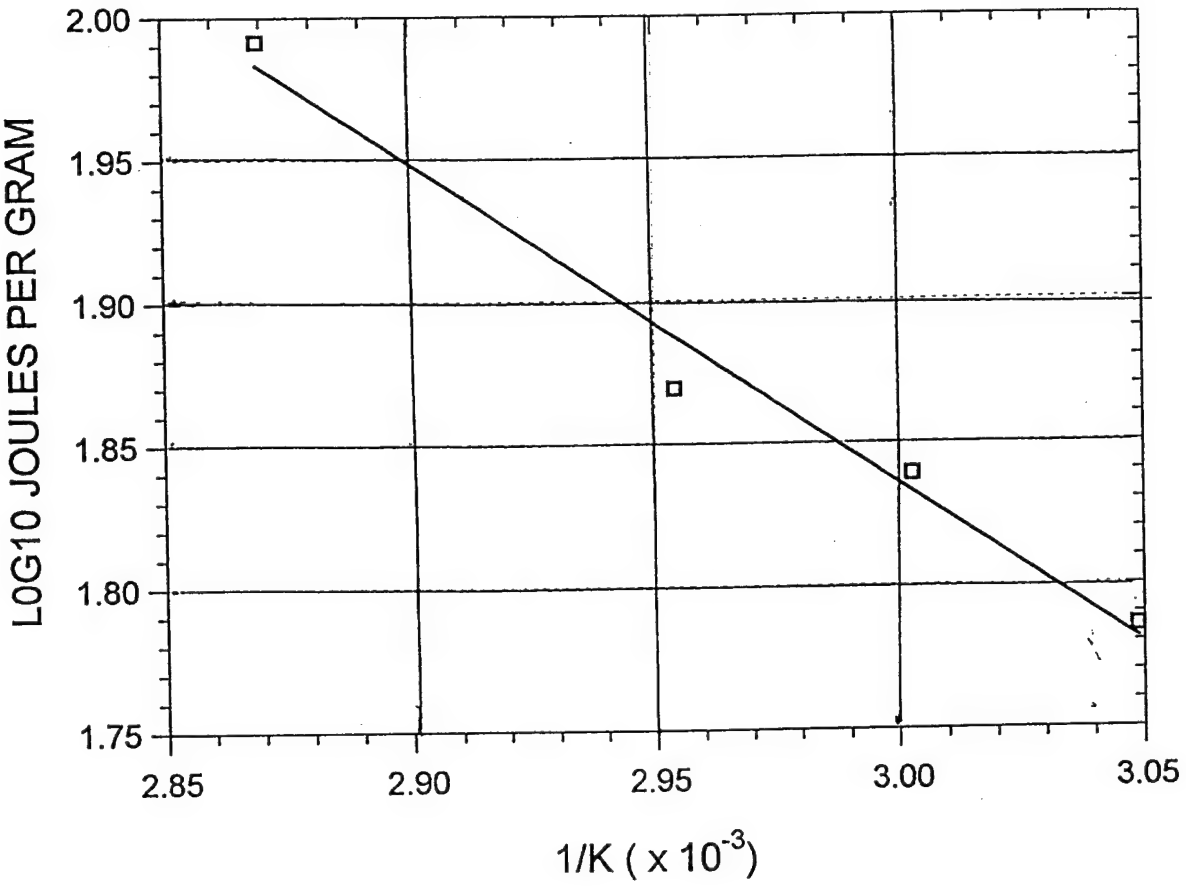

Figure 9. IMC Arrhenius plot of HTPB propellant + sealant A.

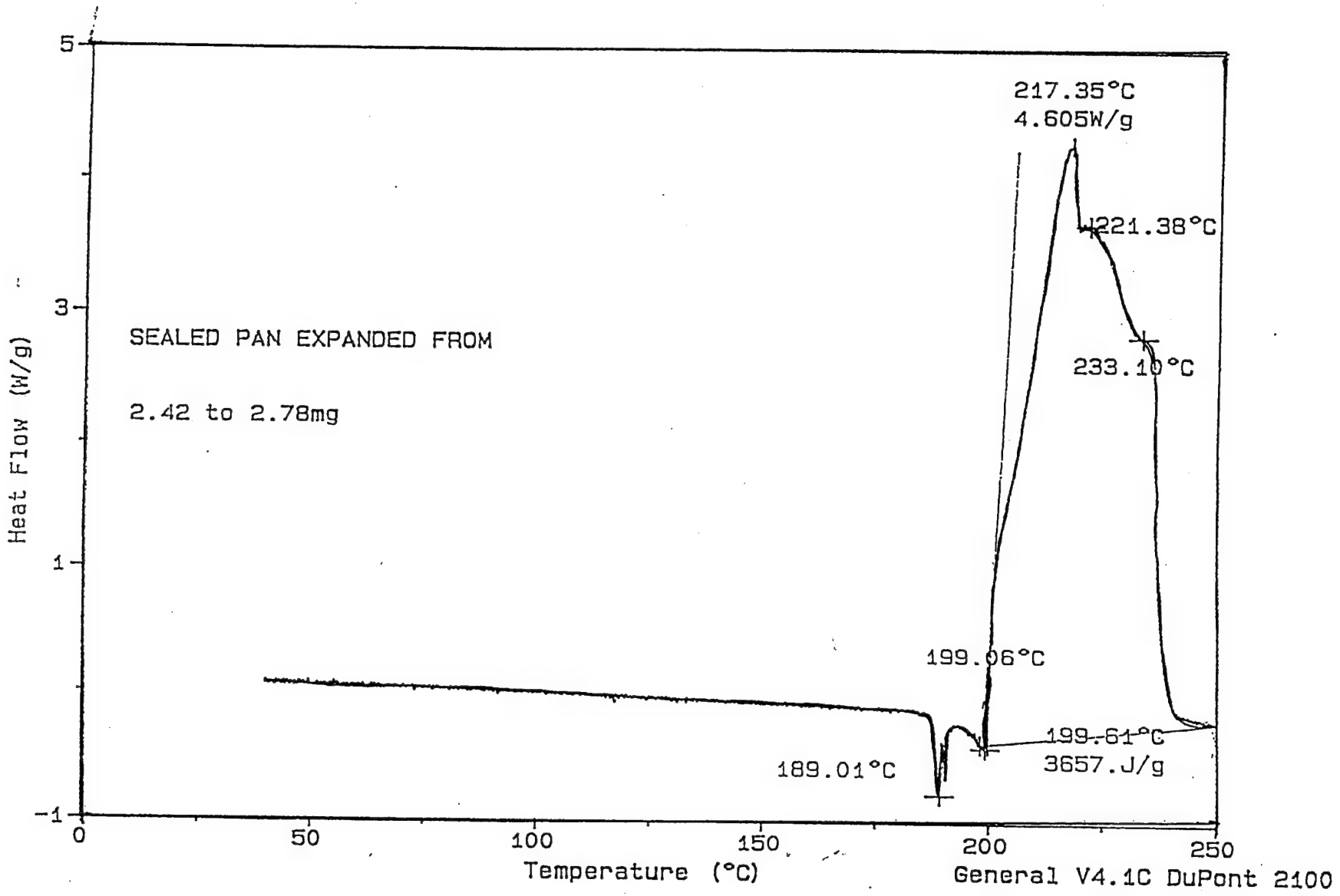

Figure 10. DSC curve of ground RDX in a sealed pan at 2°C/min.

Q20

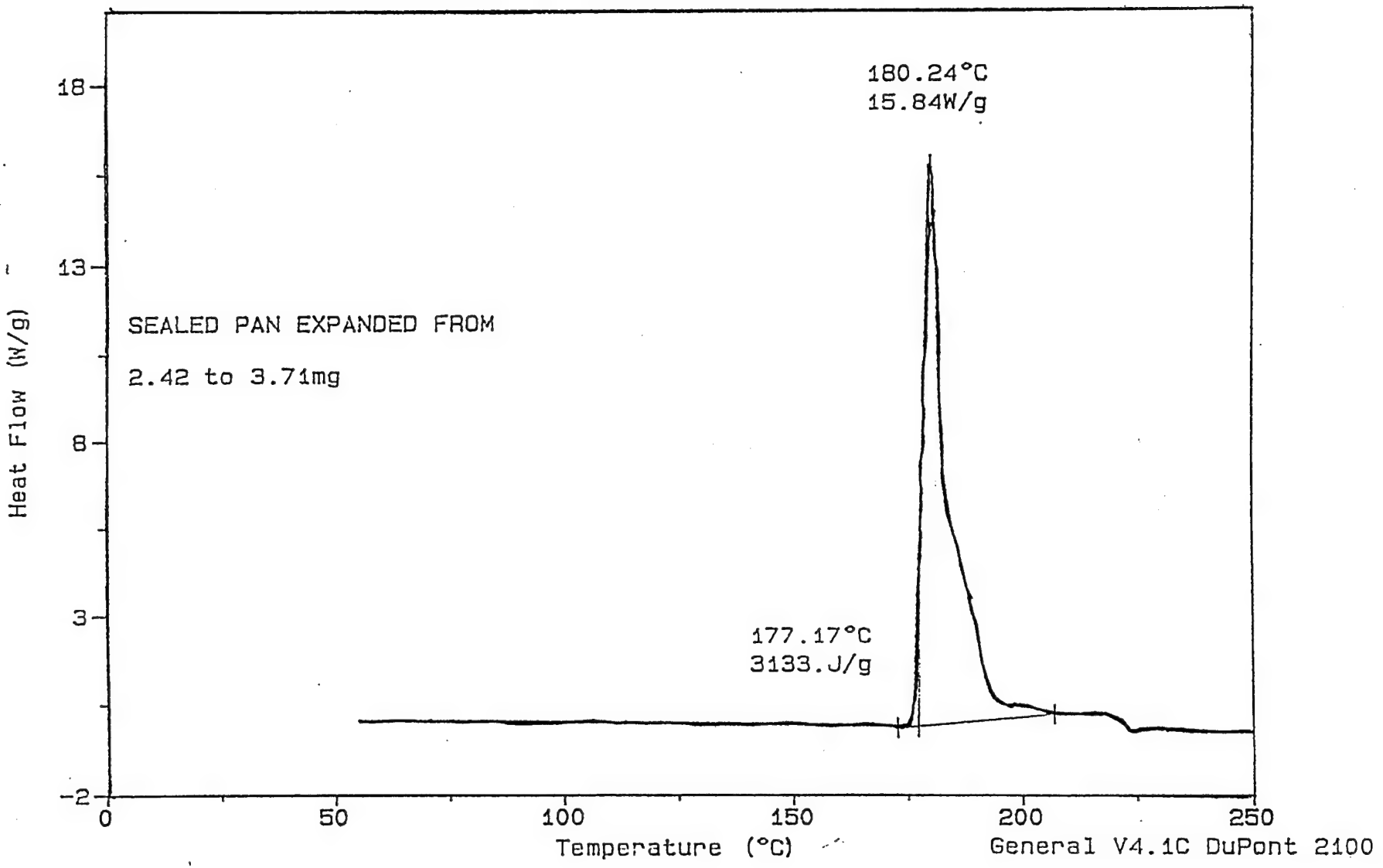

Figure 11. DSC curve of ground RDX + ammonium benzoate in a sealed pan at 2°C/min.

SMALL SCALE REUSABLE METAL CRUCIBLE FOR USE IN DIFFERENTIAL SCANNING CALORIMETRY AND ITS MICROCALORIMETRY APPLICATIONS

Linda D. Tuma
Merck Research Laboratories
Rahway, NJ 07065 USA

A small scale, specially designed reusable "Merck" metal crucible has been developed and evaluated for use with differential scanning calorimetry. Its applications include: 1) determination of exothermic activity in a closed system, 2) Syringe Injection Calorimety (SIC) to determine heats of reactions and 3) Small Scale Isothermal Age (SSIA) to determine exothermic onset temperatures. Each technique uses less than 75 micrograms of material and produces accurate and reproducible results.

The metal crucibles are constructed of either 316L, Hastelloy B or tantalum lined Hastelloy B. The crucibles are reusable, with a screw on cap containing a replaceable 400 psi "rupture disk" seal. They have an operating temperature range of <0°C to ~ 300°C and a volume of ~60µls. The problems associated with the use of a crimped aluminum sample pan, with its low pressure containment and chemical reactivity, are overcome with the use of these crucibles.

The metal crucibles and both the SIC and SSIA techniques, which use these crucibles, have been calibrated and presented in published papers.

SMALL SCALE METAL REUSABLE CRUCIBLE

A. DESIGN

High Pressure DSC or crimped aluminum pans are in standard use to determine the presence of exotherms in closed reaction systems. Problems with the chemical reactivity of the aluminum pans, noisy baselines and difficulties in the duplication of High Pressure DSC results are typical. These are overcome with the use of the "Merck" metal reusable crucible[1]. While many of the commercially available high pressure cells are not reusable and are difficult to seal, the "Merck" crucible consists of a threaded bottom and a screw on cap and is reusable (figure 1). The crucibles are constructed of either 316L, or Hastelloy or tantalum lined. The bottom of the crucible is ~ 0.25 inches in diameter and has a capacity of ~60 µl. The cap has a replaceable Teflon rupture disk, ~20 µm thick, and can withstand a pressure of ~400 psi. A set of specially designed wrenches (figure 2) are used to hold the bottom of the assembly and in tightening the cap. The crucible has an operating temperature range from 0 to ~300°C

B. CALIBRATION

This crucible has been calibrated with respect to the calibration coefficient (E), heat transference, repeatability of traces, quantitative data generation and pressure generation. This calibration factors are compared to those of a crimped aluminum pan.

The calibration coefficient (E) was determined using both a constant weight of indium and varying the heating rate and a constant heating rate and varying the weight of indium. E was determined using a TA thermal analytical instrument, a TA 910 DSC cell and the TA general analysis program[2]. The results are presented in Tables 1 and 2 and in Figures 2 and 3 respectively. The results indicate that the coefficient E increases linearly with increase in mass and heating rate, and the values obtained are consistent with those reported by Van Humbeeck and Bijvoet[3].

Heat transference was evaluated through the determination of the thermal resistance factor for the two test cells and is visually shown by overlaying the plots of the indium melt for each test cell. The indium melt curves used the same weight of indium and a 5°C min^{-1} heating rate. The results are presented in Table 3 and shown in Figure 4. The results indicate that the thermal resistance of the closed bomb is approximately twice that of the crimped aluminum pan.

Repeatability of results was evaluated by carrying out a series of runs on a consistent weight of indium. The results are compared by the offset overlay of the indium melt curves and are presented in Figure 5. The repeatability for both test cells is good.

The quantitative measurement of data is shown by the comparison of decomposition exotherms for three proprietary Merck compounds using the two test cells and are reported in Table 4. The results indicate that the sizes of the decomposition exotherms for the closed bomb are consistent if the pressure generation is within the rating of the aluminum pan.

Vapor pressure containment was evaluated by holding water, ethanol and acetone at ~10°C above their boiling points for ~16 hours and comparing the weight of the solvents before and after age. The two test cells were heated at 5°C min^{-1} until the seal ruptured to determine the closed bomb's pressure rating. The results are presented in Table 5. The results indicate that the closed bomb pressure rating is over ~400 psi with weight losses of less than 0.1 mg ($\leq$ 0.14% weight loss) with highly volatile compounds.

USE OF THE SMALL SCALE METAL REUSABLE CRUCIBLE

A. DETERMINATION OF EXOTHERMS IN CLOSED REACTION SYSTEMS

The reusable metal crucible is capable of providing accurate and reproducible thermal data for exotherms present in closed reaction systems. The use of this closed crucible can provide information on the size, rate of heat release and initiation temperature of exothermic decomposition/oxidation which are present in closed reaction systems. Sample size can be varied from < 5 up to ~75 milligrams, with heating rates from 1°C min^{-1} to 25°C min^{-1}.

B. SYRINGE INJECTION CALORIMETRY

Syringe Injection Calorimetry (SIC), which uses the small scale metal crucible, is applicable for use with liquid/liquid and liquid/solid reactions where the reaction takes place rapidly at room temperature, the reaction is not affected by air or moisture, the reactants mix readily, the mixture is homogeneous after the reaction is complete and where there is negligible gas generation during the reaction. For reactions which meet these requirements, SIC can provide rapid and accurate data.

B1. Experimental Technique – Syringe Injection Calorimetry

A weighted amount of reactant A is injected into the metal crucible and allowed to come to thermal equilibrium before an excess amount of the second reactant is injected into the system. Heat flow is recorded verses time and is integrated using a sigmoidal baseline with E equal to 1. The results are then adjusted using a calibration factor, E_{SIC}.

B2. Calibration of the Syringe Injection Calorimetry Technique

The procedure by which the Syringe Injection Calorimetry technique is calibrated and the use of E_{SIC} is used is described below:

Step 1:

Determine the calibration coefficient E for the metal crucible as described in the calibration of the metal crucibles. The results are presented in Table 6 and are plotted in Figure 6 with E being equal to .0121 Q + 1.1611 determined using linear regression.

Step 2:

Determine the SIC calibration coefficient E_{SIC}, to compensate for the amount of unmeasured heat which is lost due to the configuration of the system.

To establish Esic, the reaction HCl + NaOH $\rightarrow$ NaCl + H_2O is run using 0.5, 1.0, 2.0, 3.0, and 4.0 NaOH solution. The solutions must be assayed to determine the exact weight percent of NaOH present in each solution. Heat flow versus time is measured and the heat of reaction (ΔH) is obtained by integration using a sigmoidal baseline with the E set to 1.000. The experimental heat of reaction, ΔH_{HRX} (Kcal/mole of A) is calibrated using the following equation, where ΔH is the measured heat of reaction

$$\Delta H_{HRX} = \frac{\Delta H \times M.W.}{1000 \times 4.184} \qquad (1)$$

Step 3:

ΔH_{HRX} is then corrected to that of the theoretical value through the following four steps:

1) determine the E_{EXP} calibration coefficient:

$$E_{EXP} = \frac{\Delta H_{TH}}{\Delta H_{HRX}} \qquad (2)$$

where E_{EXP} = the calibration coefficient E for the specific SIC run

ΔH_{TH} = the theoretical heat of reaction
(includes the heat of dilution) in Kcal\mole of NaOH

ΔH_{HRX} = heat of reaction in Kcal per mole of reactant A as determined from the DSC value as per equation (1)

2) determine the total heat Q:

$$Q = \frac{\Delta H \times W}{1000} \qquad (3)$$

where ΔH = the DSC value for the heat of reaction in joules per gram

W = the weight of NaOH used in mgs

3) plot Q verses E_{EXP} to determine the calibration coefficient E_{SIC}

$$\text{where } E_{SIC} = mQ + b \qquad (4)$$

The plot of Q verses E_{EXP} for the HCl + NaOH reaction is linear over the range of 0.4 to 3.0 joules of total heat measured and has a positive slope which is consistent with the data published by Van Humbeek and Bijvoet and with our indium calibration of the metal crucibles. The results are presented in Table 7 and are plotted in Figure 7 for both the experimental and Corrected E values (E_{SIC}) determined from the linear regression where e = 0.0242 + 1.3803.

4) determine the corrected heat of reaction, ΔH_{CORR}

$$\Delta H_{CORR} = \Delta H_{HRX} \times E_{SIC} \qquad (5)$$

where ΔH_{CORR} = the corrected heat of reaction in Kcal/mole of reactant A

The results for the HCl + NaOH reaction are presented in Table 8 and are plotted in Figure 8 for both the uncorrected and corrected heat of reaction values.

B3. Case Studies

Several classical heats of reaction, heats of solutions and heats of dilution have been studied using the syringe injection calorimetry technique. The results are presented in Table 9 and are reported as percentages of the theoretical heat of reaction values.

In addition , SIC was used to obtain heats of reaction for several Merck proprietary reactions and compared with either a calculated or an independently determined experimental heat of reaction. The results are presented in Table 10.

B4. Conclusions

Syringe Injection Calorimetry (SIC) is capable of providing accurate, rapid and reproducible results for heats of reactions. A typical reaction can be studied in less than two hours using milliliters or milligrams of reactants. The heat of reaction data determined using the SIC technique are within $\pm$ 3% of the theoretical values. From these results, it has been shown that SIC is an appropriate technique for measuring heats of reaction when the reaction in question meets the following criteria: The reaction occurs rapidly at room temperature; the reactants mix easily; the solution is homogenous after the reaction; and there is negligible gas evolution.

C. SMALL SCALE ISOTHERMAL AGE TECHNIQUE TO DETERMINE EXOTHERMIC ONSET TEMPERATURES

The Small Scale Isothermal Age technique (SSIA) was developed to provide reliable information as to exothermic onset temperature using 50 to 75 milligrams of material[4]. This is a novel DSC technique which utilizes the small scale metal reusable crucibles. The sample is held isothermally at a preset temperature for an extended period of time, usually overnight, with the aged sample being reevaluated for any change in the size of original exotherm. A decrease in the size of the original exotherm indicates that heat was evolved during the age. The consequences of the initiation of the exotherm must be further evaluated via Fauske Reactive System Screening Tool (RSST), Vent Size Packaging (VSP) or other suitable methodology in order to determine the consequences of initiation on chemical processing[5].

C1. Experimental

There are four steps in the experimental technique:

Step 1: Determine Exothermic Decomposition Onset Temperature.

A temperature scan from ambient ot ~300°C at 2°C min^{-1} is run on a sample to determine the exothermic onset temperature. The sealed metal crucible with a typical sample weight of 5 to 10 milligrams is used.

Step 2: Isothermal Age

A DSC isothermal age, in a sealed metal crucible, is run at the exothermic onset temperature determined in Step 1 for at least 12 hours. The sample is packed tightly, with the crucible being filled almost to the top to minimize heat loss from the sample. A typical sample quantity used is from 50 to 75 milligrams for a solid and about 65 microliters for a liquid sample. When using a liquid sample, the sealed metal crucible must be weighed both before and after the age so that any weight loss can be compensated for in calculating the size of the exotherm after the age.

Step 3: DSC Scan on Aged Sample

A DSC scan, utilizing the sealed metal crucible, was run on the aged sample from Step 2, utilizing a TA 2200 system. The size of the resulting exotherm was compared to the original exotherm in the unaged sample. The cell base, metal crucible, sample weight and heat-up rate were identical to those used to determine the exotherm size in the unaged sample in Step 1. A decrease in the size of the exotherm indicates that heat was evolved during the age, and thus the exotherm initiated during the age.

Step 4: Determination of DSC Decomposition Onset Temperature

Steps 2 and 3 are repeated at lower temperatures in ~5°C increments, until no change in the size of the exotherm is observed for the aged sample.

C2. Calibration Experimental – Small Scale Isothermal Age Technique

The SSIA techniques was calibrated using solid dicumyl peroxide and a 40% weight solution in ethyl benzene. A Round-Robin testing program, sponsored by the DIERS Users Group, indicated the onset temperature for the decomposition for a 40% weight solution of dicumyl peroxide in ethyl benzene using standard DSC, ARC, RSST and VSP test cells and procedures[6].

Four different test systems/methods utilizing four different test cells: 1) Fauske RSST with standard glass and Merck designed dewar cell, ASI[7] Radex with standard glass and Merck-designed dewar cell, TA 2200 DSC with the small scale metal reusable crucible and adiabatic dewar with standard dewar cell and a specially designed temperature-controlled oven, were used to determine the exothermic onset temperatures for three

different compounds. Two different heat profile programs were used: a temperature scan utilizing a constant heat-up rate and an isothermal age technique using a set temperature.

The results for the Step 1 decomposition onset temperature determination are reported and compared to those of the DIERS Round-Robin test results in Table 11. The results of the reevaluation of the isothermally aged samples are reported in Table 12. See Figures 9 and 10 for a comparison of the DSC reruns of the isothermally aged solid and ethyl benzene solution of dicumyl peroxide.

C3. Case Studies

The exothermic decomposition onset temperature for two Merck proprietary compounds were determined using the SSIA technique and compared to those determined using standard adiabatic dewar, RSST and Radex dewar studies. The results are presented in Table 13 and 14. Both proprietary compounds were isothermally aged in the metal crucibles, RSST and Radex Merck designed dewar cells at three predetermined temperatures, and then rerun in a metal crucible with the results compared to the unaged sample. The results are presented in Tables 15 and 16.

C4. Sensitivity

Calibration of the SSIA technique, using dicumyl peroxide, has indicated that the system has a sensitivity level lower (0.01 to 0.013°C min^{-1}) than that selected for the ARC studies (0.02°C min^{-1}) in the DIERS Round-Robin Test. The results are presented in Table 17.

C5. Conclusions

Calibration of the SSIA technique, using dicumyl peroxide indicates that the test method is capable of predicting decomposition onset temperatures comparable to that of an ARC and better than those obtainable using standard dewar temperature scan runs. A sensitivity level of 0.01 to 0.013°C min^{-1} was determined for the SSIA technique.

This methodology is useful for determining onset temperatures only. The consequences of the initiation of the decomposition must be further evaluated via RSST, VSP or other suitable techniques in order to determine the consequences of initiation on processing.

CONCLUSIONS FOR THE USE OF THE "MERCK" SMALL SCALE REUSABLE METAL CRUCIBLE

The "Merck" small scale reusable metal crucible is capable of providing accurate and reproducible data using milligram/milliliters of sample to:

1. determine whether exothermic activity is present in a closed reaction sytem

2. determine accurate, rapid and reproducible heats of reaction for appropriate reaction systems and

3. determine accurate exothermic decomposition onset temperatures which are comparable to those determined using an ARC.

REFERENCES

1. L.D. Tuma, "A Reusable Metal Crucible for Use in Differential Scanning Calorimetry Analysis of Closed Reaction System Samples", *Thermichima Acta,* 212 (1992) 179-197.

2. TA Instruments, New Castle, DE.

3. J. Van Humbeeck and Bijvoet, "A Calibration Study of the DuPont 910 Module", *Thermichima Acta,* 120 (1987) 55.

4. L. D. Tuma, "Small Scale Isothermal Age Technique to Determine Exothermic Onset Temperatures" 284 (1996) 135-144.

5. Fauske and Associates, Inc., Burr Ridge, IL.

6. DIERS Users Group Phase VII Round-Robin Testing Results Presented at DIERS Users Group Meeting, Boston MA, September 30, 1994.

7. Astra Scientific International, Inc. Pleasanton, CA.

TABLE 1

METAL CRUCIBLE CALIBRATION USING INDIUM
CONSTANT WEIGHT
(9.2 MGS)

CRUCIBLE	WEIGHT OF INDIUM (MGS)	ONSET OF MELTING (°C)	E[1]	E CORRECTED[2]
Al Pan[4]	1	27.661	1.0278	1.0414
Al Pan[4]	2	27.169	1.0464	1.0449
Al Pan[4]	5	26.929	1.0557	1.0552
Al Pan[4]	10	26.422	1.0760	1.0724
Al Pan[4]	20	25.370	1.1206	1.1069
Al Pan[4]	50	23.609	1.2042	1.2102
Metal Crucible[5]	1	26.570	1.0700	1.1035
Metal Crucible[5]	2	26.397	1.0770	1.1097
Metal Crucible[5]	5	25.590	1.1110	1.1283
Metal Crucible[5]	10	24.519	1.1595	1.1592
Metal Crucible[5]	20	23.791	1.1950	1.2211
Metal Crucible[5]	50	20.235	1.4050	1.4068

TABLE 2

METAL CRUCIBLE CALIBRATION USING INDIUM
CONSTANT HEATING RATE
(5°C MIN^{-1})

CRUCIBLE	WEIGHT OF INDIUM (MGS)	ONSET OF MELTING (°C)	E[6]	E CORRECTED[7]
Al Pan[4]	5.5	27.919	1.0183	1.0302
Al Pan[4]	9.2	27.169	1.0464	1.0464
Al Pan[4]	15.0	26.429	1.0757	1.0630
Al Pan[4]	19.4	26.049	1.0914	1.0781
Al Pan[4]	24.7	25.949	1.0956	1.0964
Al Pan[4]	29.8	25.658	1.1080	1.1140
Metal Crucible[5]	5.5	26.426	1.0758	1.0835
Metal Crucible[5]	9.2	25.589	1.1110	1.0963
Metal Crucible[5]	15.0	25.126	1.1315	1.1198
Metal Crucible[5]	19.4	24.551	1.1580	1.1377
Metal Crucible[5]	24.7	24.199	1.1748	1.1591
Metal Crucible[5]	29.8	23.729	1.1981	1.1780

TABLE 3

HEAT TRANSFER ABILITY

SAMPLE HOLDER	THERMAL CONDUCTIVITY (CAL/CM-SEC-°C)	ONSET OF MELTING (°C)	E CORRECTION
Aluminum Pan	0.2203	26.929	1.0557
Metal Crucible[3]	0.4386	25.590	1.1110

FOOTNOTES

Theoretical heat to fusion for indium = 28.43 J gm^{-1}.

[1]For heat of fusion data E was set to 1.000.

[2]$E_{EXP} = \frac{\text{theoretical heat of fusion}}{\text{experimental heat of fusion}}$

[3]E corrected is the result of the straight line fit of data points where $y = mx + b$.

[4]Al pan = crimped Al pan.

[5]Sealed crucible.

[6]For heat of fusion data E was set to 1.00

[7]$E_{CAL} = \frac{\text{heat of fusion theoretical}}{\text{heat of fusion experimental}}$

TABLE 4

COMPARISON OF DECOMPOSITION EXOTHERMS USING THE TWO SAMPLE HOLDERS

	SEALED METAL CRUCIBLE	ALUMINUM PAN
1	248.40	163.53[1]
2	55.00	8.18[1]
3	38.76	38.24

TABLE 5

SEALED METAL CRUCIBLE'S VAPOR PRESSURE CONTAINMENT

SAMPLE[3]	LOWEST RUPTURE PRESSURE[4] (Psia)	HIGHEST RUPTURE PRESSURE (Psia)[4]	AVERAGE RUPTURE PRESSURE (Psia)[4]
ACETONE	~433	~518	~462
METHANOL	~445	~530	~498
WATER	~414	~452	~498

SAMPLE[3]	WEIGHT OF SAMPLE BEFORE AGE (mg)	WEIGHT OF SAMPLE AFTER AGE (mg)	% WEIGHT LOSS
ACETONE	67.4	67.3	0.15
METHANOL	61.1	61.1	0.00
WATER	58.5	58.5	0.00

TABLE 6

INSTRUMENT CALIBRATION USING INDIUM

INDIUM				
14.60	24.474	0.36	1.1616	1.1759
36.43	24.145	0.88	1.1775	1.1803
77.69	24.000	1.86	1.1886	1.1846
115.59	23.895	2.76	1.1898	1.1965
169.46	23.475	3.98	1.2111	1.2069

TABLE 7

SIC CALIBRATION USING
$HCl + NaOH \rightarrow NaCl + H_2O$

0.5	0.36	9.862	13.668	1.386	1.389
1.0	0.70	9.992	13.986	1.399	1.397
2.0	1.44	10.453	14.807	1.417	1.415
3.0	2.17	10.921	15.649	1.433	1.433
4.0	2.92	11.359	16.471	1.450	1.451

FOOTNOTES

[1]The lid either leaked or was blown off, before the exotherm was complete.
[2]The sample was heated until the teflon seal ruptured.
[3]Each run was repeated 5 times.
[4]The psia values reported are taken from Lange's "Handbook of Chemistry".
[5]Each sample was heated to ~10°C above its boiling point and held at that temperature for ~16 hours.
[6]The theoretical heat of fusion for indium = 28.43 Joules $gram^{-1}$.
[7]For the heat of fusion data, E was set to 1.000.
[8]For experimental heat of reaction data (H_{EXP}), E was set to 1.000.
[9]The H_{TH} and H_{HRX} include a heat of dilution effect.
[10]Δ_{TH} was calculated by interpolation using data tables from Lange's "Handbook of Chemistry".

TABLE 8

SYRINGE INJECTION CALORIMETRY[1]

$HCl + NaOH \rightarrow NaCl + H_2O$

0.5	0.36	13.668	13.698	72.15	100.02
1.0	0.70	13.959	13.959	71.44	99.81
2.0	1.44	14.807	14.791	70.59	99.89
3.0	2.17	15.649	15.649	69.78	100.00
4.0	2.92	16.482	16.482	68.96	100.07

TABLE 9

SIC EXPERIMENTAL RESULTS

$HCl + NaOH$	0.5	100.2
$HCl + NaOH$	1.0	99.8
$HCl + NaOH$	2.0	99.9
$HCl + NaOH$	3.0	100.0
$HCl + NaOH$	4.0	100.1
$HNO_3 + NaOH$	1.0	100.3
$HNO_3 + NaOH$	2.0	98.1
$HNO_3 + NaOH$	3.0	99.0
$HNO_3 + NaOH$	4.0	98.2
$KCl + H_2O$	-	99.0
$CaSO_4 + H_2O$	-	97.6
$H_2SO_4 + H_2O$	-	102.5

TABLE 10

SIC RESULTS ON PROPRIETARY REACTIONS

90.0	-	-	89.0
82.5	91.0	-	-
10.5	-	10.0	-

TABLE 11

COMPARISON OF EXOTHERM ONSET TEMPERATURES FOR DICUMYL PEROXIDE SOLID AND 40% WT IN EtBZ

DIERS ROUND-ROBIN[3]	DSC	STAINLESS STEEL	TEST NOT RUN	109.4 TO 159.2 (AVG. 150 ± 6.1 °C)
SSIA CALIBRATION	DSC	HAST B CRUCIBLE	125	124
DIERS ROUND-ROBIN[3]	RADEX	GLASS CELL	NOT AVAILABLE	NOT AVAILABLE
SSIA CALIBRATION	RADEX	GLASS CELL	112	117
DIERS ROUND-ROBIN	RSST	GLASS CELL	NOT AVAILABLE	110 TO 125 (AVG. 115.2 ± 4.1 °C)
SSIA CALIBRATION	RSST	GLASS CELL	112.5	118
DIERS ROUND-ROBIN[3]	ARC	REGULAR TEST CELL	NOT AVAILABLE	97 TO 107 (AVG. 103.4 ± 3.2 °C)
SSIA CALABARINE	RADEX	SPECIAL DEWAR CELL[4]	103	105
SSIA CALIBRATION	RSST	SPECIAL RSST CELL[4]	104	103
SSIA CALIBRATION	ADIABATIC DEWAR OVEN	REGULAR DEWAR	104	TEST NOT RUN

FOOTNOTES

[1]The ΔH_{TH} includes a heat of dilution.

[2]All ΔH's are in Kcal/mole of reactant A.

[3]DIERS Users Group Phase VII Round-Robin Testing Results Presented at DIERS Users Group Meeting, Boston MA, September, 1994.

[4]L. D. Tuma and A. A. Wieczorek, "Novel Small Scale Techniques to Identify Exothermic Initiation Temperatures Under Adiabatic Conditions" presented at 23rd NATAS Conference, Toronto, Canada.

TABLE 12

SSIA DETERMINATION OF ECTOTHERM ONSET TEMPERATURE FOR DICUMYL PEROXIDE SOLID AND 40 WT IN EtBZ

DSC	HAST B CRUCIBLE	12	90	0	0
RADEX	DEWAR CELL[1]	12	90	0	0
RSST	DEWAR CELL[1]	12	90	0	0
DSC	HAST B CRUCIBLE	12	92.5[2]	-1.5	-1.9
DSC	HAST B CRUCIBLE	12	95	-9.8	-10.2
RADEX	DEWAR CELL[1]	12	95	-10.2	-9.4
RSST	DEWAR CELL[2]	12	95	-9.6	-10.3
DSC	HAST B CRUCIBLE	12	100	-13.4	-14.5
RADEX	DEWAR CELL[1]	12	100	-13.3	-14.6
RSST	DEWAR CELL[2]	12	100	-14.9	-13.4

TABLE 13

COMPARISON OF EXOTHERM ONSET TEMPERATURE FOR PROPRIETARY COMPOUND #1

DSC	HAST B	NONE	108.3	175.3
RADEX	GLASS CELL	NONE	109.2	179.9
RADEX	DEWAR CELL[1]	58.7	108.6	173.4
RSST	GLASS CELL	NONE	108.3	178.1
RSST	DEWAR CELL[1]	58.3	108.6	173.4
ADIABATIC DEWAR OVEN	REGULAR DEWAR	51.4	108.3	175.0

TABLE 14

COMPARISON OF EXOTHERM ONSET TEMPERATURE FOR PROPRIETARY COMPOUND #2

DSC	HAST B	70.0	122.0
RADEX	GLASS CELL	72.5	125.5
RADEX	DEWAR CELL[1]	57.6	124.5
RSST	GLASS CELL	66.8	125.0
RSST	DEWAR CELL[1]	51.5	120.5
ADIABATIC DEWAR OVEN	REGULAR DEWAR	48.3	125.0

FOOTNOTE

[1]L. D. Tuma and A. A. Wieczorek, "Novel Small Scale Techniques to Identify Exothermic Initiation Temperatures Under Adiabatic Conditions" presented at 23rd NATAS Conference, Toronto, Canada.

[2]The data for the 92.5°C is provided to allow for the determination of the sensitivity level of the SSIA technique.

TABLE 15

SSIA DETERMINATION OF EXOTHERM ONSET TEMPERATURE FOR PROPRIETARY COMPOUND #1

DSC	HAST B CRUCIBLE	12	30	0
DSC	HAST B CRUCIBLE	12	35	0
RADEX	DEWAR CELL[1]	12	35	0
RSST	DEWAR CELL[1]	12	35	0
DSC	HAST B CRUCIBLE	12	40	-5.85
RADEX	DEWAR CELL[1]	12	40	-6.63
RSST	DEWAR CELL[1]	12	40	-5.23
DSC	HAST B CRUCIBLE	12	50	-21.30
RADEX	DEWAR CELL[1]	12	50	-16.34
RSST	DEWAR CELL[1]	12	50	-16.6

TABLE 16

SSIA DETERMINATION OF EXOTHERM ONSET TEMPERATURE FOR PROPRIETARY COMPOUND #2

DSC	HAST B CRUCIBLE	12	30	0
DSC	HAST B CRUCIBLE	12	35	0
RADEX	DEWAR CELL[1]	12	35	0
RSST	DEWAR CELL[1]	12	35	0
DSC	HAST B CRUCIBLE	12	45	-1.21
RADEX	DEWAR CELL[1]	12	45	-1.74
RSST	DEWAR CELL[1]	12	45	NOT AVAILABLE[2]
DSC	HAST B CRUCIBLE	12	55	-3.50
RADEX	DEWAR CELL[1]	12	55	-3.06
RSST	DEWAR CELL[1]	12	55	-2.82
DSC	HAST B CRUCIBLE	12	65	-4.59
RADEX	DEWAR CELL[1]	12	65	-3.89
RSST	DEWAR CELL[1]	12	65	-4.98

FOOTNOTES

[1]L. D. Tuma and A. A. Wieczorek, "Novel Small Scale Techniques to Identify Exothermic Initiation Temperatures Under Adiabatic Conditions", presented at 23rd NATAS Conference, Toronto, Canada.

[2]The percent change in the size of the exotherm at 45°C could not be measured due to sample decomposition upon storage.

TABLE 17
COMPARISON OF SENSITIVITY (°C/MIN) OF TEST METHODS

TEST METHOD	SAMPLE TEST	
ARC[1]	DICUMYL PEROXIDE LIQUID 40 WT IN EtBZ	0.02[2]
SSIA	DICUMYL PEROXIDE LIQUID 40 WT IN EtBZ	0.013[3]
SSIA	DICUMYL PEROXIDE SOLID	0.01[3]
SSIA	PROPRIETARY COMPOUND #1	0.025[3]
SSIA	PROPRIETARY COMPOUND #2	0.011[3]

[1]DIERS Users Group Phase VII Round-Robin Testing Results Presented at DIERS Users Group Meeting, Boston MA, September, 1994.
[2]Sensitivity level used in DIERS Round Robin Test.
[3]The sensitivity was calculated by dividing the heat release in cal/gram by the time in minutes. This result was divided by the heat capacity (0.5cal/gram°C assumed).

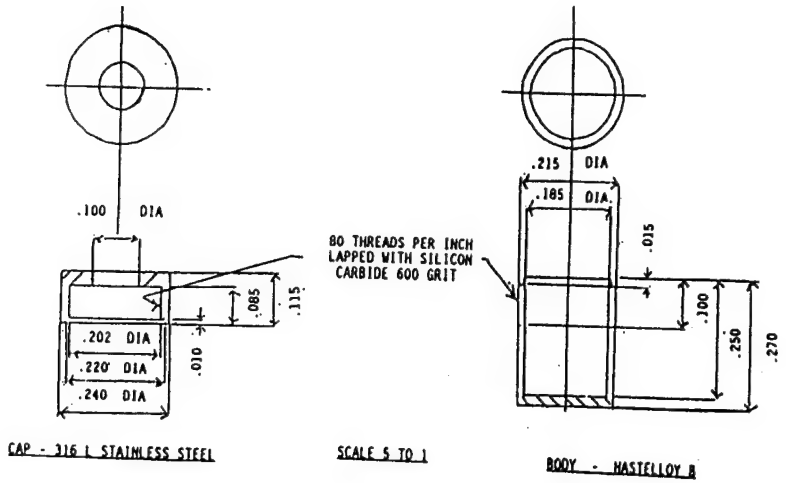

SAMPLE CRUCIBLES

FIGURE 1

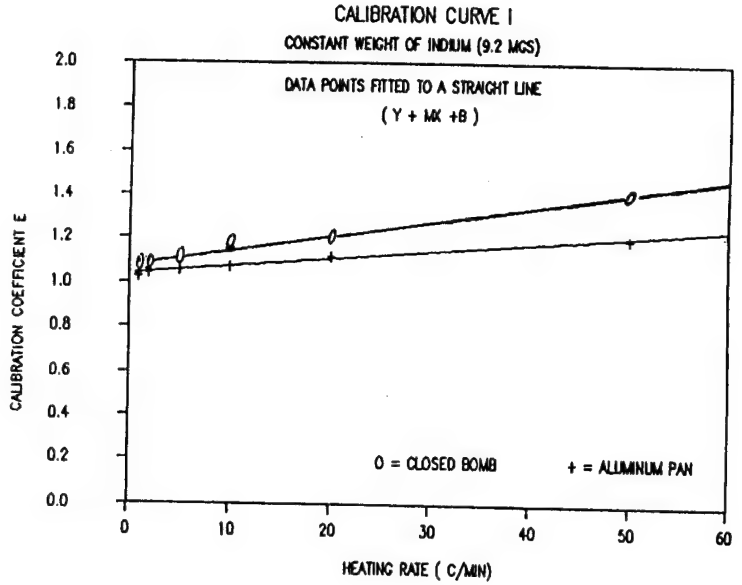

FIGURE 2

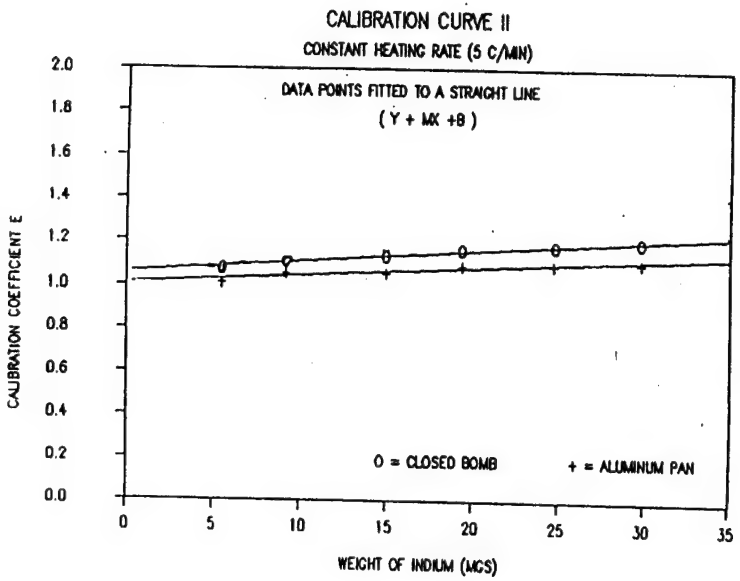

FIGURE 3

R16

FIGURE 4

COMPARISON OF DSC INDIUM MELT CURVES FOR THREE SAMPLE CONTAINERS

HEAT TRANSFER ABILITY

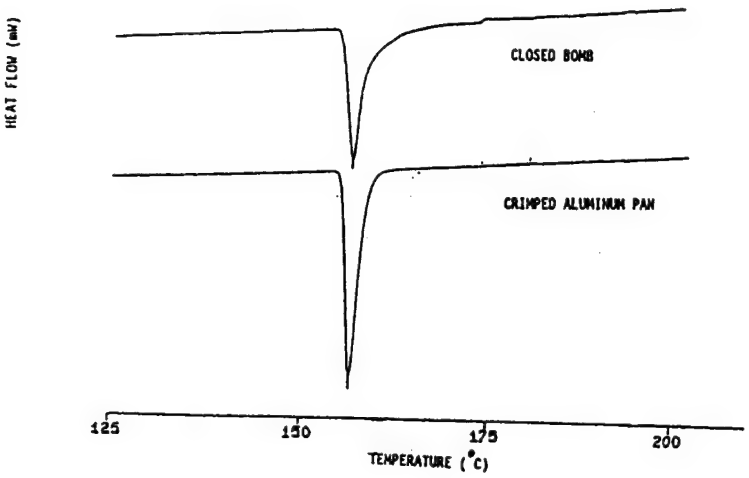

FIGURE 5

COMPARISON OF DSC INDIUM MELT CURVES FOR THREE SAMPLE CONTAINER

REPRODUCIBILITY

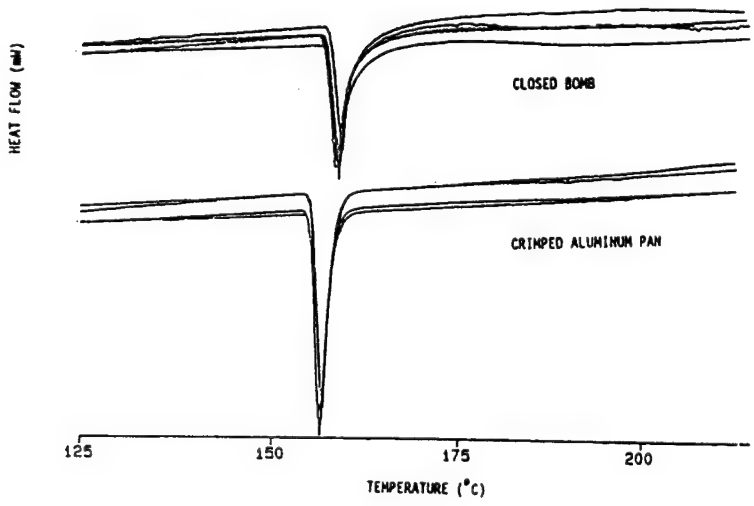

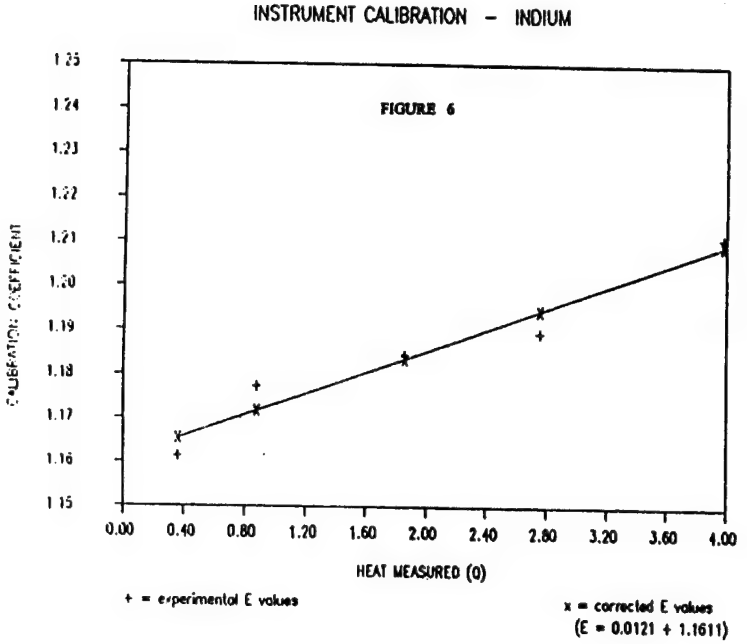
INSTRUMENT CALIBRATION - INDIUM
FIGURE 6
CALIBRATION COEFFICIENT
1.25
1.24
1.23
1.22
1.21
1.20
1.19
1.18
1.17
1.16
1.15
0.00 0.40 0.80 1.20 1.60 2.00 2.40 2.80 3.20 3.60 4.00
HEAT MEASURED (Q)
+ = experimental E values
x = corrected E values
(E = 0.0121 + 1.1611)

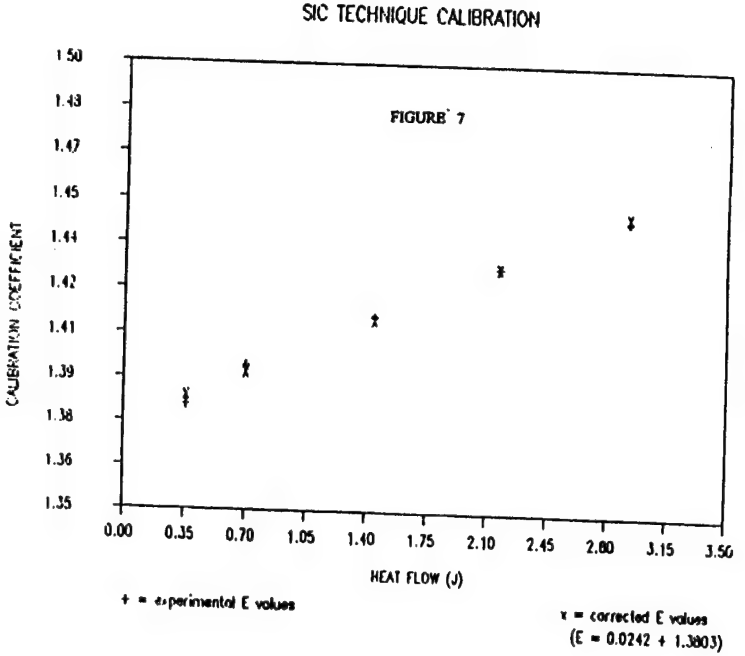
SIC TECHNIQUE CALIBRATION
FIGURE 7
CALIBRATION COEFFICIENT
1.50
1.48
1.47
1.45
1.44
1.42
1.41
1.39
1.38
1.36
1.35
0.00 0.35 0.70 1.05 1.40 1.75 2.10 2.45 2.80 3.15 3.50
HEAT FLOW (J)
+ = experimental E values
x = corrected E values
(E = 0.0242 + 1.3803)

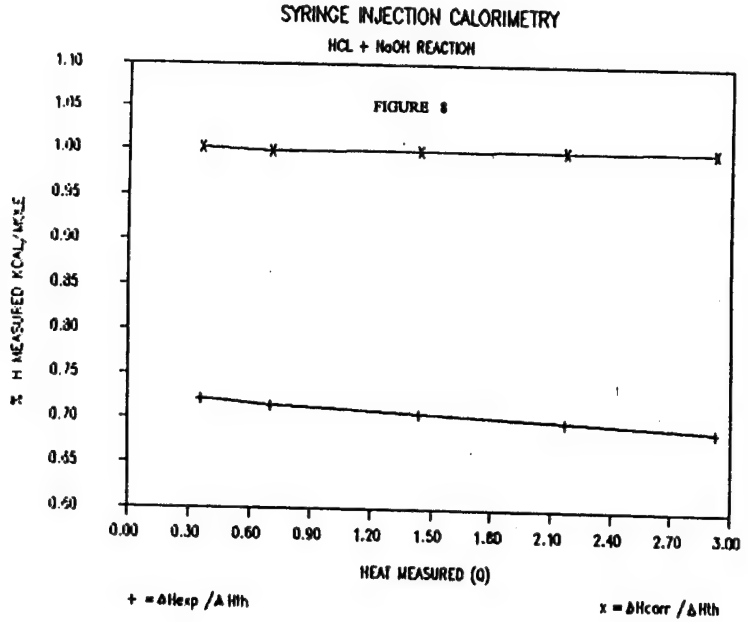
SYRINGE INJECTION CALORIMETRY
HCL + NaOH REACTION
FIGURE 8
% H MEASURED KCAL/MOLE
1.10
1.05
1.00
0.95
0.90
0.85
0.80
0.75
0.70
0.65
0.60
0.00 0.30 0.60 0.90 1.20 1.50 1.80 2.10 2.40 2.70 3.00
HEAT MEASURED (Q)
+ = ΔHexp /Δ Hth
x = ΔHcorr /Δ Hth

DSC RUNS OF UNAGED DICUMYL PEROXIDE VERSUS SSIA DSC AGED SAMPLES
(IN ETHYL BENZENE)

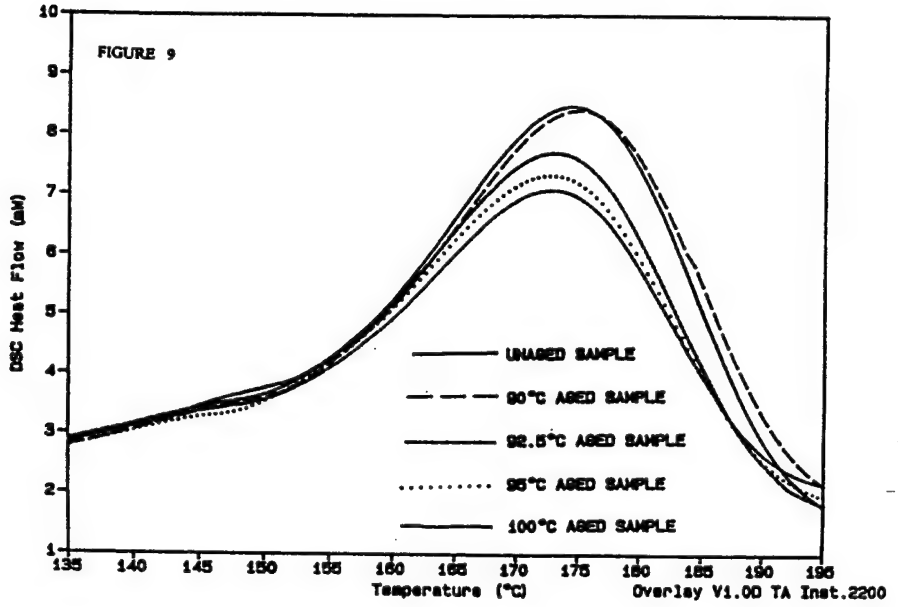

DSC RUNS OF UNAGED DICUMYL PEROXIDE VERSUS SSIA DSC AGED SAMPLES
(SOLID)

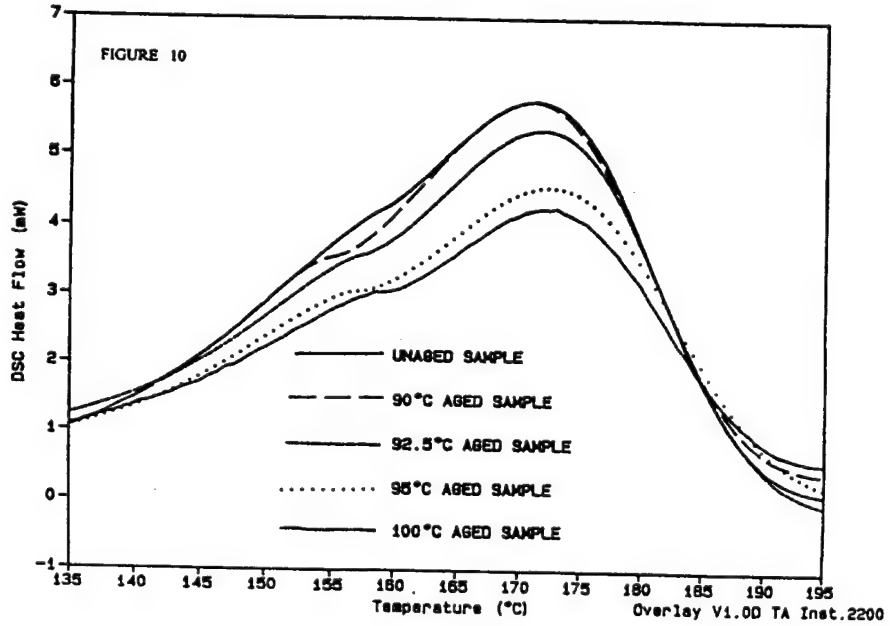

International Round Robin Test to Determine the Stability of DB Ball Propellants by Heat Flow Calorimetry [1]

Stephan Wilker [#], Pierre Guillaume [*]

Abstract

This report summarises the results of the Round Robin Test in which a method for the determination of the slow decomposition of propellants by heat flow calorimetry (HFC) was tested amongst eight laboratories in six countries. As it is known that small changes of sample preparation and measuring procedure affect the HFC signal very much it was very easy to detect whether the operational procedure was conducted in a comparable way. The results show that – besides the initial effects – the standard deviation of the HFC curves at 80°C were very low which means that the measuring principle proposed by PB Clermont and WIWEB was good enough to be reproduced. This method should thus be integrated into a STANAG „HFC of DB ball propellants".

Additionally the kinetics of the decomposition reaction was calculated and the chemistry of the stabiliser depletion was investigated under different reaction conditions.

Introduction

In April 1997 ten scientists agreed to participate in a Round Robin Test dealing with microcalorimetric measurements of double base ball propellants. The aim was to harmonize the measurement conditions and the evaluation procedure and to compare the obtained data. The DPA stabilised propellant K 6210 was chosen because the decomposition of this propellant was intensively investigated during the past three years [1]. Lot 225 was taken for this test.

Participants of the Round Robin Test „Heat Flow Calorimetry"

Affilation	Name	Address		
ETBS	Dr. C. Balès	Route de Guerry	F-18015	Bourges
ICT	Dr. M.A. Bohn	J-v-Fraunhofer-Str. 7	D-76327	Pfinztal
Nitrochemie Wimmis	Mrs. R. Sopranetti		CH-3752	Wimmis
PB Clermont S.A.	Dr. P. Guillaume	Rue de Clermont, 176	B-4480	Engis
Puolustusvoimien Tutkimuskeskus	Mrs. M. Hihkiö	PL 5	SF-34111	Lakiala
SNPE – CRB	Mme M. Rat	Boîte Postale N° 2	F-91710	Vert-le-Petit
TNO P.M. Laborat.	Dr. N. v.d. Meer	Postbus 45	NL-2280AA	Rijswijk
WIWEB	Dr. S. Wilker	Großes Cent	D-53913	Swisttal

[1] Actualised and revised version from the one published at the 29th International ICT Conference 1998

[#] Wehrwissenschaftliches Institut für Werk-, Explosiv- und Betriebsstoffe (WIWEB), Großes Cent, D-53913 Swisttal

[*] PB Clermont SA, 176 Rue de Clermont, B-4480 Engis

Program

To conduct a Round Robin Test it is necessary to define as exactly as possible the measuring conditions. This includes sample preparation, preconditioning, measurement temperature and time and calibration.

The following method was evaluated at PB Clermont and WIWEB/BICT during the past years and has proved to be satisfactory for HFC measurements of DB ball propellants. Its advantage is that it's very convenient, reproducible and it gives results within a few weeks. The measuring conditions are well-defined and are – what is very important – analogous to the conditions in small caliber ammunition.

Operational procedure of HFC measurements

This is the operational procedure for heat flow calorimetric measurements (HFC) of double base ball propellants (DB propellants) within the "Round Robin Test" arranged during the TTCP workshop at Leeds April 1997. It has changed in detail from the original version distributed amongst the participants.

The sample measured is a DB ball propellant of type K 6210-13, lot 225. It is stabilised with DPA and its decomposition chemistry is better known than of any other propellant.

1 Sample preparation

1.1 Particle size
The grains should be taken as they are (no cutting necessary).

1.2 Preconditioning
The sample should be stored in 65-70% RH (21°C) environment for some days and for comparison reasons under ambient conditions. At least the moisture content of the samples has to be known (Karl-Fischer titration).

1.3 Filling grade
The measuring ampoules should be filled up to the top so that the amount of air inside is minimal. The loading density is thus approx. 0,9 to 1,0 (2,7 - 3,0 g for a 3 ml ampoule).

1.4 Closing of the ampoules
The closing of the ampoules must be complete so that the top can not be turned around manually. In some cases the closure has to be done with two different clamps. The closing can be easily controled by looking at the HFC curve (see page 7).

2 Measurement

2.1 Temperature program
The measurements (always double or triple measurements are recommended) start at 80°C, followed by 60°C, 50°C and 40°C. 35 or 30°C measurements can also be tried, but they are quite tricky and depend on a good room temperature/rH constance. An inverse temperature program (from 40 up to 80°C) with fresh samples is not useful because the initial effects last very long at lower temperatures. But it is possible to check the 50/60°C data after the whole temperature program.

2.2 Calibration

The calibration must be done very carefully. Please wait for a stable baseline (minimum 12 h of stability). Use empty ampoules on the reference side. Use the next measuring range for calibration and measurement (e.g. 300 µW for 80°C, 100 µW for 60°C, 30 µW for 50°C and 10 µW for 40°C). Use the „Switch technique" to be sure of the niveau of the true baseline at 50/40°C measurements. Doing this please leave the switched sample for at least 20 min in the park position before putting it down into the measuring position. Otherwise the thermal equilibrium might be disturbed too much. The switched measurement should last at least several hours (e.g. over night).

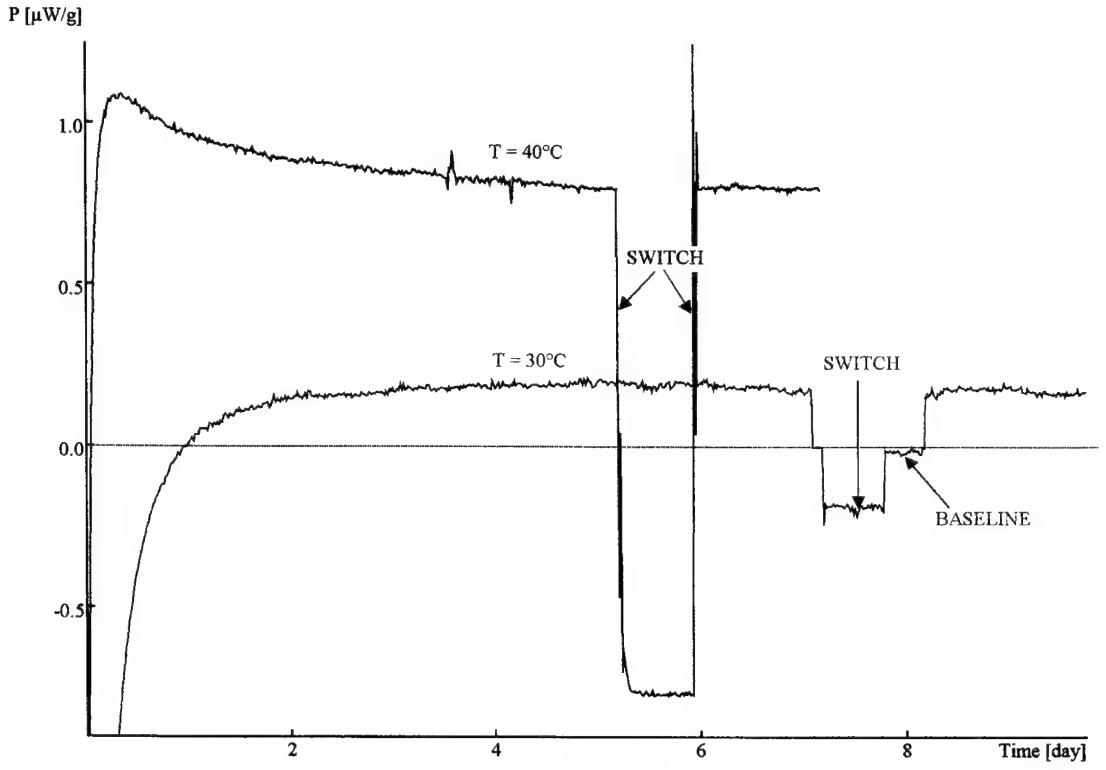

Fig. 1. Measurements showing a Switch and a combined Switch-baseline experiment

2.3 Measurement

The measuring time of 8 days at 80°C is recommended to reach a constant niveau. The lower temperature HFC measurements should be run until a constant level is reached. Constant level in this case means a variation of 3-6% within a period of 24 h. The use of the park position for about 20 minutes prior to measurement is possible but not really necessary.

If endothermic peaks due to gas evolution occur at the end of the 80°C measurement the control of the closing of the ampoules is recommended before they are measured at lower temperatures.

If water has to be refilled into the pre-heater please it should be done slowly to avoid some sharp peaks due to temperature drops in the bath. For this reason a dropping funnel is recommended.

3 Evaluation

3.1 Raw data

The data must be reduced to one gram of propellant. Double measurements at 80°C should show a very small difference in value and in time (until the 2nd maximum is reached). If this is not the case the measurements must be repeated.

3.2 Data format

The data should be readable to DIGITAM v 3.0® because not all participants do have the DIGITAM for WINDOWS® version. Alternatively the data should be converted to ASCII and evaluated by EXCEL 5® for Windows 3.1®.

3.3 Calculation

The calculation of service life occurs analogously to the formula presented in the German TL and at the TTCP workshop. The first step is to establish an Arrhenius plot (formula 1). The determination of the correlation coefficient is useful to get a feeling for the quality of the data. As in nearly all cases a change in slope at about 60°C occurs two Arrhenius plots (the first with the 80/60°C values; the second with the 60/40°C values) have to be established.

From the lower temperature range the heat flow value P40 must be calculated. Using formula (2) the time until 1,5% energy* is lost is then calculated. It should be around 3 to 3½ years. The value for heat of explosion is 4075 J/g for this lot.

$$P = C * e^{\frac{-E_a}{R*T}} \qquad (1)$$

$$t_{40} = \frac{Q_{ex} * 0{,}015}{P_{40} * 86400 * 365{,}25} \qquad (2)$$

using

P = heat flow [µW/g]

C = preexp. factor [W/kg]

E_a = activation energy [kJ/mol]

T = temperature [K]

R = universal gas constant [0,00831 $kJ \cdot K^{-1} \cdot mol^{-1}$]

t = time [years]

P_{40} = from (1) calculated heat flow at 40°C

Q_{ex} = heat of explosion [4,075 kJ/g]

4 Analysis

The samples should weighed after the HFC measurement to see whether a remarkable weight loss has occurred. If the samples had been closed good enough this should not be the case. After that the samples should be analysed after the HFC measurements by HPLC and/or GPC to look at the changes of the stabiliser content and distribution (this is also a control for the closing of the ampoules) and to look at the molecular mass decay under the measured conditions.

As well the moisture content of the samples after measurement should be checked. If enough measured sample is left, the heat of explosion might also be determined. To do

* The original value taken was 3% energy loss. As we know by now, a 1.5% energy loss definitively has no negative effect on the ballistical behaviour of this ball propellant. So we decided to calculated the t_{40} times with 1.5 % energy loss to be sure to be on the „safe side".

that it is necessary to refer to the original weight of the sample before the HFC measurement.

5 Data exchange

The data should be collected and sent to Germany (WIWEB) by diskette and in printed format. WIWEB will make the evaluation and comparison of the data.

HFC Results

At first the values at different temperatures deriving from all laboratories are compared to look at the „qualitiy" of measurement. As mentioned before the shape of the 80°C curve is very dependent on the humidity of the propellant, on the degree of filling and on the closing of the ampoules[2]. So we separated the evaluation into samples with and without preconditioning. We took out values and time of some very special points of the curve (1st maximum, „Knick", 1st minimum, intersection value, 2nd maximum and the 2nd minimum) and compared the results from different laboratories. The intersection point is consistent with the graphically estimated point of intersection where the tangent of the decreasing part of the curve meets the tangent going through the point of inflexion between the first minimum and the second

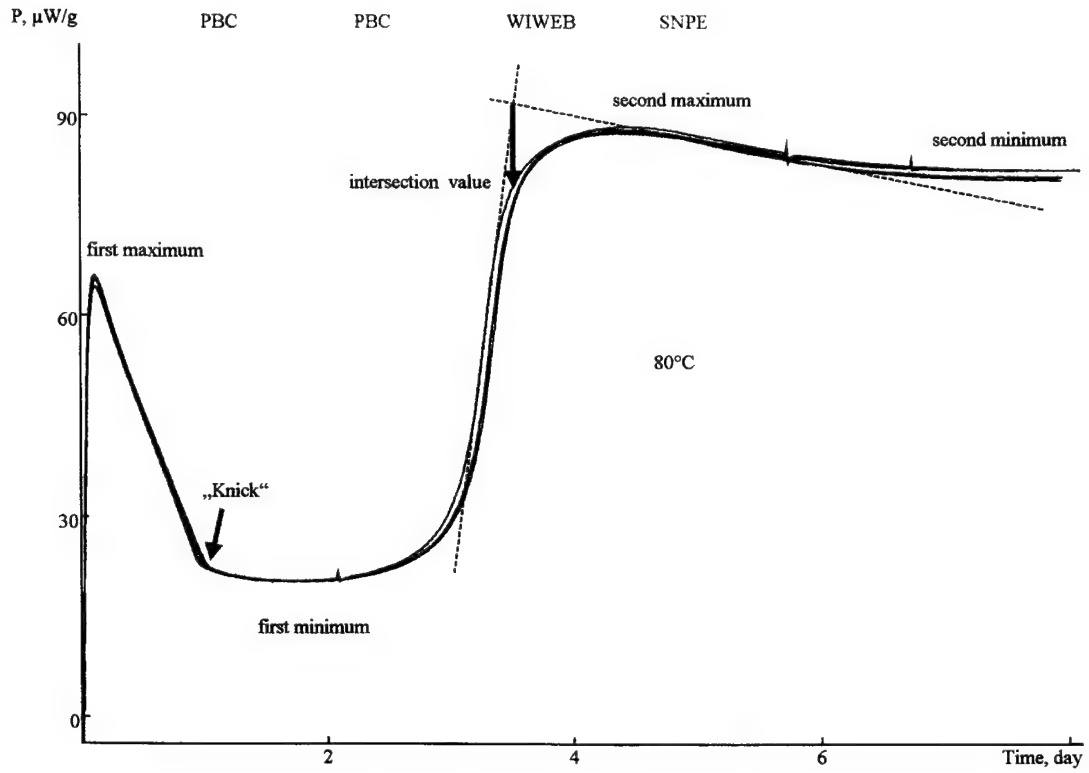

Fig. 2. Explanation of maxima, minima, „Knick", and inters. value (see text). K 6210, lot 223.

[2] Results of HFC measurements in leaking (not closed) ampoules, in ampoules with a lower filling grade and under different atmospheric conditions are presented in [9].

maximum (see fig. 2). It is taken because it is much easier to determine in time and heat flow than the second maximum itself. Its value is about 90% of the heat flow of the 2nd maximum.

All average values are collected in table 1 (80°C). The results of the 60/50/40°C measurements are collected in tables 2-4.

Table 1. Averages of measurements at T = 80°C

labs A-G	precond.	P/1. max.	t/1. max.	P/Knick	t/Knick	P/1. min.	t/1. min.
		[µW/g]	[h]	[µW/g]	[d]	[µW/g]	[d]
Average [a)]	Y	72,4	1,70	22,7	1,11	21,1	1,69
Standard deviation [a)]	Y	8,65	1,43	1,30	0,09	1,34	0,16
Rel. standard dev. [a)]	Y	11,9 %	84,4 %	5,7 %	7,9 %	6,4 %	9,7 %
Average [a)]	N	66,2	2,48	22,8	1,14	20,9	1,72
Standard deviation [a)]	N	4,35	1,42	0,66	0,19	0,74	0,09
Rel. standard dev. [a)]	N	6,6 %	57,3 %	2,9 %	16,6 %	3,5 %	5,4 %

Explanation: labs A-G: laboratories participated in these measurements; precond. = preconditioning (Yes/No); P/1.max. = value at the 1st maximum; t/1. max = time of 1st maximum; P/Knick = value of Knick; t/Knick = time of Knick; P/1. min. = value at 1st minimum; t/1. min. = time of 1st minimum

Table 1 (contd). Averages of measurements at T = 80°C

labs A-G	precond.	P/inters	t/inters	P/2. max.	t/2. Max.	P/end	t/end	Qg
		[µW/g]	[d]	[µW/g]	[d]	[µW/d]	[d]	[J/g]
Average [a)]	Y	81,1	3,43	87,6	3,99	79,1	8,00	43,5
Standard deviation [a)]	Y	4,85	0,18	4,8	0,23	b)	b)	4,60
Rel. standard dev. [a)]	Y	6,0 %	5,2 %	5,5 %	5,9 %	b)	b)	10,6 %
Average [a)]	N	78,2	3,42	86,2	4,15	79,1	8,7	42,0
Standard deviation [a)]	N	1,62	0,18	1,86	0,21	b)	b)	1,12
Rel. standard dev. [a)]	N	2,1 %	5,2 %	2,2 %	5,0 %	b)	b)	2,7 %

a) excluding stragglers; b) not useful (different times of end of measurement)

Explanation: P/inters = value at the intersection point; t/inters = time of the intersection point; P/2.max. = value at the 2nd maximum; t/2. max = time of 2nd maximum; P/end = value of the end of measurement; Qg = total energy released during measurement.

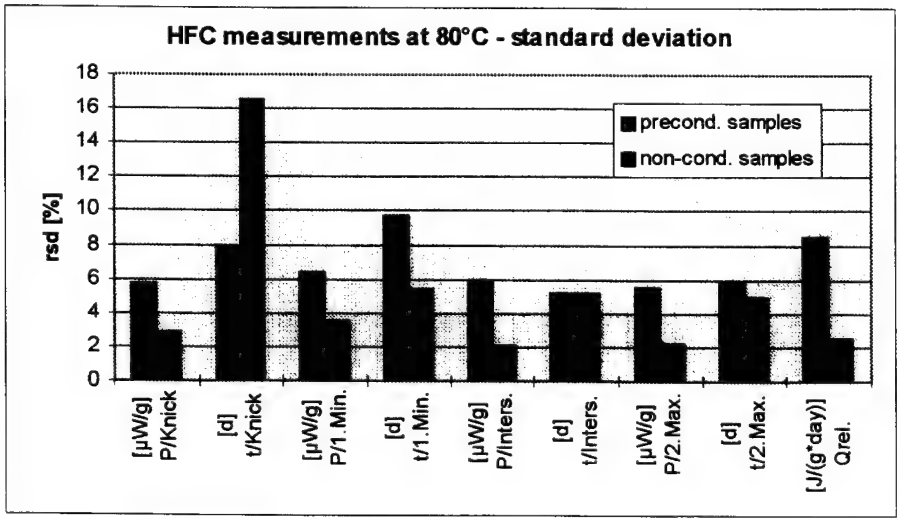

Fig. 3. Comparison of preconditioned and non-conditioned samples at 80°C

Table 2. Averages of measurements at T = 60°C

labs A-F	precond.	P/2d	P/4d	P/6d	P/8d	meas. time	Qg	Qrel
		[µW/g]	[µW/g]	[µW/g]	[µW/g]	[d]	[J/g]	[J/(g*day)]
average	Y	8,14	7,26	6,84	6,54	4 - 12	2 - 10	0,64
std. dev.	Y	0,59	0,54	0,42	0,42	-	-	0,04
average	N	7,81	7,20	6,93	6,72	4 - 11	1 - 8	0,62
std. dev.	N	0,98	0,93	1,08	0,53	-		0,07

The first 60°C series of laboratory A (see entries A016, A026 and A036) showed a big difference (stragglers) to the other experiments. So they were taken out from the average value, which means a significant decrease of the standard deviation (compared to [7]).

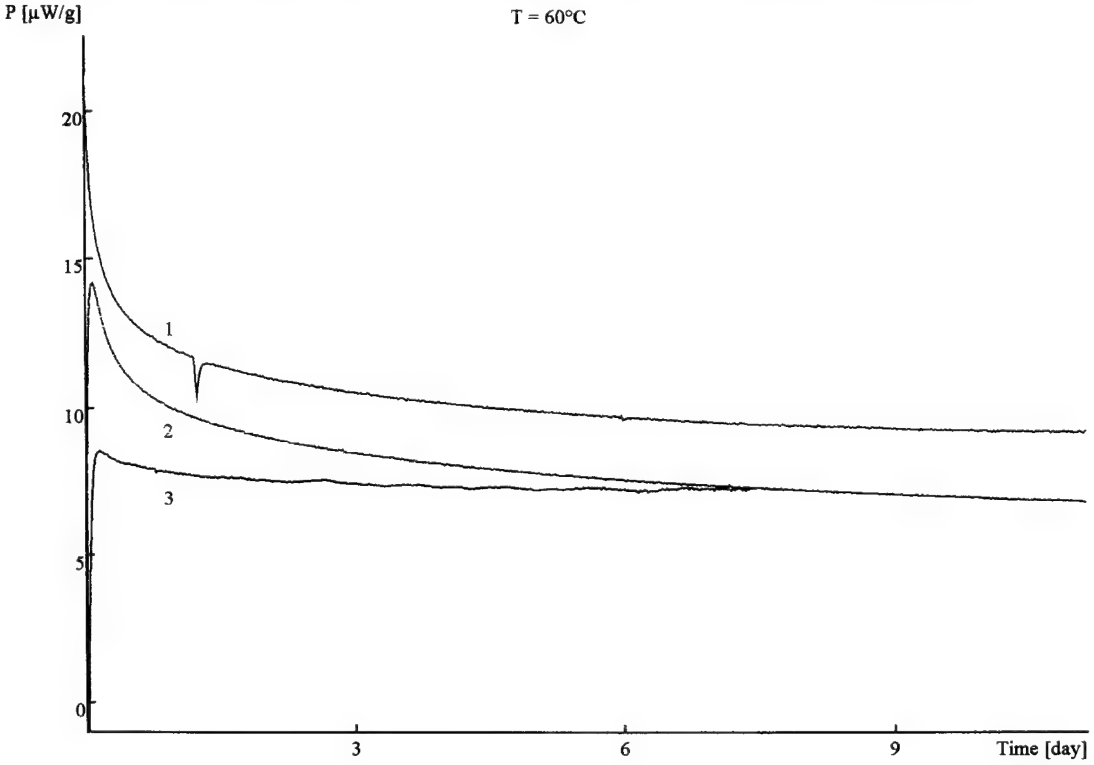

Fig. 4. Comparison of results at 60°C.
1 = lab. A; conditioned sample; measured at 80 → 60°C
2 = lab. B; unconditioned sample; measured at 80 → 60°C
3 = lab. C; unconditioned sample; measured at 80 → 70 → 60°C

Table 3. Averages of measurements at T = 50°C

labs A-F	precond.	P/2d	P/4d	P/6d	P/8d	meas. time	Qg	Qrel
		[µW/g]	[µW/g]	[µW/g]	[µW/g]	[d]	[J/g]	[J/(g*day)]
average	Y	2,06	1,90	1,80	1,72	6 - 9	1 - 2,3	0,170
std. dev.	Y	0,14	0,13	0,12	0,07	-	-	0,011
average	N	1,90	1,76	1,70	1,73	6 - 23	0,8 - 4,8	0,156
std. dev.	N	0,26	0,27	0,26	0,16	-	-	0,021

The first 50°C series of laboratory A (see entries A015, A025 and A035 in table A5 [10]) showed a big difference (stragglers) to the other experiments. So they were taken out from the average value, which means a significant decrease of the standard deviation (compared to [7]).

Table 4. Averages of measurements at T = 40°C [a)]

labs A-F	precond.	P/2d	P/4d	P/6d	P/8d	meas. time	Qg	Qrel
		[µW/g]	[µW/g]	[µW/g]	[µW/g]	[d]	[J/g]	[J/(g*day)]
average	Y	0,697	0,613	0,580	0,579	6 - 20	0,3 - 1,0	0,051
std. dev.	Y	0,079	0,069	0,081	0,038	-	-	0,003
average	N	0,778	0,602	0,572	-	6,5 - 20	0,2 - 1,0	0,045
std. dev.	N	0,093	0,116	0,113	-	-	-	0,016

a) all values taken for calculation of the average are corrected by Switch and/or baseline experiments (see fig.1)

In case of laboratory D no Switch was made thus these values are not collected in the average.

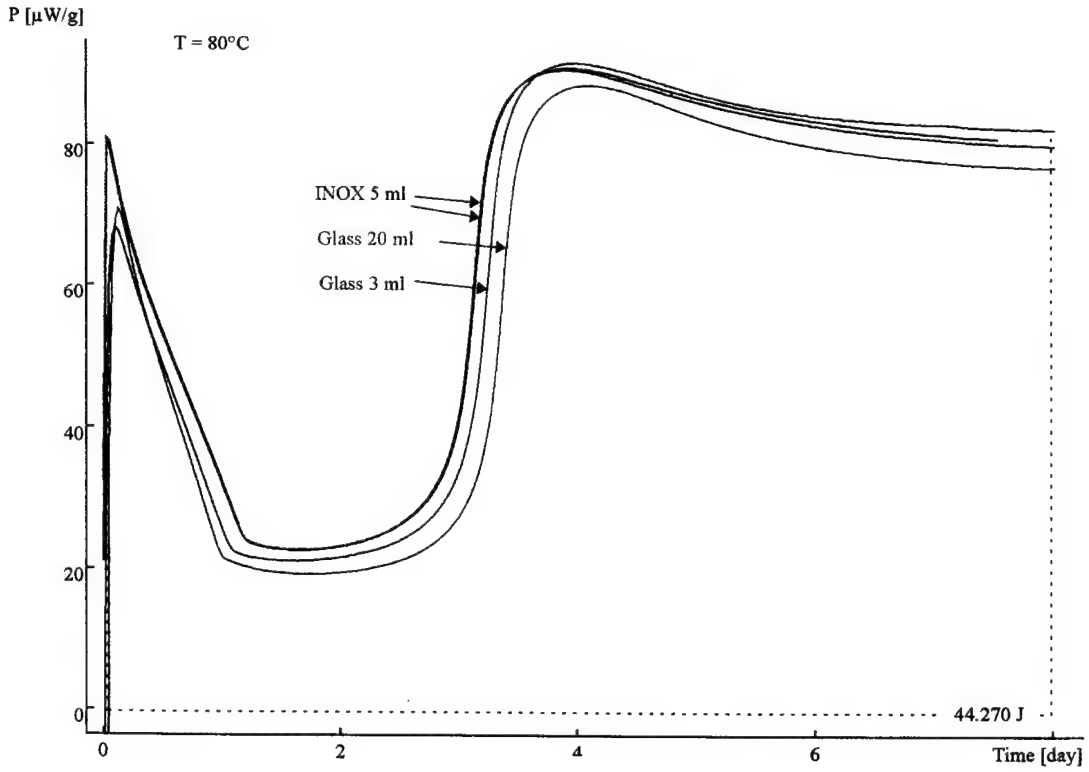

Fig. 5. Influence of the sample cell and cell volume on the HFC signal. Samples preconditioned.

Discussion

After all the data were collected and analysed by comparison (see tables 5-7) and by statistical analysis (see table 8). To find out the differences between samples with and without preconditioning they were evaluated separately. It was also necessary to give details of the measuring conditions (type of cell used). Some examples are picked out in the following tables.

The preconditioning has large effects at **80°C** only on the samples of laboratory D because the measurements were conducted in winter with a very low humidity in the laboratory. Especially the value of the second maximum of the 80°C measurement differs between conditioned and unconditioned samples. In all other cases the effects of preconditioning were negligible and differ in both directions (higher and lower values can be found) from the values of unconditioned samples.

Whereas the first maximum is quite dependent of the experimental procedure in the beginning the following points of the 80°C curves are quite indifferent towards it. So there are big standard deviations of heat flow and time of the first maximum. The best agreement was the time and the value of the second maximum. This is the period where the DPA is nearly totally consumed.

The second maximum indicates the maximum of N-NO-DPA content and the reduction of DPA to a very low value. DPA reaches nearly zero after 8 days at 80°C. Comparing the measurements of conditioned and unconditioned samples there is no big difference between the two (neither in value nor in time; and the standard deviation is quite comparable) except for the measurements in laboratory D as mentioned earlier. It is probably not useful to discuss in detail small differences in HFC value. What can be seen is that the standard deviation of HFC values is somewhat smaller using nonconditioned samples compared with the preconditioned ones.

Table 5. Details of 80°C measurements. (Average = average of all measurements of precond. samples). Abbreviations see table 1.

Sample N°	ampoule	V	precondition.	P/1. max.	t/1. max.	Knick	t/Knick
		[ml]		[µW/g]	[h]	[µW/g]	[d]
E23	Glass	3	65%rH/>1mo	77,6	0,50	24,2	1,08
A01	INOX	5	65%r.H./3 d	73,4	3,18	23,6	1,23
B12	Glass	3	65%r.H./3 d	62,2	3,10	22,3	1,05
C41	Glass	3	no	66,0	3,22	22,9	0,96
D42	Glass	3	no	62,4	0	22,0	1,46
G47	Glass	3	no	63,8	2,2	22,6	0,99
F26	Glass	20	0%r.H.	59,0	5,02	19,7	1,34
Average				**72,8**	**1,72**	**22,6**	**1,10**

Table 5 (contd.)

Sample N°	P/1. min.	t/1. min.	P/inters	t/inters	P/2. max.	t/2. Max.	P/end	t/end	Qg
	[µW/g]	[d]	[µW/g]	[d]	[µW/g]	[d]	[µW/d]	[d]	[J/g]
E23	21,9	1,67	80,1	3,35	87,8	3,88	77,1	8,01	43,1
A01	22,5	1,67	86,1	3,45	-	-	87,2	8,00	44,3
B12	20,4	1,73	77,6	3,56	85,0	4,10	72,6	7,76	39,5
C41	20,4	1,79	78,4	3,56	87,9	4,36	80,8	7,89	40,8
D42	20,6	1,83	60,6	3,17	67,2	3,83	54,3	6,33	41,1
G47	20,6	1,64	77,3	3,35	84,5	3,92	73,8	8,00	40,8
F26	18,4	1,91	60,2	3,70	66,9	4,18	46,6	8,00	30,0
Average	**20,9**	**1,69**	**81,5**	**3,46**	**88,4**	**4,03**	**79,1**	**8,00**	**43,5**

Interestingly there is nearly no difference between measurements in glass or in steel (Inox) ampoules if the other parameters like closing, degree of filling and preconditioning are comparable, see figure 5.

The difference between preconditioning and no preconditioning is not much bigger at **60°C**. This is in opposite to our first report made for the ICT conference [7]. The standard deviation decreased with the increasing number of samples and a re-measurement of laboratory A (their first three measurements were taken out as stragglers). So after 6 days for example the average value differs between 6,8 µW/g (precond. samples) and 6,9 µW/g (non cond. samples). To show the slow decrease we put the values at the end of the measurement and at one day before the end in two columns. The reduction of the value is about 50-80 nW in the last 24 hours so it can be regarded as being constant enough for an Arrhenius evaluation.

Table 6. Detailed values at 60°C.

exp. N°	V	ampoule	precond.	meas. program	P/2d	P/4d	P/6d	P(end-1d)	P/end	meas. time	Qg
	[ml]		[%r.H]		[µW/g]	[µW/g]	[µW/g]	[µW/g]	[µW/g]	[d]	[J/g]
A046	5	INOX	65	80 → 60	8,70	7,69	7,08	6,42	6,30	10,96	7,39
B116	3	GLASS	65	80 → 60	8,48	7,37	6,87	6,12	6,04	12,21	7,75
D166	3	GLASS	69	80 → 60	7,43	7,10	7,00	6,99	7,02	6,50	4,25
D1661	3	GLASS	69	80,60,50, 40 → 60	5,71	5,47	-	5,79	5,47	4,00	1,81
B366	3	GLASS	no	80 → 60	9,04	8,10	7,58	6,95	6,85	11,10	7,74
C4076	3	GLASS	no	80 → 70 → 60	7,56	7,21	7,21	7,21	7,31	7,02	4,46
F266	20	GLASS	0	80 → 60	4,75	4,23	3,93	3,93	3,81	7,13	2,72
average [a)]		-	-	-	**8,14**	**7,26**	**6,84**	**6,54**	-	-	-

a) average of all preconditioned samples. precond. = %rH of preconditioning; meas. program = temperature program; P/2d = heat flow after 2 days; P(end-1d) = heat flow one day before the end of the measurement; P/end = heat flow at the end. See also table 1.

Interestingly laboratory D had measured the sample again at 60°C after the whole temperature program (table 6, entry D1661). The HFC value has dropped down to about 4 µW/g, reaching a constant level quite fast. Even the sample C4076 (no preconditioning) that had been measured at 70°C prior to 60°C shows a lower heat flow value than the others. The time to reach a constant niveau is also much faster. The (possible) reason for this is explained later on. The dried sample (lab. F) shows severe differences in HFC value compared to the other samples.

The first three experiments done by laboratory A were also taken out as stragglers. So the difference between conditioned and non-conditioned samples also went down at **50°C** (tables 3 and 7). The average was 1,80 µW/g (precond.) and 1,70 µW/g (non cond.) after 6 days. At the end the signal was constant enough for evaluation (decrease of 10-40 nW in the last 24 hours).

If the sample comes directly from 80°C to 50°C the HFC value is much higher (see entry C3955) and the time to reach a constant level is much longer whereas if 70°C had also been measured this time is much shorter. This shows that an exact temperature program must be kept to obtain comparable results and that there is no time gain when measurements for a complete Arrhenius plot are done with only two temperatures!

Table 7. Detailed values at 50°C. Abbreviations see table 1.

exp. N°	V	ampoule	precond.	meas. program	P/2d	P/4d	P/6d	P (end - 1d)	P/end	meas. time	Qg
	[ml]		[% r.H.]		[µW/g]	[µW/g]	[µW/g]	[µW/g]	[µW/g]	[d]	[J/g]
B115	3	GLASS	65	80,60,50	2,07	1,90	1,78	1,71	1,70	8,07	1,26
F275	4	GLASS	65	80,60,50	2,15	2,01	1,91	1,87	1,84	8,05	1,38
E215	3	GLASS	65	80,60,50	1,89	1,75	1,76	1,66	1,64	8,07	1,43
A315	5	INOX	no	80,60,50	1,94	1,77	1,65	1,63	1,61	8,00	1,31
C3955	3	GLASS	no	80,50	3,50	2,90	2,58	1,76	1,72	**22,68**	4,69
C4075	3	GLASS	no	80,70,60, 50	2,03	2,00	1,98	1,98	2,01	6,86	1,09
F445	20	GLASS	no	80,60,50	2,23	2,06	1,97	1,94	1,91	8,05	1,32
average [a)]					**2,58**	**2,42**	**2,30**	**1,75**	**1,74**	-	**1,26**

a) of non-cond. samples

The average of the preconditioned samples (0,58 vs. 0,57 µW/g after 6 days) at **40°C** (see table 4) is the same than that of the non-conditioned ones. Nearly all measurements are corrected with the Switch. The baseline is never at zero but differs about 50 to 80 nW in both directions. This is in the range of the value of the detection limit which we know from calibration experiments we conducted in the last months [2]. They show that the „correct" values can be slightly different from the observed ones. If the data evaluation is done by Arrhenius plot these small differences can cause a change in slope and though in activation energy and preexponential factor, especially at lower temperatures.
At the end the signal was constant enough for evaluation (decrease of 10-60 nW per day).

Statistical evaluation of data

By calculating the performance index using formula (3) the quality of the obtained data can be checked. As the 80°C measurement does not deliver a single value (like in HPLC tests) but a complex curve we took out the intersection point (see explanations to table 1) and looked at the value and at the time of it. The results are divided into conditioned and unconditioned samples.

$$PI = \sum_{i=1}^{N}\left[\frac{c_i}{c_i^*} - 1\right]^2 * \frac{10.000}{N} \qquad (3)$$

c_i = average of laboratory; c_i^* = average of all laboratories; N = number of samples (= 1); s_i = standard deviation of all samples

Because there is no „true value" for the HFC measurement we took the average of all measurements (but preconditioned and non-conditioned separately) as c_i^*. The $|z|$ score is calculated with formula (4); the average value of the unconditioned samples does not contain the µW values of laboratory D, because they are much lower due to low humidity of the propellant (see above). A performance index < 100 and a $|z|$ score < 2 can be regarded as satisfactory. In fact for both value and time of the intersection point all laboratories reach this goal.

$$|z| = \frac{\left(c_i - c_i^*\right)}{s_i} \qquad (4)$$

Table 8. Performance index and |z| scores for the intersection value and time at 80°C

	cond. samples				uncond. samples			
Lab.	PI value	PI time	|z| score value	|z| score time	PI value	PI time	|z| score value	|z| score time
A	2,50	0,00	0,72	0,03	1,82	26,80	-1,26	-1,54
B	1,43	2,89	-0,58	0,66	0,77	2,70	0,95	0,56
C	75,78	22,98	-2,13	1,25	0,19	6,89	0,46	0,90
D	11,72	1,79	-0,84	-0,35	*238,56*[a)]	21,39	*-11,79*[a)]	-1,12
E	0,67	2,44	0,40	-0,82	-	-	-	-
F	3,11	26,93	-0,31	0,96	0,42	1,51	-0,50	-0,30
G	-	-	-	-	0,34	1,77	-0,44	-0,32
H	-	-	-	-	4,23	15,79	1,41	1,08

PI = performance index; a) = value not in average

Additionally other statistical parameters were calculated for the 80°C measurements, such as the repeatability standard deviation, the repeatability standard deviation within one laboratory, the repeatability limit, the reproducibility limit, and the limits within a 95% probability . All these data are collected in the final report [10]. In addition the standard deviation was re-calculated by excluding the stragglers (both stragglers of type 1 (= one out of several measurements in one laboratory which differs markedly) and type 2 (= all values of one laboratory are markedly different from all other laboratories)). Which experiments were excluded is indicated in tables A12 and A13 in the final report [10]. All statistical parameters were calculated from formulas presented in the literature [5].

From all these calculations derives that the differences within each laboratory were quite small – and what is more important – between all laboratories only small differences could be observed which makes the Round Robin Test a success, because shows a satisfying reproducibility.

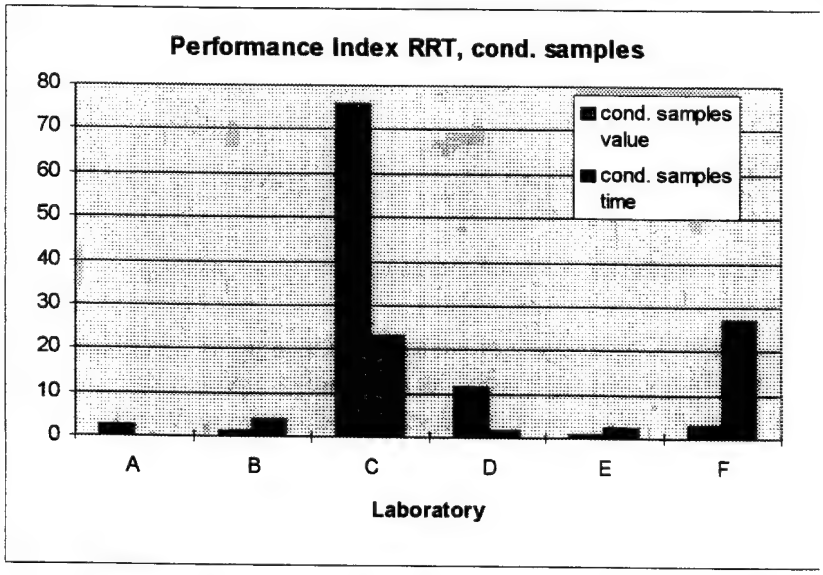

Fig. 6. Performance Index of heat flow at the intersection point – precond. samples

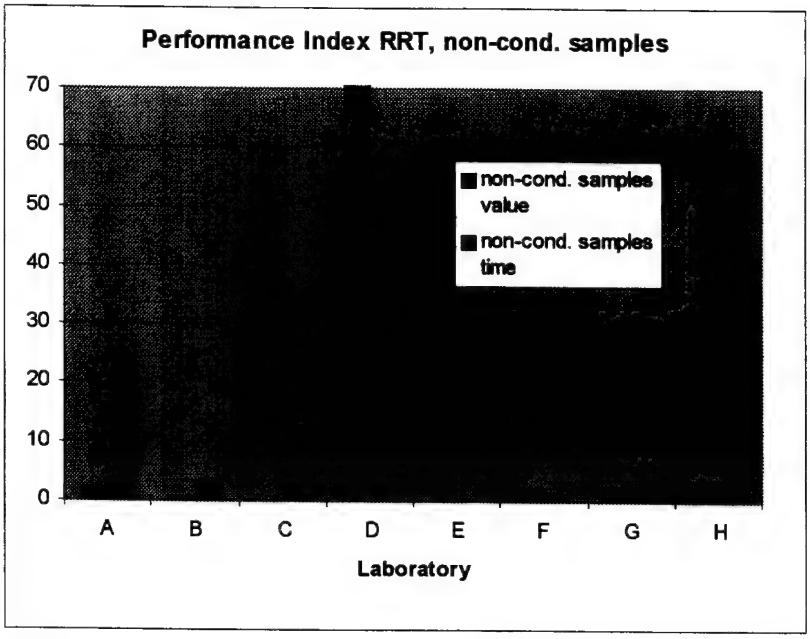

Fig. 7. Performance Index of heat flow at the intersection point – non cond. samples

The higher performance index and $|z|$ score of time of the intersection value of the unconditioned samples is due to some differences between early (labs A, D) and late (labs B, C) second maximum, which is also visible in the relatively high standard deviation.

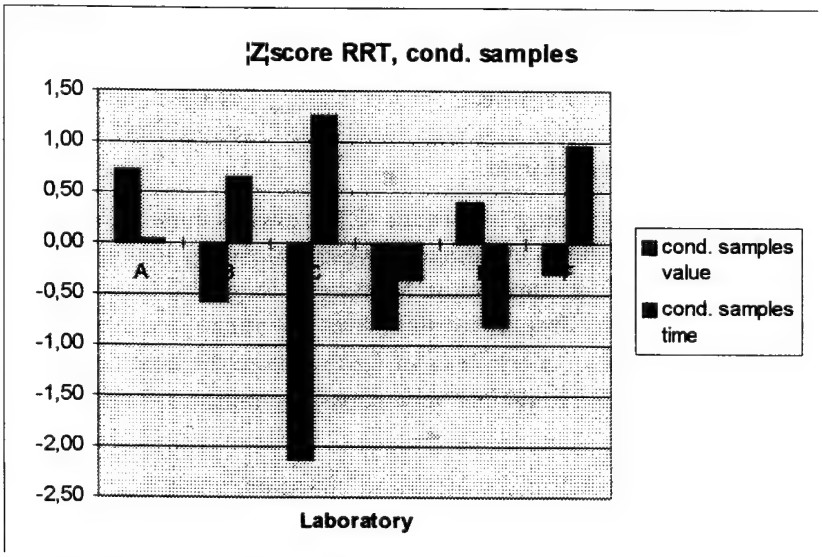

Fig. 8. $|z|$ score of intersection point – precond. samples. Except of one (lab. C) all laboratories fit the limit of $-2 < |z| < 2$, which is also true for the heat flow at the intersection point.

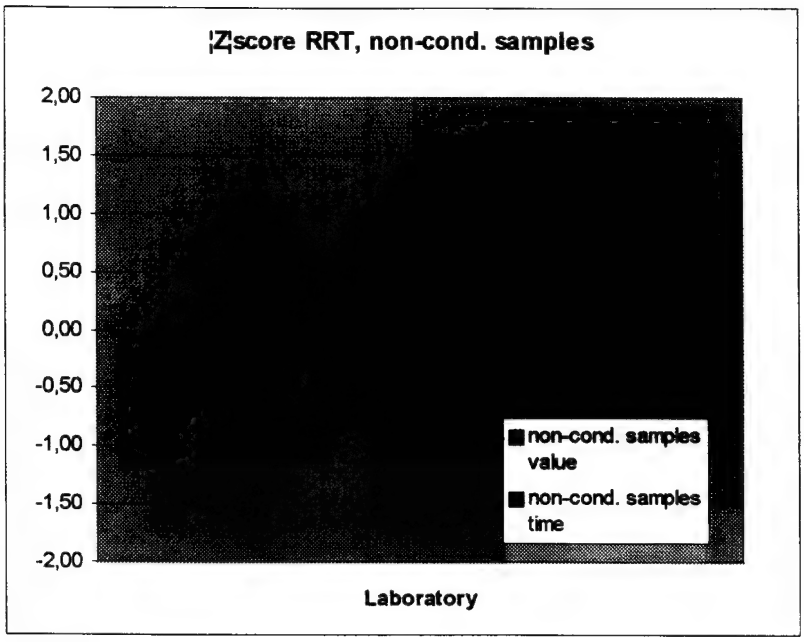

Fig. 9. $|z|$ score of intersection point – non cond. samples. Except of one (lab. D, not shown) all laboratories fit the limit of $-2 < |z| < 2$, which is also true for the heat flow at the intersection point.

Evaluation of the kinetics of the decomposition

There are two possibilities of evaluation for this purpose. One is the calculation of service life analogously to the formula presented at the TTCP workshop [1]. The first step is to establish an Arrhenius plot (formula 1). The determination of the correlation coefficient from all measurements is useful to get a feeling for the quality of the data [3]. As in nearly all cases a change in slope at about 60°C occurs two Arrhenius plots (the first with the 80/60°C values; the second with the 60/50/40°C values) have to be established.

The calculation of the time of 3% energy loss according to formula (2) as always done by WIWEB is not useful any more because there is no direct evidence between 3% energy loss and a significant and limiting loss of v_0 at this stage of decomposition. Moreover, long time experiments show that the decomposition rate does not remain constant over this range of energy loss ($\approx$ 120 kJ/mole) [3]. So we took the time of an energy loss of 1,5%, where the heat flow is $\pm$ constant and where is evidence for an acceptable ballistical behaviour [unpublished results from WTD 91, Meppen, Germany].

The calculation of the kinetic parameters had been done by MathCad® program using every single value (for table 9) resp. average values of each laboratory of the end of the measurements (table 10). In the following table it can be seen that there are only small differences in activation energy and pre-exponential factor between conditioned and unconditioned samples. It is also of importance that the time of the low-temperature values differs from laboratory to laboratory.

[3] As a general rule it can be said that if KK > 0.999 all values can be described by the same straight line. If KK < 0.999 then a change in slope must be assumed which means there is no constant activation energy in the whole temperature range.

If the values 80, 60 and 50°C are taken together for the calculation of the high temperature activation energy, the activation energy changes a little bit (see an example in table 10). In the case of non conditioned samples the correlation coefficient is even a little bit better if the 50°C measurement is integrated into the higher temperature area.

The grey marked values are not taken for the average calculation.

Table 9. Calculation of kinetic parameters from different laboratories

	Ea 80-60	lg pF 80-60	Ea 60-40	lg pF 60-40	KK 80-60	KK 60-40
sample precond.						
Lab.	[kJ/mole]	[W/kg]	[kJ/mole]	[W/kg]	-	-
A [a)]	124	17,2	117	16,1	0,99989	0,9999
B	129	17,3	101	13,6	0,99978	0,9910
D	122	17,0	102	13,7	0,99894	0,9924
E	126	17,5	104	14,0	0,99770	0,9937
F	121 [b)]	16,7	110	15,1	0,99957	0,9999
sample non cond.						
A	124	17,3	101	13,6	0,99968	0,9966
B	121	16,9	98	13,1	0,99997	0,9967
C [c)]	124	17,2	124	17,1	0,99999	0,9988
D	117	16,1	93	12,1	0,99989	0,9962
F	120	16,6	114	15,7	0,99988	0,9987
sample dried						
F	132	18,2	120	16,2	0,99964	0,9987

Ea = activation energy, pF = pre-exponential factor, KK = correlation coefficient

a) only samples A04X-A07X are taken, b) high-temperature values incl. 50°C, c) incl. 70°C values

There is a small change in slope of the Arrhenius plot at about 50-60°C. This can be found with any gun propellant as far as we know. The „detection limit" of the activation energy is about 3 kJ/mole [2] which means that these effects are real.

The second method for evaluation of stability is to measure the time of the 2nd minimum or a comparable point in the curve (e.g. the time until 60 J/g ≙ 1.5% of the heat of explosion) is reached and extrapolate it with the activation energy on storage temperatures of e.g. 30°C. As we know that the shape of the curve of fresh samples is very comparable also at 70, 60, and 50°C [1] the time of the 2nd minimum is an „iso-α-point" and therefore the calculation method is reliable. The problem of this method is the very long measuring time of fresh samples at 60°C or 50°C [9].

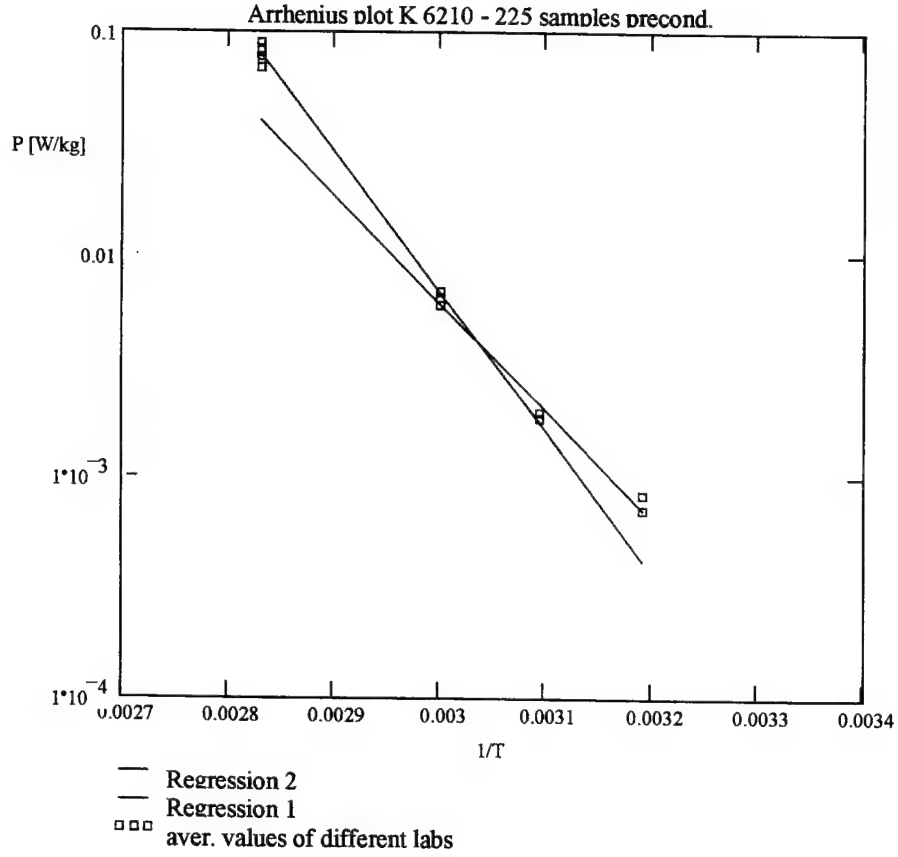

Fig. 10. Arrhenius plot (all laboratories; conditioned samples)

Table 10. Activation energy and preexp. factor from all measurements

	sample precond.			sample non cond.		
temp. range	activation energy	preexp. factor	corr. coeff.	activation energy	preexp. factor	corr. coeff.
[°C]	[kJ/mole]	[W/kg]		[kJ/mole]	[W/kg]	
60-40	108	14,8	0,9960	108	14,7	0,9911
80-60	124	17,2	0,9996	120	16,6	0,9989
80-50	121	16,8	0,9995	120	16,7	0,9991
t_{50}	1,05			1,01		
t_{40}	3,81			3,63		
t_{30}	15,0			14,2		

t50, t40, t30 = times to reach an energy loss of 61 J/g (1,5%), given in years.

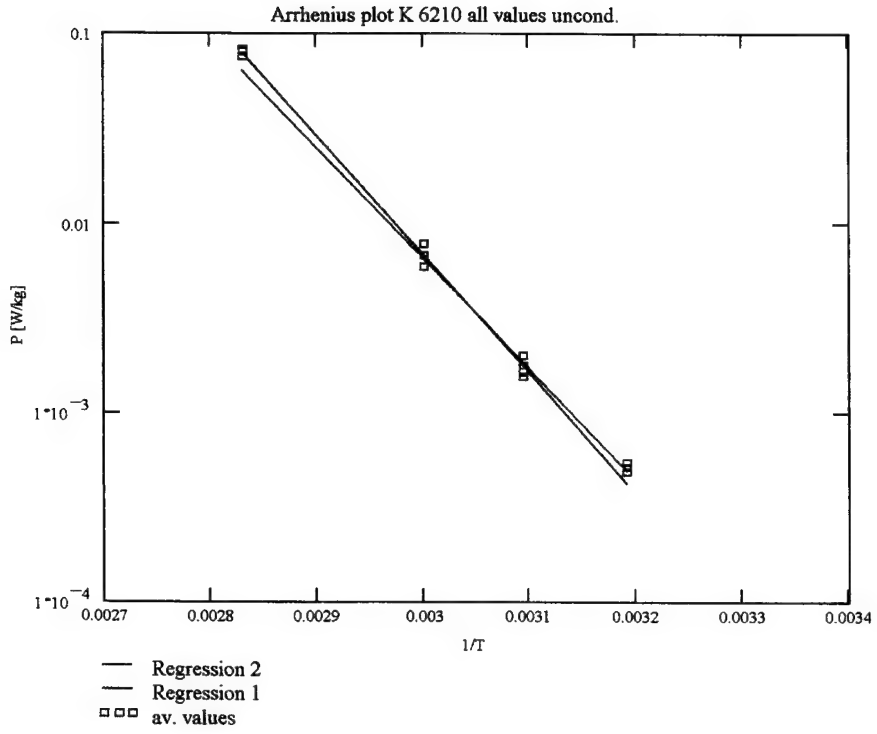

Fig. 11. Arrhenius plot (all laboratories; unconditioned samples)

Chemical analysis after measurement

To be sure of the correctness of closing of the ampoules the samples were analysed after the HFC measurements by HPLC and/or GPC to look at the changes of the stabiliser content and its reaction products and at the molecular mass decay under the measured conditions.

Especially the correlation between energy loss and stabiliser depletion is looked at. There is no big difference in α (reaction degree) of the samples B - E2, thus only small differences in chemical composition are observed.

Tables 11/12 show the stabiliser content of the K 6210 propellant (samples preconditioned) after different stages of HFC measurement.

Table 13 shows the stabiliser content of the K 6210 propellant (samples non conditioned) after different stages of HFC measurement.

The results of the HPLC analyses of the samples aged in a leaky ampoule and in an ampoule with low loading density are collected in [9].

Table 11. Results of preconditioned samples (labs. A and D)

Sample N°	before	A06	A046	A055	A074	A014-034	D1646
Ampoule used	-	glass cell 3 ml	inox cell 5 ml	inox cell 5 ml	glass cell 20 ml	samples mixed	glass cell 3 ml
Energy loss during HFC experiments [J/g]	0	44	50	53	49	56	60
Water content (KF method)	0,60	nm	nm	nm	0,62	0,77-0,85	0,4
Stabiliser (%)							
DPA	0,49	< 0,01	< 0,01	nd	nd	< 0,01	0,04
NNO-DPA	0,46	0,71	0,69	0,55	0,56	0,55	0,685
2-NDPA	0,02	0,01	0,01	< 0,01	< 0,01	< 0,01	nm
4-NDPA	0,02	< 0,01	< 0,01	nd	nd	0,01	nm
NNO-2NDPA	nd	0,06	0,07	0,05	0,05	0,06	nm
NNO-4NDPA	nd	0,13	0,14	0,10	0,09	0,18	nm
4,4'-DNDPA	nd	0,01	0,01	0,01	0,01	0,04	nm
2,2'-DNDPA	nd	0,02	0,02	0,02	0,01	0,05	nm
2,4'-DNDPA	nd	0,02	0,02	0,01	0,01	0,07	nm
Nitroglyerin	19,2	nm	nm	nm	19,2	19,05	18±1
heat of explosion [J/g]	4072	nm	nm	nm	4021	3962	nm
GPC: NC M_w	276.000	nm	nm	156.000	153.000	153.000	nm

nd = not detected; nm = not measured

Ageing:

A06 After heating at 80°C in the calorimeter

A046 After heating at 80°C and 60°C in the calorimeter

A055 After heating at 80°C, 60°C and 50°C in the calorimeter

A074, A014-034 After heating at 80°C, 60°C, 50°C and 40°C in the calorimeter

D1646 After heating at 80°C, 60°C, 50°C, 40°C and 60°C in the calorimeter

There is strong evidence that the stabiliser DPA is converted to N-NO-DPA until the second maximum is reached. At this point N-NO-DPA shows its highest concentration and decreases slowly afterwards. The appearance of N-NO-2-NDPA and N-NO-4-NDPA reveals that there is a slow nitration of N-NO-DPA occuring when no more DPA is present. Interestingly the original content of 2-NDPA and of 4-NDPA is also decreasing just in the moment of the DPA disappearance. This is in good correlation with the observations of some Russian scientists [6] and with the relative ratios of reactivity according to Bohn [8]. We suspect that both mono-nitro-DPAs are nitrosated on the nitrogen atom and are thus not very stable under the conditions in the ampoule. The appearance of dinitro-DPA in closed ampoules is only seen at the end of the storage time.

Table 12. HPLC results of preconditioned samples from laboratory E after HFC

Sample N°	original	E20	E22	E246	E256	E215	E234
Ampoule used	-	glass cell 3 ml					
Energy loss during HFC experiments [J/g]	0	45	46	56	51	50	52
Stabiliser (%)							
DPA	0,53	0,13	0,11	0,11	0,11	0,14	0,12
NNO-DPA	0,40	0,67	0,70	0,68	0,67	0,63	0,67
2-NDPA	0,03	nd	nd	< 0,01	< 0,01	nd	< 0,01
4-NDPA	< 0,01	< 0,01	< 0,01	< 0,01	< 0,01	< 0,01	< 0,01
NNO-2NDPA	nd	0,06	0,06	0,06	0,06	0,06	0,06
NNO-4NDPA	nd	nd	nd	nd	nd	nd	nd
4,4'-DNDPA	nd	nd	nd	nd	nd	nd	nd
2,2'-DNDPA	nd	0,01	0,02	0,02	0,01	0,01	0,01
2,4'-DNDPA	nd	0,01	0,01	0,03	0,02	nm	0,01
Nitroglyerin	19,52	19,0	19,22	18,34	18,32	19,60	19,31
weight loss [%]	-	0,13	0,28	0,23	0,11	0,12	0,12

nd = not detected; nm = not measured

Ageing:

original	Before measurement
E20, E22	After heating at 80°C in the calorimeter
E246, E256	After heating at 80°C and at 60°C in the calorimeter
E215	After heating at 80°C, 60°C, and at 50°C in the calorimeter
E234	After heating at 80°C, 60°C, 50°C, and at 40°C in the calorimeter

Table 13. HPLC results of unconditioned samples (laboratories A and D) after HFC

Sample N°	before	A314-A334	D4246-D4346
Ampoule used	-	samples mixed	glass cell 3 ml
Energy loss during HFC experiments [J/g]	0	43	41
Water content (KF method)	0,44	0,50	
Stabiliser (%)			
DPA	0,49	<0,01	0,04
NNO-DPA	0,46	0,71	0,65
2-NDPA	0,02	0,02	nm
4-NDPA	0,02	<0,01	nm
NNO-2NDPA	nd	0,06	nm
NNO-4NDPA	nd	0,13	nm
4,4'-DNDPA	nd	0,01	nm
2,2'-DNDPA	nd	0,02	nm
2,4'-DNDPA	nd	0,03	nm
Nitroglyerin	19,2	19,1	18±1
heat of explosion [J/g]	4042	4008	nm
GPC: NC M_w	269.000	154.000	nm

Explanations to table 13:

nd = not detected; nm = not measured

A0314-0334	After heating at 80°C, 60°C, 50°C and 40°C in the calorimeter (sample unconditioned)
D4246	After heating at 80°C, 60°C, 50°C, 40°C and 60°C in the calorimeter (sample unconditioned)

Conclusion

The results show a very good comparability and reproducibility leading to the conclusion that the Round Robin Test was a success. Thus a STANAG method „HFC of DB ball propellants" should be established using the HFC method described in this paper.

Very surprising was the fact that the standard deviation of all measurements at 80°C was – besides the initial effects – very low and that even the preconditioning of the propellant is not really necessary. This is not true if the measurement is prepared and conducted in a cold winter (then the humidity of the propellant is too low). At measuring temperatures below 80°C the preconditioning also has nearly no effect. If the evaluation of data is done by Arrhenius equation the preconditioned samples show the same activation energy and preexponential factor.

What is as well surprising is that a measurement at e.g. 60°C after the whole temperature program shows different results than the first 60°C measurement because between both measurements there are only some J/g energy difference in the propellant. That means that both measurements are done nearly at the same stage of decomposition (iso-α). One explanation for this might be that the thermal decomposition is superimposed by long lasting endothermic evaporation and exothermic condensation or diffusion processes probably of moisture and/or nitroglycerin. If the equilibrium is not completely established deviations of the signal in both directions may occur depending on the conditions of the experiment (e.g. duration of the experiment, the measuring temperature before, the treatment and the time between two measurements). A hint in this direction has been obtained by HFC testing of single base propellants [4] where an equilibrium is reached within 1-2 days, which is faster than here.

The stabiliser consumption measured after HFC measurements shows that the closing of the ampoules was good enough (mainly N-NO-DPA), because if the ampoule is not closed correctly then dinitro- and trinitro-DPAs are dominating.

Acknowledgements. The authors want to thank all participants for their engagement and time they spent into this project. I also want to thank Dr J Bellerby for fruitful dicussions about the stabiliser depletion chemistry in open and closed ampoules.

References

[1] P. Guillaume, A. Fantin, M. Rat, S. Wilker, G. Pantel, „Stability Studies of Spherical Propellants", *ICT-Jahrestagung* **27**, 16-1 - 16-14 (1996); M. Rat, P. Guillaume, S. Wilker, G. Pantel, „Practical Application of the HFC for the determination of the Stability of Propellants", *Proc. 1. TTCP Workshop Leeds* 4/**1997**; P. Guillaume, M. Rat, S. Wilker, G. Pantel, „Microcalorimetric and Chemical Studies of Propellants", *ICT Jahrestagung* **28** (1998).

[2] S. Wilker, U. Ticmanis, G. Pantel, P. Guillaume, „Detailed investigation of sensitivity and reproducibility of HFC measurements", *11. Symp.Chem.Probl.Conn. Stabil. Explos.*, Båstad **1998**.

[3] D.S. Ellison, A. Chin, „Common Factors that May Affect the Accuracy of Microcalorimetric Data" *Proc. TTCP Workshop Leeds* 4/**1997**; A. Chin, D.S. Ellison, „20 mm Gun Propellant Safety Service Life Study Using Microcalorimetry/HPLC Correlation Diagrams", *Proc. TTCP Workshop Leeds* 4/**1997**.

[4] U. Ticmanis, G. Pantel, L. Stottmeister, „Stabilitätsuntersuchungen einbasiger Treibladungspulver – Mikrokalorimetrie im Grenzbereich", *ICT Jahrestagung* **28** (1998).

[5] L. Dinkloh et al., „Ringversuche in der Wasseranalytik – II. Auswertung", *Z.Wasser Abwasser Forschung* 13, 174-187 (**1980**); DIN-ISO-Norm 5725, „Precision of test methods – Determination of repeatibility and reproducibility for a Standard Test Method by inter-laboratory tests", edition 1986; L. Dinkloh et al., „Ringversuche in der Wasseranalytik – III. Beispiel einer Ringversuchsauswertung und Vergleich mit dem DIN-ISO-Entwurf 5725", *Z.Wasser Abwasser Forschung* 13, 174-187 (**1980**).

[6] LS Lussier, H Gagnon, „The Canadian Gun Propellant Surveillance Program", *Proc. AGARD Conf.* **87**, 18-1 - 18-13 (1996); Svetlov, BS, Shelaputina, VP, Maksimova, LD, Jevtushenkov, VP, „Reaction of Nitroglycerin with Diphenylamine" (Original in russian), *Moskovskii chim.-technol. Inst. im. Mendeleeva,* **83**, 35-40 (1974).

[7] S. Wilker, P. Guillaume, „International Round Robin Test to Determine the Stability of DB Ball Propellants by Heat Flow Calorimetry", *ICT Jahrestagung* **29**, 132 (1998).

[8] M.A.Bohn, „Use of Kinetic Equations to Evaluate the Ageing Behaviour of Energetic Materials – Possible problems", *11. Symp.Chem.Probl.Conn. Stabil. Explos.*, Båstad **1998**.

[9] P. Guillaume, M. Rat, G. Pantel, S. Wilker, „Heat Flow Calorimetry of Propellants – Effects of Sample Preparation and Measuring Conditions", *Proc. 2. TTCP Workshop Leeds* (**1999**).

[10] S. Wilker, P. Guillaume, „International Round Robin Test of HFC Measurements with Propellant K 6210-13", Final Report 30 Nov. 1998.

Heat Flow Calorimetry of Propellants – Effects of Sample Preparation and Measuring Conditions [1]

by Pierre Guillaume [#], Mauricette Rat [§], Gabriele Pantel [♣], and Stephan Wilker [♣]

Abstract

Isothermal microcalorimetry measurements were performed on double base ball propellant K 6210. The influence of different sample preparation techniques and measuring conditions are discussed. The most important parameter is the atmosphere above the propellant. If air is replaced by nitrogen a reduction of primary effects can be observed. A replacement by oxygen leads to a complete different decomposition reaction. Comparable effects are achieved when the ampoules are only filled to ¼. In this case also oxidation reactions can be observed. Working in ampoules that are not closed tightly also changes the decomposition reaction. All experiments were also accompanied by stabiliser analyses (HPLC) that as well demonstrate the different decomposition reactions. By changing the temperature but leaving the sample preparation and measurement conditions unchanged heat flow curves that are similar in shape are observed. That means that the decomposition reactions are nearly comparably activated. Reducing the volume to lower the sample amount is not possible by adding glass balls. In this case adsorption/desorption reactions cover the first part of the decomposition reaction. If a glass rod is taken there is no change in the shape of the curve.

1 Introduction

The slow decomposition of nitrocellulose based propellants has been investigated for many years by using different techniques [1]. One of them is the isothermal microcalorimetry [2]. Since very sensitive and precise calorimetres are available it is possible to monitor the small amounts of heat that are evolved by the slow decomposition processes directly [3]. In contrast to most of the other techniques like stabiliser depletion or molecular mass decay microcalorimetry is a summarizing method [4]. It covers all chemical and physical processes that generate heat. The most important safety criteria can be directly derived from the heat flow curve like self-ignition and the kinetics of the decomposition [5].

The aim of this work was to detect the influence of different measuring conditions on the heat flow curve of double base propellants. Different measuring conditions in this concern are variations of the atmosphere, of the loading density/filling grade, of the closing of the ampoule, of the preconditioning of the samples etc. In parallel the stabiliser consumption under different measuring conditions was monitored.

---

[1] Submitted for publication in *Propellants, Explosives, Pyrotechnics*

[#] PB Clermont SA, Rue de Clermont, B-4480 Engis

[§] SNPE, Boîte Postale N°2, F-91710 Vert-le-Petit

♣ WIWEB, Großes Cent, D-53913 Swisttal

2 Experimental

Heat flow measurements were conducted with a "Thermal Activity Monitor" TAM 2277 (Thermometrics AB, Sverige). The measurements were performed in 3 mL glass ampoules. Usually the ampoules are completely filled (sample amount ≈ 2.8 g) and sealed. For the determination of the influence of different measuring conditions we varied the standard method by

- using unsealed ampoules
- filling the ampoule to only 85%, 50%, 25%, 16%
- working under pure oxygen and pure nitrogen
- reducing the volume of the ampoule with glass balls and glass rods
- preconditioning the propellant with different humidities

The propellant taken for this investigation is a double base ball propellant K 6210 with a nitroglycerin content of about 19%. It is stabilised with diphenylamine (DPA).

The stabiliser content was monitored by aging propellant samples in the microcalorimeter under different conditions (details see below) and in completely filled and sealed HFC ampoules in an oven at 80°C. Prior to measurement the propellants were dissolved in 10 mL of acetonitrile, and then 40 mL methanol are added. The nitrocellulose was precipitated by adding 50 mL of water. The solution was filtered through a filter syringe and directly passed into the HPLC autosampler flasks. The stabilisers were detected with a Gynkotek HPLC system consisting of a pump M480S, an automatic sampler Gina 50, a column oven and a diode array detector UVD 320S (λ = 200-356 nm). The detection resulted at 225 nm. The column (Lichrospher 100RP18 - 5µm; 250·4 mm with a pre-column 20·4 mm) was tempered at 25°C. A methanol/water mixture (67/33) was used as mobile phase and pumped with a flow rate of 1.2 mL/min.

The stabiliser depletion products N-NO-2-NO_2-DPA and N-NO-4-NO_2-DPA were synthetised according to literature methods from 2-NO_2-DPA (resp. 4-NO_2-DPA) and $NaNO_2$ [6].

3 Heat flow measurements of double base propellants

We observed the slow decomposition process of double base gun propellants by microcalorimetry [7]. In parallel the stabiliser consumption was investigated. All DPA stabilised propellants show a very typical heat flow curve which is presented in fig. 1. The different stages of the decomposition process are summarised in table 1.

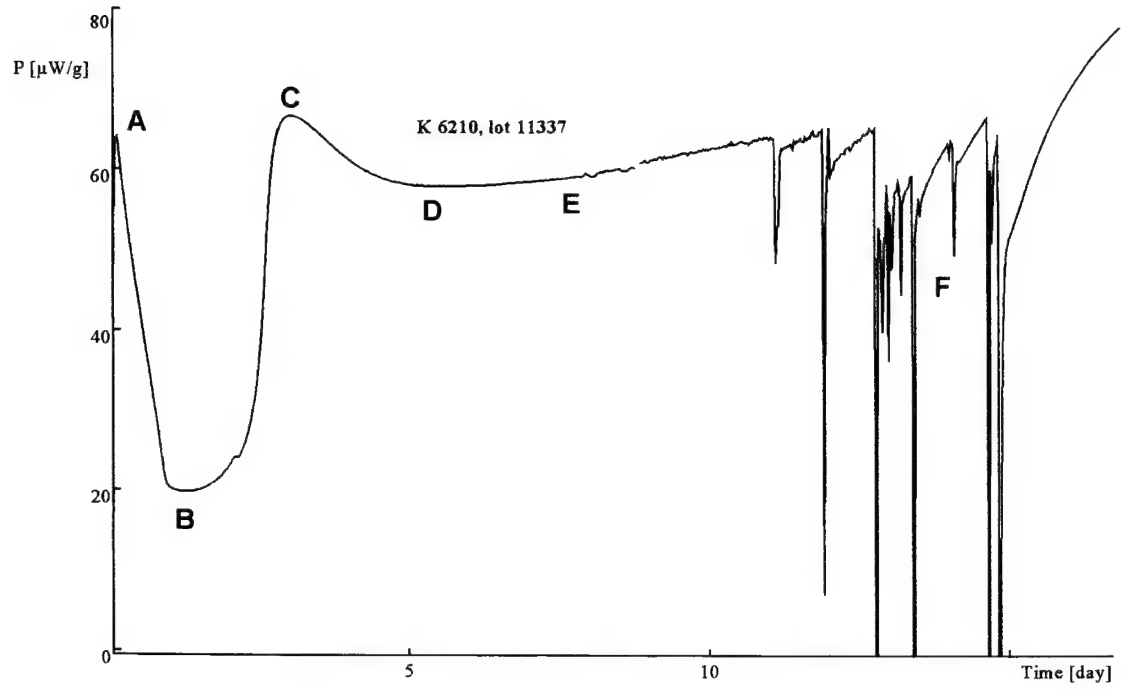

Figure 1. Heat flow measurement of DB ball propellant K 6210, lot 11337, at 80°C

Table 1. Description of the different stages of the decomposition of propellant K 6210

stage	explanation
1. maximum **A**	Primary reaction of the propellant with oxygen. The integral correlates both with the DPA content and the amount of oxygen in the atmosphere.
1. minimum **B**	Constant decomposition of the propellant accompanied by consumption of DPA.
2. maximum **C**	After the consumption of DPA is completed the next stabiliser product (N-NO-DPA) is slowly decreasing. The time of the second maximum and its height depend on the moisture content of the propellant. The higher the moisture content is, the later and higher is the value of the second maximum.
2. minimum **D**	constant N-NO-DPA-decomposition rate ($\rightarrow$ formation of N-NO-NO_2-DPA). The value of the heat flow in this period is usually taken for the determination of the Arrhenius parameters. The sample is taken out of the calorimeter and measured at lower temperatures (60, 50, 40°C; "decreasing temperature program").
beginning autocatalysis **E**	Slow, but long lasting increase of heat flow reaching a maximum after 30-50 days. Increasing pressure in the ampoule is indicated by endothermic peaks (leaking ampoule, **F**).

4 Results and Discussion

4.1 Influence of the closing of the ampoule and the filling grade on the HFC signal

The influence of the closing of the ampoule on the heat flow signal can be seen in fig. 2a-2c where three different closing methods were applied.

It is obvious that all three experiments show a very different behaviour of the propellant under the different measuring conditions. Whereas the "normal" experiment (fig. 2a; closed ampoule, completely filled) shows the typical shape with two maxima and minima and a slight autocatalytic increase after 3 days at 89°C, the second experiment (fig. 2b; leaking ampoule, completely filled) does not show any autocatalytic increase within 16 days at 89°C. The third experiment (fig. 2c; closed ampoule, filled to only ¼) has a completely different pattern with a sharp maximum, followed by a minimum at about one day. The autocatalytic increase begins directly after that minimum. Compared with the other experiments the specific heat production rate is higher.

The chemistry of stabiliser consumption as well as the weight loss was monitored at different stages of decomposition with a non-closed and a completely closed ampoule. The points where the samples are taken out of the calorimeter are indicated by the letters a-e, m-q, and w-z in figures 2a-2c. The following tables 2-4 show the results of the HPLC analyses of the samples pre-aged in the calorimeter under three different conditions (see also [8]).

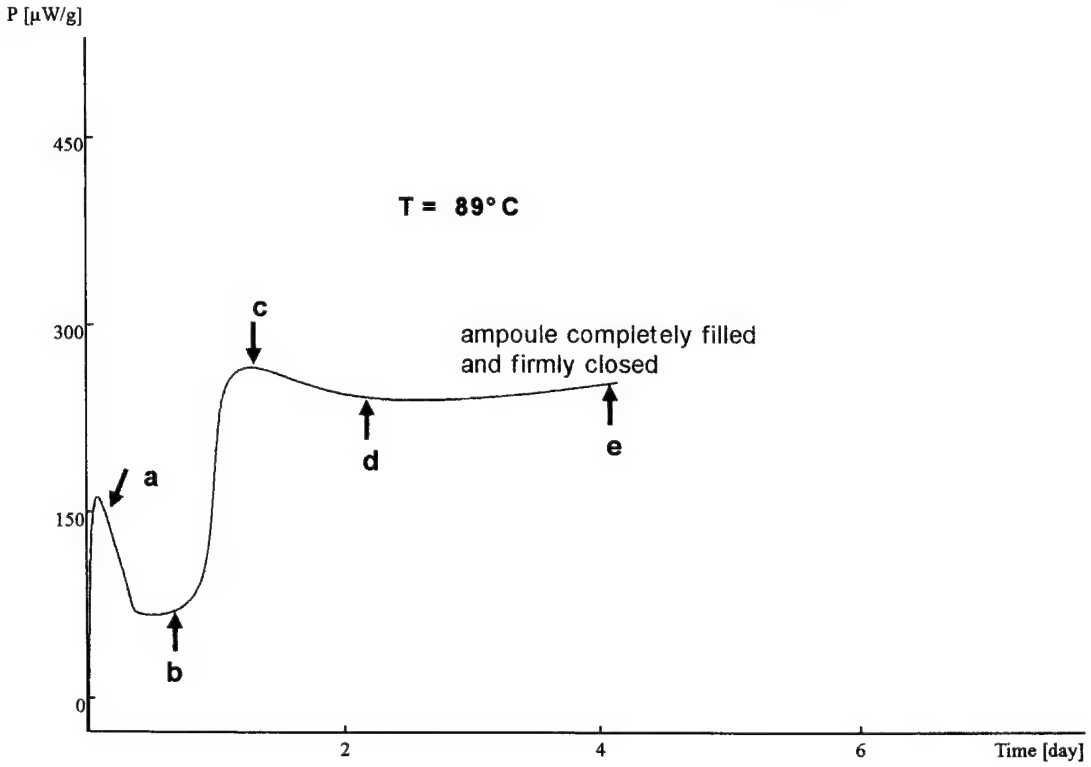

Figure 2a. Heat flow measurement of DB ball propellant K 6210, closed and filled ampoule at 89°C. The letters refer to different points of stabiliser analysis

The first experiment shows that the primary stabiliser DPA is consumed within the first 24 h. This is the time when the HFC curve reaches its second maximum. At the same time N-NO-DPA has its maximum concentration, but it drops down only very slightly after this point. Very surprising is the fact that both 2-NDPA and 4-NDPA are also consumed after the DPA is used up. Probably these two compounds are "better stabilisers" than N-NO-DPA under this conditions. Both N-NO-DPA and the mononitro-DPAs react with the NOx evolved from the propellant to form N-NO-mononitro-DPA. It is not clear whether a direct nitration of N-NO-DPA occurs or whether a rearrangement of N-NO-DPA to the mono-nitro-DPA and their subsequent nitrosation takes place. Anyway, the composition of the stabiliser products differs markedly from that of the second experiment (table 3).

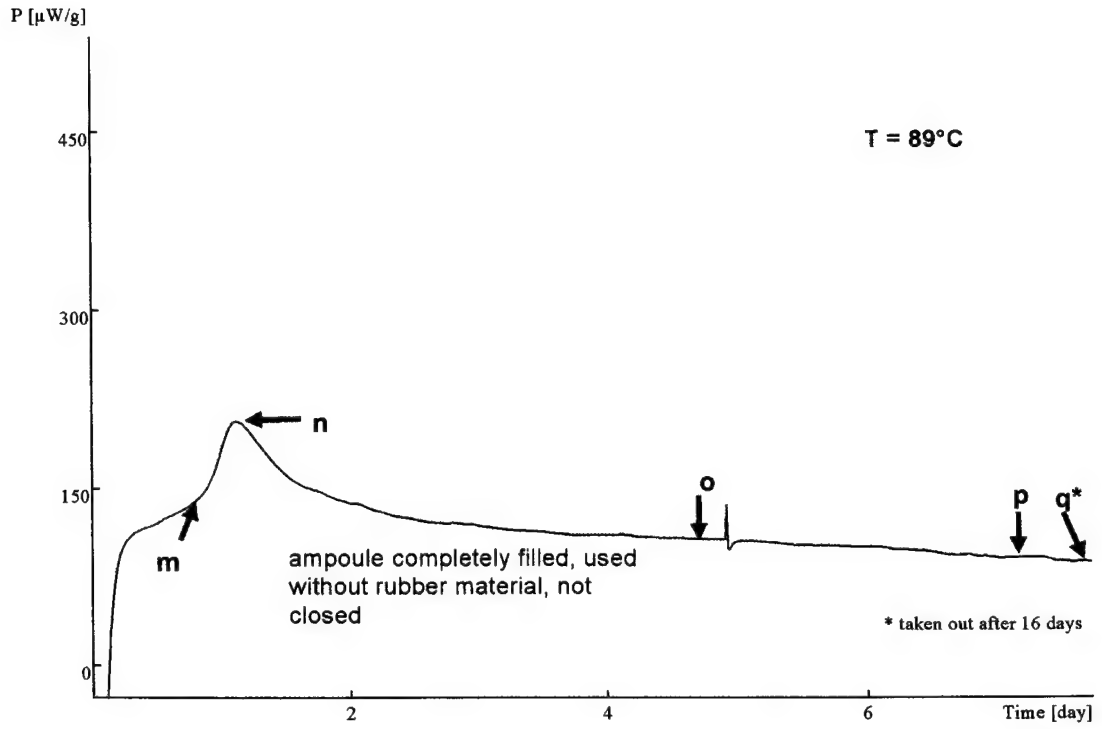

Figure 2b. Heat flow measurement of DB ball propellant K 6210, leaking filled ampoule at 89°C. The letters refer to different points of stabiliser analysis

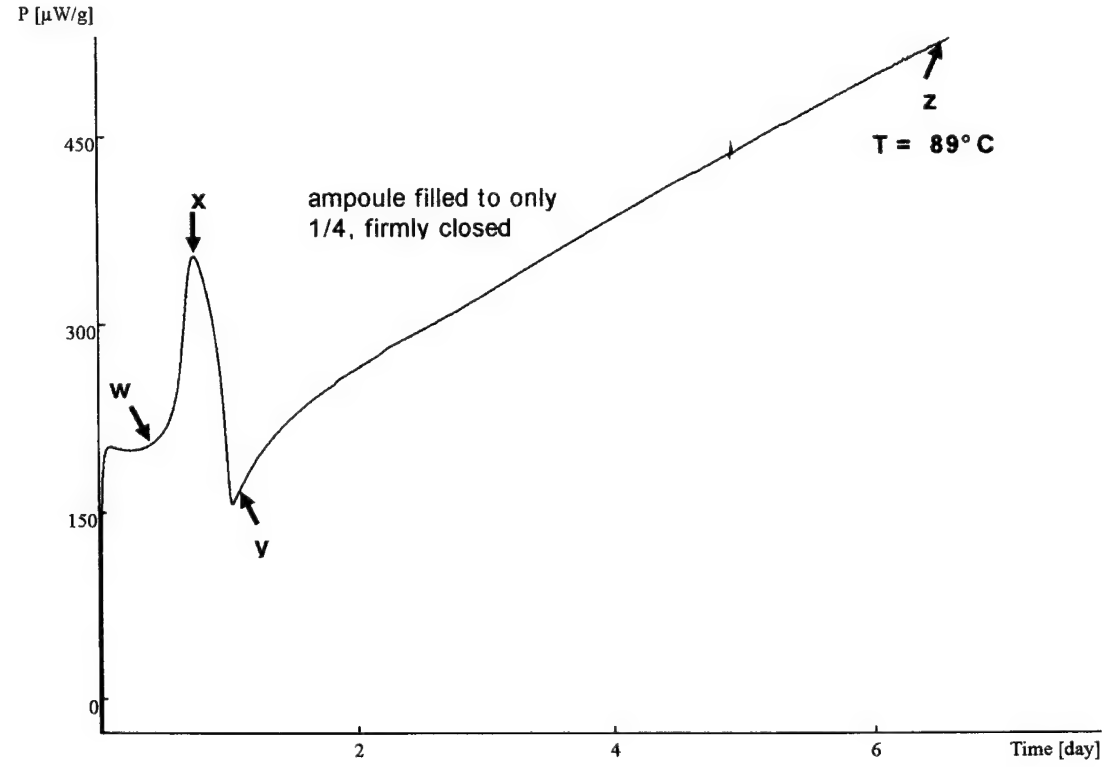

Figure 2c. Heat flow measurement of DB ball propellant K 6210, closed, ¼filled ampoule at 89°C. The letters refer to different points of stabiliser analysis

Table 2. Stabiliser depletion of propellant K 6210 in closed, completely filled HFC ampoules

sample	fresh	a	b	c	d	e
time at 89°C [d]	0	0,09	0,51	1,23	2,08	3,67
energy released [J/g]	0	1,5	4,5	14,5	32	65
Ngl	18,9	n.d.	n.d.	n.d.	19,0	18,5
DPA	0,53	0,37	0,044	0,007	-	-
N-NO-DPA	0,39	0,50	0,81	0,84	0,84	0,60
2-NDPA	0,02	0,02	0,043	0,023	-	-
4-NDPA	0,02	0,02	0,008	0,017	-	-
N-NO-2-NDPA	-	-	0,008	0,055	0,094	- [a)]
N-NO-4-NDPA	-	-	0,006	0,082	0,15	0,325
2,2'-DNDPA	-	-	-	-	-	0,024
2,4'-DNDPA	-	-	-	-	0,011	0,044
tri-NDPAs (sum)	-	-	-	-	-	-
tetra-NDPAs (sum)	-	-	-	-	-	-

a) The decrease of the N-NO-2-NDPA was also observed by other authors [10]. Probably it can rearrange much faster than the other derivative (N-NO-4-NDPA) to the dinitro compound. Also reversible nitrosation-denitrosation reactions must be taken into account.

Table 3. Stabiliser depletion of propellant K 6210 in leaking completely filled HFC ampoules

sample	fresh	m	n	o	p	q
time at 89°C [d]	0	0,83	1,04	1,75	7,0	16,0
energy released [J/g]	0	7	10	22	77	127
weight loss [%]	-	1,78	0,64	0,83	1,55	8,4
Ngl	18,9	19,1	17,9	18,2	15,5	14,2
DPA	0,53	0,006	0,008	-	-	-
N-NO-DPA	0,39	0,444	0,189	0,068	-	-
2-NDPA	0,02	0,087	0,073	0,062	-	-
4-NDPA	0,02	-	-	-	-	-
N-NO-2-NDPA	-	-	-	-	-	-
N-NO-4-NDPA	-	-	-	-	-	-
2,2'-DNDPA	-	0,007	0,028	0,020	0,014	-
2,4'-DNDPA	-	0,105	0,191	0,143	-	-
2,4,4'-TNDPA	-	-	0,009	0,009	0,400	0,170
2,2',4-TNDPA	-	-	-	-	0,119	0,112
2,2',4,4'-tetra-NDPA	-	-	-	-	0,097	0,296

Table 4. Stabiliser depletion of propellant K 6210 in closed, ¼ filled HFC ampoules

sample	fresh	w	x	y	z
time at 89°C [d]	0	0,69	0,88	1,13	8,00
energy released [J/g]	0	12,9	17,7	22,5	253
weight loss [%]	-	0,04	0,09	0,03	0,32
Ngl	18,9	18,9	19,2	19,6	18,2
DPA	0,53	0,007*	0,007*	-	-
N-NO-DPA	0,39	0,457	0,601	0,371	0,256
2-NDPA	0,02	0,070	0,059	0,062	0,006
4-NDPA	0,02	0,110*	0,059	-	-
N-NO-2-NDPA	-	-	-	-	-
N-NO-4-NDPA	-	0,233	0,106	-	-
2,2'-DNDPA	-	0,005	-	0,021	0,054
2,4'-DNDPA	-	0,080	-	0,111	0,160
2,4,4'-TNDPA	-	-	-	-	0,034
2,2',4-TNDPA	-	-	-	-	0,009
tetra-NDPAs (sum)	-	-	-	-	-

* impurities in the chromatogram (overlapping with another compound)

In the "leaking" experiment the DPA disappears roughly as fast as in the experiment in the closed ampoules. As well as in the first experiment N-NO-DPA reaches its maximum at this point. But its concentration is much lower than in the first experiment and it is disappearing very fast within less than 7 days by the formation of mono- and di-nitro-DPA derivatives. They also are used up to give tri- and tetra-nitro-DPAs. No formation of N-NO-mononitro-DPA could be observed. Thus it must be assumed that they are not stable under the conditions in this experiment.

4.2 Influence of the atmosphere on the HFC signal

The influence of the atmosphere above the propellant was investigated by preparing the samples (a) under air, (b) under pure oxygen, and (c) under pure nitrogen. All experiments were performed with completely filled and closed ampoules. The results are presented in fig. 3.

It is obvious that the sample prepared under pure oxygen shows a very different pattern of the HFC curve than the other two experiments. Especially the sharp maximum after about 2 days, followed by a sharp minimum is very typical. Also the endothermic gas evolution peaks that appear quite early have to be noticed. The shape of this curve is somewhat comparable to the HFC curve in fig. 2c (¼ filled ampoule). In both cases there is enough oxygen available to oxidise the NO into NO_2 evolved from the nitrocellulose which then oxidises the nitrocellulose chain and the N-NO-DPA that is formed during the ageing of the propellant.

In the case of the experiment under nitrogen the initial effects nearly disappear. As there is always traces of air inside the propellant grains they might be responsible for the small first maximum. In addition the second maximum (the point when DPA is used up) takes place about one day later. This shows the influence of oxygen (in the air above the grains) on the decomposition velocity.

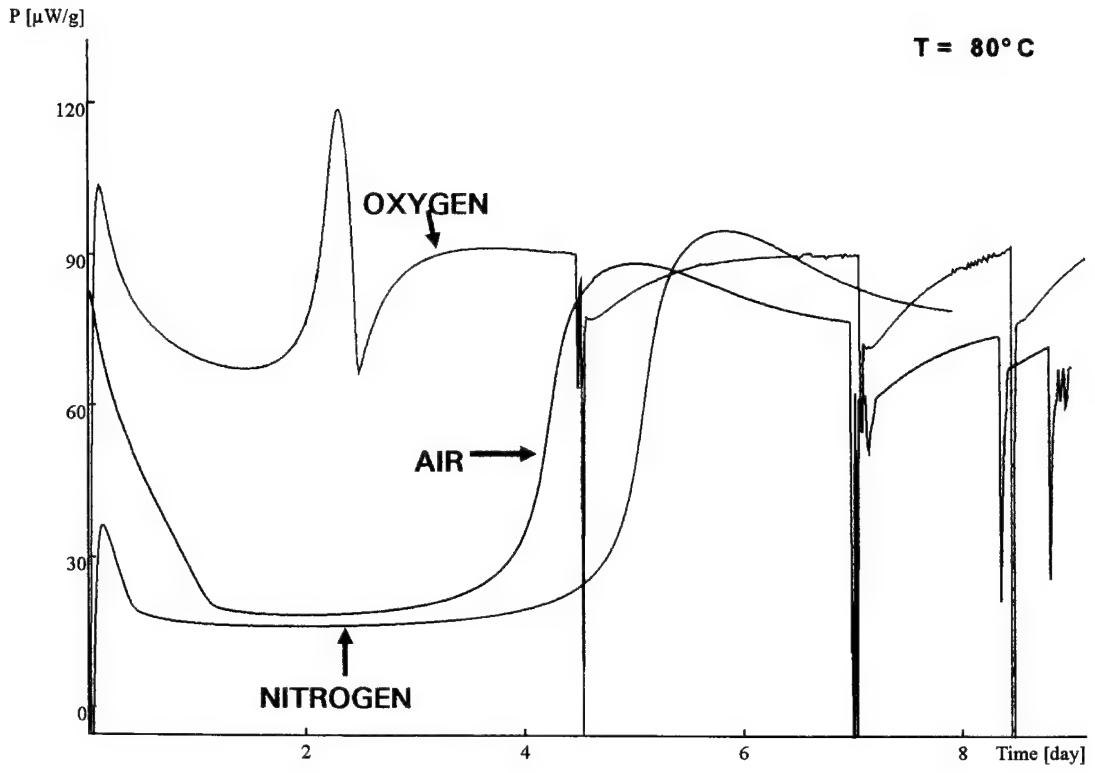

Figure 3. Heat flow measurement of DB ball propellant K 6210, different atmospheres, 80°C (each sample 3.50 g, non-conditioned propellant grains)

4.3 Influence of preconditioning of the propellant on the HFC signal

During the International Round Robin Test performed in 1997/98 we looked at the influence of the preconditioning of the propellant under different humidities on the HFC signal. The results of a typical experiment are presented in fig. 4.

The shape of the curve always remains the same if the same sample handling (closing of the ampoule and the filling grade) is applied. The differences arise in the heat flow levels and in the time when the second maximum is reached. Both the first maximum and the first minimum remain nearly unchanged in all three experiments. The big difference is the specific heat production rate which rises from 67 µW/g (0% rH) to 88 µW/g (65%rH). Table 5 summarises all results.

Table 5. Specific heat production rate of propellant K 6210 (lot 225), preconditioned under different humidities (T = 80°C)

preconditio-ning	1st maximum [µW/g]	1st minimum [µW/g]	2nd maximum [µW/g]	2nd maximum [days]	energy released within 5 days [J/g]
65 % rH	61,7	20,7	87,7	4,23	20,2
no	56,8	20,0	82,2	4,07	21,8
0% rH	57,9	17,6	67,0	4,26	16,5

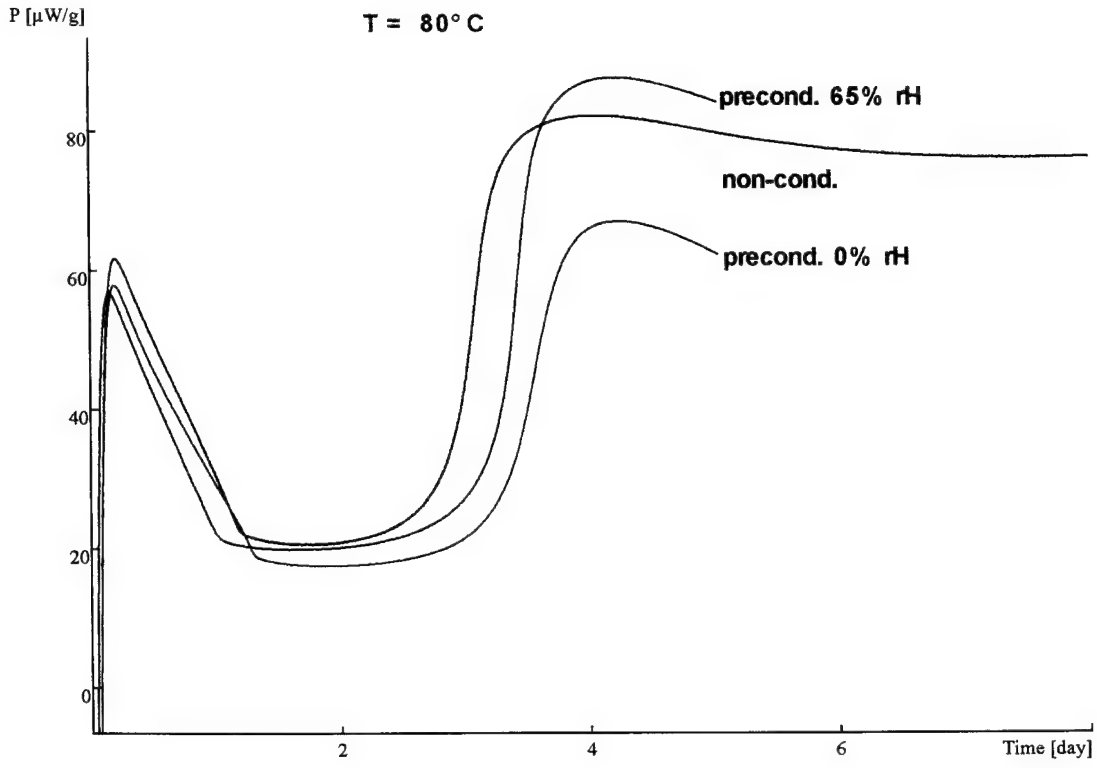

Figure 4. Heat flow measurement of DB ball propellant K 6210, different preconditioning, 80°C (each sample 3.50 g, atmosphere: air, closed ampoules)

4.4 Influence of temperature on the HFC signal

The determination of the temperature dependence on the HFC signal is of great importance to find out the activation energy and to calculate the safe shelf life of it. We performed measurements at 89°C, 80°C, 70°C, 60°C, and 50°C with fresh samples lot 225 of propellant K 6210. All HFC curves show a comparable pattern with a first maximum, a first minimum, a second maximum and a second minimum, followed by a slow increase into the autocatalysis.

Interestingly all chemical reactions that are responsible for this quite complicated decomposition procedure are comparably activated. We calculated the activation energy for iso-α-points of the curve between 89°C and 60°C. They are collected in table 6. A superposition of three measurements at 89°C and 80°C is presented in figure 5.

Besides the first maximum, where the different rates of heating up the sample at different temperature play an important role, and the first minimum, which is lower activated (≈ 120 kJ/mole) all following steps of the decomposition reaction show an activation energy of about 135-140 kJ/mole. The rapid increase into the second maximum shows also a different activation energy, if the value of the heat flow is looked at (Ea (P)). It seems that the increase shifts to a lower reaction degree when the temperature is increased.

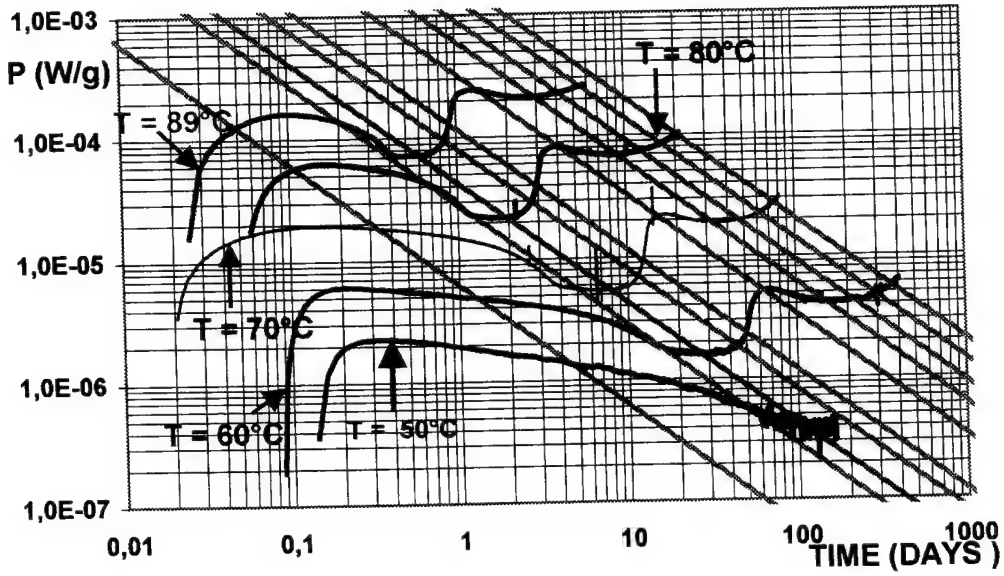

Figure 5a. Heat flow measurements of propellant K 6210 at 89°C, 80°C, 70°C, 60°C and 50°C with fresh samples (ampoule filled and closed, propellant non-conditioned)

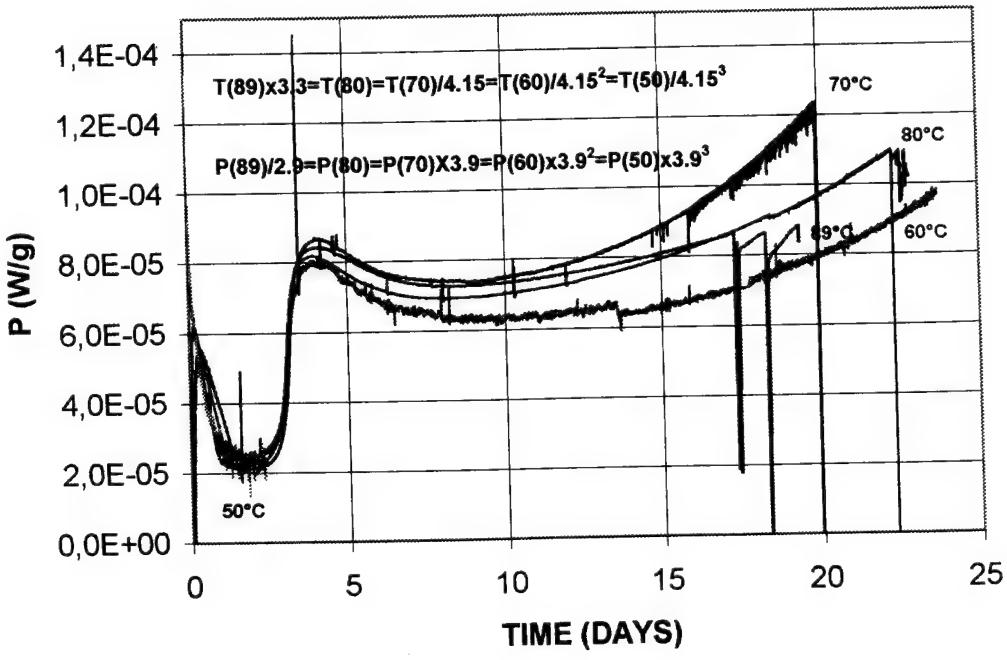

Figure 5b. Heat flow measurements of propellant K 6210 at 89°C, 80°C, 70°C, 60°C and 50°C with fresh samples (ampoule filled and closed, propellant non-conditioned); reduced x- and y-axis

Table 6. Activation energies calculated from iso-α-points of the measurements at 89°C, 80°C, 70°C, and 60°C. Ea (P) refers to the heat flow at the iso-α-points, Ea (t) refers to the time when an iso-α-point is reached. The grey marked values belong to the increase into the second maximum and are higher activated.

Q [J/g]	Ea (P) 89-80°C	Ea (t) 89-80°C	Ea (P) 89-70°C	Ea (t) 89-70°C	Ea (P) 89-60°C	Ea (t) 89-60°C
1	116	97	123	108	124	105
2	118	102	126	114	125	115
3	105	108	122	116	122	118
4	120	108	132	119	123	119
5	137	114	136	124	129	121
6	145	120	142	127	134	123
7	147	127	147	131	142	127
8	154	131	147	135	139	129
9	148	131	147	137	147	132
10	143	132	142	136	147	133
15	140	134	136	137	137	135
20	140	134	136	137	136	134
30	143	136	137	137	138	135
40	145	138	138	137	140	136
50	144	139	139	138	141	137
60	143	139	140	138	141	137
70	141	139	139	138	142	138
75	141	140	139	138	141	138

The activation energies Ea (P) are graphically presented in figure 6.

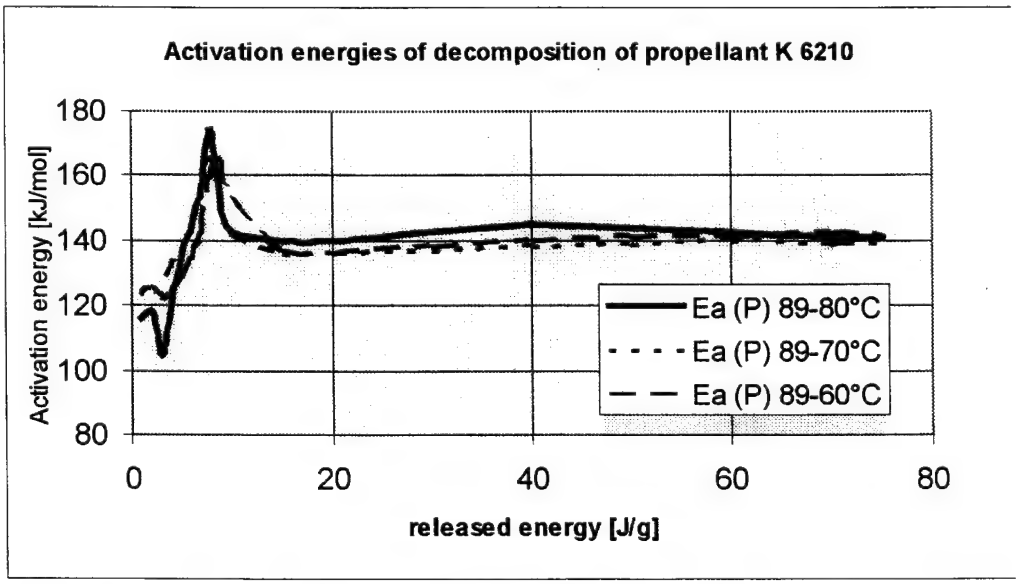

Figure 6. Activation energies of the decomposition of propellant K 6210 at temperatures between 89°C and 60°C

4.5 Experiments to reduce the volume of the glass ampoule

The comparable activation energy of the decomposition process at different temperatures and the availability of high temperature heat flow calorimeters that allow measurements above 89°C makes measurements at e.g. 100°C or 110°C very attractive because measuring times can thus be reduced markedly. With increasing temperatures the heat flow values also rise so that at 100°C the range of the TAM calorimeter (3000 µW) is reached. As we know from the experiments above a reduction of sample amount in the ampoule to reduce the heat production rate is not possible (different shape of the curve and different decomposition chemistry, see fig. 2c and table 4) it was necessary to lower the volume of the sample cell by adding glass to the propellant. We took glass balls (around 1,5 g of propellant and 2,25 g of glass balls) of different diameters and glass rods to reduce the volume of the glass ampoule. The aim of these experiments was to find out whether this additional glass material has an influence on the shape of the curve. Figure 7 shows the results.

The use of glass balls does not lead to the same shape of the HFC curve. It does not depend whether the propellant is above or below the glass material. It can be seen that the first minimum appears later and has a higher level. It also is much shorter, leading to a rapid and early increase into the second maximum which is always lower than that of the pure propellant ("normal measurement"). The effects are bigger when very small glass balls are used. There is no influence on the HFC signal whether the glass is above or below the propellant grains. A homogeneous mixture of glass balls and propellant grains shows a very different HFC signal. All these effects must be related to absorption/desorption phenomena on the glass surface and probably different relative humidities in the sample cell because the biggest differences arise in the first part of the measurement. After the second maximum is reached all heat flow curves are more or less comparable to the original one.

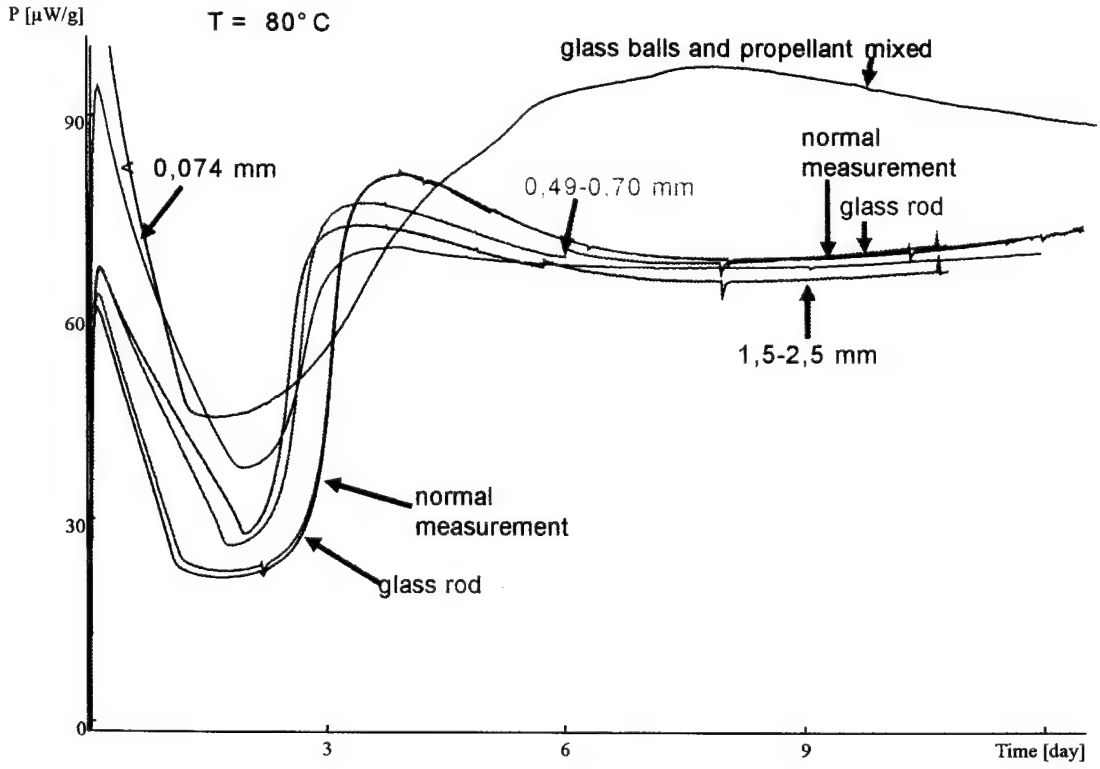

Figure 7. Experiments to reduce the volume of the glass ampoule, T = 80°C. The figures indicate the diameter [mm] of the glass balls used.

Nearly no change in shape or in value is reached when a single glass rod is used to reduce the volume of the ampoule. In this case the glass surface is not much bigger than in the glass ampoule without a glass rod. So the absorption/desorption phenomena are negligible.

5 Conclusion

It is of big importance to know the influence of sample preparation and measuring conditions on the heat flow signal. With the knowlegde of the effects of these parameters on the sample reliable and reproducible measurements can be realised [9]. Increased oxygen concentration and moisture contents seem to stimulate the degradation process.

The conditions that we prefer for gun propellants are completely filled and firmly closed glass ampoules of 3 or 4 mL. The reason for this is the comparability of these conditions with those in the ammunition where also a nearly filled and firmly sealed cartridge is common. Anyway – other arrangements in the ammunition must be as well realised experimentally if necessary. The closing of the ampoule also is important for the reaction mechanism of the stabiliser. If both oxygen is available and NO_x gases can escape through the cap of the ampoule polynitroDPAs dominate while in the closed case the stabiliser reaction stops at the step of N-NO-nitro-DPAs and a much faster autocatalysis is observed. The effects of the humidity of the propellant on the HFC results are less important but must be taken into account if the reproducibility of measurements is not good enough. To reduce the volume of the sample cell (this is necessary in high temperature applications) a glass rod should be taken. Adsorption/ desorption effects dominate the decomposition reaction if glass balls are used. The strong dependence of atmospheric conditions on the HFC signal and the composition of the stabiliser products make it necessary that a comparison of results is only allowed if the environmental conditions used in the experiment are identical.

Acknowledgements

The authors wish to thank all persons that are involved in this project of international collaboration.

References and Notes

[1] Out of the many papers dealing with this subject we picked out some of the most important ones: A. Sopranetti, H.U. Reich, "Comparison of high-temperature stability tests with studies of stabilizers in single-base propellants", *Symp.Chem.Probl. Connected Stabil.Explos.* **5**, 459-477 (1979); L.S. Lussier, H. Gagnon, "The Canadian Gun Propellant Surveillance Program", *Proc. AGARD Conf.* **87**, 23-1 – 23-12 (1996); G. Holl, S. Wilker, M. Kaiser, P. Guillaume, "Former and Modern Methods for the Determination of the Service Life of Double Base Propellants", *Proc. AGARD Conf.* **87**, 18-1 - 18-13 (1996).

[2] D.S. Ellison, A. Chin, "Common Factors that May Affect the Accuracy of Microcalorimetric Data" *Proc. TTCP Workshop Leeds* **4/1997**; A. Chin, D.S. Ellison, "20 mm Gun Propellant Safety Service Life Study Using Microcalorimetry/HPLC Correlation Diagrams", *Proc. TTCP Workshop Leeds* **4/1997**.

[3] Hansson, J., "Testing Propellants by Calorimetry", *LKB Application Note 337* **(1983)**; L.-G. Svensson, P.E. Lagerkvist, C.J. Elmqvist, "Ampoule Microcalorimetry for stability and Compatibility Testing of Explosives and Materials", *LKB Application Note* 332 **(1983)**; C.J. Elmqvist, P.E. Lagerkvist, L.-G. Svensson, "Stability and Compatibility Testing Using a Microcalorimetric Method", *J.Haz.Mater. 7*, 281-285 **(1983)**, E. Lion, M. Rat, "Application de la Microcalorimétrie Isotherme a L'Étude de la Stabilité des Poudres pour Armes", *SNPE Bericht* 93/83/CRB/NP (1983); L.-G. Svensson, C. K. Forsgren, P.O. Backman, "Microcalorimetric Methods in Shelf Life Technology", *Proc. Symp. Compatibility of Plastics and other Materials with Explosives, New Orleans* **(1988)**, 132-137; M. Leveque, O. Ruault, "Influence de l'humidité sur l'évolution des poudres à temperature ambiente", *ICT Jahrestagung* 14, 509-520 **(1983)**; M. Frey, "Stabilitätsuntersuchungen an TLP und Sprengstoffen mittels Wärmeflußkalorimetrie", *Symp.Chem.Probl.Connected Stabil.Explos.* 5, **(1979)**; S. Wilker, U. Ticmanis, G. Pantel, P. Guillaume, "Detailed investigation of sensitivity and reproducibility of HFC measurements", *11. Symp.Chem.Probl.Conn. Stabil. Explos.*, Båstad **1998**.

[4] M.A. Bohn, "Bewertung von Methoden zur Beurteilung und Prognose der Sicherheit von Rohrwaffentreibmitteln", *ICT-Bericht* 29. Juli 1998.

[5] C.J. Dahn, "Large caliber gun propellant thermal stability prediction", *DoD Explosives Safety Seminar* **19**, 699-725 (1980).

[6] Stoermer, Hoffmann, *Chem.Ber.* 31, 2535 [Beilstein XII, page 728].

[7] M. Rat, P. Guillaume, S. Wilker, G. Pantel, "Practical Application of Microcalorimetry to the Stability Studies of Propellants", *Proc. TTCP Workshop, Leeds UK* **1997**; P. Guillaume, A. Fantin, M. Rat, S. Wilker, G. Pantel, "Stability Studies of Spherical Propellants", *ICT-Jahrestagung* **27**, 16-1 - 16-14 (1996); P. Guillaume, M. Rat, S. Wilker, G. Pantel, "Microcalorimetric and Chemical Studies of Propellants", *ICT Jahrestagung* **29**, 133 (1998).

[8] A.H. Heemskerk, "Stability of Nitrocellulose Propellants", *Symp.Chem.Probl.Connected Stabil. Explos.* **8**, 137-148 (1988).

[9] S. Wilker, P. Guillaume, "International Round Robin Test to Determine the Stability of DB Ball Propellants by Heat Flow Calorimetry", *ICT Jahrestagung* **29**, 132 (1998).

[10] J.M. Bellerby, "Is 4-NDPA a better stabiliser than 2-NDPA?", *Proc. 2nd Internat. WIWEB Workshop on Microcalorimetry/Stability*, p. 50-53 **(1999)**.

DISCUSSIONS AND COMMENTS ON PAPERS

THE USE OF HEAT FLOW CALORIMETRY / OPTIMISE THE SERVICE LIFE EVALUATION OF GUN PROPELLANT

J. WILSON

Do you check the HFC results against stabiliser depletion?

We have but generally the HFC trace is used. When a new propellant is introduced a baseline between HPLC results and HFC traces are determined, after this the HFC curve is used to evaluate the stabiliser depletion. We are not interested in stabiliser depletion once it is determined that the propellant is stabilised.

Can you be sure that decomposition is the only process or does diffusion etc play a part?

Ageing is the primary driving force but we are aware that automatic loading systems break seals allowing ingress of moisture and thus changing the decomposition.

Is the propellant surface modified or is it homogeneous?

The surface is modified. We are also trying to look at real hardware and not to consider the propellant in isolation.

INFLUENCE OF STORAGE ON AGEING OF GUN PROPELLANTS IN MUNITION ARTICLES OR IN GLASS BOTTLES.

W. de CLERK

How do you solve the critical diameter?

Heat Flow Calorimetry is a good method for estimating the critical diameter.

How do you assess the criteria as critical diameter is an artificial quantity?

From the Heat Flow curve, when the propellant becomes unstable then it is taken to below the critical diameter.

From the traces of the bag propellant what was the temperature of the measurements?

The temperature of the run was 85°C for one week from which we predicted a surveillance time equivalent to 8 - 10 years.

MICROCALORIMETRY: A TECHNIQUE FOR DETERMINING PROPELLANT STABILITY

R.G. JEFFREY

Does size matter, one slide showed differences between ground and block propellant, is there an explanation for this?

In block samples when propellant decomposes, the resultant gases are retained within the grain thus accelerating the ageing. For the ground samples the decomposition gas has more chance of escaping from the propellant.

When you use glass ampoules how do you seal?

When glass ampoules are used the aim is to retain any evolved gases within the ampoule therefore after sealing each ampoule is tested for leaks. In 70-80% of the ampoules the sealing is satisfactory but in the remainder they have to be re-sealed.

During the presentation you said you had problems with the salt solutions, can you explain why?

At the temperature of the test, i.e., 80°C, nitroglycerine and plasticiser evaporates from the propellant and can then be adsorbed by the salt solution. For double-base propellants the salt solution turns brown.

For propellant Type 3 the results shown are higher than the NATO standard, is the a reason from this?

There is no explanation, however the percentage of ethyl centralite was low which could give rise to variation in the HPLC results or it may be due to the extra glassware used.

In your experiments with different humidities what results were expected?

Solutions were prepared to give different levels of humidity and the expectation was the heat flow would increase with increase humidity. Unfortunately the results obtained were very poor.

THE APPLICATION OF MICROCALORIMETRY FOR OBTAINING THE CORRECT HEAT GENERATION RATES FOR PREDICTING THERMAL RUNAWAY IN NITROCELLULOSE BASED PROPELLANTS.

D ELLISON

What is the name of the microcalorimeter?

The concept was to build a scanning calorimeter by using Peltier elements used in power compensation. The idea is to use the temperature to control the reaction so that the reaction does not go autocatalytic due to the temperature rises.

The idea was proposed that in a TAM experiment there is a time lag between the temperature of the sample and the heat flow reaching the recording Peltiers which would lead to a "false" activation energy.

As a TAM user, would the idea of knowing the temperature lead to a change in the reaction path or give a higher activation energy?

What we are trying to achieve is the true temperature, so that the true rate is obtained and hence a more accurate activation energy. (See Annex A.)

HEAT CONDUCTION CALORIMETERS: PHYSICAL MODELS, AN APPROACH TO INCREASED ACCURACY.

C.E. AUGUET

How do you find parameters such as air gaps, heat conductivities in these systems?

We try alternative values for the heat flow and validate the experimental and theoretical results.

DETERMINATION OF THE KINETIC DATA OF THE THERMAL DECOMPOSITION OF ENERGETIC PLASTICIZERS AND BINDER BY ADIABATIC SELF HEATING.

M.A. BOHN

You dilute the GAP so as to control thermal runaway. If you reduced the size of the GAP sample would the same result be obtained?

It is possible but there are disadvantages with the liquid system. The ARC has a reflux system and if you use pure GAP it distils off and does not drop back thus changing the sample weight.

Does dilution of the GAP change the mechanism?

I do not think the dilution of the GAP changes the mechanism.

Working in a closed system is there air in the sample cell?

The cell was completely filled with sample and not flushed with nitrogen.

In your experience of lower concentration of products and the reaction mechanism do you observe an autocatalytic system?

An autocatalytic system is not observed by this method.

SELF IGNITION MODELLING BASED ON MICROCALORIMETRY MEASUREMENTS.

A. FABRE

How do you determine the activation energy and is it correct?

The power release after 45 hours is used to calculate the activation energy and yes it is correct. Sometimes the heat flow curve is not constant and the thermal conductivity is measured. The Chairman (Dr Wilker) informed the Workshop that a Swedish company have produced a good instrument for measuring heat conductivities which will help in calculations such as those referred to.

What is the temperature of the chamber?

The temperature was 66°C which corresponds to the asymptotic temperature that is non-self-ignition. There is a narrow band between non-ignition and ignition.

A STUDY OF THERMAL STABILITY AND PERFORMANCE OF ENERGETIC MATERIALS USING HEAT FLOW CALORIMETRY.

D. ELLISON

Mr Ellison reiterated the hypothesis that the temperature of the block is not the temperature of the sample and that the true activation energy is not being measured since the reaction rate is changing in an exponential fashion. He stated that this could be an explanation why different laboratories get different results on the same sample, because an accurate temperature is not being measured.

RECENT DEVELOPMENTS IN MICROCALORIMETRY USING AUTOMATED AND LARGE SCALE SAMPLING SYSTEMS.

J WILSON

In the automatic sampling carousel how are the samples put into the Thermal Active Monitor (TAM)?

An arm lifts the ampoule and the carousel moves to a large hole through which it is dropped into the instrument.

Is the autosampler at the same temperature as the TAM?

Yes, that was the aim when it was designed and built.

How long is each individual sample in the calorimeter?

After equilibrium each individual sample is measured for 15 minutes.

NOVEL METHODS OF CHARACTERISATION OF ADSORBENT SURFACES BY FLOW ADSORPTION MICROCALORIMETRY.

A. J. GROSZEK

The zeolite used, was it a commercial sample or was it specially prepared?

It was prepared in the laboratory as the ammonium salt.

Heats of reaction can they be measured?

The heats of adsorption are the heats of reaction in chemisoption experiments.

AN ABSOLUTE CALIBRATION METHOD FOR MICROCALORIMETERS.

P. BUNYAN

What is the temperature drop used in the specific heat determination?

About 1°C but 0.9987°C was measured. The TAM's thermostat decade resistor settings were determined by trial and error.

Would you recommend a calibration for every change in temperature?

Results indicate that it does not matter.

If calibration was required would you get a large change in the heat factor?

Because it is a relatively small heater I do not think it is applicable, but I would need to think about this.

USE OF RH PERFUSION AMPOULE IN TAM AT ELEVATED TEMPERATURES.

M.A. PHIPPS

If the water is being adsorbed then using 2 mass flow controllers one at 20°C and the still water at 25°C then by measuring the concentration changes you would know exactly how much water (was adsorbed.)

I do not dispute this but we try to make life easy and have the humidifier chambers equilibrated and therefore do not have to worry about thermostats.

Did you use salt solutions to verify the RH?

Yes, this was the method used to verify the RH.

At higher temperatures there is the possibility of running out of water, do you correct for this?

Sort of, we can reduce the flow rate.

MICROCALORIMETRIC METHOD TO DETERMINE THE CORROSION RATE OF LIQUID PROPELLANT AND METAL CONTAINER.

D. ELLISON

How do you measure corrosion?

It was measured from the heat flow, 1mm of corrosion was equivalent to 1mj/mole.

THE DEVELOPMENT OF A NEW DIFFUSION CONTROLLED CALIBRATION DEVICE FOR MICROCALORIMETERS.

L. WADSO

What is the diameter of the tube between the two chambers in the calibration ampoule and what was the temperature of the calibration runs?

The diameter was 0.66mm diameter and the calibration temperature was 25°C.

Have you run calibrations at other temperatures?

No, for different temperatures you may have to change the system but in principle it should work.

What was the concentration of the sulphuric acid used?

The concentration of the sulphuric acid used was 97 mass percent.

Would you expect any contribution from corrosion?

Originally some corrosion was experienced but this was eliminated by the design of a new chamber.

You mentioned the problem of having two cells above and below each other, if they were side by side would this overcome the problem?

A paper was previously published on this, the volume is small and this configuration did not work as well.

NB. At the end of his presentation Dr Wadso showed a calculation he had made on the earlier hypothesis suggested by Mr Ellison, i.e., that the temperature recorded is not the true temperature of the sample. This calculation is reproduced as Annex A.

MICROCALORIMETRY AND DSC STUDY OF THE COMPATIBILITY OF ENERGETIC MATERIALS.

A. TOMPA

In isothermal compatibility you integrated the signal instead of taking the mircowatt reading, was there a reason for this?

In some cases the joule plot looked better.

SMALL SCALE REUSABLE METAL CRUCIBLE FOR USE IN DIFFERENTIAL SCANNING CALORIMETRY AND ITS MICROCALORIMETRIC APPLICATION

L TUMA

How much higher pressure will the new cell withstand compared to aluminium pans?

100 psi , however, this depends on how well the cell is sealed. The pressure increase over aluminium pans is consistently a factor 2 to 4 higher.

Your company designed these new cell in Merck metal, can you name the vendor and give further details?

Each crucible costs about $250 to manufacture. They are made from Hastelloy B and can be lined with tantalum. Each cell will last for 6 months of constant use and has a capacity of about 75 milligrams or 65 microlitres. The size of the cells are limited by the size of the platens.

INTERNATIONAL ROUND ROBIN TEST TO DETERMINE THE STABILITY OF DB BALL PROPELLANTS BY HEAT FLOW CALORIMETRY.

S. WILKER

What is the reason for the reproducibility being less between 40-60°C as it is very good at 80°C?

This depends on the signal level and the history of the sample. On longer measuring times a further degradation stage occurs, also the reproducibility is not so good when different laboratories used different measuring times.

Could you improve the reproducibility by taking the log of the signal?

There are "tricks" that can be used to improve reproducibility such as taking a larger sample, stopping the experiment before the critical temperature or taking the log of the signal to obtain a straight line.

At 80°C there was a drop down to the first minimum, why?

Yes this is so and is discussed in our second paper.

HEAT FLOW CALORIMETRY - EFFECTS OF SAMPLE PREPARATION AND MEASURING CONDITIONS.

S. WILKER

No questions were asked.

FINAL DISCUSSION

LEAD BY DR PETER LAYE

The final session of the Workshop consisted of a discussion led by Dr Laye and supported by a panel of experts consisting of Mr de Klerk, Mr Ellsion and Dr Wilker.

Dr Laye opened the discussion by reiterating the conclusions from the 1997 Workshop which were headed: instrumentation, samples and interpretation. The main tools for calibration and problems with the Relative Humidity Perfusion unit. With sampling the problem was sealing the ampoules and how ampoules should be filled. Interpretation was measuring the activation energy and understanding the reaction mechanisms and the effects of humidity/moisture on the results.

Dr Laye posed the question where are we today? Two papers have been presented on new calibration methods, the manufacturer of the RHP unit suggested modification and changes to the flow rate to overcome the condensation problems. Also a successful round robin exercise showed the reproducibility that could be obtained on propellant samples by adopting a standard method.

Discussion started with a question, What about the Thermometric and Bofors flow through units compared with ampoules, are we happy with the system? Dr Wilker responded, that a round robin exercise for flow through cells containing magnesium sulphate or potassium chloride had been proposed and although interest was showed in laboratories participating, no-one wanted to organise the exercise. Mr Jeffries said there was a problem with flow through cells when studying double base propellants due to the loss of nitroglycerine, giving a change in composition which results in different results. Mr Ellison suggested not to use the flow through cell in a continuous mode but to introduce slugs which could be injected into a closed loop. He said there may even have to be a separate type of cell.

Dr Laye stated that other themes noted at the Workshop was a tendency to larger samples and automated sampling. Mr Ellison, who is the person mainly involved in this said that to keep track of samples he uses a logging system and at present a card system is used to track samples. However, in future a bar-code on the sample bottle could be a way forward. With the automatic sample the aim was to improve the software so that changes to the data could be made during an experiment. Also, he would like to see a standard data format so that data could be transferred between laboratories.

Dr Laye posed the question, in the interpretation of results is the isothermal rate low first order kinetics when discussing decomposition of propellants? Dr Wilker said he had give presentations on this at an ICT conference and at the last Workshop, but one must know more about the reactions. To simplify the calculations a global reaction

has to be considered for once the DPA stabiliser had been used up many reactions occur and the reaction mechanism is almost un-solvable. It is for this reason that the shape of the curves have to be considered. Mr de Klerk said if you want to know the activation energy there are other methods available but again for propellants the reactions are complex. For some propellants a single activation energy cannot be applied as other factors such as diffusion rate influences the kinetics.

The point was then made that the functionality of the propellant was the next most important parameter. Dr Laye asked if there was any information comparing microcalorimetry results against performance? Mr Ellison said he wished to do such a study, he had started t age 20mm rounds in an oven at 52.2°C and would fire the aged rounds. He would then like to duplicate the ageing in the calorimeter so he could compare heat flow with performance.

Mr de Klerk, the STANAG states if the stabiliser content is satisfactory then all materials can be stored together but complex changes can occur and the critical diameter, depending on the storage, can be smaller than expected. Dr Wilker said they had started measuring heat conductivities, with a new Swedish system, to give a heat transfer number.

Dr Laye thought the results from the round robin exercise, carried out since the last Workshop was very important. The question was asked if it was planned to write up the method used in the round robin exercise. Dr Wilker stated that a draft had been written and submitted to the committee for agreement.

In an IUPAC study a similar exercise was carried out using the hydrolysis of triacetin as the reaction, and in which eight or nine laboratories had participated. The results are being collated and analysed. Anyone wanting further details should contact Ed Lewis, Calorimetry Science Corporation.

Mr Jeffries said the results from the propellant round robin showed good agreement and similar traces but how could this be used to indicate whether a propellant was good or bad? The only way is through experience and it must be remembered that the results only indicate good or bad in terms of decomposition kinetics and gives no indication of functionality.

Looking to the future it was decided to hold another Workshop in about 2 years time, however, this could clash with a Swedish meeting on microcalorimetry. To avoid this the aim would be to consider a date around September 2001.

It was put to the organisers of the meeting that they consider expanding the scope of the meeting to include DSC and ARC papers.

Dr Griffiths closed the Workshop by giving thanks to all who attended, the authors of papers, the Chairmen of the Sessions and to his many helpers.

ANNEX A CRITIQUE OF TRUE TEMPERATURE IN A HEAT FLOW CALORIMETRIC EXPERIMENT.

During the conference Dr Ellison had proposed that during a Heat Flow Calorimeter experiment that a finite time was required for the temperature at the centre of the sample to transfer to the temperature sensors, therefore the temperature recorded was not the true temperature. Since the heating rate curve was an exponential then this time lag could lead to errors in the predictions of shelf life. In reply to this Dr Lars Wadso made a presentation of a calculation he had made. First he showed a diagram to show the parameters to be measured within the instrument.

Assumptions made were:

constant temperature of the bath:

all heat passes through thermocouples (safe side):

there are no rapid changes $\Rightarrow$ therefore a steady state is produced (this assumption is OK since the length of experiments presented were long):

Air gap : k= 35000 ; T = 80°C.

The sample is 6mm radius, 20mm length then λ (thermal conductivity) was taken as 0.17 W/mK (ref FABRE's paper) and ρ = 100 μw.

2CP = K = 0.115 W/K

16 TCP = K = 0.992 W/K

From this were calculated.

ANNEX A CRITIQUE OF TRUE TEMPERATURE IN A HEAT FLOW CALORIMETRIC EXPERIMENT.

During the conference Dr Ellison had proposed that during a Heat Flow Calorimeter experiment that a finite time was required for the temperature at the centre of the sample to transfer to the temperature sensors, therefore the temperature recorded was not the true temperature. Since the heating rate curve was an exponential then this time lag could lead to errors in the predictions of shelf life. In reply to this Dr Lars Wadso made a presentation of a calculation he had made. First he showed a diagram to show the parameters to be measured within the instrument.

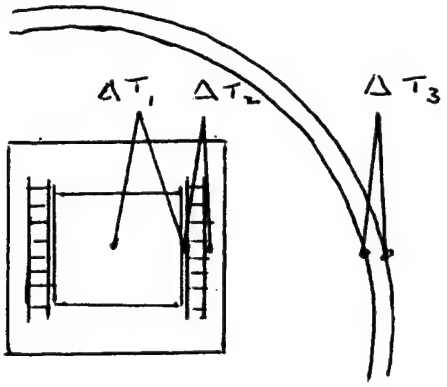

Assumptions made were:

constant temperature of the bath:

all heat passes through thermocouples (safe side):

there are no rapid changes ⇒ therefore a steady state is produced (this assumption is OK since the length of experiments presented were long):

Air gap : k= 35000 ; T = 80°C.

The sample is 6mm radius, 20mm length then λ (thermal conductivity) was taken as 0.17 W/mK (ref FABRE's paper) and ρ = 100 μw.

2CP = K = 0.115 W/K

16 TCP = K = 0.992 W/K

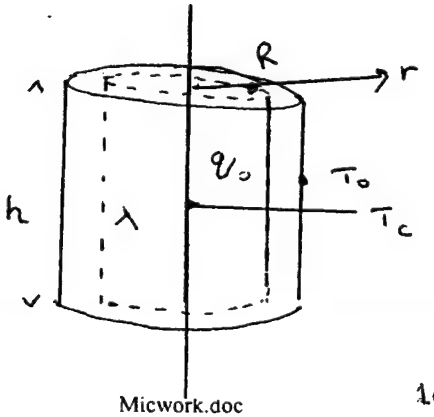

From this ΔT_1, ΔT_2, ΔT_3 were calculated.

ΔT_1

$$\text{Heat Flux} = -\lambda \frac{dT}{dr}$$

$$-\frac{q_0 r}{2\lambda} = \frac{dT}{dr};\ q_0 = \frac{P}{\pi R^2 H}$$

$$\Rightarrow T_r = \frac{-q_0 r^2}{4\lambda} + T_c;\ T(R) = 0$$

$$-\frac{E_a}{RT} \Rightarrow \Delta T = \frac{P}{4\pi\lambda H}$$

$$\Delta T_1 = 2.3mK$$

$$\Delta T_2 = \frac{P}{k} = \{0.9mK(2TCP),\ 0.1mK(16TCP)$$

$$\Delta T_3 = \frac{P}{k} = 0.2mK$$

$$\Delta T_1 + \Delta T_2 + \Delta T_3 = 3.4mK$$

$$\text{rate} \sim e^{-\frac{E_a}{RT}}$$

$$\frac{\text{rate}(80°C + \Delta T}{\text{rate}(80°C)} = \frac{e^{-\frac{35000}{R(273+80+3.4mK)}}}{e^{-\frac{35000}{R(273+80)}}}$$

$$= 1.0001$$

Thus proving that the difference between the temperature at the centre of the sample and the recorded temperature would be very small and hence have little affect on the rate of reaction and that the results as recorded are valid.

LIST OF ATTENDEES

BELGIUM	
Dr Pierre Guillame	PB Clermont SA
DENMARK	
Mr Niels Frederiksen	Naval Material Command
FINLAND	
Mrs Maija Hihkiö	Finnish Research Centre of Defence Forces
Dr Irmeli Tuukkanen	Defence Material Establishment Headquarters
FRANCE	
Mr Alain Fabre	ETBS DPY/CME
Mr Eric Thomas	Dessault Aviation
GERMANY	
Dr Manfred Bohn	Fraunhofer-Institut Fuer Chemische Technologie
Dr Stephan Wilker	BICT
THE NETHERLANDS	
Mr Wim De Klerk	TNO - PML
Dr Niels Van Der Meer	TNO - PML
Dr Leo Van Leersum	Royal Netherlands Navy.
REPUBLIC OF SOUTH AFRICA	
Mrs Helge Schimansky	Somchem
SPAIN	
Dr Carlota Auguet	Universitat Politecnia de Catalunya
SWEDEN	
Ms Veronica Andersson	DYNO NOBEL
Dr Ulf Bemm	Defence Research Establishment (FOA)
Mrs Marja-Liisa Petterson	Defence Research Establishment (FOA)
Dr Lars Wadso	Lund University

UNITED KINGDOM

Dr Paul Bunyan	DERA, Fort Halstead
Mr Tony Cardell	DERA, Fort Halstead
Dr Michael Cartwright	RMCS, Cranfield University
Prof Ted Charsley	University of Huddersfield
Dr Nigel Davies	RMCS, Cranfield University
Mr William Fletcher	MOD, Procurement Executive
Dr Octavia Frota	RMCS, Cranfield University
Ms Sarah Goodall	University of Huddersfield
Dr Trevor Griffiths	DERA, Fort Halstead
Dr Aleksander Groszek	Microscal Ltd
Mr Ronald Jeffrey	DERA, Fort Halstead
Dr Peter Laye	University of Leeds
Dr Mark Phipps	Thermometric Ltd
Mr Jim Queay	CESO (Navy)
Mr Jim Rooney	Univeristy of Huddersfield
Mr Robert Taylor	Thermometric Ltd
Mr Neil Turner	CESO (Navy)
Dr Tracy Vine	DERA, Fort Halstead
Dr Richard White	AWE, Aldermastion

UNITED STATES OF AMERICA

Dr Bernie Douda	NSWC, Crane
Der Daniel Ellison	NSWC, Crane
Dr Bill Hubble	NSWC, Crane
Mr Alan Phipps	NSWC, Crane
Dr Albert Tompa	NSWC, Indian Head
Ms Linda Tuma	Merck
Mr James Wilson	NSWC, Crane

DISTRIBUTION LIST

Dr P Barnes

Dr I Wallace

Dr G Lindsley

Dr K Smit

DRIC, (2 copies)

Public Records Office

DERA Information Centre (2 copies)

All Attendees of the Workshop.

CESO (Navy), Bath, UK

VP(SS) Ordnance Board

DSc (Land) 1

DSTO, Australia